Morpho-structural variability in wings of selected dragonflies with special reference to *Pantala flavescens* (Fabricius, 1798) (Libellulidae): Gut bacterial microbiome, development, and characterisation of wing resilin protein

Thesis submitted in
partial fulfillment of the requirements
for the award of the degree of

DOCTOR OF PHILOSOPHY IN ZOOLOGY

By

GAYATHRI. M

Under the Guidance of

Dr. Y. SHIBU VARDHANAN

BIOCHEMISTRY & TOXICOLOGY DIVISION
DEPARTMENT OF ZOOLOGY
UNIVERSITY OF CALICUT
KERALA, INDIA

APRIL, 2024

കാലിക്കറ്റ് സർവ്വകലാശാല
ജന്തുശാസ്ത്ര പഠനവിഭാഗം
കാലിക്കറ്റ് സർവ്വകലാശാല (പി.ഒ.), മലപ്പുറം (ജില്ല),
കേരള, ഇന്ത്യ - 673 635

UNIVERSITY OF CALICUT
DEPARTMENT OF ZOOLOGY
Calicut University (P.O.), Malappuram (Dt.),
Kerala India - 673 635
Tel: 0494 - 2407420 (Head), 0494 - 2407419 (Off.)

Dr. Y. Shibu Vardhanan
Professor

Re-Accredited by NAAC with "A" Grade

No: 362/4C /ZOO/2024-2025 Date: 23rd October 2024

CERTIFICATE

This is to certify that this dissertation entitled **"Morpho-structural variability in wings of selected dragonflies with special reference to *Pantala flavescens* (Fabricius, 1798) (Libellulidae): Gut bacterial microbiome, development, and characterisation of wing resilin protein"** is an authentic record of independent work done by **Gayathri. M.,** Department of Zoology, the University of Calicut under my guidance and supervision for the partial fulfillment of the requirements for **the Degree of Doctor of Philosophy in Zoology** and further no part of this dissertation has been presented before for any other Degree or Diploma.

Dr. Y. Shibu Vardhanan

Dr. Y. Shibu Vardhanan
Professor
Department of Zoology,
University of Calicut, Malappuram,
Kerala, India. PIN: 673635

DECLARATION

I do hereby declare that project entitled **"Morpho-structural variability in wings of selected dragonflies with special reference to *Pantala flavescens* (Fabricius, 1798) (Libellulidae): Gut bacterial microbiome, development, and characterisation of wing resilin protein"** is an authenticated record of the work carried out by me under the guidance and supervision of **Dr. Y. Shibu Vardhanan**, Associate Professor, Biochemistry & Toxicology Division, Department of Zoology, University of Calicut and that no part of this has been submitted before for the award of any other Degree or Diploma.

C.U. Campus **Gayathri, M.**

ACKNOWLEDGMENT

I would like to express my sincere gratitude to my supervisor Dr. Y. Shibu Vardhanan, Associate Professor, Department of Zoology, University of Calicut for the continuous support of my Ph.D. study, and for his patience, motivation, and immense knowledge. His guidance and encouragement have always helped me throughout the time of research and writing of this thesis. He is my mentor and a better advisor for my doctorate study beyond the imagination.

I also like to express my sincere thanks to Mr. Anand, P. P, my colleague and senior research scholar, whose sincere support, and vast knowledge helped me a lot in the completion of my Ph.D. work.

My sincere thanks to Dr. E. Pushpalatha (Former Head of the Department of Zoology), Dr. E. M. Manogem, (Former Head of the Department of Zoology), & Dr. C. D. Sebastein (Head of the Department of Zoology) for providing facilities in the department to complete my work.

I am also pleased to say thanks to Mr. Vivek Chandran A, Research scholar, Christ College Irinjalakuda for his valuable advice for the identification of specimens.

I would like to extend my Sincere gratitude to the UGC for providing financial support for doing the research.

I would like to express my heartfelt gratitude to the University of Calicut's CSIF (Central Sophisticated Instrument Facility) for providing instrumentation facilities.

I express my heartfelt thanks to all my lab mates Dr. Neethu, C.B., Dr. Seena. S., Mrs. Rahila.K., Mrs. Renu, V.V., Ms. Mehabooba, B., Mr. Abhishek Buxi., Dr. Abhilash, P. L., Ms. Priyanka, P. P, and Ms. Rameesa, P for their support and help for the completion of my work

I express my heartfelt thanks to all my teachers and non-teaching staff of the Department of Zoology, the University of Calicut for their selfless support and help.

My sincere heartfelt thanks goes to all my friends in the Department of Zoology for their enthusiastic support and help during my research.

I would like to thank my entire family: My father, mother, brother, and in-laws for their support, encouragement, and motivation to accomplish my goal. Last but not least I wish to show my heartfelt thanks to my husband Mr. Ratheesh for his unconditional, and loving support and motivation.

Gayathri M.

CONTENTS

ABSTRACT

Dragonflies, with their intricate wing venation, hold immense fascination for scientists across disciplines. These structures, particularly the forewing and hindwing venation patterns, have long fascinated biologists due to their diversity and functional significance. This thesis delves into a multifaceted exploration of dragonfly biology, encompassing their wing venation, embryology, predatory potential, gut bacterial microbiome, and wing resilin protein.

Firstly, the study examines the remarkable venation patterns of selected dragonfly species wings, elucidating their structural adaptations and aerodynamic implications. For the study purposes, we documented the wing venation pattern of 26 dragonfly species forewings and hindwings. Dragonfly wings are characterized by a network of veins and cross-veins that provide structural support and aerodynamic efficiency during flight. The forewing and hindwing of dragonflies exhibit distinct venation patterns, which vary across species. Major veins, such as the costa, subcosta, radius, and media, form the framework of the wing, while cross-veins connect these major veins, contributing to wing rigidity and flexibility. The arrangement and density of these veins and cross-veins can differ significantly between species, reflecting adaptations to specific ecological niches and flight requirements. From the study, we revealed that hindwings exhibits high level of structural variations as compared to forwings and these variations connected to the flying adaptation of an organisms. Intrestingly, the morphological modifications of wing patterns in forewing and hindwings are controlled by natural selection pressure not by evolutionary force, which confirmed that ecology play an important role in the flight adapation of dragonflies.

The gut microbiome plays a crucial role in various aspects of insect physiology, including digestion, immunity, and development. Recent studies have suggested a potential link between the gut microbiome composition and the morphological traits of insects, particularly wing size variations. For the study purposes, we compared the gut bacterial microbiome of migratory and non-migratory species: *Pantala flavescens* and *Neurothemis tullia.* There is a significant difference in the diversity of gut bacterial communities of the the dragonfly species.

Some bacterial group shows specificity towards *P. flavescens* like *Aeromonas, Paraclostridium, Myroides, Pseudocitrobacter, Vagococcus* and *Weissella*. Bacterial genus *Paracoccus, Janthinobacterium*, and *Romboutsia* are specific to *N. tullia*. In addition to that, the variation in the abundance of bacterial communities has been not limited to species wise, it also observed in the male and female dragonflies.

The wandering glider (*Pantala flavescens*) is a remarkable migratory dragonfly species known for its extensive transcontinental movements. This thesis investigates the migratory behavior of wandering gliders, focusing on the embryonic and post-embryonic development stages, as well as their predatory potential. For the embryonic and post-embryonic development, we developed a novel culture method, developed a nutrient solution for the mass rearing of wandering glider. The predatory potential of wandering glider is proved that the wandering glider could be used as a strong biocontrol agent for mosquito control in an ecological effective manner. The novel nutrient composition increases the physiological activies as well as the predatory potential of the wandering glider.

The intricate relationship between dragonfly wing morphology and the role of resilin proteins in providing structural integrity and elasticity to the wings. By investigating the intricate details of dragonfly wing structure and the properties of resilin proteins, this research aims to shed light on the adaptive mechanisms that enable dragonflies to achieve exceptional flight performance. This is the first study deals with the isolation, sequencing and characterization of wing resilin. As per the current records, only two resilin proteins identified from the two species of the dragonfly species. As per the records, in India there is no proper study related to wing resilin proteins. Furthermore, the role of wing resilin protein in conferring mechanical resilience and flexibility to dragonfly wings is investigated, unveiling strategies for biomimetic material design and engineering applications.

Collectively, these diverse facets of dragonfly biology present a rich tapestry of research opportunities with implications ranging from fundamental science to technological innovation. Harnessing insights from dragonfly biology holds promise for advancements in fields as varied as bioinspired design, ecological conservation, and biomedical engineering.

സംഗ്രഹം

ഷഡ്പദങ്ങളുടെ കൂട്ടത്തിൽ നിന്ന് തന്നെ വളരെയധികം വ്യത്യസ്തത പുലർത്തുന്ന ജീവിവർഗ്ഗമാണ് തുമ്പികൾ. 30 കോടി വർഷങ്ങളായി ഇവർ ഭൂമിയിൽ ജീവിക്കുന്നുണ്ടെന്നാണ് കരുതപ്പെടുന്നത്. ലോകത്താകമാനം 3,000-ത്തിൽപ്പരം സ്പീഷിസുകളുള്ള ഇവ നിറത്തിലും രൂപത്തിലുമെല്ലാം മറ്റൊന്നിൽ നിന്ന് വ്യത്യസ്തമായിരിക്കും. ഇന്ത്യയിൽ ഇതുവരെ കണ്ടെത്തിയ അഞ്നൂറോളം ജാതി തുമ്പികളില് നൂറ്റിഎഴുപതിലേറെ ഇനത്തെ കേരളത്തില് കാണാം. ആറുകാലുകളുണ്ടെങ്കിലും നടത്തത്തിൽ വളരെ പിന്നിലുള്ള ജീവികളാണ് ഇവർ. പക്ഷേ വേഗത്തിൽ പറക്കാൻ അപാര കഴിവാണ് ഇവയ്ക്കുള്ളത്. മണിക്കൂറിൽ 48 കിലോമീറ്റർ വേഗതയിൽ വരെ പറക്കാൻ കഴിയുന്ന ഇക്കൂട്ടർ ലോകത്തിലെ ഏറ്റവും വേഗതയുള്ള ഷഡ്പദങ്ങളാണ്. പിന്നിലേക്ക് പറക്കാനും ഇവയ്ക്ക് സാധിക്കും. ജലാശയങ്ങൾക്ക് സമീപമുള്ള ചൂടുള്ള പ്രദേശങ്ങളിലാണ് ഇവ പ്രധാനമായും കാണപ്പെടാറുള്ളത്. ലോകത്തിൽ പലരീതിയിലുള്ള പഠനം നടന്നുവരുന്നുണ്ടെങ്കിലും ഏറെ ശ്രദ്ധയാകർഷിക്കുന്ന പഠനമേഖലയാണ് ഇവയുടെ ചിറകുകളുടെ ഘടനയും കൂടാതെ അതിവേഗത്തിൽ പറക്കാനുള്ള കഴിവും.

തിരഞ്ഞെടുത്ത തുമ്പികളുടെ ചിറകുകളുടെ ഘടന, അവയുടെ പരിണാമം, കൂടൽ ബാക്കീരിയ വൈവിധ്യം - ദേശാടനം നടത്തുന്നവയും അല്ലാത്ത തുമ്പികളിലൂടെയുമാണ് ഈ പഠനത്തിന്റെ ആദ്യ ഭാഗം കേന്ദ്രീകരിക്കുന്നത്. 26 സ്പീഷീസ് കേന്ദ്രികരിച്ചുള്ള പഠനത്തിൽ, ഒരോ സ്പീഷീസ് തുമ്പികളുടെ മുൻചിറകുകൾ, പിൻചിറകുകൾ വെനേഷൻ പാറ്റേൺ (Venation pattern) പഠനത്തിന് വിധേയമാക്കിയത്. ഓരോ തുമ്പികൾക്കും അവയുടെ ജീവിതരീതിക്അനുസരിച്ചാണ് അവയുടെ ചിറകിന്റെ വെനേഷൻ പാറ്റേൺ നിജപ്പെടുത്തിരിയിരിക്കുന്നത്. ഈ ചിറകുകളുടെ ഘടനയിൽ വരുന്ന മാറ്റങ്ങൾ ജീവിവർഗ്ഗികരണത്തിന് ഒരു വലിയ മുതൽക്കൂട്ടാണ് എന്ന് ഈ പഠനത്തിലൂടെ തെളിയിക്കുവാൻ സാധിച്ചു. കൂടാതെ ഈ ഘടനയിൽ വരുന്ന മാറ്റങ്ങൾ പരിണാമ തിരഞ്ഞെടുപ്പ് സമ്മർദ്ദത്തേക്കാൾ (Natural selection pressure) പാരിസ്ഥിതിക തിരഞ്ഞെടുപ്പിന്റെ സമ്മർദ്ദത്താലാണ് (Environmental selection pressure) എന്നത് ഈ പഠനത്തിന്റെ വലിയ നേട്ടമാണ് .

ജപ്പാനിൽ നിന്ന് ഇന്ത്യയിലേക്ക്, ഇന്ത്യയിൽ നിന്ന് ആഫ്രിക്കയിലേക്ക് അവിടെ നിന്ന് അമേരിക്കയിലേക്ക്. ഇങ്ങനെ ഭൂഖണ്ഡങ്ങള് തോറും കൂട്ടമായി സന്ദർശനം നടത്തുന്നവരുമുണ്ട് തുമ്പികളുടെ കൂട്ടത്തില്. പന്താലാ ഫ്ളേവ്സെന്സ് (*Pantala flavescens*) എന്നാണ് ഇവയുടെ പേര്. സമുദ്രോപരിതലത്തിലെ കാറ്റിനനുസരിച്ചാണ് ഇവ പലപ്പോഴും വന്കരകളില് നിന്ന് വന്കരകളിലേക്ക് യാത്ര ചെയ്യുക. തുമ്പി കേരളത്തിലെത്തുമ്പോൾ ഇവിടെ ഓണം. മാലദ്വീപിലെത്തുമ്പോൾ തുലാമഴയുടെ തുടക്കം. ആഫ്രിക്കയിലെത്തുമ്പോൾ വിത തുടങ്ങാനുള്ള സമയം. ഇങ്ങനെ ലോകത്തിന്റെ പല ഭൂഖണ്ഡങ്ങളിലും ഐശ്വര്യം കൊണ്ടുവരുന്ന ശുഭസൂചനയാണ് പാന്റലാ ഫ്ളേവ്സെന്സ് എന്നറിയപ്പെടുന്ന ഓണത്തുമ്പി. ഹിമാലയം, ഗോവ, കേരളം, മാലദ്വീപു വഴി ആഫ്രിക്ക. ഒരു വർഷം കൊണ്ട് ഈ ചക്രം പൂർത്തിയാക്കുമ്പോഴേക്കും പിറ്റേവർഷത്തെ യാത്രയ്ക്കുള്ള സമയമാകും. ശരാശരി മൂന്നു–നാല് മാസമാണ് തുമ്പിയുടെ ആയുസ്. കേരളത്തിൽ മുട്ടിയിട്ട് പറന്നയരുന്ന തുമ്പി മാലദ്വീപിലെത്തുമ്പോഴേക്കും നാമാവശേഷമാകും. തൊട്ടുപുറകേ എത്തുന്ന കുഞ്ഞുങ്ങളുടെ ബാച്ചാണ് ആ യാത്ര പൂർത്തിയാക്കി ആഫ്രിക്കയിലെത്തുക. ഹിമാലയത്തിൽ നിന്നു പുറപ്പെടുന്നവയുടെ അഞ്ചാം തലമുറയാകും ലക്ഷ്യത്തിൽ എത്തുക.

ഇത്രയധികം പ്രത്യകത ഉള്ള തുമ്പിയുടെ ജീവിതരീതി, ഭ്രൂണവും ഭ്രൂണാനന്തര വികസനവും, പ്രീഡറ്റോറി പൊറ്റന്റില് (Predatory potential) കൂടാതെ ചിറകുകൾക്ക് അസാധാരണമായ പറക്കാനുള്ള കഴിവിന് കാരണമാകുന്ന പ്രോട്ടീൻ ആയ റെസിലിൻ (Resilin) എന്നിവയെകുറിച്ചു പ്രതിപാദിക്കുന്നതാണ് ഈ പഠനത്തിന്റെ ബാക്കി ഭാഗങ്ങൾ. മുട്ടവിരിഞ്ഞു വരുന്ന കുഞ്ഞുങ്ങൾ (Naids) ജലത്തിലാണ് കഴിച്ചുകൂട്ടുന്നത്. മത്സ്യക്കുഞ്ഞുങ്ങൾ ഉൾപ്പെടെയുള്ള ചെറു ജലജീവികളാണ് അവയുടെ ഭക്ഷണം. എട്ട്ഘട്ടങ്ങളായിട്ടാണ് ഇവയുടെ ബ്രൂണത്തിന്റെ വളര്ച്ച അവസാനിക്കുന്നത്. ഈ തുമ്പിയുടെ ജീവിതരീതിയും അവയെ കൂട്ടത്തോടെ വളർത്തിയെടുക്കാനുള്ള സാങ്കേതികതരീതിയും ഈ പഠനത്തിലൂടെ വികസിപ്പിച്ചെടുത്തിട്ടുണ്ട്. തുമ്പികൾ ഇല്ലെങ്കിൽ നമ്മുടെ ജീവിതം ദുസ്സഹമായിരിക്കും. കാരണം കൊതുകുകളാണ് ചിലയിനം തുമ്പികളുടെ ഇഷ്ടഭക്ഷണം. ദിവസവും നൂറുകണക്കിന് കൊതുകുകളെ ഓരോ തുമ്പിയും പിടിച്ചുതിന്നാറുണ്ട്. വെള്ളത്തിൽ ജീവിക്കുന്ന ഇവയുടെ കുഞ്ഞുങ്ങളും കൊതുകുകളുടെ കൂത്താടികളെ ഭക്ഷിക്കാറുണ്ട്. കൃഷിയെ നശിപ്പിക്കുന്ന കീടങ്ങളെയും തുമ്പികൾ യഥേഷ്ടം പിടിച്ചുതിന്നാറുണ്ട്. ഈ പഠനത്തിലൂടെ വികസിപ്പിച്ചെടുത്ത പ്രത്യേക പോഷക പരിഹാരം (Special nutrient solution) വലിയ രീതിയിൽ തുമ്പിയെ വളർത്തിയെടുക്കാൻ (Mass rearing and culturing) ഉതകുന്നതാണ് . ഇങ്ങനെ വളർത്തിയെടുക്കുന്ന തുമ്പികളെ ജൈവരീതിയിൽ കീടങ്ങളെ ഇല്ലാതാക്കാൻ സഹിക്കുന്നതാണ്.

പല പ്രാണികളിലും മറ്റ് ആർത്രോപോഡുകളിലും കാണപ്പെടുന്ന ഒരു എലാസ്റ്റോമെറിക് പ്രോട്ടീനാണ് റെസിലിൻ. ഇത് യാന്ത്രികമായി സജീവമായ അവയവങ്ങൾക്കും ടിഷ്യൂകൾക്കും മൃദു റബ്ബർ-ഇലാസ്റ്റിറ്റി നൽകുന്നു; ഉദാഹരണത്തിന്, പല ജീവിവർഗങ്ങളിലുമുള്ള പ്രാണികളെ അവയുടെ ചിറകുകൾ കാര്യക്ഷമമായി ചാടാനോ പിവറ്റ് ചെയ്യാനോ ഇത് പ്രാപ്തമാക്കുന്നു. ചിറകിൻ്റെ മൂലകങ്ങളുടെ രൂപഭേദം വരുത്തുന്നതിൽ നിന്ന് വീണ്ടെടുക്കുന്നതിനും ചിറകിന് അനുഭവപ്പെടുന്ന വായു ചലനാത്മക ശക്തികളെ തളർത്തുന്നതിനും റെസിലിൻ പ്രധാനപങ്കുവഹിക്കുന്നുണ്ട്. റെസിലിൻ ഒരു ക്രമരഹിതമായ പ്രോട്ടീൻ ആണ്; എന്നിരുന്നാലും അതിൻ്റെ സെഗ്മെൻ്റുകൾ വ്യത്യസ്ത സാഹചര്യങ്ങളിൽ ദ്വിതീയ ഘടനകൾ സ്വീകരിച്ചേക്കാം. തുമ്പികളുടെ ചിറകുകളിൽ ഉള്ള റെസിലിനെ കുറിച്ചുള്ള ഗവേഷങ്ങൾ വളരെ വിരളമാണ്. തുമ്പികളിൽ, രണ്ടു സ്പീഷീസ് നിന്നുള്ള റെസിലിൻ പ്രോട്ടീൻ മാത്രമാണ് നിലവിൽ ലഭ്യമാവുന്നത്. പന്താലാ ഫ്ളേവ്സെന്സ് റെസിലിൻ പ്രോട്ടീൻ ഇതുവരെ ഒരു പഠനവും നടന്നിട്ടില്ല. ഈ പഠനത്തിലൂടെയാണ് ആദ്യമായി റെസിലിൻ പ്രോട്ടീൻ വേർതിരിച്ചെടുക്കുന്നതും അതിൻറെ ഘടനയെകുറിച്ചും വിശകലനം ചെയ്യുന്നത്. റെസിലിന്റെ ശ്രദ്ധേയമായ റബ്ബർ ഇലാസ്തികത കാരണം, വൈവിധ്യമാർന്ന മെറ്റീരിയൽ, മെഡിക്കൽ ആപ്ലിക്കേഷനുകൾക്കായി പുനഃസംയോജന പതിപ്പുകൾ പര്യവേക്ഷണം ചെയ്യാൻ കഴിയുന്നതാണ്. ഓട്ടോഫ്ലൂറസെൻസ് കാരണം റെസിലിന് ഒരു പ്രോട്ടീൻ മാർക്കറായി ഉപയോഗിക്കാവുന്നതാണ്. ഈ പഠനത്തിലൂടെ റെസിലിന് പ്രോട്ടീൻ അടിസ്ഥാന ഗുണങ്ങൾ മാത്രമാണ് വിശകലനം ചെയ്യുന്നത്. കൂടുതൽ ഗവേഷണത്തിലൂടെമാത്രമാണ് ഇവയുടെ ബയോമെഡിക്കൽ എഞ്ചിനീയറിംഗ്, മെഡിസിൻ എന്നീ മേഖലകളിൽ ഉപയോഗത്തെക്കുറിച്ചു മനസിലാക്കാൻ കഴിയുകയുള്ളു .

GENERAL INTRODUCTION

Odonata is one of the ancient groups of insects, and this order appeared about 250 million years ago during the Carboniferous era (Subramanian, 2005). The insect Order Odonata comprises three suborders: the Zygoptera (damselflies), the Anisoptera (dragonflies), and the Anisozygoptera. Over 6300 Odonate species have been identified worldwide, 493 in India, 196 in the Western Ghats, and 175 in Kerala (Jose & Chandran, 2020). Among these, the damselflies are very thin-bodied insects with very weak flying ability, whereas the dragonflies are active fliers with robust body types. These are hemimetabolous insects with three life stages: egg, naiads, and adult stage. The naiads of Odonata are aquatic, and their adult forms are terrestrial. These adult Odonates are mainly seen near the water bodies. Most of the Odonates show sexual dimorphism when they attain maturation, but the newly emerged male and female dragonflies will look similar.

An adult dragonfly's body is divided into a head, thorax, and abdomen. The head region of Odonates is mostly covered with compound eyes, which gives them 360° vision, and helps them capture prey. Their antenna is tiny, with about 3 to 7 antennal segments. As these Odonates are predatory insects, they exhibit biting mouthparts. The dragonfly thorax consists of three segments: prothorax, mesothorax, and metathorax. The meso-and meta thorax of these insects fused to form the pterothorax. The three pairs of legs and two pairs of wings are attached to the thoracic region of the dragonflies. The legs of Odonates help them catch and hold the prey. The abdomen of the dragonflies is long and cylindrical with ten abdominal segments, and the tenth abdominal segment bears the anal appendages.

The male dragonflies' second and third abdominal segments are modified to bear the secondary genitalia.

The naiads and adult forms of dragonflies and damselflies are carnivorous. Birds, fishes, lizards, and frogs are some of the primary predators of these insects. Economically, these Odonates play many significant roles. These dragonflies are major predators of many noxious pests and vectors (mosquitoes, blackflies, etc). Also, these Odonates are very sensitive to pollution, so they are good bioindicators of water quality, eg., *Brachythemis contaminata* (Libellulidae), which is mainly seen near polluted water bodies. Dragonflies also play a significant role in the wetland ecosystem. Any threats to the aquatic ecosystem like pollution, eutrophication, overexploitation, degradation of the habitats, exotic species invasion, etc., will directly affect the life of Odonates. The long-term conservation of these Odonates can be attained through appropriate conservation programmes of the freshwater ecosystem.

The Odonate wings are uncoupled. Their forewing and hindwings are not attached so they can beat their wings independently. The insect wing morphology plays a crucial role in its flight performance. The cuticular membranes and the veins form the insect wings. In dragonflies and damselflies, the flight performance of the wing is critical for their predatory behaviour, long-distance migration, predator avoidance, and courtship behaviour. The flexural rigidity and the elastic deformation of the dragonfly’s wing are determined by the size and arrangements of the wing veins (Combes & Daniel, 2003; Meresman & Ribak, 2017; Wehmann et al., 2019).

Studying their wing morphology, venation patterns, and evolutionary relationships will help to understand how this wing differs between short and long-distance dispersal and between the migratory and non-migratory species of dragonflies. The evolution of several traits and many structural modifications will occur in the migratory species (Dingle, 1996), and it is essential to conduct evolutionary studies on migration.

The insect gut microbiome plays a significant role in their health and fitness, its phenotype, innate immunities, sexual performance, oviposition, etc. (Gavriel et

al., 2010; Sharon et al., 2010; Mueller & Sachs, 2015; Lynch & Hsiao, 2019). Studying the gut content of the dragonflies will give an idea about their potential as a predator and also help us understand if there are any differences between migratory and non-migratory dragonflies. A comparative study of the gut content of migratory and non-migratory species will give some details about this. We conducted a detailed study on this by comparing the gut-associated bacterial communities in *Pantala flavescens* (migratory) and *Neutothemis tullia* (non-migratory). The molecular and morphological phylogenetic analysis of dragonflies showed that these two species share the same clade so we selected these dragonflies for further studies. The *P. flavescens* (Libellulidae), the wandering glider or globe skimmer, is one of the longest known migratory species covering about 18,000 km and is also a good predator of some major agricultural pests and vectors like mosquitoes. It is a seasonal dragonfly species mainly seen in the paddy fields. *N. tullia* is a non-migratory small dragonfly commonly found in paddy fields and a good predator of paddy pests.

Copulation of the insect group Odonata occurs mainly during their flight by forming a wheel position, which may last from a few seconds to hours. The eggs of Odonata are divided into two groups, endophytic eggs, and exophytic eggs, based on their deposition of eggs in plants or water. Damselflies mostly exhibit the endophytic mode of oviposition, and their eggs are elongated types, but most dragonflies exhibit exophytic oviposition, and their eggs are broad and elliptical. The number of eggs the female Odonates lays varies between species, ranging from a few hundred to thousands. The egg-hatching time of these groups varies between species and takes a few days to several months.

The eggs of Odonata hatch to form the naiads with many instars. These instars of the naiads of dragonflies are not fixed, and they vary between species and even within species, ranging from 9 to 12 or 16 instars. They are bottom-living organisms, and during their early instars, they mainly feed on tiny aquatic organisms like Daphnia, protozoans, etc. However, in the later stages of the naiads, they feed on larger prey like fishes, tadpoles, mosquito larvae, etc. The dragonfly naiads show

cannibalism. That is, they even prey upon naiads of their species. The body of naiads is also divided into three as that of their adult forms: head, thorax, and abdomen. The extensible labium is the unique feature of the dragonfly naiads. Their thoracic region bears three pairs of legs and two pairs of wing sheaths. They ventilate the rectal gills by pumping water inside through the anal area. The naiad's life stage of Odonata varies from several months to years depending upon the species and environmental factors like temperature. They are good predators of many pests and vectors, especially in controlling some major agricultural pests, and these dragonflies can easily control vectors like mosquitoes. The growth and development of the naiads mainly depended upon the availability of food and the external temperature. So, by providing a suitable environment for the growth of naiads, we can easily culture them in the laboratory and release them into the field for pest and vector control.

The wings and an elastomeric protein called resilin of dragonflies had a significant role in their migratory behaviour of dragonflies. So, the studies on the resilin protein and its role in migratory species like *P. flavescens* are critical. Different parts of the wings have different roles; the wing vein joints, pterostigma, costa, and nodus are some of the parts participating in the flight of dragonflies (Marrocco et al., 2010). The resilin protein is seen in the insect cuticle, and it helps to increase flexibility, improve efficiency, reduce stress, and store elastic energy (Chapman, 1998; Mistick et al., 2016; Mountcastle & Combes, 2013; Gorb, 1999; Michels et al., 2016). This resilin protein in the dragonfly's and damselflies' wing vein joints gives flexibility to the wings. Studies on this protein, especially in a migratory species like *P. flavescens* will give a good understanding of how this resilin protein helps in the migratory behaviour of dragonflies. Studies of this resilin protein's structural, mechanical, and functional properties will also be applied to biotechnology and medicine.

We have studied the morphology and venation patterns of the wings of dragonflies and also conducted morphological and molecular phylogenetic analysis to understand the similarities and differences between the migratory and non-

migratory dragonfly species. Then we selected one migratory (*P. flavescens*) and one non-migratory (*N. tullia*) species sharing similar clades in the phylogenetic tree analysis for studying the relationships of gut-associated microorganisms, migration, and predation. Then, we selected *P. flavescens* for further studies because this species is more abundant in India during post-monsoon, September to December, and was found to be a good predator of pests and vectors. So, we standardised a new protocol for the mass rearing of *P. flavescens* in the laboratory that can be utilized in Integrated Pest Management. As a long-distance migratory species, it is very important to study how the wings influence its migratory behaviour. Thus, we conducted a detailed study on that and found the importance of wing resilin protein in its flight.

OBJECTIVES

1. Morpho-structural variability in wings of selected dragonflies with their morpho-and molecular phylogenetic relationship.

2. Comparative gut bacterial microbiome diversity in selected dragonfly species: Migrator *vs.* Non- migrator.

3. Embryonic, post-embryonic, predatory potential of the Wandering glider, *P. flavescens* (Fabricius, 1798) (Libellulidae).

4. Isolation, Sequencing, and molecular structural characterisation of wing resilin of Wandering glider, *P. flavescens* (Fabricius, 1798) (Libellulidae).

REFERENCES

Chapman, R. F. (1998). *The Insects: Structure and Function*, (4th ed). Cambridge, UK: Cambridge University Press.

Combes, S. A., & Daniel, T. L. (2003). Flexural stiffness in insect wings I. Scaling and the influence of wing venation. *Journal of Experimental Biology*. 206, 2979–2987. doi:10.1242/jeb.00523

Dingle, H. (1996). *Migration: The Biology of Life on the Move*. New York, NY: Oxford University Press.

Gavriel, S., Jurkevitch, E., Gazit, Y., & Yuval, B. (2010). Bacterially enriched diet improves sexual performance of sterile male Mediterranean fruit flies. *Journal of Applied Entomology*, 135(7), 564-573. https://doi.org/10.1111/j.1439-0418.2010.01605.x

Jose, J., & Chandran, A. V. (2020). *Introduction to Odonata with identification keys for dragonflies & damselflies commonly found in Kerala*. Society for Odonate Studies. DOI: 10.13140/RG.2.2.35429.32486

Lynch, J. B., & Hsiao, E.Y. (2019). Microbiomes as sources of emergent host phenotypes. *Science*. 365, 1405–1409. https://doi.org/10.1126/science.aay0240.

Marrocco, J., Demasi, L., & Venkataraman, S. (2010). Investigating the structural dynamics implication of flexible resilin joints on dragonfly wings. *ACSESS Proc*. 10, 9.

Meresman, Y., & Ribak, G. (2017). Allometry of wing twist and camber in a flower chafer during free flight: how do wing deformations scale with body size? *Royal Society Open Science.* 4, 171152. doi:10.1098/rsos.171152

Michels, J., Appel, E., & Gorb, S.N. (2016). Functional diversity of resilin in arthropoda. *Beilstein Journal of Nanotechnology*, 7, 1241–1259

Mistick, E. A., Mountcastle, A. M., & Combes, S. A. (2016). Wing flexibility improves bumblebee flight stability. *Journal of Experimental Biology*. 219, 3384–3390.

Mountcastle, A. M., & Combes, S. A. (2013). Wing flexibility enhances load-lifting capacity in bumblebees. *Proceedings of the Royal Society B*. 280(1759), 20130531. http://doi.org/10.1098/rspb.2013.0531

Mueller, U. G., & Sachs, J. L. (2015). Engineering microbiomes to improve plant and animal health. *Trends Microbiol*. 23(10), 606–617. DOI: 10.1016/j.tim.2015.07.009

Subramanian, K. A. (2005). *Dragonflies and damselflies of peninsular India-A field guide.* Bangalore, India: Indian academy of sciences.

Wehmann, H. N., Heepe, L., Gorb, S. N., Engels, T., & Lehmann, F. O. (2019). Local deformation and stiffness distribution in fly wings. *Biology Open,* 8(1), bio038299. doi:10.1242/bio.038299

Chapter 1

Morpho-structural variability in wings of selected dragonflies with their morpho-and molecular phylogenetic relationship

CONTENTS

LIST OF FIGURES

LIST OF TABLES

1

Morpho-structural variability in wings of selected dragonflies with their morpho-and molecular phylogenetic relationship

1.1 INTRODUCTION

The flight performance of insects is influenced by the complex interactions between their body morphology, behavior, and environment (Norberg, 1995; Berwaerts et al., 2002; Clark & Dudley, 2009; Outomuro et al., 2013). The wing morphology of insects directly influences their flight performance (Meresman et al., 2020) and strongly influences the aerodynamic performance of insects (Aiello et al., 2021). In insects, long and slender wings help in long-duration flight, whereas short and broad wings help in slow and agile flight (Betts & Wootton, 1988; DeVries et al., 2010). In addition to the size and shape differences of the wings, the flight performance of the migratory species is also affected by some modifications in the thoracic pilosity, wing microtrichia, wing venation distribution, and wing corrugation (Wakeling & Ellington, 1997; Tillyard, 1917; Dudley, 2000). These insect wings are composed of cuticular membrane and wing veins (Wootton, 1992). The size and arrangement of these wing veins determine the flexural rigidity and elastic deformation of the wings (Combes & Daniel, 2003; Meresman & Ribak, 2017; Wehmann et al., 2019). The flight of insects is important for many aspects of their life history including migration, dispersal, predator avoidance, feeding, and courtship behaviours (Aiello et al., 2021). The wing shape of insects plays an important role in their flight performance and thus studying the phylogenetic

changes in the wing shape will help in understanding the evolution of flight in insects (Outomuro et al., 2013).

Migratory behaviour of animals can be defined as the displacement of an individual from one location to another with better survival conditions (Suarez-Tovar & Sarmiento, 2016). Most of the dragonflies show short-distance dispersal from their emergence site, but some dragonflies migrate several kilometers to avoid seasonal changes like drought (Corbet, 1999; Wikelski et al., 2006). The migratory behaviour of individuals needs the evolution of several traits and these changes may lead to several structural modifications (Dingle, 1996). This makes the evolutionary studies on migration more interesting because natural selection directly reflects on various morphological traits (Suarez-Tovar & Sarmiento, 2016). Dragonflies are excellent models for conducting studies on evolutionary responses to flight because, in dragonflies, this trait evolved a long time ago and thus exhibits the diversity of flight strategies (Dudley, 2000; Dickinson, 2006). Approximately 50 of 5800 species of Odonata have been recorded as migratory species (Wikelski et al., 2006), and 70% of these Odonates belong to the family Libellulidae (Suarez-Tovar & Sarmiento, 2016). The migration of Odonate species usually occurs at night (Feng et al., 2006).

In insects, the shape of the wing exhibits high heritability and thus the wing morphology especially the wing venation of insects has been widely used in phylogenetic analysis studies (Moraes et al., 2004; Grimaldi & Engel, 2005; Nel et al., 2012) because the insect wing veins and the intersections of the veins are homologous (Ross, 1936). The use of insect wing venation for the traditional classification of insects was first introduced by Comstock (1893). It is one of the major characteristics used in the identification and classification of insects (Wheeler et al., 2001; Trautwein et al., 2012).

Before the arrival of DNA sequencing, inferring the phylogenetic relationships among animals was one of the most challenging problems in systematic biology (Field et al., 1988). Morphology-based phylogenesis was most common at that time and later molecular phylogenetics became the standard for

phylogenetic relationship studies (Ziemert & Jensen, 2012; Zhao et al., 2023). Although molecular-based phylogenetic analysis has many advantages over morphology-based phylogenesis, we cannot completely replace or neglect them from the study of phylogenesis (Zhao et al., 2023). The shape and its variations among organisms are important in the studies of evolution and interactions between genotype, phenotype, and environmental spaces (Monteiro et al., 2002) and this shape is also a part of phylogenetic and cladistic studies (Pretorius, 2005).

In recent decades, geometric morphometrics has become an efficient analysis tool for the evaluation of morphological variations in insects (Tatsuta et al., 2018; Santos et al., 2019). Geometric morphometrics was developed in the 1980s by Fred Bookstein, James Rolf, Ian Dryden, and others (Mitterocker, 2021). It is a valid tool that can be used in wing shape analysis and can also be applied to the evolutionary and ecological Odonate research (Cordoba-Aguilar, 2008).

Geometric morphometrics is a promising alternative technique for species identification using landmarks (Bookstein, 1982). This landmark collection is a cost-effective technique and it requires only little entomological experience compared to the standard morphological identification (Sauer et al., 2020). For the analysis of shape and size differences of insect morphological features like wings, genitals, mandibles, and for other structures we can use landmark-based geometric morphometrics as it utilizes powerful and comprehensive statistical procedures (Adam et al., 2004), while the traditional morphometric methods were mainly based on the measurement-based techniques (Rohlf & Marcus, 1993) and thus it provides poor information about the shape. Insect wings have been widely used in the past few years for geometric morphometric studies (Rohlf & Slice, 1990). Different tps series of programs that are used in the geometric morphometric analysis for statistic studies has been developed by Rohlf and he provides an overview of this technique and its use in phylogenetic studies (Rohlf, 1993; 2001; 2002)

In the geometric morphometric analysis, the shapes are expressed as geometric coordinates and are subjected to mathematical and statistical techniques (Zelditch et al., 2004) and this method allows the visualization of shapes

independent of size (Rohlf & Marcus, 1993; Adams et al., 2004). An advancement in quantitative biological shape analysis has happened after the revolution of geometric morphometrics in this field (Mitteroecker & Gunz, 2009; Lawing & Polly, 2010). The geometric morphometric analysis has been successfully used in many systematics and evolutionary biology studies (Klingenberg & Zaklan, 2000; Wappler et al., 2012; Outomuro & Johansson, 2015).

This chapter deals with the study of dragonfly wing morphology, wing venation, geometric morphometric analysis of the wings, and morpho- and molecular phylogenetic analysis of dragonflies. We conducted a detailed study on the wing venation patterns of some Anisopteran dragonflies and compared the venation patterns of migratory species with the non-migratory species. We used a Geometric morphometrics tool to study the wing-based morpho-phylogenetic relationship among the dragonflies.

1.2 REVIEW OF LITERATURE

Many previous studies have been conducted on the wings of dragonflies. The size and shape of the dragonfly wings play an important role in its flight performance and thus studies on the wings of dragonflies are an interesting area of research for many researchers. Geometric morphometric methods have been used by Kiyoshi and Hikida (2012) to study the morphological variations among the golden-ringed dragonfly *Anotogaster sieboldii* by comparing its hindwing shape. Romero-Lebron et al. (2020) used a geometric morphometrics tool for the interpretation of the egg-laying behavior of endophytic Odonates, and this method helped them to make inferences about the oviposition behavior of an Odonate that lived around 52 million years ago. Villalobos-Jimenez and Hassall (2019) compared the *Ishnura elegans* wing shape among different land use types with the help of geometric morphometrics. Sadeghi et al. (2009) studied the wing shape variations in the damselfly *Calopteryx splendens*. Cabuga et al. (2017) studied sexual dimorphism by using geometric morphometric analysis in the wings of *Neurothemis terminata* and their results showed significant differences between the female and male populations. Tuzun et al. (2017) studied the effect of urbanization on the damselflies

by conducting a comparative study between the damselflies in the urban and rural areas. They used geometric morphometrics for the comparative study and their study showed an increase in the flight performance of the urban damselflies. Bots et al. (2012) studied the influence of wing shape on territorial contests in the damselfly *Calopteryx virgo*. For this study, they have used geometrics morphometrics to compare the wing shape between winner and loser damselflies. Kiyoshi and Hikida (2012) studied the morphological variations in the wing shape of *Anotogaster sieboldii* by using geometric morphometric methods and by using molecular phylogenetics. The wing size and shape variations in the damselfly *Argia sedula* due to environmental factors have been studied by Stewart and Vodopich (2018) and their study revealed that seasonal and environmental variations will influence the wing shape and size in insects. Hassall et al. (2007) studied the wing shape variations in the damselfly *Coenagrion puella* using geometric morphometrics and showed that the wing shape varies between different range margins. Gallesi et al. (2015) conducted a comparative study on the wing shape between andromorph females of *Calopteryx splendens* with their male population using geometric morphometrics.

Outomuro et al. (2013) used geometric morphometrics and phylogenetic comparative approaches to study the evolution of wing shape in calopterygid damselflies and they also studied the wing size and shape relationship in 37 taxa of calopterygid damselflies. Zikie et al. (2017) studied the evolutionary relationships of wing venation and wing size and wing shape in the parasitic wasp Aphidiinae by using geometric morphometrics and phylogenetic comparative methods. GMM was used by Lopez-Aguirre et al. (2020) to study the phylogenetic, ecological, and biological variations in the humeral morphology of bats. Perrard et al. (2016) used the wing shape data of social wasps, hornets, and yellow jackets for the phylogenetic analysis by using landmarks. Zhang et al. (2019) used geometric morphometrics to study the morphological diversity and evolution of stag beetles. Pretorius and Scholtz (2001) studied the evolution of Scarabaeoidea by using geometric morphometric analysis. Zhao et al. (2023) investigated the phylogeny of the cantharid beetles by applying geometric morphometrics in the hindwings. Fang et al. (2024) investigated the interspecific relationship of *Lyponia* s. str. using geometric

morphometrics and phylogenetic morphometric methods and their studies were based on the shape of male genitalia. Santos et al. (2019) evaluated the phylogenetic morphological variations among the *Plebeia* species by using geometric morphometrics on the wings of stingless bee species.

Many previous studies have shown that molecular data based interspecific relationships and morphology based interspecific relationships are consistent with each other if the morphological characteristics are chosen correctly (Grzywacz et al., 2017; Noguerales et al., 2018). Huang et al. (2020) compared the morphology and molecular based phylogenesis using dragonfly wing morphology and their study showed that there is some interspecific phylogenetic information in the wing shape of dragonflies. The study conducted by Marin et al. (2017) on Euptychiina butterflies showed that morphology based phylogenesis and molecular based phylogenesis are comparable. Bocek et al. (2017) conducted a detailed comparative study on the molecular and morphology based phylogenesis of trichaline net-winged beetles. Marinov et al. (2016) assessed the morphological and molecular variations of the damselfly *Xanthocnemis sobrina*, for the morphological examination they used landmark-based geometric morphometrics, and for molecular analysis they targeted the 28S and 16S rRNA genes.

Aiello et al. (2021) studied how the evolution of aerodynamically important traits of bombycoid moths, is linked to clade divergence by using landmark-based morphometrics. GM was used by Champakaew et al. (2021) to discriminate between mosquito species and they constructed the phenetic relationship to illustrate the discrimination pattern of different genera and species of mosquitos.

The Odonate evolutionary history and the relationships among them were first published in the twentieth century (Fraser, 1954; Munz, 1919). The molecular phylogenetic studies on the suborders Anisoptera and Zygoptera have been conducted by many scientists (Dijkstra et al., 2014; Carle et al., 2015; Letsch et al., 2016). Johansson et al. (2009) studied the evolution of the wing shape in Anisopteran dragonflies and their study showed that migration and mate guarding behaviour of the dragonflies affects the shape of their wings.

1.3 MATERIALS AND METHODS

1.3.1 Data collection

The dragonflies were collected from the randomly selected regions of Palakkad district, Kerala using a sweep net. The collected specimens were used for morphological identification by using various taxonomic keys and with the help of taxonomists. The comparative taxonomic documentation of wing venation of selected dragonfly species was done according to Fraser 1936.

1.3.2 Image acquisition

Forewings and hindwings of the collected dragonfly species were dissected, appropriately mounted in a clean, dry slide, and photographed using Canon EOS 7D digital camera macro-lense, 180 mm, Japan (F-stop: f/ 22, Focal length 180 mm, ISO-1000 and Expo. time 1/25). Damaged and abnormal wings were excluded from our analyses.

GMM methods allow one to describe the shape of rigid structures using a set of variables that can be used for statistical hypothesis testing, and to generate a graphical representation of shape differences as variability/deformations. However, when the landmarks (set of variables) chosen for an analysis span multiple rigid structures that articulate, variation describing the position of landmarks on one structure relative to those on another is also present in the data.

1.3.3 Selection and digitization of landmarks

For geometric morphometric analysis, we selected 26 landmarks (Fig. 1.1) from the forewing (Table 1.1), and 31 from the hindwings (Table 1.2) (N=30). To avoid an error in the landmarking procedure, a sample of individuals was photographed and landmarked twice. Images are initially converted to mathematical coordinates using tpsUtil V 1.68. Landmarking was done by tpsDig v2.26 software.

Table 1.1: Description of landmarks used in the forewings

Landmark	Anatomical description	Abbreviation
1	Proximal end of the Costa	C
2	Proximal end of the Subcosta	Sc1
3	Proximal end of the Radius + media	R + M
4	Proximal end of the Cubitus	Cu
5	Proximal end of the 1st anal vein	A/IA
6	Basal end of the Arculus	Arc
7	Proximal end of the anterior margin of the triangle	T1
8	Distal end of the anterior margin of the triangle	T2
9	Posterior end of the triangle	T3
10	Origin of Radial branches	R2 and R4
11	Origin of intercalary vein	IR3
12	Nodus	N
13	Distal end of the Subcosta	Sc2
14	Distal end of the Radius	R
15	Origin of the Radial branches	R2 and R3
16	Anterior end of the 2nd crossvein between Radial branches	R2 and IR3a
17	Posterior end of the 1nd crossvein between Radial branches	R2 and IR3b
18	Posterior end of the 2nd crossvein between Radial branches	R2 and IR3c
19	Distal end of anterior media	MV
20	Distal end of	R4
21	Distal end of the intercalary radial vein	IR2
22	Distal end of Radial branch	R2
23	Antero-lateral and distal end of the pterostigma	P1
24	Postero-lateral and distal end of the pterostigma	P2
25	Antero-lateral and proximal end of the pterostigma	P3
26	Postero-lateral and proximal end of the pterostigma	P4

Table 1.2: Description of landmarks used in the hindwings

Landmark	Anatomical description	Abbreviation
1	Proximal end of the Costa	C
2	Proximal end of the Radius + media	R+M
3	Proximal end of the media	M
4	Proximal end of the Cubitus	Cu
5	Posterior end of the anal crossing	Ac
6	Basal end of the Arculus	Arc
7	Posterior and proximal vertex of the hypertrigone	ht1
8	Anterior and proximal vertex of the hypertrigone	ht2
9	Posterior and proximal vertex of the subtrigone	t1
10	Distal vertex of the subtrigone	t2
11	Second branch of cubital vein	Cu2a
12	Distal end of the cubito-anal vein	Cu2b
13	Distal end of the posterior cubital vein	Cu1
14	Origin of Radial branch	R4
15	Origin of the intercalary radial vein	IR3
16	Nodus	N
17	Distal end of the subcosta	Sc
18	Distal end of the radius	R
19	Origin of the Radial branches	R2 and R3 a
20	Anterior end of the 2nd cross-vein between Radial branches	R2 and R3 b
21	Posterior end of the 2nd cross-vein between Radial branches (R2 and R3); origin of Radial supplement	Rspl
22	Distal end of the Anterior media	AM
23	Distal end of Radial branch	R4
24	Distal end of the Intercalary Radial vein	IR3
25	Distal end of Radial branch	R3
26	Distal end of intercalary radial vein	IR2
27	Distal end of Radial branch	R2
28	Antero-lateral and distal end of the pterostigma	P1
29	Postero-lateral and distal end of the pterostigma	P2
30	Antero-lateral and proximal end of the pterostigma	P3
31	Postero-lateral and proximal end of the pterostigma	P4

1.3.4 Data analysis

All GMM analysis was conducted in MorphoJ. Morpho-space boundary analysis was done using different statistical tools like Principal Component Analysis (PCA), Discriminant Function Analysis (DFA), Canonical Variate Analysis (CVA), and Partial Least Square (PLS). One way Procrustes ANOVA was performed to estimate the landmarking error in the datasets.

1.3.5 Phylogenetic signal analysis

In GM, phylogenetic signals were used to see if the size and shape of the taxa's morphological structures evolved due to shared evolutionary history or environmental factors. The Mesquite v3.61 modular system was used to reconstruct ancestral states. 10000 permutational analysis was performed to estimate the statistical significance. The phylogeny analysis has no phylogenetic signal ($p>0.05$), indicating that ecology has acted as one of the primary selective forces in diversifying dragonflies. *vice versa*, in phylogenetic signal ($p<0.05$), presence of evolutionary constraints.

1.3.6 Molecular phylogenetic analysis

Cytochrome oxidase I (CO1) of selected dragonfly species FASTA sequences were retrieved from NCBI GenBank. Sequences were aligned in MUSCLE. Maximum-Likelihood phylogeny, Tamura-Nei model phylogenetic tree constructed in MEGA X tool. Bootstrap value 100.

1.4 RESULT

A total of 26 Anisopteran species representing four families and 21 genera were analysed in this study (Table 1.3). Of these, 4 species come under the genus *Orthetrum*, 2 from *Tramea,* and 2 from *Trithemis.*

Table 1.3: List of species collected

Sl. No	Species	Code	Family	Common name	Remarks
1	*Aethriamanta brevipennis* (Rambur, 1842)	AB	Libellulidae	Scarlet marsh hawk	Passive, short flight
2	*Acisoma panorpoides* (Rambur, 1842)	AP	Libellulidae	Trumpet tail	Very weak and short flight
3	*Brachythemis contaminata* (Fabricius, 1793)	BC	Libellulidae	Ditch jewel	Passive, short flight
4	*Bradinopyga geminata* (Rambur, 1842)	BG	Libellulidae	Granite ghost	Active, short flight
5	*Crocothemis servilia* (Drury, 1770)	CS	Libellulidae	Scarlet skimmer	Active, short flight
6	*Diplacodes trivialis* (Rambur, 1842)	DT	Libellulidae	Ground skimmer	Active, short flight
7	*Epophthalmia vittata* (Burmeister, 1839)	EV	Macromiidae	Torrent hawk	Active
8	*Gynacantha dravida* (Lieftinck, 1960)	GD	Aeshnidae	Indian duskhawker	Active, short flight
9	*Hylaeothemis apicalis* (Fraser, 1942)	HA	Libellulidae	Blue hawklet	Active
10	*Ictinogomphus rapax* (Rambur, 1842)	IR	Gomphidae	Common clubtail	Active
11	*Lathrecista asiatica* (Fabricius, 1798)	LA	Libellulidae	Asiatic blood tail	Active
12	*Neurothemis tullia* (Drury, 1773)	NT	Libellulidae	Pied paddy skimmer	Very weak and short flight
13	*Orthetrum glaucum* (Brauer, 1865)	OG	Libellulidae	Blue marsh hawk	Passive
14	*Orthetrum luzonicum* (Brauer, 1868)	OL	Libellulidae	Tri-coloured marsh hawk	Passive

15	*Orthetrum pruinosum* (Burmeister, 1839)	OP	Libellulidae	Crimson-tailed marsh hawk	Passive
16	*Orthetrum sabina* (Drury, 1770)	OS	Libellulidae	Green marsh hawk	Passive
17	*Potamarcha congener* (Rambur, 1842)	PC	Libellulidae	Yellow-tailed ashy skimmer	Active
18	*Pantala flavescens* (Fabricius, 1798)	PF	Libellulidae	Wandering glider	Active, long, migrator
19	*Palpopleura sexmaculata* (Fabricius, 1787)	PS	Libellulidae	Blue-tailed yellow skimmer	Active, short flight
20	*Rhyothemis variegata* (Linnaeus, 1763)	RV	Libellulidae	Variegated flutterer	Passive, short
21	*Trithemis aurora* (Burmeister, 1839)	TA	Libellulidae	Crimson marsh glider	Passive
22	*Tramea basilaris* (Palisot de Beauvois, 1817)	TB	Libellulidae	Keyhole glider	Active, long, migrator
23	*Trithemis festiva* (Rambur, 1842)	TF	Libellulidae	Black stream glider	Passive
24	*Tramea limbata* (Desjardins, 1832)	TL	Libellulidae	Black marsh trotter	Active
25	*Tholymis tillarga* (Fabricius, 1798)	TT	Libellulidae	Coral-tailed cloudwing	Passive, migrator
26	*Zyxomma petiolatum* (Rambur, 1842)	ZP	Libellulidae	Long-tailed duskdarter	Passive

1.4.1 Wing morphology and venation pattern

The wing morphology and venation pattern of all the species' forewings and hindwings were compared (Theischinger & Gunther, 2006). Significant differences observed in the forewings of collected species are mainly found in the veins of the triangle, hyper triangle, sub-triangle, arculus, distal antenodals, and the regions of the discoidal field. In the hindwings, the anal loop region, triangle, hypertriangle, arculus, hindwing base, and distal antinodals are some of the areas that showed variations among the species.

1. *Aethriamanta brevipennis*

a. Forewing

Forewing triangle and hypertriangle free. Subtriangle single celled. Arculus situated between the first two antenodal cross-veins, closer to the first cross-vein. Sectors of arculus fused at their origin, forming a short stalk. Distal antenodal is complete, both costal and subcostal cross-vein present. The discoidal field not widens towards the wing margin. Single row of cells between IR3 and Rspl (Fig. 1.2A).

b. Hindwing

Hindwing triangle and hypertriangle free. Basal side of the triangle at the line of arculus. Sectors of the arculus fused closer to arculus, forming short stalk separating closer to arculus. Hindwing rounded at the base. Anal loop well developed, stocking-shaped, closed at the tip. Arculus situated between the first and second antenodal cross-vein, closer to the first antenodal cross-vein. Single row of cells between IR3 and Rspl. Distal antenodal is complete, both costal and subcostal cross-veins present (Fig. 1.2B).

2. *Acisoma panorpoides*

a. Forewing

Forewing triangle and hypertriangle free. Subtriangle single celled. Arculus situated between the first two antenodal cross-veins. Sectors of arculus fused more extensive, forming a large stalk. Distal antenodal is complete, both costal and subcostal cross-vein present. The discoidal field widens towards the wing margin (Fig. 1.2A).

b. Hindwing

Hindwing triangle and hypertriangle free. Basal side of the triangle at the line of arculus. Sectors of arculus fused more extensive, forming large stalk separating closer to the first cross-vein beyond arculus. Hindwing rounded at

the base. Anal loop well developed, stocking-shaped, closed at the tip. Arculus situated between first and second antenodal cross-vein, closer to the second antenodal cross-vein. Single row of cells between IR3 and Rspl. Distal antenodal is complete, both costal and subcostal cross-veins present (Fig. 1.2B).

3. *Brachythemis contaminata*

a. Forewing

Forewing triangle crossed. hypertriangle free. Subtriangle three celled. Arculus situated between the first two antenodal cross-veins. Sectors of arculus fused more extensive, forming a large stalk. Distal antenodal is incomplete, subcostal cross-vein absent. The discoidal field widens slightly towards the wing margin. Some double cells between IR3 and Rspl (Fig. 1.3A).

b. Hindwing

Hindwing triangle and hypertriangle free. Basal side of the triangle at the line of arculus. Sectors of arculus fused more extensive, forming large stalk separating in the middle of arculus and the first cross-vein beyond arculus. Hindwing rounded at the base. Anal loop well developed, stocking-shaped, closed at the tip. Arculus situated between the first and second antenodal cross-vein, closer to the first antenodal cross-vein. Some double cells between IR3 and Rspl. Distal antenodal is complete, both costal and subcostal cross-veins present (Fig. 1.3B).

4. *Bradinopyga geminata*

a. Forewing

Forewing triangle crossed, hypertriangle free. Subtriangle four celled. Arculus situated between the first two antenodal cross-veins. Sectors of arculus fused more extensive, forming a large stalk. Distal antenodal is

incomplete, subcostal cross-vein absent. The discoidal field widens towards the wing margin (Fig. 1.3A).

b. Hindwing

Hindwing triangle and hypertriangle free. Basal side of the triangle at the line of arculus. Sectors of arculus fused more extensive, forming large stalks separating closer to the first cross-vein beyond arculus. Hindwing rounded at the base. Anal loop well developed, stocking-shaped, closed at the tip. Arculus situated between the first and second antenodal cross-vein. Some double cells between IR3 and Rspl. Distal antenodal is complete, both costal and subcostal cross-veins present (Fig. 1.3B).

5. *Crocothemis servilia*

a. Forewing

Forewing triangle crossed, hypertriangle free. Subtriangle three celled. Arculus situated between first two antenodal cross-veins, closer to second antenodal cross-vein. Sectors of arculus fused more extensive, forming a large stalk. Distal antenodal is incomplete, subcostal cross-vein absent. The discoidal field widens towards the wing margin (Fig. 1.4A).

b. Hindwing

Hindwing triangle and hypertriangle free. Basal side of the triangle at the line of arculus. Sectors of arculus fused more extensive, forming large stalk separating at the middle of arculus and the first cross-vein beyond arculus. Hindwing rounded at the base. Anal loop well developed, stocking-shaped, closed at the tip. Arculus situated between the first and second antenodal cross-vein, closer to second antenodal cross-vein. Single row of cells between IR3 and Rspl. Distal antenodal is complete, both costal and subcostal cross-veins present (Fig. 1.4B).

6. *Diplacodes trivialis*

a. Forewing

Forewing triangle crossed, hypertriangle free. Subtriangle three celled. Arculus situated between first two antenodal cross-veins. Sectors of arculus fused more extensive, forming a large stalk. Distal antenodal is incomplete, subcostal cross-vein absent. The discoidal field widens towards the wing margin. Single row of cells between IR3 and Rspl (Fig. 1.4A).

b. Hindwing

Hindwing triangle and hypertriangle free. Basal side of the triangle at the line of arculus. Sectors of arculus fused more extensive, forming large stalk separating at the middle of arculus and the first cross-vein beyond arculus. Hindwing rounded at the base. Anal loop well developed, stocking-shaped, closed at the tip. Arculus situated between the first and second antenodal cross-vein. Single row of cells between IR3 and Rspl. Distal antenodal is complete, both costal and subcostal cross-veins present (Fig. 1.4B).

7. *Epophthalmia vittata*

a. Forewing

Forewing triangle crossed, hypertriangle crossed with three cross-veins. Subtriangle poorly developed. Arculus situated between first two antenodal cross-veins. Sectors of arculus fused more extensive, forming a large stalk. Distal antenodal is complete, both costal and subcostal cross-vein present. The discoidal field widens towards the wing margin. Single row of cells between IR3 and Rspl (Fig. 1.5A).

b. Hindwing

Hindwing triangle crossed. Hypertriangle crossed with two cross-veins. Basal side of the triangle far beyond arculus, separated it by a distance equal to the length of arculus. Sectors of arculus fused more extensive, forming

large stalk separating closer to the first cross-vein beyond arculus. Anal margin of the hindwing angulated, forming anal triangle crossed with one cross-vein. Anal loop round and poorly developed with ten cells. Arculus situated between the first and second antenodal cross-vein, closer to second antenodal cross-vein. Single row of cells between IR3 and Rspl. Distal antenodal is complete, both costal and subcostal cross-veins present (Fig. 1.5B).

8. ***Gynacantha dravida***

a. Forewing

Forewing triangle is elongated along wing axis with cross-veins. Hypertriangle crossed with six cross-veins. Arculus situated between second and third antenodal cross-veins. Sectors of arculus not fused. Distal antenodal is complete, both costal and subcostal cross-vein present. The discoidal field widens towards the wing margin. IR3 Fork present with three cell rows (Fig. 1.5A).

b. Hindwing

Hindwing triangle crossed with cross-veins forming cells inside it. Hypertriangle crossed with six cross-veins. The basal side of the triangle far beyond the base of the arculus, separated by a distance larger than the length of arculus. Sectors of arculus not fused, it is separated. Hindwing rounded at the base in females, angulated in males forming an anal triangle with three cells. Anal loop rounded, poorly developed with many cells. Arculus situated between second and third antenodal cross-vein, closer to second antenodal cross-vein. Distal antenodal is complete, both costal and subcostal cross-veins present. IR3 Fork present with 3-4 cell rows (Fig. 1.5B).

9. ***Hylaeothemis apicalis***

a. Forewing

Forewing triangle free, hypertriangle crossed with one cross-vein. Subtriangle single celled. Arculus situated between second and third

antenodal cross-veins. Sectors of arculus fused more extensive, forming a large stalk. Distal antenodal is complete, both costal and subcostal cross-vein present. The discoidal field widens towards the wing margin (Fig. 1.6A).

b. Hindwing

Hindwing triangle free, hypertriangle crossed with one cross-vein. Basal side of the triangle beyond the base of arculus. Sectors of arculus fused more extensive, forming large stalk separating away from the first cross-vein beyond arculus. Hindwing rounded at the base. Anal loop rounded, poorly developed with four cells. Arculus situated between second and third antenodal cross-vein, closer to second antenodal cross-vein. Distal antenodal is complete, both costal and subcostal cross-veins present (Fig. 1.6B).

10. *Ictinogomphus rapax*

a. Forewing

Forewing triangle crossed, forming three cells. Hypertriangle crossed with two cross-veins. Subtriangle two celled. Arculus situated between first two antenodal cross-veins. Sectors of arculus not fused. Distal antenodal is complete, both costal and subcostal cross-vein present. The discoidal field widens towards the wing margin (Fig. 1.6A).

b. Hindwing

Hindwing triangle transversed by cross-veins. Hypertriangle crossed with two cross-veins. Basal side of the triangle beyond the base of arculus, which is equal to the length of arculus. Sectors of arculus not fused. Hindwing anal margin angulated, forming anal triangle with five cells. Anal loop rounded, poorly developed with five cells. Arculus situated between the first and second antenodal cross-vein. Distal antenodal is incomplete (Fig. 1.6B).

11. *Lathrecista asiatica*

a. Forewing

Forewing triangle crossed, hypertriangle free. Subtriangle three celled. Arculus situated between second and third antenodal cross-veins, very closs

to second cross-vein. Sectors of arculus fused more extensive, forming a large stalk. Distal antenodal is incomplete. The discoidal field slightly widens towards the wing margin. Single row of cells between IR3 and Rspl (Fig. 1.7A).

b. Hindwing

Hindwing triangle and hypertriangle free. Basal side of the triangle is beyond the base of arculus, very closer to the arculus base. Sectors of arculus fused more extensive, forming large stalk separating closer to the first cross-vein beyond arculus. Hindwing rounded at the base. Anal loop well developed, stocking-shaped, closed at the tip. Arculus situated between the second and third antenodal cross-vein. Single row of cells between IR3 and Rspl. Distal antenodal is complete, both costal and subcostal cross-veins present (Fig. 1.7B).

12. ***Neurothemis tullia***

a. Forewing

Forewing triangle crossed, hypertriangle crossed with two cross-veins. Subtriangle four celled. Arculus situated between first two antenodal cross-veins. Sectors of arculus fused more extensive, forming a large stalk. Distal antenodal is incomplete. The discoidal field not widens towards the wing margin (Fig. 1.7A).

b. Hindwing

Hindwing triangle and hypertriangle crossed with one cross-vein. Basal side of the triangle at the line of arculus. Sectors of arculus fused more extensive, forming large stalk separating closer to the first cross-vein beyond arculus. Hindwing rounded at the base. Anal loop well developed, stocking-shaped, closed at the tip. Arculus situated between the first and second antenodal cross-vein. Distal antenodal is complete, both costal and subcostal cross-veins present (Fig. 1.7B).

13. *Orthetrum glaucum*

a. Forewing

Forewing triangle and hypertriangle crossed with single cross-veins. Subtriangle three celled. Arculus situated between second and third antenodal cross-veins, closer to second cross-vein. Sectors of arculus fused more extensive, forming a large stalk. Distal antenodal is complete, both costal and subcostal cross-vein present. The discoidal field widens towards the wing margin. Single row of cells between IR3 and Rspl with some double cells in between (Fig. 1.8A).

b. Hindwing

Hindwing triangle and hypertriangle free. Basal side of the triangle at the line of arculus. Sectors of arculus fused more extensive, forming large stalk separating closer to the first cross-vein beyond arculus. Hindwing rounded at the base. Anal loop well developed, stocking-shaped, closed at the tip. Arculus situated between second and third antenodal cross-vein, closer to second antenodal cross-vein. Single row of cells between IR3 and Rspl with some double cells. Distal antenodal is complete, both costal and subcostal cross-veins present (Fig. 1.8B).

14. *Orthetrum luzonicum*

a. Forewing

Forewing triangle and hypertriangle crossed with one cross-vein. Subtriangle three celled. Arculus situated at the base of second antenodal cross-veins. Sectors of arculus fused more extensive, forming a large stalk. Distal antenodal is complete, both costal and subcostal cross-vein present. The discoidal field widens towards the wing margin. One row of cells with some double row of cells between IR3 and Rspl (Fig. 1.8A).

b. Hindwing

Hindwing triangle and hypertriangle free. Basal side of the triangle at the line of arculus. Sectors of arculus fused more extensive, forming large stalk

separating at the middle of arculus and the first cross-vein beyond arculus. Hindwing rounded at the base. Anal loop well developed, stocking-shaped, closed at the tip. Arculus situated between at or very close to second antenodal cross-vein. Single row of cells between IR3 and Rspl with some double cells in between. Distal antenodal is complete, both costal and subcostal cross-veins present (Fig. 1.8B).

15. *Orthetrum pruinosum*

a. Forewing

Forewing triangle and hypertriangle crossed with single cross-vein. Subtriangle three celled. Arculus situated at the base of second antenodal cross-veins. Sectors of arculus fused more extensive, forming a large stalk. Distal antenodal is complete, both costal and subcostal cross-veins present. The discoidal field widens towards the wing margin (Fig. 1.9A).

b. Hindwing

Hindwing triangle transversed with one cross-vein, hypertriangle free. Basal side of the triangle at the line of arculus. Sectors of arculus fused more extensive, forming large stalk separating closer to the first cross-vein beyond arculus. Hindwing rounded at the base. Anal loop well developed, stocking-shaped, closed at the tip. Arculus situated between second and third antenodal cross-vein, closer to second antenodal cross-vein. Single row of cells between IR3 and Rspl with some double cells. Distal antenodal is complete, both costal and subcostal cross-veins present (Fig. 1.9B).

16. *Orthetrum sabina*

a. Forewing

Forewing triangle and hypertriangle crossed with one cross-vein. Subtriangle three celled. Arculus situated at the base of second antenodal cross-veins. Sectors of arculus fused more extensive, forming a large stalk. Distal antenodal is complete, both costal and subcostal cross-vein present. The

discoidal field widens towards the wing margin. Single and some double cells in between IR3 and Rspl (Fig. 1.9A).

b. Hindwing

Hindwing triangle and hypertriangle free. Basal side of the triangle at the line of arculus. Sectors of arculus fused more extensive, forming large stalk separating closer to the first cross-vein beyond arculus. Hindwing rounded at the base. Anal loop well developed, stocking-shaped, closed at the tip. Arculus situated at or very close to the base of second antenodal cross-vein. Single row of cells between IR3 and Rspl with some double cells. Distal antenodal is complete, both costal and subcostal cross-veins present (Fig. 1.9B).

17. *Potamarcha congener*

a. Forewing

Forewing triangle crossed, hypertriangle free. Subtriangle three celled. Arculus situated at or very close to second antenodal cross-vein. Sectors of arculus fused more extensive, forming a large stalk. Distal antenodal is incomplete. The discoidal field slightly widens towards the wing margin. Single cell row between IR3 and Rspl with some double cells (Fig. 1.10A).

b. Hindwing

Hindwing triangle crossed with single cross-vein, hypertriangle free. Basal side of the triangle at the line of arculus. Sectors of arculus fused more extensive, forming large stalk separating closer to the first cross-vein beyond arculus. Hindwing rounded at the base. Anal loop well developed, stocking-shaped, closed at the tip. Arculus situated between at the base of second antenodal cross-vein. Single row of cells between IR3 and Rspl with few double cells. Distal antenodal is complete, both costal and subcostal cross-veins present (Fig. 1.10B).

18. *Pantala flavescens*

a. Forewing

Forewing triangle crossed, hypertriangle free. Subtriangle with many cells. Arculus situated between first two antenodal cross-veins. Sectors of arculus fused more extensive, forming a large stalk. Distal antenodal is incomplete. The discoidal field reduces towards the wing margin. Single row of cells between IR3 and Rspl with some double cells (Fig. 1.10A).

b. Hindwing

Hindwing triangle and hypertriangle free. Basal side of the triangle at the line of arculus. Sectors of arculus fused more extensive, forming large stalk separating at the middle of arculus and the first cross-vein beyond arculus. Hindwing rounded at the base. Anal loop well developed, stocking-shaped, closed at the tip. Arculus situated between the first and second antenodal cross-vein, closer to first antenodal cross-vein. Single row of cells between IR3 and Rspl with some double cells. Distal antenodal is complete, both costal and subcostal cross-veins present (Fig. 1.10B).

19. *Palpopleura sexmaculata*

a. Forewing

Forewing triangle and hypertriangle crossed. Subtriangle three celled. Arculus situated between first two antenodal cross-veins. Sectors of arculus fused at the base of arculus forming short stalk. Distal antenodal is incomplete. The discoidal field widens towards the wing margin. Single row of cells between IR3 and Rspl (Fig. 1.11A).

b. Hindwing

Hindwing triangle crossed with single cross-vein, hypertriangle free. Basal side of the triangle at the line of arculus. Sectors of arculus fused close to the arculus, forming small stalk separating closer to arculus. Hindwing rounded

at the base. Anal loop well developed, stocking-shaped, closed at the tip. Arculus situated between the first and second antenodal cross-vein. Single row of cells between IR3 and Rspl. Distal antenodal is complete, both costal and subcostal cross-veins present (Fig. 1.11B).

20. *Rhyothemis variegata*

a. Forewing

Forewing triangle and hypertriangle crossed. Subtriangle many celled. Arculus situated between first two antenodal cross-veins, closer to first antenodal cross-vein. Sectors of arculus fused at their origin. Distal antenodal is incomplete. The discoidal field not widens towards the wing margin. Sigle row of cells between IR3 and Rspl with some double cells (Fig. 1.11A).

b. Hindwing

Hindwing triangle and hypertriangle free. Basal side of the triangle at the line of arculus. Sectors of arculus fused more extensive, forming large stalk separating closer to the first cross-vein beyond arculus. Hindwing rounded at the base. Anal loop well developed, stocking-shaped, closed at the tip. Arculus situated between the first and second antenodal cross-vein, closer to first antenodal cross-vein. Single row of cells between IR3 and Rspl with some double cells. Distal antenodal is complete, both costal and subcostal cross-veins present (Fig. 1.11B).

21. *Trithemis aurora*

a. Forewing

Forewing triangle crossed, hypertriangle free. Subtriangle three celled. Arculus situated between first two antenodal cross-veins. Sectors of arculus fused more extensive, forming a large stalk. Distal antenodal is incomplete. The discoidal field not widens towards the wing margin. Single row of cells between IR3 and Rspl with some double cells (Fig. 1.12A).

b. Hindwing

Hindwing triangle and hypertriangle free. Basal side of the triangle at the line of arculus. Sectors of arculus fused more extensive, forming large stalk separating closer to the first cross-vein beyond arculus. Hindwing rounded at the base. Anal loop well developed, stocking-shaped, closed at the tip. Arculus situated between the first and second antenodal cross-vein, closer to second antenodal cross-vein. Single row of cells between IR3 and Rspl with some double cells. Distal antenodal is complete, both costal and subcostal cross-veins present (Fig. 1.12B).

22. *Tramea basilaris*

a. Forewing

Forewing triangle and hypertriangle free. Subtriangle three celled. Arculus situated between first two antenodal cross-veins. Sectors of arculus fused at their origin, forming a short stalk. Distal antenodal is complete, both costal and subcostal cross-vein present. The discoidal field slightly widens towards the wing margin. Single row of cells between IR3 and Rspl (Fig. 1.12A).

b. Hindwing

Hindwing triangle and hypertriangle free. Basal side of the triangle at the line of arculus. Sectors of arculus fused at the base of arculus, forming short stalk separating closer to arculus. Hindwing rounded at the base. Anal loop well developed, stocking-shaped, closed at the tip. Arculus situated between the first and second antenodal cross-vein, closer to the first antenodal cross-vein. Single row of cells between IR3 and Rspl. Distal antenodal is complete, both costal and subcostal cross-veins present (Fig. 1.12B).

23. *Trithemis festiva*

a. Forewing

Forewing triangle crossed, hypertriangle free. Subtriangle three celled. Arculus situated between first two antenodal cross-veins. Sectors of arculus

fused more extensive, forming a large stalk. Distal antenodal is incomplete. The discoidal field not widens towards the wing margin. Single row of cells between IR3 and Rspl with some double cells (Fig. 1.13A).

b. Hindwing

Hindwing triangle and hypertriangle free. Basal side of the triangle at the line of arculus. Sectors of arculus fused more extensive, forming large stalk separating closer to the first cross-vein beyond arculus. Hindwing rounded at the base. Anal loop well developed, stocking-shaped, closed at the tip. Arculus situated between the first and second antenodal cross-vein. Single row of cells between IR3 and Rspl with some double cells. Distal antenodal is complete, both costal and subcostal cross-veins present (Fig. 1.13B).

24. *Tramea limbata*

a. Forewing

Forewing triangle crossed with two cross-vein, hypertriangle free. Subtriangle not well defined. Arculus situated between first two antenodal cross-veins. Sectors of arculus fused closer to arculus, forming a short stalk. Distal antenodal is incomplete. The discoidal field widens towards the wing margin. Single row of cells between IR3 and Rspl with some double cells (Fig. 1.13A).

b. Hindwing

Hindwing triangle and hypertriangle free. Basal side of the triangle at the line of arculus. Sectors of arculus fused, with short stalk separating closer to arculus. Hindwing rounded at the base. Anal loop well developed, stocking-shaped, closed at the tip. Arculus situated between the first and second antenodal cross-vein, closer to the first antenodal cross-vein. Single row of cells between IR3 and Rspl with some double cells. Distal antenodal is complete, both costal and subcostal cross-veins present (Fig. 1.13B).

25. *Tholymis tillarga*

a. Forewing

Forewing triangle crossed, hypertriangle free. Subtriangle three celled. Arculus situated between first two antenodal cross-veins. Sectors of arculus fused more extensive, forming a large stalk. Distal antenodal is incomplete. The discoidal field reduces towards the wing margin. Single row of cells between IR3 and Rspl with some double cells (Fig. 1.14A).

b. Hindwing

Hindwing triangle and hypertriangle free. Basal side of the triangle at the line of arculus. Sectors of arculus fused more extensive, forming large stalk separating at the middle of arculus and the first cross-vein beyond arculus. Hindwing rounded at the base. Anal loop well developed, stocking-shaped, closed at the tip. Arculus situated between the first and second antenodal cross-vein. Single row of cells between IR3 and Rspl with some double cells. Distal antenodal is complete, both costal and subcostal cross-veins present (Fig. 1.14B).

26. *Zyxomma petiolatum*

a. Forewing

Forewing triangle crossed, hypertriangle free. Subtriangle three celled. Arculus situated between first two antenodal cross-veins. Sectors of arculus fused at their origin, forming a short stalk. Distal antenodal is incomplete. The discoidal field not widens towards the wing margin. Single row of cells between IR3 and Rspl (Fig. 1.14A).

b. Hindwing

Hindwing triangle and hypertriangle free. Basal side of the triangle at the line of arculus. Sectors of arculus fused more extensive, forming large stalk separating closer to arculus. Hindwing rounded at the base. Anal loop open on one side of midvein. Arculus situated between the first and second antenodal cross-vein, closer to second antenodal cross-vein. Single row of

cells between IR3 and Rspl. Distal antenodal is complete, both costal and subcostal cross-veins present (Fig. 1.14B).

1.4.2 Geometric Morphometric Analysis of forewings

The morphometric analysis of the wings of 26 Anisopteran dragonfly species was performed in this study. Three of these 26 species were migratory, *P. flavescens*, *T. tillarga,* and *T. basilaris*.

1.4.2.1 Centroid size analysis

The centroid size analysis demonstrated the presence of variations in the wing size among the Anisopteran species (Fig. 1.15). The wing centroid sizes of 26 Anisopteran species were compared, *E. vittata* (83.41 ± 0.03) had the largest forewing, and then *G. dravida* (80.39 ± 2.13). *T. limbata* (71.69 ± 1.7), and *P. flavescens* (68.92 ± 1.44) are the other species with larger forewings after *E. vittata,* and *G. dravida. A. panorpoides* (32.85 ± 0.55) and *P. sexmaculata* (32.9 ± 1.86) are the species with the smallest forewing size. *O. pruinosum* (60.13 ± 0.26), and *O. sabina* (60.01 ± 1.04) had similar forewing sizes. *P. congener* (58.79 ± 1.5), *B. geminata* (58 ± 1.01) and *R. variegata* (58.97 ± 2.84) also had identical forewing size.

1.4.2.2 GPA and % Variance analysis

48 PCs explained the 100% variance among the forewings of 26 Anisopteran species. The first three PCs covered about 74.76 % variation (PC1 explained 38.12 % variation, PC2 covered 22.12 % variation, and PC3 explained 14.52 %) (Fig. 1.16). The forewings triangle region, apical area, pterostigmal region, and cubital region showed more variations in the GPA analysis (Fig. 1.16).

1.4.2.3 Morphospace boundary analysis

PCA and CVA methods validated the distribution of the forewings morphospace. A total of 48 PCs were present in the forewing analysis. In the PCs-morphospace boundary analysis, the first two covered about 60.24% variation (PC1 explained 38.12 % variation, while PC2 covered 22.12 %). *E. vittata*, *I. rapax* and *T. tillarga* were clustered separately in the PCs morphospace. All other species were found to be clustered closely in the morphospace (Fig. 1.17A).

In the CVA- Morphospace boundary analysis of the forewings, we found many separate clusters, and the overlapping clusters were very low, indicating variations among the wings of Anisopteran species (Fig. 1.17B).

1.4.2.4 Partial Least Square analysis (PLS)

In size, PLS analysis of the forewing of 26 Anisopteran species, many species show similarities, but *E. vittata* and *G. dravida* do not show any similarities with other species (Fig. 1.18A). The shape PLS analysis of the forewing *E. vittata* and *H. apicalis* showed the highest dissimilarities (Fig. 1.18B).

1.4.2.5 phylogenetic signal analysis

No phylogenetic signals were observed in the size and shape-related phylogenetic signal analysis of the forewings of 26 dragonfly species. The phylogeny tree length for the forewing size was 2127.751, with a P=0.108, (Fig. 1.19A) and the phylogeny tree length for the shape was 0.03889, P=0.147 (Fig. 1.19B). This result indicates that the shape and size of the forewing are modulated by environmental selection pressure rather than evolutionary force.

1.4.2.6 Hierarchical cluster dendrogram analysis

Based on the morphological data, the phylogenetic history of the wings of 26 dragonfly species was constructed. The 26 Anisopteran species were found to be diverged into different clades, and closely related species were arranged closely in the cluster dendrogram based on their similarities. In this analysis, the 26 dragonfly species were first divided into two major clades at 0% similarities (Fig. 1.20). Clade 1 includes the species *A. panorpoides, O. glaucum, O. luzonicum, B. geminata, I. rapax, G. dravida, R. variegata, T. tillarga, H. apicalis, L. asiatica, P. sexmaculata,* and *T. aurora*. Clade 2 includes *A. brevipennis, E. vittata, T. limbata, Z. petiolatum, B. contaminata, T. basilaris, T. festiva, P. flavescens, C. servilia, N. tullia, D. trivialis, P. congener, O. sabina,* and *O. pruinosum*. In clade 1, *L. asiatica* is the most distantly related species; in clade 2, *O. pruinosum* is the most distantly related species. In the forewing dendrogram analysis, *R. variegata* and *T. tillarga* showed the highest similarities of 78% as per the dendrogram and diverged from clade 1. *T. limbata,* and *Z. petiolatum* diverged from clade 2 with 76% similarities. *B. geminata,*

and *I. rapax* showed 77% similarities and diverged from clade 1. *G. dravida* diverged from clade 1 with 70% similarities.

1.4.3 Geometric Morphometric Analysis of Hindwings

1.4.3.1 Centroid Size Analysis

The centroid size analysis demonstrated the presence of variations in the hindwing size among the Anisopteran species (Fig. 1.21). The hindwing centroid sizes of 26 Anisopteran species were compared, *G. dravida* (93.22 ± 2.76) had the largest hindwing, and then the *E. vittata* (89.06 ± 0.03). *T. limbata* (76.46 ± 1.79) and *P. flavescens* (76.79 ± 2.05) are the other species with larger hindwings after *G. dravida* and *E. vittata. P. sexmaculata* (33.27 ± 1.97) and *A. panorpoides* (34.62 ± 0.63) have the smallest forewing size. The species *O. glaucum* (65.13 ± 2.19), *O. pruinosum* (65.39 ± 0.62), and *O. sabina* (65.32 ± 1.18) has similar hindwing size. *B. geminata* (62.85 ± 1.47), *L. asiatica* (62.84 ± 1.27), and *R. variegata* (62.04 ± 2.83) also had similar hindwing size.

1.4.3.2 GPA and % Variance analysis

A total of 57 PCs explained the 100% variance among the hindwings. The first three PCs covered about 75.14 % variation (PC1 explained 32.23 % variation, PC2 covered 28.35 % and PC3 explained 14.56 %) (Fig. 1.22). In hindwings GPA analysis, the anal region showed the maximum variations, then the wing apical region and the pterostigmal regions also showed some variations (Fig. 1.22).

1.4.3.3 Morphospace boundary analysis

PCA and CVA methods validated the distribution of the hindwings morphospace. A total of 57 PCs were present in the forewing analysis. In the PCs-morphospace boundary analysis (Fig. 1.23A), the first two PCs covered about 60.58% variation (PC1 explained 32.23 % variation, and PC2 covered 28.35 % variation). *E. vittata*, *I. rapax*, *T. tillarga, and P. congener* were clustered separately in the PCs morphospace. All other species were found to be clustered closely in the morphospace. The hindwings' CVA- Morphospace boundary analysis showed separate clusters for most species (Fig. 1.23).

1.4.3.4 Partial Least Square analysis (PLS)

In size PLS analysis of the hindwings of 26 Anisopteran species, many species show similarities, but *E. vittata, H. apicalis,* and *G. dravida* do not show any similarities with other species (Fig. 1.24A). The shape PLS analysis of the hindwings *E. vittata, I. rapax, G. dravida,* and *B. contaminata* showed the highest dissimilarities (Fig. 1.24B).

1.4.3.5 phylogenetic signal analysis

No phylogenetic signals were observed in the size and shape-related phylogenetic signal analysis of the hindwings of 26 dragonfly species. The tree length for the size phylogeny of the hindwing was 2842.877 and P=0.128 (Fig. 1.25A), and for shape phylogeny, P=0.173 (Fig. 1.25). This result indicates that the shape and size of the hindwing are modulated by environmental selection pressure rather than evolutionary force.

1.4.3.6 Hierarchical cluster dendrogram analysis

Based on the morphological data, the phylogenetic history of the wings of 26 dragonfly species was constructed. The 26 Anisopteran species were found to be diverged into different clades, and closely related species were arranged closely in the cluster dendrogram based on their similarities (Fig. 1.26). *P. sexmaculata* is the most distantly related species in the hindwing dendrogram analysis. The remaining 25 species were divided into two major clades. The clade 1 includes the species *O. luzonicum, B. geminata, G. dravida, R. variegata, T. tillarga, H. apicalis, L. asiatica, Z. petiolatum, T. festiva, C. servilia, P. congener, O. sabina, O. pruinosum,* and *T. aurora*. Clade 2 includes *A. panorpoides, O. glaucum, A. brevipennis, E. vittata, T. limbata, B. contaminata, T. basilaris, P. flavescens, N. tullia, D. trivialis,* and *I. rapax*. In the hindwing dendrogram analysis, *G. dravida* and *B. geminata* showed the highest similarities of 86% and diverged from clade 1. *H. apicalis* and *O. luzonicum* diverged from clade 1 with 84% similarities. *T. tillarga* and *Z. petiolatum* showed 74% similarities and diverged from clade 1. The highest percentage of similarities shown by the clade 2 species is 40%.

1.4.4 Molecular phylogeny

The COI gene sequences were used for the molecular phylogenetic tree construction (Table 1.4). The species phylogenetic tree was constructed based on the Maximum likelihood method and Tamura-Nei model. 26 Anisopteran species were used for the phylogenetic analysis to check the similarities and differences between the migratory and non-migratory species (Figure 1.46). The three migratory species *P. flavescens*, *T. basilaris*, and *T. tillarga* were found in the different clades. At the same time, the non-migratory species like *N. tullia* and the migratory species *P. flavescens* were found to be diverged at the same time. This analysis concluded that CO1-based phylogenetic analysis does not help categorize the molecular evolutionary analysis of migratory and non-migratory species.

Table 1.4: Collected specimens with NCBI accession number

Sl. No	Species	Accession No.
1	*Aethriamanta brevipennis* (Rambur, 1842)	KC287158.1
2	*Acisoma panorpoides* (Rambur, 1842)	MN689142.1
3	*Brachythemis contaminata* (Fabricius, 1793)	MN345273.1
4	*Bradinopyga geminata* (Rambur, 1842)	JX306648.1
5	*Crocothemis servilia* (Drury, 1770)	MF774561.1
6	*Diplacodes trivialis* (Rambur, 1842)	JF839454.1
7	*Epophthalmia vittata* (Burmeister, 1839)	MW509733.1
8	*Gynacantha dravida* (Lieftinck, 1960)	MK990607.1
9	*Hylaeothemis apicalis* (Fraser, 1942)	ON255470.1
10	*Ictinogomphus rapax* (Rambur, 1842)	MF358743.1
11	*Lathrecista asiatica* (Fabricius, 1798)	MN202659.1
12	*Neurothemis tullia* (Drury, 1773)	MH881325.1
13	*Orthetrum glaucum* (Brauer, 1865)	OR287446.1
14	*Orthetrum luzonicum* (Brauer, 1868)	MZ092847.1
15	*Orthetrum pruinosum* (Burmeister, 1839)	MF358753.1
16	*Orthetrum sabina* (Drury, 1770)	KX670387.1
17	*Potamarcha congener* (Rambur, 1842)	MG885276.1
18	*Pantala flavescens* (Fabricius, 1798)	OM945866.1
19	*Palpopleura sexmaculata* (Fabricius, 1787)	MN159179.1
20	*Rhyothemis variegata* (Linnaeus, 1763)	MN345757.1
21	*Trithemis aurora* (Burmeister, 1839)	PP032031.1
22	*Tramea basilaris* (Palisot de Beauvois, 1817)	MK038728.1
23	*Trithemis festiva*, (Rambur, 1842)	OM919689.1
24	*Tramea limbata* (Desjardins, 1832)	KX055147.1
25	*Tholymis tillarga* (Fabricius, 1798)	MZ127380.1
26	*Zyxomma petiolatum* (Rambur, 1842)	MZ093432.1

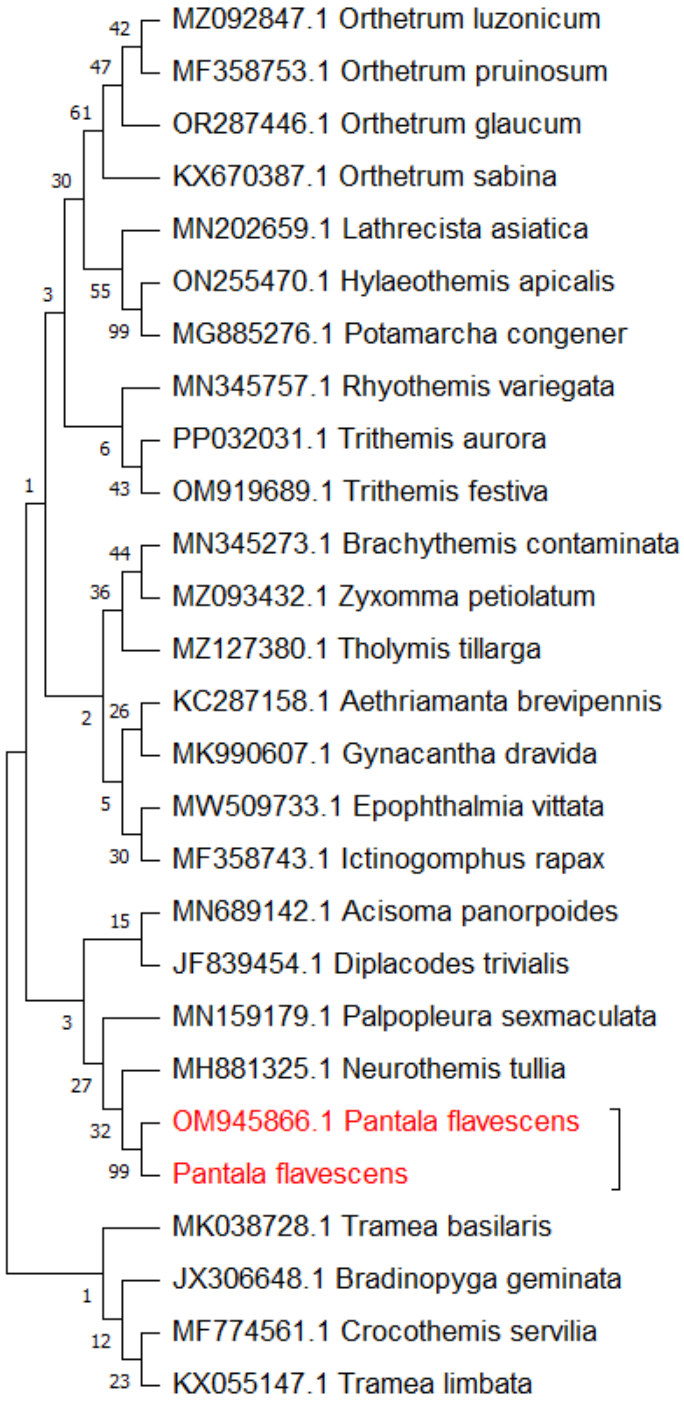

Figure 1.46: Maximum-likelihood phylogeny analysis of collected species with previously deposited CO1sequence, Tamura-Nei model, and MUSCLE alignment. Bootstrap value 100.

1.5 DISCUSSION

1.5.1 Wing morphology and venation pattern

The wing morphology of insects affects flight performance, including manoeuvrability, agility, lift, and thrust production (Dudley, 2000; Berwaerts et al., 2002; Bots et al., 2012). We conducted a detailed comparative study on the wing morphology and venation patterns of 26 Anisopteran dragonflies. A study conducted by Johansson et al. (2009) showed that the anal lobe of the hindwings is more prominent in the migrating dragonfly species. Also, the apex region of the forewing will be more prominent in the migratory species. The anal lobe of the hindwing helps in the gliding of dragonflies, possibly by reducing the drag, and this gliding is an adaptive behaviour of migration (Corbet, 1962). In our study, we observed well developed, stocking-shaped, closed anal loop in all three migratory species, and the anal margin is rounded in all three species. In contrast, *E. vittata, G. dravida,* and *I. rapax* had poorly developed rounded anal loops with angulated anal margins forming a triangle with one to three cells in that area. Even though these three species have the largest wing size, they cannot able to move long distances due to the poorly developed anal loop and anal margin.

The hindwing of migratory dragonfly species has an expansion called a lobe (Johansson, 2009), which helps in gliding, an adaptive behavior of migratory dragonflies (Corbet, 1962). The wing vein distribution influences manoeuvrability and energy usage during the flight of insects (Tillyard, 1917; Corbet, 1999; Dudley, 2000; Wootton & Newman, 2008; Zhao et al., 2012). When we compared the morphological features and the venation patterns of the forewing and hindwings of 26 dragonfly species, we found many differences between them. The anal loop region and the anal area of the hindwing showed more variations. These variations in the hindwing make the differences in the flight of 26 dragonfly species: some are active fliers, some are passive, and some are very weak fliers. Our study collected three migratory species: *P. flavescens, T. basilaris*, and *T. tillarga*. The venation pattern of the hindwings of all three migratory species are showing similarities, especially the anal area. However, the forewings of *P. flavescens* showed some

differences in the venation pattern compared to the other two migratory species. The discoidal field of the forewings, triangle, arculus sectors, and distal antenodals shows the differences. Centroid size differences of the fore and hindwing between these three species have also been noticed, in which *P. flavescens* had larger wings than the other two migratory species. *T. tillarga* and *T. basilaris* had almost similar wing sizes. *P. flavescens* is the longest known migratory species (Hobson et al., 2012; May, 2013; Chapman et al., 2015), and it migrates around 14000 to 18000 km, including a migration distance of about 1000 km over the open Indic Sea (Anderson, 2009). Thus, all these changes in the wings might be an adaptation for its long-distance migration.

1.5.2 Geometric morphometric analysis

In the 26 species of dragonflies, the largest centroid size of forewing and hindwing was observed in *E. vittata* and *G. dravida*. Then, we observed the highest centroid size in the three migratory species *P. flavescens*, *T. tillarga,* and *T. basilaris*. The wing centroid size of *I. rapax* was more prominent than *T. basilaris*. According to Suarez-Tovar & Sarmiento (2016), the migratory dragonfly species will have larger wings and smaller ridge regions in both the forewings and hindwings. The size differences of the wings alone cannot differentiate the migratory and non-migratory species; the shape of the wings also plays a vital role in them.

According to Suarez-Tovar & Sarmiento (2016), the wings of migratory dragonflies will have a smaller pterostigma and more proximally located nodus. The GPA analysis of the forewing and hindwings of the 26 species also showed some variations between species. In the forewings, the major variations were observed in the wing triangle, apical, and the regions of pterostigma. The hindwing showed more variations in the anal region. The regions of pterostigma, discoidal field, and apical area of the hindwing also show some variations. In our study shape related variations are found to be more than the size-related variations (PLS analysis), especially in the anal region of the hindwings (GPA analysis) and our results agree with the fact that the shape of the flight-related structures is the better descriptors of evolutionary response to selective factors rather than the size of flight-related

structures (Johansson et al., 2009; Garcia & Sarmiento, 2012; Outomuro et al., 2013; Suarez-Tovar & Sarmiento, 2016).

Dragonflies are one of the oldest living groups of insects, showing high variations in wing morphology and shape (Wootton, 1991). In our study, shape-related variations were more than the size-related variations among the 26 Anisopteran dragonfly species, verified by PLS analysis. In wing morphology, the size and shape of the wing may function as independent components (Debat et al., 2003). The shape of the wing determines the flying ability of the dragonflies. The Aisopteran dragonflies show variations in their wing shape among genera, and the interspecific variations in the wing shape might be partly due to the selection (Johansson et al., 2009).

The wings of insects, birds, and bats are major morphological adaptations that contribute to their evolutionary success (Dudley, 2002; Hedenstrom, 2002; Sane, 2003). The morphological evolution of populations can be easily explored using geometric morphometric analysis (Cooke & Terhune, 2015; Baylac et al., 2003). The phylogenetic history of shape changes, the diversification and spreading of clades through the space of morphometric variables can be graphically visualized by the cluster dendrogram (Klingenberg & Marugan-Lobon, 2013). 26 dragonfly species were arranged in different clades based on their similarities and differences in the wing. Similar species were arranged closely in the dendrogram. In the forewing and hindwing cluster dendrogram analysis *P. flavescens* and *T. basilaris* occupied the same clade (clade 1), but *T. tillarga* occupied clade 2.

For the morphospace analysis, we used PCA and CVA methods. The CVA analysis explained the interspecific variations among the 26 Anisopteran dragonfly species. Some species were found to be clustered together in the morphospace, which shared similar wing morphological characters. The hindwing and forewing CVA analysis of the dragonflies showed a clear separation of the species *E. vittata, G. dravida, H. apicalis,* and *I. rapax*; these species occupied a distinct area in the morphospace because these species show an apparent morphological variation in their wing venation pattern, like poorly developed rounded anal loop area in the

hindwings with angulated anal margin forming triangle with one to three cells in that area but in *H. apicalis* the anal margin is rounded.

1.5.3 Molecular and morphological phylogenetic signal analysis

The migratory behavior of insects is also an essential aspect of evolutionary studies because the effect of natural selection is more reflected in various insect's morphological traits, especially in wing morphology (Suarez-Tovar & Sarmiento, 2016). In geometric morphometrics, the phylogenetic signal analysis was performed to understand if the size and shape of taxa's morphological structures evolved by evolutionary history or by environmental factors (Klingenberg & Gidaszewski, 2010). In this study, we analyzed the size and shape phylogenetic signal of the forewing and hindwings of 26 dragonfly species. We found no size and shape-related phylogenetic signal in the forewing and hindwings. This indicates that the size and shape-related variations in the forewing and hindwings, not the evolutionary ones.

The molecular phylogenetic relationship among the 26 dragonflies has also been studied. The three migratory species *P. flavescens*, *T. tillarga,* and *T. basilaris* have been found to occupy different clades, showing no relationship between them. Suarez-Tovar and Sarmiento (2016) studied the morphologies of two major migration-evolved clades of Libellulid dragonflies. They found no differences in the shape of the wing especially in the hindwing anal area. Their study concluded that parallel pleiotropic changes might be responsible for similar morphological modifications (Prudhomme et al., 2006). In our study, we could not find any close relationship between migratory and non-migratory dragonfly species, and this irregularity in the relationship among them might be indicated as this behaviour may evolve due to natural selection pressure nor by the evolutionary selection.

At present, only few studies were attempt to reveal the wing phenotypic variations and their functional role. As we know odonates is the oldest living group and their venation pattern not showed too much variations, and their venation pattern is highly conserved. The flying mechanism and behvioural pattern connected with the molecular and morphological feature of an organisms. However, more studies are required to understand the flying mechanism of odonates in connection with the migratory vs. non. migratory.

1.6 KEY FINDINGS

- A total of 26 dragonfly species wing venation patterns (fore- and hindwings) were studied.
- The wing venation patterns are correlated with the flight behavioural patterns, especially the hindwing anal lobe and longitudinal vein arrangements.
- GMM analysis proved that wing venation patterns can be used as a valid tool for identifying dragonfly species.
- Each species occupied a unique morphospace boundary, verified in PCA, CVA, and PLS analysis. It indicated that, each species had its own unique wing venation patterns.
- As compared to size, shape-related variations are prominent in selected dragonfly species, which was verified in PLS analysis.
- There is no size and shape-related phylogenetic signal in forewing and hindwings among the selected dragonfly species. This indicates that the size and shape-related variations were modulated by environmental selection pressure, not by evolutionary force.

1.7 REFERENCES

Adams, D. C., Rohlf, F. J., & Slice, D. E. (2004). Geometric morphometrics: Ten years of progress following the 'revolution'. *Italian Journal of Zoology,* 71(1), 5–16. https://doi.org/10.1080/11250000409356545

Aiello, B. R., Tan, M., Sikandar, U. B., Alvey, A. J., Bhinderwala, B., Kimball. K. C., … & Sponberg, S. (2021). Adaptive shifts underlie the divergence in wing morphology in bombycoid moths. *Proceedings of the Royal Society B: Biological Sciences*, 288 (1956). https://doi.org/10.1098/rspb.2021.0677

Anderson, R.C. (2009). Do dragonflies migrate across the western Indian Ocean? *J. Trop. Ecol*. 25, 347–358.

Berwaerts, K., Dyck, V, H., & Aerts, P. (2002). Does flight morphology relate flight performance? An experimental test with the butterfly *Pararge aegeria*. *Functional Ecology*, 16, 484-491.

Betts, C. R., & Wootton, R. J. (1988). Wing shape and flight behaviour in butterflies (Lepidoptera: Papilionoidea and Hesperioidea): a preliminary analysis. *Journal of Experimental Biology*, 138, 271–288.

Bocek, M. & Bocak, L. (2017). The comparison of molecular and morphology-based phylogenies of trichaline net-winged beetles (Coleoptera: Lycidae: *Metriorrhynchini*) with description of a new subgenus. *PeerJ*. 5, e3963. doi: 10.7717/peerj.3963.

Bookstein, F. L. (1982). Foundations of morphometrics. *Annu. Rev. Ecol. Syst*. 13, 451–470.

Bots, J., Breuker, C. J., Kaunisto, K. M., Koskimaki, J., Gossum, H. V., & Suhonen, J. (2012). Wing shape and its influence on the outcome of territorial contests in the damselfly *Calopteryx virgo*. *Journal of insect science*, 12(96).

Cabuga, C. C., Estaño, L. A., Abelada, J. J., Cruz, I. N., Angco, M. K., Joseph, C. C., … & Martinez, P. J. (2017). Landmark based geometric morphometric analysis describing sexual dimorphism in wings of *Neurothemis terminata* (Ris, 1911) from Mt. Hilong-Hilong, Philippines. *Computational Ecology and Software*, 7(2), 65-81.

Carle, F. L., Kjer, K. M., & May, M. L. (2015). A molecular phylogeny and classification of Anisoptera (Odonata). *Arthropod Syst. Phylogeny,* 73, 281–301.

Champakaew, D., Junkum, A., Sontigun, N., Sanit, S., Limsopatham, K., Saeung, A., … & Pitasawat, B. (2021). Geometric morphometric wing analysis as a tool to discriminate female mosquitoes from different suburban areas of Chiang Mai province, Thailand. *PLoS ONE*, 16(11), e0260333. https://doi.org/10.1371/journal.pone.0260333

Chapman, J. W, Reynolds, D. R., & Wilson, K. (2015). Long-range seasonal migration in insects: mechanisms, evolutionary diverse and ecological consequences. *Ecology Letters,* 18(3), 287–302. https:// doi. org/ 10. 1111/ ele. 12407

Clark, C. J., & Dudley, R. (2009). Flight costs of long, sexually selected tails in hummingbirds. *Proceedings of the Royal Society B: Biological Sciences*, 276, 2109–2115.

Combes, S. A., & Daniel, T. L. (2003). Flexural stiffness in insect wings I. Scaling and the influence of wing venation. *Journal of Experimental Biology*. 206, 2979–2987. doi:10.1242/jeb.00523

Comstock, J. H. (1893). *Evolution and Taxonomy: An essay on the application of the theory of natural selection in the classification of animals and plants, illustrated by a study of the evolution of the wings of insects*. Ithaca, New- York: The Wilder Quarter-Century Book.

Corbet, P. (1999). *Dragonflies: Behavior and Ecology of Odonata*. New York, NY: Cornell University Press.

Corbet, P. S. (1962). *A biology of dragonflies*. London: Whiterby.

Corbet, P. S. (1999). *Dragonflies: behavior and ecology of Odonata*. New York, NY: Comstock publishing Associates.

Cordoba-Aguilar, A. (2008). *Dragonflies and Damselflies. Model Organisms for Ecological and Evolutionary Research*. Oxford University Press.

Debat, V., Bégin, M., Legout, H., & David, J. R. (2003). Allometric and nonallometric components of drosophila wing shape respond differently to developmental temperature. *Evolution,* 57, 2773–2784

DeVries, P. J., Penz, C. M., & Hill, R. I. (2010). Vertical distribution, flight behaviour and evolution of wing morphology in Morpho butterflies. *Journal of Animal Ecology*, 79, 1077–1085.

Dickinson, M. (2006). Insect flight. *Current Biology*. 16, R309–R314.

Dijkstra, K. B., Kalkman, V. J., Dow, R. A., Stokvis, F. R., & Van Tol, J. A. N. (2014). Redefining the damselfly families: a comprehensive molecular phylogeny of Zygoptera (Odonata). *Systematic Entomology*. 39, 68–96.

Dingle, H. (1996). *Migration: The Biology of Life on the Move*. New York, NY: Oxford University Press.

Dudley, R. (2000). *The Biomechanics of Insect Flight: Form, Function, Evolution*. Princeton, NJ: Princeton University Press.

Dudley, R. (2002). Mechanisms and implications of animal flight maneuverability. *Integrative and Comparative Biology*, 42,135–140.

Fang, C., Yang, Y., Yang, X., & Liu, H. (2024). A Phylogenetic Morphometric Investigation of Interspecific Relationships of *Lyponia* s. str. (Coleoptera, Lycidae) Based on Male Genitalia Shapes. *Insects*, 15, 11. https://doi.org/10.3390/insects15010011

Feng, H., Wu, K., Ni, Y., Cheng, D., & Guo, Y. (2006). Nocturnal migration of dragonflies over the Bohai Sea in northern China. *Ecological Entomology*. 31, 511–520.

Field, K. G, Olsen, G. J., Lane, D. J., Giovannoni, S. J., Ghiselin, M. T., Raff, E. C., … & Raff, R. A. (1988). Molecular phylogeny of the animal kingdom. *Science*, 239(4841), 748–753. https://www.science.org/doi/abs/10.1126/science.3277277

Fraser, F.C. (1954). The origin and descent of the order Odonata based on the evidence of persistent archaic characters. *Proceedings of the Royal Entomological Society (B),* 23, 89-94

Gallesi, M. M., Sacchi, R., & Hardersen, S. (2015). Does wing shape of andromorph females of *Calopteryx splendens* (Harris, 1780) resemble that of males? *International Journal of Odonatology*, 18(4), 305-315, DOI: 10.1080/13887890.2015.1085457

Garcıa, Z., & Sarmiento, C.E. (2012). Relationship between body size and flying-related structures in Neotropical social wasps (Polistinae, Vespidae, Hymenoptera). *Zoomorphology*, 131, 25–35.

Grimaldi, D. A., & Engel, M. S. (2005). *Evolution of the Insects*. Cambridge, UK: Cambridge University Press.

Grzywacz, B., Heller, K. G., Warchalowska-sliwa, E., Karamysheva, T. V., & Chobanov, D. P. (2017). Evolution and systematics of Green Bush-crickets (Orthoptera: Tettigoniidae: *Tettigonia*) in the Western Palaearctic: testing concordance between molecular, acoustic, and morphological data. *Organisms Diversity and Evolution*, 17(1), 213-228. DOI 10.1007/s13127-016-0313-3.

Hassall, C., Thompson, D. J., & Harvey, I. F. (2008). Wings of *Coenagrion puella* vary in shape at the northern range margin (Odonata: Coenagrionidae). *International Journal of Odonatology*, 11(1), 35-41, DOI:10.1080/13887890.2008.9748310

Hedenstrom, A. (2002). Aerodynamics, evolution and ecology of avian flight. *Trends in Ecology & Evolution*. 17, 415–422.

Hobson, K. A., Anderson, R. C., Soto, D. X., & Wassenaar, L. I. (2012). Isotopic evidence that dragonflies (*Panata flavescens*) migrating through the Maldives come from the northern Indian subcontinent. *PLoS One*, 7, e52594. https:// doi. org/ 10. 1371/ journ al. pone. 00525 94

Huang, S. T., Wang, H. R., Yang, W. Q., Si, Y. C., Wang, Y. T, Sun, M. L, … & Bai, Y. (2020). Phylogeny of Libellulidae (Odonata: Anisoptera): comparison of molecular and morphology-based phylogenies based on wing morphology and migration. *PeerJ*, 8, e8567. doi: 10.7717/peerj.8567.

Johansson, F., Soderquist, M. & Bokma, F. (2009). Insect wing shape evolution: independent effects of migratory and mate guarding flight on dragonfly wings. *Biological journal of the Linnean Society*, 97(2), 362-372. https://doi.org/10.1111/j.1095-8312.2009.01211.x.

Kiyoshi, T. & Hikida, T. (2012). Geographical Variation in the Wing Morphology of the Golden-ringed Dragonfly *Anotogaster sieboldii* (Selys, 1854) (Odonata, Cordulegastridae) Detected by Landmark-based Geometric Morphometrics. *Bull. Natl. Mus. Nat. Sci., Ser. A*, 38(2), 65-73.

Kiyoshi, T., & Hikida, T. (2012). Dragonfly *Anotogaster sieboldii* (Selys, 1854) (Odonata, Cordulegastridae) Detected by Landmark-based Geometric Morphometrics. *Bull. Natl. Mus. Nat. Sci., Ser. A*, 38(2), 65–73

Klingenberg, C. P., & Gidaszewski, N. A. (2010). Testing and quantifying phylogenetic signals and homoplasy in morphometric data. *Systematic biology*, 59(3), 245–261. https://doi.org/10.1093/sysbio/syp106

Klingenberg, C. P., & Zaklan, S. D. (2000). Morphological intergration between development compartments in the Drosophila wing. *Evolution; international journal of organic evolution*, 54(4), 1273–1285. https://doi.org/10.1111/j.0014-3820.2000.tb00560.x

Lawing, A. M. & Polly, P. D. (2010). Geometric morphometrics: recent applications to the study of evolution and development. *Journal of Zoology*, 280(1), 1-7. https://doi.org/10.1111/j.1469-7998.2009.00620.x

Letsch, H., Gottsberger, B., & Ware, J. L. (2016). Not going with the flow: a comprehensive time-calibrated phylogeny of dragonflies (Anisoptera: Odonata: Insecta) provides evidence for the role of lentic habitats on diversification. *Molecular Ecology*. 25 (6), 1340–1353.

Lopez-Aguirre, C., Hand, S.J., Koyabu, D., Tu, V. T., & Wilson, L. A. B. (2020). Phylogeny and foraging behaviour shape modular morphological variation in bat humeri. *Journal of Anatomy*, 238, 1312-1329. DOI: 10.1111/joa.13380.

Marcus, L. F., & Corti, M. (1996). *Overview of the new, or geometric morphometrics*. In: Marcus LF, Corti M, Loy A, Naylor GJP, Slice, DE (Eds) Advances in morphometrics. (pp. 1–13). Springer.

Marin, M. A., Pena, C., Uribe, S. I., & Freitas, A. V. L. (2017). Morphology agrees with molecular data: phylogenetic affinities of Euptychiina butterflies (Nymphalidae: Satyrinae). *Systematic Entomology,* 42(4), 768-785. DOI 10.1111/syen.12245.

Marinov, M., Amaya-Perilla, C., Holwell, G. I., Varsani, A., Bysterveldt, K. V., Kraberger, S., … & Paterson, A. (2016). Geometric morphometrics and molecular systematics of *Xanthocnemis sobrina* (McLachlan, 1873) (Odonata: Coenagrionidae) and comparison to its congeners. *Zootaxa*, 4078(1), 84–120. https://doi.org/10.11646/zootaxa.4078.1.9

May, M. L. (2013). A critical overview of progress in studies of migration of dragonflies (Odonata: Anisoptera), with emphasis on North America. *Journal of Insect Conservation*, 17,1–15. https:// doi. org/ 10. 1007/s10841- 012- 9540-x

Meresman, Y., & Ribak, G. (2017). Allometry of wing twist and camber in a flower chafer during free flight: how do wing deformations scale with body size? *Royal Society Open Science.* 4, 171152. doi:10.1098/rsos.171152

Meresman, Y., Husak, J. F., Ben-Shlomo, R. & Ribak, G. (2020). Morphological diversification has led to inter-specific variation in elastic wing deformation during flight in scarab beetles. *Royal Society Open Science*, 7(4). http://dx.doi.org/10.1098/rsos.200277

Mitterocker, P. (2021). *Morphometrics in Evolutionary Developmental Biology*. In: Nuno de la Rosa, L., Müller, G.B. (Eds) Evolutionary Developmental Biology. Springer, Cham. https://doi.org/10.1007/978-3-319-32979-6_119

Mitteroecker., P. & Gunz, P. (2009). Advances in Geometric Morphometrics. *Evolutionary Biology*, 36, 235-247.

Monteiro, L. R., Diniz-Filho, A. F., dos Reis, S. F., & Araujo, E. D. (2002). Geometric estimates of hereditability in biological shape. *Evolution,* 56, 563–572.

Moraes, E. M., Spressola, V. L., Prado, P. R. R., Costa, L. F., & Sene, F. M. (2004). Divergence in wing morphology among sibling species of the *Drosophila buzzatii* cluster. *Journal of Zoology Systematics Evolutionary Research*, 42, 154–158. https://doi.org/10.1111/j.1439-04-69.2004.00256.x

Munz, P. A. (1919). A Venational Study of the Suborder Zygoptera (Odonata): With Keys for the Identification of Genera. *Memoirs of the American Entomological Society*, 3, 1-78.

Nel, A., Prokop, J., Nel, P., Grandcolas, P., Huang, D., Roques, P., … & Szwedo, J. (2012). Traits and evolution of wing venation pattern in paraneopteran insects. *Journal of Morphology*, 273, 480–506.

Noguerales, V., Cordero, P. J., & Ortego, J. (2018). Integrating genomic and phenotypic data to evaluate alternative phylogenetic and species delimitation hypotheses in a recent evolutionary radiation of grasshoppers. *Molecular Ecology*, 27(5), 1229-1244. DOI 10.1111/mec.14504.

Norberg, U. M. (1995). How a long tail and changes in mass and wing shape affect the cost for flight in animals. *Functional Ecology*, 9, 48–54.

Outomuro, D., & Johansson, F. (2015), Bird predation selects for wing shape and coloration in a damselfly. *Journal of Evolutionary Biology*, 28, 791-799. https://doi.org/10.1111/jeb.12605

Outomuro, D., Adams, D. C., & Johansson, F. (2013). The Evolution of Wing Shape in Ornamented-Winged Damselflies (Calopterygidae, Odonata). *Evolutionary Biology*. 40, 300-309. DOI 10.1007/s11692-012-9214-3

Perrard, A., Lopez-Osorio, F., & Carpenter, J. M. (2016). Phylogeny, landmark analysis and the use of wing venation to study the evolution of social wasps (Hymenoptera: Vespidae: Vespinae). *Cladistics*, 32, 406-425.

Pretorius, E. (2005). Using geometric morphometrics to investigate wing dimorphism in males and females of Hymenoptera – a case study based on the genus *Tachysphex* Kohl (Hymenoptera: Sphecidae: Larrinae). *Australian Journal of Entomology*, 44, 113-121.

Pretorius, E., & Scholtz, C. H. (2001). Geometric morphometrics and the analysis of higher taxa: a case study based on the metendosternite of the Scarabaeoidea (Coleoptera). *Biological Journal of the Linnean Society*, 74, 35-50. doi: l0.1006/bij1.2001.0568

Prud'homme, B., Gompel, N., Rokas, A., Kassner, V. A., Williams, T. M., Yeh, S. D., … & Carroll, S. B. (2006). Repeated morphological evolution through cis-regulatory changes in a pleiotropic gene. *Nature,* 440, 1050–1053.

Rohlf, F. J. (1993). NTSYS-pc, *version* 1.80. Exeter Software, Setauket, USA.

Rohlf, F. J. (2001). Comparitive methods for the analysis of continuous variables: geometric interpretations. *Evolution*, 55, 2143–2160.

Rohlf, F. J. (2002). *Geometric Morphometrics and Phylogeny. In: Morphology, Shape and Phylogenetics*. In P. Forey; N. Macleod (Eds), 175–193. London, UK, Francis & Taylor.

Rohlf, F. J., & Marcus, L. F. (1993). A revolution morphometrics. *Trends in Ecology & Evolution,* 8(4), 129-32. doi:10.1016/0169-5347(93)90024-J.

Rohlf, F. J., & Slice, D. E. (1990). Extensions of the Procrustes method for the optimal superimposition of landmarks. *Systematic Zoology,* 39(1), 40–59. doi:10.2307/2992207

Romero-Lebron, E., Gleiser, R. M., & Petrulevicius, J. F. (2020). Geometric morphometrics to interpret the endophytic egg-laying behavior of Odonata (Insecta) from the Eocene of Patagonia, Argentina. *Journal of Paleontology*, 93(6), 1126-1136. https://doi.org/10.1017/jpa.2019.30

Ross, H. H. (1936). The ancestry and wing venation of the Hymenoptera. *Annals of the Entomological Society of America,* 29, 99–111.

Sadeghi, S., Adriaens, D., & Dumont, H. J. (2009). Geometric morphometric analysis of wing shape variation in ten European populations of *Calopteryx splendens* (Harris, 1782) (Zygoptera:Odonata). *Odonatologica,* 38(4), 343-360

Sane, S. P. (2003). The aerodynamics of insect flight. *Journal of Experimental Biology.* 206, 4191–4208.

Santos, C. F. D., Santos, P. D. S. D., Marques, D. M., Da-Costa, T., & Blochtein, B. (2019). Geometric morphometrics of the forewing shape and size discriminate *Plebeia* species (Hymenoptera: Apidae) nesting in different substrates. *Systematic Entomology*, 44, 787-796. DOI: 10.1111/syen.12354.

Sauer, F. G., Jaworski, L., Erdbeer, L., Heitmann. A., Schmidt-Chanasit, J., Kiel, E., & Luhken, R. (2020). Geometric morphometric wing analysis represents a robust tool to identify female mosquitoes (Diptera: Culicidae) in Germany. *Scientific Reports,* 10, 17613 (2020). https://doi.org/10.1038/s41598-020-72873-z

Stewart, S. S., & Vodopich, D. S. (2018). Environmental effects on wing shape and wing size of *Argia sedula* (Odonata: Coenagrionidae), *International Journal of Odonatology*, DOI: 10.1080/13887890.2018.1523752

Suarez-Tovar, C. M., & Sarmiento, C. E. (2016). Beyond the wing planform: morphological differentiation between migratory and nonmigratory dragonfly species. *Journal of Evolutionary Biology*, 29, 690-703. doi: 10.1111/jeb.12830.

Tatsuta, H., Takahashi, K. H., & Sakamaki, Y. (2018). Geometric morphometrics in entomology: basics and applications. *Entomological Science*, **21**, 164–184.

Theischinger, G., & Hawking, J. (2006). *The Complete Field Guide to Dragonflies of Australia*, Australia, CSIRO Publishing.

Tillyard, R. (1917). *The Biology of Dragonflies (Odonata or Paraneuroptera)*. London, UK, Cambridge University Press.

Trautwein, M. D., Wiegmann, B. M., Beutel, R., Kjer, K. M., & Yeates, D. K. (2012). Advances in insect phylogeny at the dawn of the postgenomic era. *Annual Review of Entomology*. 57, 449–468.

Tuzun, N., Beeck, L, O., & Stoks, R. (2017). Sexual selection reinforces a higher flight endurance in urban damselflies. *Evolutionary Applications*. 10(7), 694-703. doi: 10.1111/eva.12485.

Villalobos-Jiménez, G., & Hassall, C. (2019). Wing shape patterns among urban, suburban, and rural populations of *Ischnura elegans* (Odonata: Coenagrionidae). *International Journal of Odonatology*, 22 (1), 37-49.

Wakeling, J. & Ellington, C. (1997). Dragonfly flight. I. Gliding flight and steady-state aerodynamic forces. *Journal of Experimental Biology*. 200, 543–556.

Wappler, T., Labandeira, C. C., Rust, J., Frankenhauser, H., & Wilde, V. (2012). Testing for the Effects and Consequences of Mid Paleogene Climate Change on Insect Herbivory. *PLoS ONE*, 7(7). https://doi.org/10.1371/journal.pone.0040744

Wehmann, H. N., Heepe, L., Gorb, S. N., Engels, T., & Lehmann, F. O. (2019). Local deformation and stiffness distribution in fly wings. *Biology Open,* 8(1), bio038299. doi:10.1242/bio.038299

Wheeler, W. C., Whiting, M., Wheeler, Q. D., & Carpenter, J. M. (2001). The phylogeny of the extant hexapod orders. *Cladistics*, 17, 113–169.

Wikelski, M., Moskowitz, D., Adelman, J. S., Cochran, J., Wilcove, D. S., & May, M. L. (2006). Simple rules guide dragonfly migration. *Biology Letters*, 2, 325–329.

Wootton, R. & Newman, D. (2008). *Evolution, Diversification, and Mechanics of Dragonfly Wings*. New York, Oxford University Press..

Wootton, R. J. (1991). The functional morphology of the wings in Odonata. *Advanced Odonatologica*, 5, 153–169.

Wootton, R. J. (1992). Functional morphology of insect wings. *Annual Review of Entomology*. 37, 113–140. doi:10.1146/annurev.en.37.010192.000553

Zelditch, M. L., Swiderski, D. L., Sheets, H. D., & Fink, W. L. (2004). *Geometric morphometrics for biologists*: A primer. Amsterdam, Elsevier. doi:10.1016/B978-0-12-778460-1.X5000-5

Zhang, M., Ruan, Y., Wan, X., Tong, Y., Yang, X., & Bai, M. (2019). Geometric morphometric analysis of the pronotum and elytron in stag beetles: insight into its

diversity and evolution. *ZooKeys*, 833, 21–40. https://doi.org/10.3897/zookeys.833.26164

Zhao, H., Yin, Y., & Zhong, Z. (2012). Multi-levels, multi-scales and multi-functions in the fine structure of the wing veins in the dragonfly *Pantala flavescens* (Fabricius) (Anisoptera: Libellulidae). *Odonatologica,* 41, 161–172.

Zhao, W., Liu, H. Y., Ge, X. Y., & Yang, Y. X. (2023). Evaluating the significance of wing shapes in inferring phylogenetic proximity among the generic taxa: an example of Cantharinae (Coleoptera, Cantharidae). *Arthropod Systematics & Phylogeny*, 81, 303–316. https://doi.org/10.3897/asp.81.e101411

Ziemert, N., & Jensen, P. R. (2012). Phylogenetic approaches to natural product structure prediction. *Methods in Enzymology,* 517, 161–182. https://doi.org/10.1016/B978-0-12-404634-4.00008-5

Zikie, V., Stankovie, S. S., Petrovie, A., Milosevie, M. I., Tomanovie, Z., Klingenberg, C. P., & Ivanovie, A. (2017). Evolutionary relationships of wing venation and wing size and shape in Aphidiinae (Hymenoptera: Braconidae). *Organisms Diversity and Evolution*, 17, 607-617. DOI 10.1007/s13127-017-0338-2

Chapter 2

Comparative Gut Bacterial Microbiome Diversity in Selected Dragonfly Species: Migrator vs. Non-migrator

CONTENTS

LIST OF FIGURES

LIST OF TABLES

2

Comparative Gut Bacterial Microbiome Diversity in Selected Dragonfly Species: Migrator vs. Non-migrator

2.1 INTRODUCTION

The host-microbiome is the colonisation of microbes like bacteria, fungi, archaea, and viruses in the mucosal surfaces, such as digestive, respiratory tissues, and urogenital tracts (Woodhams et al., 2020). The bacterial communities associated with the insect gut are a mix of mutualist, pathogenic, and commensal bacteria (Jones et al., 2013). The symbiotic association of the host and microbiome is either endosymbiotic or ectosymbiotic association based on whether the microbiota is living within the host tissue cells or in the lining or lumen of the body cavity walls (Pan, 2020). The microbiome's relationship with its host is complex and will change over time due to external and internal fluctuations (West et al., 2018). Recent advances and developments in molecular and bioinformatics have made the study of gut-associated bacterial taxa and assemblages of insects easier (Morrill et al., 2024).

The gut microorganism and their beneficial association with the host played an essential role in the evolutionary success of the insects (Kaufman & Klug, 1991; Dillon & Charnley, 2002; Engel & Moran, 2013). These insect gut microorganisms are also crucial in many other fields like medicine, agriculture, and ecology (Engel & Moran, 2013). These microbiome plays a significant role in the host's health and fitness (Mueller & Sachs, 2015) and shape the host phenotype (Lynch & Hsiao, 2019). They can regulate the host's innate immunity and affect pathogen or parasite

susceptibility (Koch & Schmid-Hempel, 2012; Cariveau et al., 2014; Li et al., 2017), control the sexual performance, mating preferences, and oviposition of the host (Gavriel et al., 2010; Sharon et al., 2010). The gut microbiota of insects may also harmfully interact with the host (Hurst & Jiggins, 2000). Insects usually generate an immune response against the pathogenic bacteria but can also able to selectively maintain the beneficial microbes (Mikonranta et al., 2014). Some insects like mosquitoes and fruit flies have erratic gut communities with environmental bacteria which even shows variations among individuals (Engel & Moran, 2013; Wong et al., 2013; Bost et al., 2018; Pais et al., 2018) and some insects like termites (Brune & Dietrich, 2015), cockroaches (Tinker & Ottesen, 2016), bees (Kwong & Moran, 2016), and beetles (Ceja-Navarro et al., 2019; Nardi et al., 2006) harbour gut bacterial communities largely restricted to the host gut (Warnecke et al., 2007; Martinson et al., 2011; Anderson et al., 2012; Sudakaran et al., 2012).

The importance of gut microbiota has been tested by conducting many experiments with microbiota lacking animals and found reduced growth and abnormal organ development in germ-free mice (Lee & Hase, 2014); slower development was observed in experiments conducted on germ-free drosophila (Shin et al., 2011). Even a single host gene mutation can alter the microbiome composition and is experimentally tested in mice and fruit flies (Ley et al., 2005; Ryu et al., 2008). Temperature change will also influence the host-gut microbiome relationship both negatively and positively. In some insects, an increase in temperature may reduce some beneficial bacterial communities and increase pathogenic bacterial communities, negatively affecting the host (Khosravi & Mazmanian, 2013). An increase in temperature may also increase heat-tolerant bacterial taxa in some insects that are essential for increasing the heat tolerance in the host (Sepulveda & Moeller, 2020; Sullam et al., 2018). Xenobiotic exposure of the host may also affect the bacterial community composition of the host gut, in which the bacterial species that can degrade the xenobiotics will increase, and those bacteria that are sensitive to the xenobiotics will either decrease in or disappear (Russell et al., 2011). The gut microbiome of insects is studied for many reasons, including conservation and pest/disease management (Crotti et al., 2012).

Dragonflies are generalist predators that feed on various insects and are essential in freshwater and terrestrial invertebrate food webs (Corbet, 1999). As a strong flier, dragonfly catches diverse prey and associated microbes from a broad geographical area; thus, the gut of dragonflies may serve as a reservoir of diverse bacteria (Nair & Agashe, 2016). The gut bacterial richness of the host is associated with its ecological niche, habitat, and predatory ability (Cao & Bu, 2020), and some gut bacteria are obligate symbionts of Odonata (Morrill et al., 2023). Some previous studies on the gut microbiota of adult dragonflies suggest that their microbiome community is more diverse than other carnivorous insects (Deb et al., 2018; Nobles & Jackson, 2020).

The specific lifecycle of insects, holometabolous or hemimetabolous, can also influence the gut microbiome (Price et al., 2011). Odonates are hemimetabolous insects, and thus, they have no pupal stage, which results in high variation in the gut microbial communities of other insects (Minard et al., 2013). Their nymphal stage lives in water, and the adult stage is terrestrial; these differences in their lifestyles may also influence the gut microbiome of the Odonates. The gut microbiome of the nymph and adult life stages of Odonates differ from each other; the gut of an adult dragonfly is dominated by the Gammaproteobacteria and that of dragonfly nymphs are dominated by the Alphaproteobacteria and Betaproteobacteria (Nobles & Jackson, 2020). These differences in the gut microbiome of the nymphs and adult dragonflies are mainly due to the variations in the availability of prey at their two life stages (Deb et al., 2019). There is also a possibility of retaining the whole or part of the gut microbiome of the nymph in adult flies (Nobles & Jackson, 2020)

This chapter studied the gut microbiome of two adult Libellulid dragonflies, *Pantala flavescens* the wandering glider, and *Neurothemis tullia,* the pied paddy skimmer. *N. tullia* is a non-migratory small-sized dragonfly mainly found in rice fields (Asahina et al., 1972) and is one of the significant predators of rice pests that usually predate on smaller prey (Fraser, 1936). The migratory *P. flavescens* is a typical rice field species bigger than *N. tullia*. They are stronger fliers and usually prefer bigger moving prey (Kumar, 1984). *N. tullia* is always found throughout the

year (Heckman, 1979), whereas *P. flavesecens* is a seasonal and migratory species. Both these dragonfly species are good predators of rice pests and can be used as potential biocontrol agents. This study compared the gut-associated bacteria of *P. flavescens* and *N. tullia.* Also, we attempt to compare the bacterial communities between male and female flies.

2.2 REVIEW OF LITERATURE

Many studies on insect gut microbial communities have been conducted to investigate the potential role of microbes and their impact on host ecology and evolution (Rappe & Giovannoni, 2003). The gut microbiota of adult dragonflies has already been studied in some species (Schilder & Marden, 2007; Yun et al., 2014; Nair & Agashe, 2016; Deb et al., 2018). Cao and Bu (2020) studied the gut microbiota in four dragonflies, *P. flavescens, Orthetrum sabina, Coenagrion dyeri,* and *Brachythemis contaminata,* and showed that the dragonfly's gut was rich in microbiota densities and species. Nair and Agashe (2016) analysed the gut microbial communities of eight dragonfly species. They found that host-specific variation was low, but each host species has a distinct bacterial community which is influenced by the sampling location and season. Nobles and Jackson (2020) conducted a detailed study on the effects of species, life stage, and environment on the gut microbiota of 13 dragonfly species, and their study showed that the gut microbiome of metamorphosing insects harbours different gut microbiomes at different life stages. Lim et al. (2023) investigated the gut microbiome of three adult dragonflies, *Pseudothemis zonata*, *Orthetrum lineostigma,* and *Orthetrum melania,* and the influence of host diet and specificity on the gut microbial communities.

Theys et al. (2023) studied the effect of temperature and pesticide on the gut microbiome of two damselflies *Ishnura pumilio* and *Ishnura elegans*. Theys et al. (2023) also studied the role of gut microbiota in pace-of-life differentiation and thermal adaptation in damselfly larvae. Deb et al. (2019) studied the gut bacterial communities of six species of wild dragonflies and their relation with the host dietary specialization and neutral assembly. Colman et al. (2012) conducted a

detailed study on the influence of diet and taxonomy in insect gut-associated bacterial communities.

Shao et al. (2015) isolated gut-associated fungi from *P. flavescens* larvae and studied their diversity, bacterial symbionts, and antibacterial potential. Lu et al. (2016) characterized the compounds of a gut-associated fungus *Aspergillus terreus,* of the dragonfly. Varg et al. (2022) Studied the effect of pollutants on the gut microbiome at different trophic levels by conducting experiments on the planktonic crustacean *Daphnia magna*, damselfly larvae *I. elegans,* and dragonfly larvae *Aeshna cyanea*. Yin et al. (2018) isolated and studied the antifungal metabolites from the fungus *Curvularia crepinii* that reside in the *P. flavescens* gut. Zhang et al. (2020) conducted a detailed study on the *P. flavescens* gut-associated fungus *Trichoderma harzianum*.

Yamaguchi et al. (2018) collected the fecal material from 383 damselflies and conducted a detailed study on the antibiotic-resistant bacteria Enterobacterales. Morrill et al. (2024) studied the gut-associated bacteria in three *Coenagrion* and one *Enallagma* damselfly species. Takashi et al. (2021) investigated the fecal microflora of two dragonfly species *Sympetrum frequens* and *P. flavescens,* and they isolated carotenoid-producing microorganisms from the intestinal microflora of dragonflies.

Many studies have been conducted on the insect gut microbial communities to understand the similarities, differences, and functional role of microbiota, such as in drosophila (Chandler et al., 2011), bumble bees (Cariveau et al., 2014), *Melolontha hippocastani* beetles (Arias-Cordero et al., 2012), butterfly *Heliconius erato* (Hammer et al., 2014), *Plutella xylostella* moth (Xia et al., 2017), Gypsy moth *Lymantria dispar* (Broderick et al., 2004), silkworm *Bombyx mori* (Chen et al., 2018), *Anopheles* mosquitoes (Ngo et al., 2016) etc. Jones et al. (2013) compared the insect gut-associated bacterial communities in 62 insect species from seven orders, and their study showed that insect diet and taxonomy influence the gut microbial community. Yun et al. (2014) characterised the insect gut-associated bacteria of 218 insect species from 21 taxonomic orders, and their study showed that gut bacterial diversity is higher in omnivorous insects than in carnivorous and

herbivorous insects. Dinoto et al. (2022) studied the gut bacterial community of blister beetle *Mylabris pustulata,* and the most abundant phylum in the beetle was found to be Proteobacteria. The bacterial composition and diversity of *Apis nigrocincta* gut were studied by Lombogia et al. (2020). Fredensborg et al. (2020) studied the influence of invading parasites on insect gut microbes and found that these parasites can modulate the gut microbiome. Ferguson et al. (2018) checked the effect of seasonal changes in the environment on insect gut microbiome using *Gryllus veletis* crickets as a model organism. Augustinos et al. (2019) compared the gut-associated bacterial communities in five Tephritid species, namely *Bactrocera oleae*, *Anastrepha grandis*, *Anastrepha ludens*, and two morphotypes of *Anastrepha fraterculus*, and the role of diet, taxonomy, and developmental stage in the gut microbiota.

2.3 MATERIALS AND METHODS

2.3.1 Sample collection and gut dissection

The dragonflies, *P. flavescence* (PF), and *N. tullia* (NT)were collected from the paddy fields of Palakkad district, Kerala, India. Five male (M) and female (F) individuals of both species were collected at noon and immediately before sunset. The collected specimens were immediately preserved in 70% alcohol and stored at -20°C. The whole gut of both species was dissected under a microscope using sterilized dissecting spring scissors and fine forceps and transferred to a clean sterile petri dish. The gut of all individuals of male and female dragonflies was dissected separately. The dissected guts were then transferred to sterilized 2 ml centrifuge tubes and immediately stored at -20°C till DNA extraction. DNA is isolated using the QIAamp Power Pro DNA Kit as per the manufacturer's instructions.

2.3.2 Bioinformatics Analysis

High-quality clean reads were obtained using Trimmomatic v0.38 to remove adapter sequences, ambiguous reads (reads with unknown nucleotides "N" larger than 5%), and low-quality sequences (reads with more than 10% quality threshold (QV) < 25 phred scores) along with a sliding window of 20 bp and a minimum

length of 100 bp. FLASH software was used to stitch the PE data into single-end reads. High-quality clean reads were denoised, and chimeric sequences were filtered through DADA2/Deblur. Taxonomic classification of amplicon sequence variants was performed with the q2-feature classifier using a pre-trained classifier based on the SILVA database (Fig. 2.1).

2.3.3 Alpha and Beta diversity

Diversity metrics of within-sample (alpha diversity) and between-samples (beta diversity) were calculated. Simpson Index, Simpson reciprocal, Shannon Index, and Goods Coverages were used as alpha diversity measures. A distance matrix was calculated to compare microbial communities between samples to reflect the dissimilarity between samples. The data in this distance matrix was visualized with weighted and unweighted Principal Coordinate Analysis (PCoA).

PCoA is a technique that helps to extract and visualise a few highly informative components of variation from complex, multidimensional data. This is a transformation that maps samples present in the distance matrix to a new set of orthogonal axes such that the first principal coordinate explains a maximum amount of variation, the second principal coordinate explains the second largest amount of variation, the principal coordinates can be plotted in two or three dimensions to provide an intuitive visualisation of the data structure and look at differences between the samples, and look for similarities by sample category.

2.3.4 Comparative analysis between the samples

The abundance of gut microbiome of each sample at different taxonomic levels has been represented through pie and krona charts. The comparative analysis between four samples at different taxonomic levels has been represented through stacked bar plots.

2.4 RESULTS

The gut bacterial communities of *P. flavescens* and *N. tullia* were characterised using amplicon sequencing. These two Odonate species' male and female gut bacterial communities were also compared and analysed.

2.4.1 Rarefaction analysis

Rarefactions curves showed the species richness of the four samples, **PFF**, **PFM**, **NTM**, and **NTF**. This is a plot of the number of species as a function of the number of samples. It was performed to a depth of 5000 reads. The curves for all the samples were plateau, indicating a credible number of samples have been taken (Fig. 2.2).

2.4.2 Alpha diversity

The diversity of the bacterial gut microbiome within the samples was determined for all four samples (PFF, PFM, NTF, and NTM). The alpha diversity for the four samples was determined using the Shannon index, Simpson index, Simpson reciprocal, and Goods Coverage (Table 2.1). The gut bacterial communities of *P. flavescens* male showed the highest bacterial richness value (Chao1: 837). The female *N. tullia* exhibited the highest bacterial diversity indices (Shannon Index: 8.33, Simpson Index: 1.00). The bacterial diversity indices observed in the male dragonflies (Shannon index: PFM=7.96, NTM=7.65) were lower than the females (Shannon index: PFF=7.96, NTF=8.33)

Table 2.1: Alpha diversity of the gut bacterial communities

S. No	sample	Shannon Index	Simpson Index	Observed features	Goods Coverage	Simpson Reciprocal	Chao1
1	PFM	7.96	0.99	837	1	160.26	837
2	PFF	7.97	0.99	653	1	183.78	653
3	NTM	7.65	0.99	625	1	70.64	625
4	NTF	8.33	1.00	794	1	224.38	794

2.4.3 Abundance Heatmap

The abundance heatmap was used to display the bacterial abundance distribution of the dominant phylum among all four samples: PFF, PFM, NTF, and NTM (Fig. 2.3). Each row of the heatmap corresponds to the phyla, and each column corresponds to a sample. In the heatmap, the lower relative abundance of particular phyla in a sample is indicated by purple colour, and the higher relative abundance is indicated by red colour in the heatmap.

2.4.4 Beta Diversity

Beta diversity measures the change in gut microbial diversity between samples. Principal coordinate analysis (PCoA) was used to determine the beta diversity of the four samples. The gut bacterial communities of the four samples have not shown any similarities between them, and they are clustered separately. The same species' male and female gut population also shows some dissimilarities (Fig. 2.4).

2.4.5 The similarities and differences of gut microbiota

Venn analysis was used to visualise the shared and unshared features of the gut bacterial microbiota of the samples. Venn diagram analysis showed that NTF had the highest gut bacterial feature number of 545 among all the samples. The male and female of *N. tullia* shared 4 features consisting of approximately 0.4% of all the features (Fig. 2.5B). 5 features were shared by the male and female *P. flavescens,* and the male samples had 528 features (Fig. 2.5A). The total number of features in *N. tullia* was the highest, and the shared features were also below that of the *P. flavescens*. This indicates that *N. tullia* has the highest diversity of gut bacterial communities. The Venn diagram analysis of the four samples showed that no features are shared (Fig. 2.5C).

2.4.6 Taxonomic composition of gut microbiota

A total of 26 phyla were identified in both species. The most abundant taxa at each classification are given in (Table 4.2). The taxonomic classification from the

kingdom to genus level of the gut microbiome of four samples is depicted as Krona graphs (Fig. 2.21, 2.22).

2.4.6.1 Phylum level

The gut bacterial communities of both species are dominated by the phylum Proteobacteria (PFF=55.2%, PFM=61.5%, NTF=51.6%, NTM=54.8%), Firmicutes (PFF=19.8%, PFM=13.9%, NTF=32.3%, NTM=22.9%) and Bacteroidetes (PFF=16.4%, PFM=15.6%, NTF=11.2%, NTM=14.8%). Proteobacteria was highly dominant in *P. flavescens,* with a mean abundance of 58.35%. Actinobacteriota (PFF=0.8%, PFM=1.8%, NTF=3%, NTM=3.9%) is seen in both the dragonfly's gut with less abundance. In the gut of *P. flavescens* Desulfobacterota (PFF=3.7%, PFM=2.3%), Rs-K70_termite_group (PFF=2.9%, 1.5%), and Fusobacteriota (PFF=0.2%, PFM=2.7%) are also seen but with less abundance (Fig. 2.6, 2.7,2.8). All other bacterial phyla in the four gut samples are less than 1%.

2.4.6.2 Class level

At the bacterial class level, Gammaproteobacteria (PFF=48.01%, PFM=55.64%, NTF=42.04%, NTM=33.59%), Bacteroidia (PFF=16.37%, PFM=15.56%, NTF=11.14%, NTM=14.84%), Clostridia (PFF=9.62%, PFM=5.26%, NTF=22.39%, NTM=9.23%), Bacilli (PFF=9.64%, PFM=8%, NTF=7.74%, NTM=12.59%) and Alphaproteobacteria (PFF=7.15%, PFM=5.69%, NTF=9.46%, NTM=21.2%) are dominating in all the four samples. (Fig. 2.9, 2.10, 2.11)

2.4.6.3 Order level

At the order level, Enterobacterales is most dominant in *P. flavescens* (PFF=31.35%, PFM=26.51%), and in *N. tullia* Pseudomonadales is the most dominating order (NTF=13.86%, 18.23%). Bacteroidales and Lactobacillales, are moderately abundant in all four samples. Rickettsiales are more abundant in NTM (16.09%) and Oscillospirales are abundant in NTF (13.83%), but in *P. flavescens,* these are significantly less abundant (below 3%) (Fig. 2.12, 2.13, 2.14).

2.4.6.4 Family level

At the family level, Enterobacteriaceae (PFF=16.63%, PFM=16.14%) is most prevalent in *P. flavescens*, and Moraxellaceae (NTF=13.27%, NTM=16.31%) is most dominant in *N. tullia*. Moraxellaceae is also seen in *P. flavescens* but with less abundance. (Fig. 2.15, 2.16, 2.17)

2.4.6.5 Genus level

At the genus level, *Dysgonomonas* was most dominant in female *P. flavescens* (9.9%), and *Escherichia-Shigella* (9.51%) was the dominant genus in male *P. flavescens*. In *N. tullia Actinobacter* (NTF=13.24%, NTM=16.27%) was the most prevalent bacterial genus. Only the females of *P. flavescens* and *N. tullia* contained the members of the genus Enterobacter and are absent in the males. Members of the genus *Pseudocitrobacter* are present only in female *P. flavescens* and *Ignatzschineria* is present only in female *N. tullia*. Male and female *P. flavescens* and *N. tullia* differ in the gut community richness (Fig. 2.18, 2.19, 2.20).

Table 2.2: Taxonomic hierarchy and relative abundance in different gut samples.

Taxonomy Abundance at Phylum level (Top 5)			
PFF	**PFM**	**NTF**	**NTM**
Proteobacteria (55.22%)	Proteobacteria (61.48%)	Proteobacteria (51.59%)	Proteobacteria (54.84%)
Firmicutes (19.8%)	Bacteroidota (15.56%)	Firmicutes (32.27%)	Firmicutes (22.94%)
Bacteroidota (16.37%)	Firmicutes (13.91%)	Bacteroidota (11.2%)	Bacteroidota (114.84%)
Desulfobacterota (3.71%)	Fusobacteriota (2.74%)	Actinobacteriota (3.02%)	Actinobacteriota (3.85 %)
Rs-K70-termite group (2.93%)	Desulfobacterota (2.25%)	Verrucomicrobiota (0.36%)	Planctomycetota (0.67%)
Taxonomic Abundance at Class level (Top 5)			
PFF	**PFM**	**NTF**	**NTM**
Gammaproteobacteria (48.01%)	Gammaproteobacteria (55.64%)	Gammaproteobacteria (42.04%)	Gammaproteobacteria (33.59%)
Bacteroidia (16.37%)	Bacteroidia (15.56%)	Clostridia (22.39%)	Alphaproteobacteria (21.2%)
Bacilli (9.64%)	Bacilli (8%)	Bacteroidia	Bacteroidia

		(11.14%)	(14.84%)
Clostridia (9.62%)	Alphaproteobacteria (5.69%)	Alphaproteobacteria (9.46%)	Bacilli (12.59%)
Alphaproteobacteria (7.15%)	Clostridia (5.26%)	Bacilli (7.74%)	Clostridia (9.23%)
Taxonomic Abundance at Order level (Top 5)			
PFF	**PFM**	**NTF**	**NTM**
Enterobacterales (31.35%)	Enterobacterales (26.51%)	Pseudomonadales (13.86%)	Pseudomonadales (18.23%)
Bacteroidales (10.92%)	Pseudomonadales (15.89%)	Oscillospirales (13.83%)	Rickettsiales (16.09%)
Lactobacillales (7.74%)	Bacteroidales (7.15%)	Enterobacterales (12.61%)	Lactobacillales (10.62%)
Burkholderiales (5.42%)	Lactobacillales (6.71%)	Cardiobacteriales (5.63%)	Flavobacteriales (7.08%)
Clostridiales (4.54%)	Flavobacteriales (4.96%)	Bacteroidales (5.45%)	Bacteroidales (5.84%)
Taxonomic Abundance at Family level (Top 5)			
PFF	**PFM**	**NTF**	**NTM**
Enterobacteriaceae (16.63%)	Enterobacteriaceae (16.14%%)	Moraxellaceae (13.27%)	Moraxellaceae (16.31%)
Dysgonomonadaceae (9.91%)	Moraxellaceae (11.04%)	Ruminococcaceae (12.81%)	Anaplasmataceae (12.85%)
Yersiniaceae (6.76%)	Dysgonomonadaceae (5.78%)	Wohlfahrtiimonadaceae (5.63%)	Enterococcaceae (7.48%)
Clostridiaceae (4.3%)	Morganellaceae (4.97%%)	Weeksellaceae (4.74%)	Weeksellaceae (4.74%)
Morganellaceae (3.97%)	Pseudomonadacea (4.85%)	Morganellaceae (3.73%%)	Rhodanobacteracea (5.3%)
Taxonomic Abundance at Genus level (Top 1)			
PFF	**PFM**	**NTF**	**NTM**
Dysgonomonas (9.9%)	Escherichia-Shigella (9.51%)	Acinetobacter (13.24%)	Acinetobacter (16.27%)

2.5 DISCUSSION

In this chapter, we compared the gut microbiome of two adult dragonfly species, *P. flavescens* (migratory species) and *N. tullia* (non-migratory species). We also studied the difference between male and female individual gut microbiome communities.

We have collected the *P. flavescens* and *N. tullia* from the same site. Their gut microbial communities have shown significant diversity differences. These differences shown by the two host species could be due to many reasons, such as the host species differences, prey preferences by the two host species, specific selection pressure in the gut environment of the host, host size differences, flying and predatory ability of the host, spatial differences in the distribution of host species, etc. Many previous studies on insect gut microbiome reported that host diet is one of the important determinants in altering the microbiome community of insect's guts such as termites (Mikaelyan et al., 2015), bees (Huang et al., 2018), beetles (Kudo et al., 2018; Kim et al., 2017), *Drosophila melanogaster* (Chandler et al., 2011), and dragonflies (Deb et al., 2019; Lim et al, 2023). *P. flavescens* and *N. tullia* may consume some distinct or similar prey. *P. flavescens* capture large-sized and small-sized prey but, *N. tullia* mostly prefers small prey. *P. flavescens* even predate on other Odonates (Deb et al., 2019), but *N. tullia* is not generally found to do so. Host that prefers distinct prey species will have different gut microbial communities that are acquired passively with the prey (neutral community assembly) and the gut communities of hosts that are consuming similar prey also show differences due to the specific selection pressure in the gut environment of the host (Nair & Agashe, 2016). The availability of prey in different seasons may vary, which is also an important factor determinant of the dragonfly's gut microbiome (Deb et al., 2019).

The host sex also shows variation in the gut microbial community, e.g., the gut microbial community of female bollworms was less diverse than that of males (Priya et al., 2012). The gut microbial communities of male and female *P. flavescens* and *N. tullia* also varied in our study. Nair and Agashe (2016) studied the gut microbial communities of dragonflies. They found that the community richness and composition of male and female dragonflies varied as a function of sampling month and site. The female gut microbiome diversity of adult *Spodoptera littoralis* was more significant than the male adults (Chen et al., 2016). Some bacteria are obligate gut symbionts of Odonates (Morrill et al., 2024).

The gut microbiome of *P. flavescens* and *N. tullia* is dominated by the members of the phylum Proteobacteria; these results were parallel to some previous studies on adult dragonflies (Nair & Agashe, 2016) and other insects (Hamdi et al., 2011; Jones et al., 2013). Proteobacteria is the dominant phylum in insects, and this higher abundance in the insect gut might be due to its ability to invade and proliferate within the host compared to other bacterial groups or due to the active recruitment of Proteobacteria by the host (Jones et al., 2013). In Hymenopteran insects, these Proteobacteria were found to increase the host resistance to pathogenic parasites (Kaltenpoth & Engl, 2014). A study conducted on 81 insect gut samples was also dominated by 57.4% Proteobacteria and 21.7% of Firmicutes (Colman et al., 2012). In the human gut microbiome, these Proteobacteria phyla are associated with diseases (Shin et al., 2017).

The gut of *P. flavescens* is dominated by the family Enterobacteriaceae. Most of the members in this group have a symbiotic association with the insects and contribute a nutritional benefit; they also play a significant role in the defense mechanism against some pathogens (Dillon & Dillon, 2004; Rajagopal, 2008). *Enterobacter* sp. has the anti-Plasmodium effect, producing reactive oxygen species against the *Plasmodium* (Cirimotich et al., 2011). *Enterococcus* is present in *P. flavescens* and *N. tullia*. These *Enterococcus* help lower the gut pH and maintain the alkaline condition of the host gut (Wilson & Benoit, 1993). Genus *Wolbachia* (phylum Alphaproteobacteria, family Rickettsiaceae) is prevalent in many Odonates (Lorenzo-Carballa et al., 2019). *Wolbachia* is present in both *P. flavescens* and *N. tullia* and is more abundant in *N. tullia.* These influence the thermal tolerance, reproductive behavior, nutrition, and insects survival (Lorenzo-Carballa et al., 2019). They can induce male-specific killing, feminization, cytoplasmic incompatibility, and parthenogenesis in the host (Kageyama et al., 2002; Werren et al., 2008).

Local variation in the diet may also influence the host gut bacterial communities; thus, different populations of the same host may show variations in the composition of the gut bacterial community (Nair & Agashe, 2016). We collected *N. tullia* and *P. flavescens* from the same habitat and found differences in the gut

bacterial communities. These differences in microbial communities might be due to dietary specialisation and species differences. Host species differences significantly impacted the gut microbial communities (Cao & Bu, 2020). The study by Nobles and Jackson (2020) showed that the gut microbiome of adult dragonflies is not strongly affected by the sample location and the host species. The gut of larger host species will be richer in bacterial communities (Nair & Agashe, 2016). Even though *N. tullia* is more diminutive than *P. flavescens* there is no such significant difference in the richness of gut bacterial communities observed in our study.

Nair and Agashe (2016) studied the gut bacterial communities of some dragonflies in the South Indian region. They found some rare groups, Oceanospirillales, Rhizobiales, Flavobacteriales, and Aeromonadales, in some dragonflies and were absent in *P. flavescens*. However, in our study, all these bacterial groups were present in the gut of *P. flavescens*. Their role in carnivorous insects is still being determined. Many previous works on gut bacterial communities of Odonates showed a higher abundance of Alphaproteobacteria and Gammaproteobacteria, a moderate abundance of Bacilli, and a weak representation of Actinobacteria (Corbet, 1999; Nobles & Jackson, 2020; Morrill et al., 2023), which is very similar to our data. Nevertheless, in *P. flavescens* and *N. tullia* a moderate representation of Clostridia is also seen.

Hongwei et al. (2023) conducted a detailed study on the relationship between the gut microbial diversity and the wing size of stingless bees, and their results showed that the gut bacterial richness of the bee *Tetragonula carbonaria* is positively correlated to its forewing length. In insects, the wing size is related to its flight performance (Wootton, 1992), foraging, dispersal, and migration (Johansson et al., 2009). *P. flavescens* is a migratory species and is widely distributed; their larger wing size helps to improve their flight performance and foraging, which in turn increases their gut microbial species. As a generalist predator, *P. flavescens* consumes diverse prey with excellent mobility (Cao & Wu, 2019; Larsen, 1981) and in the work of Cao and Bu (2019), they found the highest number of OTUs in *P. flavescens* compared to other three species of dragonflies. *Coenagrion dyeri,* with

the smallest body, had the second-largest number of OTUs in their study: this indicates that the size of the species does not make any significant differences in the gut microbial communities of Odonates. There is a size difference between *P. flavescens* and *N. tullia,* but our data also shows no significant differences in the gut bacterial diversity between them.

Due to its limited spatial movements, *N. tullia* is locally distributed within its breeding habitat (Salmah et al., 2000). Due to their short distance movement and weak fluttering flight (Fraser, 1936), they are always seen in the rice plant areas or the grasses around the rice field. Meanwhile, *P. flavescens* fly over longer distances and are not restricted to their reproductive areas. The small body size of *N. tullia* enables them to hover around rice plants to capture even very small pest species, making them a potential predator in the rice field (Salmah et al., 2000). Both these dragonfly species are good predators of rice fields. After harvesting, these *N. tullia* move to the surrounding grasses of the rice field and consume small prey around there. The distribution of *P. flavescens* in that habitat becomes very low after harvesting, possibly due to the unavailability of large prey. Both species were collected from the paddy fields after harvesting to analyse the gut bacterial microbiome.

A significant difference in the gut microbiome diversity was observed in the dragonfly species *P. flavescens* and *N. tullia*. The shared bacterial communities between these two dragonfly species are different. These differences in the gut microbiome of dragonflies collected from the same site and season might be due to differences in host specificity towards prey. *P. flavescens* usually catch large prey, and *N. tullia* catches small prey. Our data suggest that *P. flavescens* and *N. tullia* have a good diversity of gut microbiome communities and both are good predators of paddy pests. As a strong flier, the widespread distribution of *P. flavescens* makes them an effective predator of significant pests and vectors.

2.6 KEY FINDINGS

- There is a significant difference in the diversity of gut bacterial communities of the two dragonfly species, *P. flavescens* and *N. tullia.*
- Some bacterial group shows specificity towards *P. flavescens* like *Aeromonas, Paraclostridium, Myroides, Pseudocitrobacter, Vagococcus* and *Weissella*. Bacterial genus *Paracoccus, Janthinobacterium*, and *Romboutsia* are specific to *N. tullia*.
- Variation in the abundance of bacterial communities has been observed in the male and female dragonflies.
- Species and diet specificity of the two dragonflies are the major reasons for the variations in the gut-associated bacterial communities in our study because the samples were collected from the same habitat and season.
- The size of the host species has no major role in determining the diversity of the gut-associated microbiome in dragonflies.
- *P. flavescens* and *N. tullia* have a good diversity of microbial communities in their gut, indicating that both these Odonata species are good predators of paddy pests.
- Quantitative predatory potential assessment between two species needs to be explored in the future.

2.7 REFERENCES

Anderson, K. E., Russell, J. A., Moreau, C. S., Kautz, S., Sullam, K. E., Hu, Y. I., … & Wheeler, D. E. (2012). Highly similar microbial communities are shared among related and trophically similar ant species. *Molecular Ecology*, 21, 2282–2296.

Arias-Cordero, E., Ping, L., Reichwald, K., Delb, H., Platzer, M., & Boland, W. (2012). Comparative evaluation of the gut microbiota associated with the below- and above-ground life stages (larvae and beetles) of the forest Cockchafer, *Melolontha hippocastani. PLoS ONE*, 7(12).

Asahina, S., Wongsiri, T., & Nagatomi, A. (1972). The paddy field Odonata taken at Bangkhen, Bangkok. *Mushi,* 46, 107-109.

Augustinos, A. A., Tsiamis, G., Caceres, C., Abd-Alla, A. M. M., & Bourtzis, K. (2019). Taxonomy, diet, and developmental stage contribute to the structuring of gut-associated bacterial communities in Tephritid pest species. *Frontiers of Microbiology*, 10. https://doi.org/10.3389/fmicb.2019.02004

Bost, A., Martinson, V. G., Franzenburg, S., Adair, K. L., Albasi, A., Wells, M. T., & Douglas, A. E. (2018). Functional variation in the gut microbiome of wild *Drosophila* populations. *Molecular Ecology*, 27, 2834-2845. https://doi.org/10.1111/mec.14728.

Broderick, N. A., Raffa, K. F., Goodman, R. M., & Handelsman, J. (2004). Census of the bacterial community of the gypsy moth larval midgut by using culturing and culture-independent methods. *Applied and Environmental Microbiology*, 70(1), 293-300.

Brune, A., & Dietrich, C. (2015). The Gut microbiota of termites: digesting the diversity in the light of ecology and evolution. *Annual Review of Microbiology*. 69, 145-166.

Cao, L. & Bu, X. (2020). The composition and interaction of the gut microbiota in four species of wild dragonflies. *Annals of Applied Microbiology and Biotechnology Journal*, 4. https://dx.doi.org/10.36876/apmbj607280

Cao, L., & Wu, K. (2019). Genetic diversity and demographic history of globe skimmers (Odonata: Libellulidae) in China based on microsatellite and mitochondrial DNA markers. *Scientific Reports*, 9,8619.

Cariveau, D. P., Powell, J. E., Koch, H., Winfree, R., & Moran, N. A. (2014). Variation in gut microbial communities and its association with pathogen infection in wild bumble bees (Bombus). *ISME Journal*, 8(12), 2369-79. DOI: 10.1038/ismej.2014.68

Ceja-Navarro, J. A., Karaoz, U., Bill, M., Hao, Z., White III, R. A., Arellano, A., … & Brodie, E. L. (2019). Gut anatomical properties and microbial functional assembly promote lignocellulose deconstruction and colony subsistence of a wood-feeding beetle. *Nature Microbiology*, 4, 864-875. https://doi.org/10.1038/s41564-019-0384-y.

Chandler, J. A., Lang, J. M., Bhatnagar, S., Eisen, J. A., & Kopp, A. (2011). Bacterial communities of diverse *Drosophila* species: ecological context of a host-microbe model system. *PLoS Genetics*, 7(9). https://doi.org/10.1371/journal.pgen.1002272

Chen, B., Teh, B. S., Sun, C., Hu, S., Lu, X., Boland, W., & Shao, Y. (2016). Biodiversity and activity of the gut microbiota across the life history of the insect herbivore *Spodoptera littoralis*. *Scientific Reports*, 6, 29505. DOI: 10.1038/srep29505

Chen, B., Yu, T., Xie, S., Du, K., Liang, X., Lan, Y., … & Shao, Y. (2018). Comparative shotgun metagenomic data of the silkworm *Bombyx mori* gut microbiome. *Scientific Data,* 5, 180285. https://doi.org/10.1038/sdata.2018.285

Cirimotich, C. M., Dong, Y., Clayton, A. M., Sandiford, S. L., Souza-Neto, J. A., Mulenga, M., & Dimopoulos, G. (2011). Natural microbe-mediated refractoriness to Plasmodium infection in *Anopheles gambiae*. *Science*, 332(6031), 855-858. doi: 10.1126/science.1201618

Colman, D. R., Toolson, C. D., & Vesbach, T. (2012). Do diet and taxonomy influence insect gut bacterial communities? *Molecular Ecology*, 21(20), 5124-5137. https://doi.org/10.1111/j.1365-294X.2012.05752.x

Corbet, P. S. (1999). *Dragonflies: behaviour and ecology of Odonata*. Revised. Colchester, Harley Books.

Crotti, E., Balloi, A., Hamdi, C., Sansonno, L., Marzorati, M., Gonella, E., ... & Daffonchio, D. (2012). Microbial symbionts: a resource for the management of insect related problems. *Microbial Biotechnology*, 5, 307-317.

Deb, R., Nair, A., & Agashe, D. (2019). Host dietary specialization and neutral assembly shape gut bacterial communities of wild dragonflies. *Peer J* ,7, e8058. http://doi.org/10.7717/peerj.8058

Dillon, R. & Charnley, K. (2002). Mutualism between the desert locust *Schistocerca gregaria* and its gut microbiota. *Research in Microbiology*, 153(8), 503-509. https://doi.org/10.1016/S0923-2508(02)01361-X

Dillon, R. J., & Dillon, V. M. (2004). The gut bacteria of insects: nonpathogenic interactions. *Annual Reviews in Entomology*, 49, 71-92. https://doi.org/10.1146/annurev.ento.49.061802.123416

Dinoto, A., Noviana, Z., Efendy, O., & Julistiono, H. (2022). Metagenomic analysis of bacterial community in the gut of blister beetle *Mylabris pustulata* Thunberg. *Journal of Mathematical and Fundamental Sciences*, 54(1), 190-210.

Engel, P., & Moran, N. A. (2013). The gut microbiota of insects - diversity in structure and function. *FEMS Microbiology Reviews,* 37(5), 699-735. https://doi.org/10.1111/1574-6976.12025

Ferguson, L. V., Dhakal, P., Lebenzon, J. E., Heinrichs, D. E., Bucking, C., & Sinclair, B. J. (2018). Seasonal shifts in the insect gut microbiome are concurrent with changes in cold tolerance and immunity. *Functional Ecology*, 32(10), 2357-2368. https://doi.org/10.1111/1365-2435.13153

Fraser, F. C. (1936). *The Fauna of British India Including Ceylon and Burma: Odonata*. Vol III. Fleet Street, London.

Fredensborg, B. L., Kalvalio, I. F. I., Johannesen, T. B., Stensvold, B., Nielsen, H. V., & Kapel, C. M. O. (2020). Parasites modulate the gut-microbiome in insects: A proof-of-concept study. *PLoS ONE*, 15(1). https://doi.org/10.1007/978-981-15-7360-6_18

Gavriel, S., Jurkevitch, E., Gazit, Y., & Yuval, B. (2010). Bacterially enriched diet improves sexual performance of sterile male Mediterranean fruit flies. *Journal of Applied Entomology*, 135(7), 564-573. https://doi.org/10.1111/j.1439-0418.2010.01605.x

Hamdi, C., Balloi, A., Essanaa, J., Crotti, E., Gonella, E., Raddadi, N., … & Manino, A., (2011). Gut microbiome dysbiosis and honeybee health. *Journal of Applied Entomology*, 135, 524–533.

Hammer, T. J., McMillan, W. O., & Fierer, N. (2014) Metamorphosis of a butterfly-associated bacterial community. *PLoS ONE*, 9(1), e86995.

Heckman, C.W. (1979). *Rice field ecology in northeastern Thailand*. Junk, the Hague.

Huang, S. K., Ye, K. T., Huang, W. F., Ying, B. H., Su. X., Lin, L. H., … & Hu, J. Z. (2018). Influence of feeding type and *Nosema ceranae* infection on the gut microbiota of *Apis cerana* workers. *mSystems*, 3(6). https://doi.org/10.1128/mSystems.00177-18

Hurst, G. D., & Jiggins, F. M. (2000). Male-killing bacteria in insects: mechanisms, incidence, and implications. *Emerg. Infect. Dis*. 6, 329–336. http://dx.doi.org/10.3201/eid0604.000402

Johansson, F., Soderquist, M., & Bokma, F., (2009). Insect wing shape evolution: independent effects of migratory and mate guarding flight on dragonfly wings. *Biological Journal of Linnean Society*, 97(2), 362–372. https://doi.org/10.1111/j.1095-8312.2009.01211.x.

Jones, R. T., Sanchez, L. G., & Fierer, N. (2013). A cross-taxon analysis of insect-associated bacterial diversity. *PLoS ONE*, 8(4), e61218.

Kageyama, D., Nishimura, G., Hoshizaki, S., & Ishikawa, Y. (2002). Feminizing *Wolbachia* in an insect, *Ostrinia furnacalis* (Lepidoptera: Crambidae). *Heredity,* 88, 444–449.

Kaltenpoth, M., & Engl, T. (2014). Defensive microbial symbionts in Hymenoptera. *Functional Ecology*, 28(2), 315–327. https ://doi.org/10.1111/1365-2435.12089.

Kaufman, M. G., & Klug, M. J. (1991). The contribution of hindgut bacteria to dietary carbohydrate utilization by crickets (Orthoptera: Gryllidae). *Comparative Biochemistry and Physiology*, 98(1), 117-123. https://doi.org/10.1016/0300-9629(91)90588-4

Khosravi, A., & Mazmanian, S. K. (2013). Disruption of the gut microbiome as a risk factor for microbial infections. *Current Opinion in Microbiology*. 16, 221–227. https://doi.org/10.1016/j.mib. 2013.03.009

Kim, J. M., Choi, M. Y., Kim, J. W., Lee, S.A., Ahn, J. H., Song, J., … & Weon, H. Y. (2017). Effects of diet type, developmental stage, and gut compartment in the gut bacterial communities of two *Cerambycidae species* (Coleoptera). *Journal of Microbiology*, 55(1), 21–30. https://doi.org/10.1007/s12275-017-6561-x

Koch, H., & Schmid-Hempel, P. (2012). Gut microbiota instead of host genotype drive the specificity in the interaction of a natural host-parasite system. *Ecological Letters*, 15(10), 1095-1103. https://doi.org/10.1111/j.1461-0248.2012.01831.x

Koyanagi, T., Maoka, T. & Misawa, N. (2021). Fecal microflora from dragonflies and its microorganisms producing carotenoids. *Carotenoids: Biosynthetic and Biofunctional Approaches. Advances in Experimental Medicine and Biology*, 1261, 209-216. https://doi.org/10.1007/978-981-15-7360-6_18

Kudo, R., Masuya, H., Endoh, R., Kikuchi, T., & Ikeda, H. (2018). Gut bacterial and fungal communities in ground-dwelling beetles are associated with host food habit and habitat. *The ISME Journal*, 13(3), 676–685. https://doi.org/10.1038/s41396-018-0298-3

Kumar, A. (1984). On the life history of *Pantala flavescens* (Fabricius) (Odonata:Libellulidae). *Annals of Entomology*, 2, 43-50.

Kwong, W. K. & Moran, N. A. (2016). Gut microbial communities of social bees. *Nat. Rev. Microbiol.* 14, 374-384. https://doi.org/10.1038/nrmicro.2016.43

Larsen, T. B. (1981). Butterflies as prey for *Orthetrum austenti* (Kirby) (Anisoptera: Libellulidae). *Notulae Odonatologicae*, 1(8), 130-133.

Lee, W. J., & Hase, K. (2014). Gut microbiota-generated metabolites in animal health and disease. *Nature Chemical Biology*, 10(6), 416–424.

Ley, R. E., Backhed, F., Turnbaugh, P., Lozupone, C. A., Knight, R. D., & Gordon, J. I. (2005). Obesity alters gut microbial ecology. *Proceedings of the National Academy of Sciences of the United States of America*, 102(31), 11070–11075.

Li, J. H., Evans, J. D., Li, W. F., Zhao, Y. Z., DeGrandi-Hoffman, G., Huang, S. K., Li, Z. G., … & Chen, Y. P. (2017). New evidence showing that the destruction of gut bacteria by antibiotic treatment could increase the honey bee's vulnerability to *Nosema* infection. *PLoS ONE*, 12(11). https://doi.org/10.1111/j.1461-0248.2012.01831.x

Lim, S. H., Park, J. K., Park, W. B., Won, D. H., Kim, M. S., Hong, S. & Do, Y. (2023). Gut microbiome of three species of Odonata. *Entomological Research*, 53(4), 167-172. https://doi.org/10.1111/1748-5967.12641

Lombogia, C. A., Tulung, M., Posangi, J., & Tallei, T. E. (2020). Bacterial Composition, Community Structure, and Diversity in *Apis nigrocincta* Gut. *International Journal of Microbiology*, https://doi.org/10.1155/2020/6906921

Lorenzo-Carballa, M. O., Torres-Cambas, Y., Heaton, K., Hurst, G. D. D., Charlat, S., Sherratt, T. N., … & Beatty, C. D., (2019). Widespread *wolbachia* infection in an insular radiation of damselflies (Odonata, Coenagrionidae). *Scientific Reports*, 9, 1–13. https://doi.org/10.1038/s41598-019-47954-3.

Lu, Y. H., Jin, L. P., Kong, L. C., & Zhang, Y. L. (2016). Phytotoxic, antifungal and immunosuppressive metabolites from *Aspergillus terreus* QT122 isolated from the gut of dragonfly. *Current Microbiology*, 74, 84-89. DOI 10.1007/s00284-016-1157-y

Lynch, J. B., & Hsiao, E.Y. (2019). Microbiomes as sources of emergent host phenotypes. *Science*. 365, 1405–1409. https://doi.org/10.1126/science.aay0240.

Martinson, V. G., Danforth, B. N., Minckley, R. L., Rueppell, O., Tingek, S., & Moran, N. A. (2011). A simple and distinctive microbiota associated with honey bees and bumble bees. *Molecular Ecology*, 20(9), 619–628. https://doi.org/10.1111/j.1365-294X.2011.05464.

Mikaelyan, A., Dietrich, C., Kohler, T., Poulsen M., Sillam-Dusses, D., & Brune, A. (2015). Diet is the primary determinant of bacterial community structure in the guts of higher termites. *Molecular Ecology*, 24(20), 5284–95. https://doi.org/10.1111/mec.13376.

Minard, G., Mavingui, P., & Moro, C. V. (2013). Diversity and function of bacterial microbiota in the mosquito holobiont. *Parasites & Vectors*, 6, 146. doi: doi.org/10.1186/1756-3305-6-146

Morrill, A., Forbes, M. R., Vesterinen, E. J., Tamminen, M., Saaksjarvi, I. E., & Kaunisto, K. M. (2024). Molecular characterisation of faecal bacterial assemblages among four species of syntopic Odonates. *Microbial Ecology*, 87(16). https://doi.org/10.1007/s00248-023-02328-1

Mueller, U. G., & Sachs, J. L. (2015). Engineering microbiomes to improve plant and animal health. *Trends Microbiol*. 23(10), 606–617. DOI: 10.1016/j.tim.2015.07.009

Nair, A., & Agashe, D. (2016). Host-specific spatial and temporal variation in culturable gut bacterial communities of dragonflies. *Current Science*, 110(8), 1513-1523. doi: 10.18520/cs/v110/i8/1513-1523

Nardi, J. B., Bee, C. M., Miller, L. A., Nguyen, N. H., Suh, S. O., & Blackwell, M. (2006). Communities of microbes that inhabit the changing hindgut landscape of a subsocial beetle. *Arthropod Structure & Development*. 35, 57-68. https://doi.org/10.1016/j.asd.2005.06.003.

Ngo, C. T., Romano-Bertrand, S., Manguin, S. & Jumas-Bilak, E. (2016). Diversity of the bacterial microbiota of Anopheles mosquitoes from Binh Phuoc Province, Vietnam. *Frontiers in Microbiology*, 7, 2095. doi: 10.3389/fmicb.2016.02095

Nobles, S., & Jackson, C. R. (2020). Effects of life stage, site, and species on the dragonfly gut microbiome. *Microorganisms,* 8. https://doi.org/10. 3390/microorganisms8020183

Pais, I. S., Valente, R. S., Sporniak, M., & Teixeira, L. (2018). Drosophila melanogaster establishes a species-specific mutualistic interaction with stable gut-colonizing bacteria. *PLoS Biol*. 16, e2005710. https://doi.org/10.1371/journal.pbio.2005710.

Pan, X., Wang, X., & Zhang, F. (2020). New insights into cockroach control: using functional diversity of *Blattella germanica* symbionts. *Insects*, 11, 696.

Price, P. W., Denno, R. F., Eubanks, M. D., Finke, D. L., & Kaplan, I. (2011). *Insect ecology: Behavior, Populations and Communities.* Cambridge University Press.

Priya, N. G., Ojha, A., Kajla, M. K., Raj, A., & Rajagopal, R. (2012). Host plant induced variation in gut bacteria of *Helicoverpa armigera*. *PLoS ONE*, 7. https://doi.org/10.1371/journal.pone.0030768

Rajagopal, R. (2009). Beneficial interactions between insects and gut bacteria. *Indian Journal of Microbiology*, 49(2), 114-119. doi: 10.1007/s12088-009-0023-z

Rappe, M. S. & Giovannoni, S. J. (2003). The uncultured microbial majority. *Annual Review of Microbiology*, 57, 369-394. DOI: 10.1146/annurev.micro.57.030502.090759

Russell, R. J., Scott, C., Jackson, C. J., Pandey, R., Pandey, G., Taylor, M. C., … & Oakeshott, J. G. (2011). The evolution of new enzyme function: lessons from xenobiotic metabolizing bacteria versus insecticide-resistant insects. *Evolutionary Applications*, 4(2), 225-248. https://doi.org/10.1111/j.1752-4571.2010.00175.x

Ryu, J. H., Kim, S. H., Lee, H. Y., Bai, J. Y., Nam, Y. D., Bae, J. W., … & Lee, W. J. (2008). Innate immune homeostasis by the homeobox gene Caudal and commensal-gut mutualism in Drosophila. *Science,* 319(5864), 777–782. DOI: 10.1126/science.1149357

Salmah, M. R. C., Hassan, S. T. S., & Hassan, A. A. (2000). Local movement and feeding pattern of adult *Neurothemis tullia* (Drury) (Odonata: Libellulidae) in a rain fed rice field. *Tropical Ecology*, 41(2), 233-241.

Schilder, R. J., & Marden, J. H. (2007). Metabolic syndrome in insects triggered by gut microbes. *Journal of Diabetes Science and Technology*, 1, 794-796.

Sepulveda, J., & Moeller, A. H. (2020). The effects of temperature on animal gut microbiomes. *Front. Microbiol*. 11, 1–9. https://doi.org/10.3389/fmicb.2020.00384.

Shao, M. W., Lu, Y. H., Miao, S., Zhang, Y., Chen, T. T., & Zhang, Y. L. (2015). Diversity, bacterial symbionts and antibacterial potential of gut-associated fungi isolated from the *Pantala flavescens* larvae in China. *PLoS ONE*, 10(7). doi: 10.1371/journal.pone.0134542

Sharon, G., Segal, D., Ringo, J. M., Hefetz, A., Zilber-Rosenberg, I., & Rosenberg, E. (2010) Commensal bacteria play a role in mating preference of *Drosophila melanogaster*. *Proceedings of the National Academy of Sciences*, 107(46), 20051–20056.

Shin, N. R., Whon, T. W., & Bae, J. W. (2015). Proteobacteria: microbial signature of dysbiosis in gut microbiota. *Trends in biotechnology*, 33(9), 496-503. DOI: 10.1016/j.tibtech.2015.06.011

Shin, S. C., Kim, S. H., You, H., Kim, B., Kim, A. C., Lee, K. A., … & Lee, W. J. (2011). Drosophila microbiome modulates host developmental and metabolic homeostasis via insulin signaling. *Science,* 334(6056), 670–674.

Sudakaran, S., Salem, H., Kost, C., & Kaltenpoth, M. (2012). Geographical and ecological stability of the symbiotic mid-gut microbiota in European firebugs, *Pyrrhocoris apterus* (Hemiptera, Pyrrhocoridae). *Molecular Ecology*, 21(24), 6134–6151. DOI: 10.1111/mec.12027

Sullam, K. E., Pichon, S., Schaer, T. M. M., & Ebert, D. (2018). The combined effect of temperature and host clinal line on the microbiota of a planktonic crustacean. *Microbial Ecology*. 76, 506–517. https://doi.org/10.1007/s00248-017-1126-4.

Theys, C., Verheyen, J., Delnat, V., Janssens, L., Tuzun, N., & Stoks, R. (2023). Thermal and latitudinal patterns in pace-of-life traits are partly mediated by the gut microbiome. *Science of the Total Environment*, 855, 158829. https://doi.org/10.1016/j.scitotenv.2022.158829

Theys, C., Verheyen, J., Janssens, L., Tuzun, N., & Stoks, R. (2023). Effects of heat and pesticide stress on life history, physiology and the gut microbiome of two congeneric damselflies that differ in stressor tolerance. *The Science of the total environment*, *875*, 162617. https://doi.org/10.1016/j.scitotenv.2023.162617

Tinker, K. A., & Ottesen, E. A. (2016). The core gut microbiome of the American cockroach, *periplaneta americana*, is stable and resilient to dietary shifts. *Applied and Environmental Microbiology*. 82, 6603-6610. https://doi.org/10.1128/AEM.01837-16.

Varg, J. E., Outomuro, D., Kunce, W., Kuehrer, L., Svanback, R., & Johansson, F. (2022). Microplastic exposure across trophic levels: effects on the host–microbiota of freshwater organisms. *Environmental Microbiome,* 17, 36. https://doi.org/10.1186/s40793-022-00429-x

Warnecke, F., Luginbuhl, P., Ivanova, N., Ghassemian, M., Richardson, T. H., Stege, J. T., … & Leadbetter, J. R. (2007). Metagenomic and functional analysis of hindgut microbiota of a wood-feeding higher termite. *Nature,* 450, 560–565.

Werren, J. H., Baldo, L., & Clark, M. E. (2008). *Wolbachia*: master manipulators of invertebrate biology. *Nature Reviews Microbiology,* 6, 741.

West, A. G., Waite, D. W., Deines, P., Bourne, D. G., Digby, A., McKenzie, V. J., & Taylor, M. W. (2019). The microbiome in threatened species conservation. *Biological Conservation*, 229, 85-98.

Wilson, G. R., & Benoit, T. G. (1993). Alkaline pH activated *Bacillus thuringiensis* spores. *Journal of Invertebrate Pathology*, 62(1), 87–89.

Wong, AC-N., Chaston, J. M., & Douglas, A.E. (2013). The inconstant gut microbiota of *Drosophila* species revealed by 16S rRNA gene analysis. *ISME Journal*, 7, 1922–1932.

Woodhams, D. C., Bletz, M. C., Becker, C. G., Bender, H. A., Buitrago-Rosas, D., Diebboll, H., ... & Whetstone, R. (2020). Host-associated microbiomes are predicted by immune system complexity and climate. *Genome biology*, 21, 1-20. doi: 10.1186/s13059-019-1908-8.

Wootton, R.J., (1992). Functional morphology of insect wings. *Annual Review Entomology*, 37(1), 113–140. https://doi.org/10.1146/annurev.en 37.010192.000553.

Xia, X., Gurr, G. M., Vasseur, L., Zheng, D., Zhong, H., Qin, B., … & You, M. (2017). Metagenomic sequencing of diamondback moth gut microbiome unveils key holobiont adaptations for herbivory. *Frontiers in Microbiology*, 8, 663. doi: 10.3389/fmicb.2017.00663

Yamaguchi, Y., Okubo, T., Matsushita, M., Wataji, M., Iwasaki, S., Hayasaka, K., … & Yamaguchi, H. (2018). Analysis of adult damselfly fecal material aids in the estimation of antibiotic resistant Enterobacterales contamination of the local environment. *PeerJ*, 6. DOI 10.7717/peerj.5755

Yin, C., Jin, L., Sun, F., Xu, X., Shao, M., & Zhang, Y. (2018). Phytotoxic and Antifungal Metabolites from *Curvularia crepinii* QTYC-1 Isolated from the Gut of *Pantala flavescens*. *Molecules*, 23, 951. doi:10.3390/molecules23040951

Yun, J. H., Roh, S. W., Whon, T. W., Jung, M. J., Kim, M. S., Park, D. S., ... & Kim, J. Y. (2014). Insects gut bacterial diversity determined by host environmental habitat, diet, developmental stage and phylogeny. *Applied and Environmental Microbiology*, 80, 5254-5264.

Zhang, S., Sun, F., Liu, L., Bao, L., Fang, W., Yin, C., & Zhang, Y. (2020). Dragonfly-associated *Trichoderma harzianum* QTYC77 is not only a potential biological control agent of *Fusarium oxysporum* f. sp. *cucumerinum* but also a source of new antibacterial agents. *Journal of agricultural and food chemistry*, 68, 14161-14167. https://dx.doi.org/10.1021/acs.jafc.0c05760

Chapter 3

Exploring Embryonic, Post-embryonic, and Predatory potential of the Wandering Glider, *Pantala flavescens*

CONTENTS

LIST OF FIGURES

LIST OF TABLES

3

Exploring Embryonic, Post-embryonic, and Predatory potential of the Wandering Glider, *Pantala flavescens*

3.1 INTRODUCTION

Odonates are hemimetabolous insects, and with three distinct life stages (egg, naiad, and adult), the dragonfly naiads show the most incredible diversity in functional morphology (Suhling et al., 2015). The naiad stages of Odonata varies from a few weeks to several years, and adult life lasts only a few months (Jose & Chandran, 2020). *Pantala flavescens* complete their egg and naiad development within 50 days (Hawking & Ingram, 1994). *P. flavescens*, the wandering glider or globe skimmer, is a widely distributed migratory species (Christudhas & Mathai, 2014).

The eggs of dragonflies are mainly included in endophytic and exophytic eggs, based on their deposition of eggs into plants or in water (Hinton, 1981). *P. flavescens* exhibits an exophytic mode of oviposition, and the eggs are oval/spheroid a common feature of exophytic eggs (Corbet, 1999; Andrew, 2011). Many Libellulid females lay their eggs in small clusters during flight by making intermittent contact with the water surface (Miller, 1987). *P. flavescens* lay eggs in different open water sources, such as rice paddy fields, small ponds, swimming pools, and puddles, by stopping over during migration flight (Hawking & Ingram, 1994; Ichikawa, 2016). The oviposition site selection behaviour of dragonflies can be used as a bioindicator

tool for assessing anthropogenic impacts on the environment (Rodrigues et al., 2018).

In insects, post-embryonic development is the period from hatching to the emergence of adult insects. It consists of a series of structural developments and differentiations that give rise to the adult organism (Lerum, 1968). The dragonfly naiads can occupy different habitats as they are highly diverse in naiad form and behaviour (Suhling et al., 2015). The number of naiad instars is not the same in all Odonate species; it varies within and between species and ranges from 9 to 15 instars (Subramanian, 2005). The head region of the dragonfly naiad bears the compound eyes, three ocelli, antennae, and mouthparts; the thorax has three pairs of legs and wing sheaths in late instars; and ten abdominal segments (Tillyard, 1917; Suhling et al., 2015). They are mandibulate insects with large, extendable labium, a unique anatomical feature of the naiads of Odonata (Tennessen, 2019). Their prehensile, protractile labium helps to capture the prey (Resh & Carde, 2009). The naiad and adult dragonflies ventilate their gas exchange system by rhythmic abdominal pumping movements; the naiads tidally ventilate their rectal gill with water, while the adult uses its abdominal spiracles to pump the air into its tracheal system (Ubhi & Matthews, 2018).

The naiads of dragonflies are generalist predators; their prey includes many aquatic insects like mosquito larvae, crustaceans, molluscs, protozoans, oligochaetes, hemipterans, mayflies, some small larval fishes and amphibians, and the predators of dragonfly naiads include fish, frog, other naiads of Odonata, aquatic beetles and hemipterans (Resh & Carde, 2009). The dietary preference of dragonfly naiads includes a wide variety of prey (Akre & Johnson, 1979; Corbet, 1980; Travis et al., 1985) and thus they regulate the community structure and abundance of different species in water bodies (Stav et al., 2005). These are more aggressive towards the con- or hetero-specifics (Rowe, 1980; Baker, 1981). Different foraging modes are seen in Odonatan naiads: active foraging, sit-and-wait predation, and visual, and tactile prey detection (Sherk, 1977). Predator-prey interaction influences the diversity and abundance of many prey communities (Sih et al., 1985), and this

interaction is a crucial agent of control group selection for many species (Weis et al., 1992).

Dragonflies and damselflies have proved to be the potential biocontrol agents of mosquitoes and rice pests worldwide (Sathe & Shinde, 2016) and play a significant role in the wetland ecosystem (Subramanian, 2005). Urbanization and improper management of domestic and other polluted water have led to many mosquito breeding sites, resulting in the spread of many mosquito-borne diseases like chikungunya, dengue, filariasis, Japanese encephalitis, etc. (Shad & Andrew, 2013). Nevertheless, we always depend on chemical insecticides to control such vectors. The continuous use of chemical insecticides and pesticides causes insecticide resistance in insect pests, environmental pollution, and also adversely affects non-target organisms (Lee et al., 2001). Instead of using such harmful insecticides, we can make use of some predators and parasites of vectors to control their population. Dragonflies (both naiads and adult) are one of the primary predators of mosquitoes (Corbet, 1980), and they are often referred to as "mosquito hawks" (Kenny & Burne, 2001). The eyes and mechanoreceptors of the naiads of Odonata play an important role in detecting prey and capturing them with the labium or labial palps (Mandal et al., 2008; Nasrabadi et al., 2022). The naiads of Odonata can be used in temporary or control group habitats as a potential biocontrol agent in regulating the larval population of vector mosquitoes (Mandal et al., 2008).

Most growth and development during the naiad stages in Odonata is essential for adult fitness (Hyeun-Ji, & Johansson, 2015). The size of the dragonfly also influences its fitness, which is influenced by the naiad's ecology (Sokolovska et al., 2000). The naiads of Odonata reared under laboratory conditions have been used to conduct many studies. Reared naiads are mainly used to document the instar stages and anatomical features, developmental patterns, factors influencing growth, predator-prey interactions, behavioural and physiological responses, effects of toxicants, etc. (Rice, 2008). Nutrient conditions of the naiads are essential for rearing potential biocontrol agents like dragonflies in the laboratory. Insufficient nutrients will lead to a high death rate and cannibalism of dragonfly naiads.

This chapter includes the embryonic development, post-embryonic development, and predatory potential studies of the dragonfly *P. flavescens*. The embryonic development of *P. flavescens* was described by mainly focusing on the easily recognisable features of the transparent egg. Every stage of embryonic development was studied without destroying the egg, and we divided the embryonic development of *P. flavescens* into eight stages. The post-embryonic developmental studies were also conducted under laboratory conditions. We developed a new mass-rearing technique for the wandering glider *P. flavescens* with controlled or no cannibalism by preparing a Special nutrient solution and given as an extra source of nutrition in addition to other foods. The predatory potential of *P. flavescens* naiads over the filarial vector, *Culex quinquefasciatus* larvae, was also studied.

3.2 REVIEW OF LITERATURE

Tillyard conducted a detailed study on the biology of dragonflies in 1917. Miyakawa (1987, 1990) conducted an elaborate work on embryo rotation within the eggs of dragonflies and compared the germ rudiment position inside different dragonfly's eggs. Sahlen and Suhling (2002) studied the relationship between clutch size and egg size among species of Sympetrinae. A detailed study on the ultrastructural post-oviposition changes in the egg chorion was conducted in some of the dragonflies (Ivey et al., 1988), in *Ictinogomphus rapax* (Andrew & Tembhare, 1992), *Aeshna juncea* (Sahlen, 1994), *Zyxomma petiolatum* (Andrew & Tembhare, 1995), *Tramea virginia* (Andrew, 2002), *Libellula depressa* (Gaino et al., 2008), in *Brachydiplax sobrina* and *Orthetrum sabina* (Andrew, 2009), *P. flavescens* (Andrew et al., 2011), *Micrathyria dictynna* (Andrew & Foerster, 2015). May (1995) conducted a comparative study on the micropyle structure of Libelluloid and Cordulegastroid dragonflies.

Hemimetabolous insects show blastokinesis during their embryonic development, and it includes mainly three embryonic movements, anatrepsis, intertrepsis, and katatrepsis (Masumoto & Machida, 2006; Panfilio, 2008; Donoughe & Extavour, 2016). The embryonic and larval developmental studies of *Sympetrum danae* were carried out by Waringer in 1983. Hottenbacher and Koch (2006) studied

the influence of egg size on the egg and naiad development of the dragonfly *Sympetrum striolatum*.

Mass rearing of dragonflies and releasing them into the agroecosystem, forest ecosystem, and wetland ecosystem is a very effective biological control method for many insect pests and vectors. Rowe (1991) reared the dragonfly *Hemianax papuensis* under laboratory conditions. Gossum et al. (2003) demonstrated difficulties in rearing experiments under laboratory conditions. Rice (2008) reviewed the laboratory-rearing methods of dragonfly naiads and described a new design for the short-term maintenance of Libelluid naiads. Sathe (2013) reared dragonflies in a glass aquarium and developed the mass culture methods of different prey (paramecium, daphnia, and mosquitoes) of dragonfly naiads in laboratory conditions. Piersanti et al. (2015) described a protocol to obtain at least three generations of *Ischnura elegans* in laboratory conditions. Okude et al. (2017) developed a laboratory-rearing system for the blue-tailed damselfly, *Ishnura senegalensis.* In Thailand, the naiads of *Bradinopyga geminata* were successfully used to control *Aedes* mosquito (Subramanian, 2005). Sathe and Shinde (2016) mass-reared the dragonflies and successfully released them into the mulberry ecosystem and paddy fields of the Kolhapur region, India.

The naiads of Odonata show cannibalism, an expected behavior in dragonflies (Johansson, 1993; Hopper et al., 1996; Gossum et al., 2003). Cannibalism was one of the major problems affecting the mass rearing of dragonflies in the laboratory. Density-dependent positive correlation of cannibalism was seen in dragonfly naiads (Buskirk, 1989). In laboratory-rearing systems, this cannibalism can be avoided by rearing the naiads in separate vials (Johnson, 1965; Lockline et al., 2012). However, it is difficult as it requires more materials and laboratory space (Locklin, 2012). The body size of Odonatan naiads and cannibalism are positively correlated (Holzmann et al., 2022).

Lerum (1968) conducted a detailed study on the development of compound eye and optic ganglia in the dragonfly naiads. Sherk (1978) also studied the compound eyes development in dragonfly naiads. Goretti et al. (2001) studied the

development of dragonfly naiad, *Aeshna cyanea*. Busse et al. (2019) conducted a detailed study on the exuviae, attachment devices, and their role during dragonfly adult emergence.

Many internal and external factors affect the development of dragonfly naiads (Pritchard et al., 1996; Corbet et al., 2006). Environmental factors like temperature, photoperiod, and food availability play a significant role in the ecology and evolution of many insects (Corbet et al., 2006; Bradshaw & Holzapfel, 2007). Lutz (1974) experimented to study the effects of temperature and photoperiod on the dragonfly naiad, *Tetragoneuria cynosure*. Gresens et al. (1982) studied the effect of temperature on the functional response of the dragonfly, *Celithemis fasciata.* Hudson and Berrill (1986) conducted a study on the effect of low pH (5.1 and 3.5) on the eggs of some Odonata, *Ishnura verticalis*, *Lestes congener*, *Lestes lydia,* and *Sympetrum vicinum*. Their study revealed that the Odonatan eggs can tolerate low pH. Punzo (1988) conducted a study to determine the combined effects of low environmental pH and temperature on the embryonic survival and metabolic rates of the dragonfly, *Anax junius,* and also the role of hypoxia in the hatching process. Miller (1992) studied the effect of oxygen lack on egg hatching in *Potamarcha congener,* and his result showed that oxygen lack triggers egg hatching in *P. congener*. Koch (2015) reared the eggs of the dragonfly *Sympetrum striolatum* under different temperatures and photoperiod to study its influence on embryonic development and found that an increase in temperature causes faster egg development. The effect of temperature on the egg development of *P. flavescens* was studied by Ichikawa et al. (2017). Augustine et al. (2021) studied the effect of temperature on the growth of *P. flavescens* naiads. Holzmann et al. (2022) studied the effect of temperature on the growth and cannibalism in damselfly larvae.

Mandal et al. (2007) estimated the predatory efficacy of five Odonatan naiads, *Aeshna flavifrons*, *Coenagrion kashmirum*, *Ishnura forcipata*, *Rhinocypha ignipennis,* and *Sympetrum durum,* using *C. quinquefasciatus* mosquito larvae as prey. The study of Chatterjee et al. (2007) revealed the biocontrol efficacy of the dragonfly naiad *Brachytron pratense* against the *Anopheles subpictus* mosquito

larvae. The presence of alternative prey forms did not inhibit the regulation of the *Culiseta longiareolata* mosquito by the *Anax imperator* dragonfly naiad (Stav et al., 2005). Ellis (2013) conducted a study to find whether the presence of dragonfly naiad influences the development and survival of mosquitoes and found no influence on the development and oviposition behaviour of the mosquito. Shad and Andrew (2013) studied the predatory potency of naiads of *B. geminata* on the filarial vector, *C. quinquefasciatus*. Venkatesh and Tyagi (2013) investigated the predatory potential of larval *B. geminata* and *Ceriagrion coromandelianum* on *Aedes aegypti*. Murugan et al. (2015) extracted silver nanoparticles (AgNPs) from the *Datura metel* leaf and studied the influence of AgNPs on the predatory potential of dragonfly naiads against the malarial vector *Anopheles stephensi*. The presence of AgNPs boosted the predatory potential of dragonfly naiads. The naiads of dragonfly *B. contaminata* can be used as a biocontrol agent against mosquito larvae, and it had the highest predation efficacy against *A. stephensi*, followed by *C. quinquefasciatus* and *A. aegypti* (Singh et al., 2003). Saha et al. (2012) evaluated the predation potential of the naiads of Odonata *Ceriagrion coromandelianum* and *Brachydiplax chalybea chalybea* on the II and IV instar larvae of *C. quinquefasciatus* under laboratory condition and recommends the naiads of Odonata as a potential biocontrol agent. Kumar et al. (2008) compared the predatory efficiency of three aquatic predators, mosquitofish, dragonfly naiads, and copepods, over mosquito larvae in the presence of alternative prey. Weterings et al. (2015) also studied the predation rates of some Odonatan naiads on *A. aegypti* and *Armigeres moultoni* larvae. Ilahi et al. (2019) studied the predatory efficiency of naiads of some odonates, *I. elegans, Trithemis aurora, P. flavescens, Ladona fulva, Sympetrum decoloratum and Crocothemis servilia* on mosquito larvae *C. quinquefasciatus*. Akram and Ali-khan (2016) studied the predation performance of Odonatan naiads, *Anax parthenope, B. geminata, Ishnura forcipate, Rhinocypha quadrimaculata,* and *T. aurora* against the mosquito larvae *A. aegypti*. Moirangthem et al. (2018) conducted a comparative study to check the efficacy of three insect larvae, Odonata (*Sympatrum* sp.), Hemiptera (*Diplonychus* sp.), and Diptera (*Lutzia tigripes*), in controlling the mosquito larvae. Lamptey and Brandl (2018) conducted a field

experiment to study the effect of dragonflies on the density of mosquito larvae. The practical efficacy of using the naiads of Odonata as mosquito control agents has been evaluated by many countries in the world (Samanmali, 2018). Mataba et al. (2023) studied the interactive effects of dragonfly larvae and *Bacillus thuringiensis* var. *israelensis* on mosquito survival and oviposition behaviour. Myanmar (Sebastian et al., 1990) and India (Venkatesh & Tyagi, 2013) have successfully used many dragonflies as biocontrol agents in regulating the larval populations of mosquitoes (Mandal et al., 2008).

3.3 MATERIALS AND METHODS

3.3.1 The embryonic developmental study

Adult *P. flavescens* were collected from the paddy fields in Palakkad district, Southern Western Ghat, Kerala, India from September to November 2020, using a sweep net. Only the females were taken to the laboratory with special care to reduce the stress during transportation. The artificially induced oviposition (Krull, 1929) method was adopted to collect the eggs of *P. flavescens*. The wings of mature females were held appropriately, and the tip of the abdomen was dipped every 15 s into a Petri dish filled with 50 ml of de-chlorinated water. This process was repeated until the female completely released the eggs. Then, the females were released back to the field after collecting the eggs. The collected eggs were kept at room/water temperature (26 ± 1° C) throughout the experiment with 14:10 hours photoperiod. Every 12 hours, 60-70 % of water was replaced with de-chlorinated tap water. The embryo's developmental stages were observed and documented using a Zeiss, SteREO Discovery V20, a modular motorised stereo zoom microscope with Zeiss Axiocam 506 colour camera 19-bit full resolution CCD Sensor, Germany. Image capturing was continued until the onset of hatching. Non-distractive methods were used to visualize and document the early embryonic events of *P. flavescens*. Daily changes in the length (anterior-posterior distance) and width of the eggs were measured using ImageJ software, n = 30, and data were represented as Mean ± SD.

3.3.2 Laboratory rearing of *P. flavescens*

The eggs of *P. flavescens* for the rearing experiment were also collected from Palakkad district, Kerala, India. The eggs of *P. flavescens* were collected from the adult females by dipping the tip of the abdomen in a beaker filled with water. A single egg clutch contained about 800-900 eggs. The eggs from the same clutch were used for the postembryonic developmental study.

3.3.2.1 Preparation of culture medium

Special Nutrient Composition (SNC) (Patent No: 202441072908) with essential amino acids and nutrients has been used for the culturing of *P. flavescens* naiads.

3.3.2.2 Laboratory rearing of *P. flavescens* naiads

The experiment was conducted in the three different special nutrient compositions (SNC) SNC 1, SNC 2 and SNC 3 and one Control group with three replicas of each. Plastic trays (34 cm length, 26 cm breadth, and 5 cm height) with 5L capacities were used for culturing the naiads. Each tray was filled with three liters of de-chlorinated tap water, and some small pebbles were added to make some hiding places for the naiads. Twenty-five eggs from the same egg clutch were transferred to each tray. The eggs were hatched within 6-7 days. After egg hatching, the special nutrient solution was added to the trays accordingly. We changed the water every fifth day without disturbing the naiads.

The early instars of naiads were fed daily with artemia, paramecium, and moina; the later instars were fed with mosquito larvae and bloodworms. Paramecium was cultured in the laboratory by using dried banana leaves. The dried banana leaves were added into a glass beaker with one litre of tap water. The beaker was closed with a muslin cloth to avoid the egg laying by other insects. One or two drops of milk were also added to it to provide the required bacteria and small protozoans. The paramecium is reproduced by simple division, and enough paramecia were produced on the fifth day. Artemia tablets were used for the culture. For one artemia tablet, we used one litre of de-chlorinated tap water mixed with two tablespoons of salt and

provided continuous aeration. Moina is a crustacean mainly used as a live fish food and is commercially available. Initial cultures of the Moina were collected from an aquarium shop and cultured in cement tanks using fresh papaya leaves. Mosquito larvae culture was also maintained in the laboratory. The egg rafts of mosquitoes were collected from the cement tanks used for the Moina culture. The tanks were filled with water, a few dry mango leaves, and one large papaya leaf, which attracted the mosquitoes. We changed the papaya leaves every third day before they started decaying. The collected egg rafts were then transferred to plastic trays filled with 3 L of water. The eggs were hatched within 2 days after oviposition. Powdered dog biscuits and fish food were added to the larval trays as food. Commercially available live bloodworms were used for feeding the later instars of *P. flavescens* naiads. When the naiads reach their final instar, we provide small sticks and nets into the trays for the adults to climb and emerge because they crawl outside the water before emergence.

3.3.2.3 The naiad traits measurements

The wing sheath length ratio and head width were used to classify the naiad instars (Benke, 1970; Minot et al., 2019). The final instar naiads were described as F-0 (F = final) and the penultimate instar as F-1, F-2, and F-3 because the naiad instars are not generally fixed in dragonflies (Okude et al., 2017). F-0 naiad instars were again divided into three developmental stages (stage 1, stage 2, and stage 3) based on the changes in the wing sheath and eye shape (Okude et al., 2021). Eight different naiad traits, total naiad length, length of the abdomen, the width of the abdomen, S8 spine length, S9 spine length, epiproct length, width of the head region, and wing sheath length were selected for taking the measurements.

3.3.2.4 Estimation of ammonia and nitrate content in the naiad culture

Water ammonia and nitrate were monitored every fifth day using a benchtop LAQUA PC2000 pH/Ion meter (HORIBA), Japan. The calibration of the machine for individual tests was performed as per the manufacturer's instruction and the respective standard calibration solution provided by Horiba. Samples were collected

from all the experimental groups to quantify ammonia before changing the water. We estimated the levels of ammonia and nitrate throughout the experiment.

3.3.2.5 Elemental composition analysis using ICP-MS

Inductively Coupled Plasma Mass Spectrometry (ICP-MS) was used to measure the elements in the water samples of naiad culture. Water samples from all four experimental groups were collected every fifth day. The collected samples were stored in separate vials after digestion before analysis.

Sample preparation: 1 ml of water samples from each experimental group was taken in separate boing tubes. 4 ml nitric acid was added to each tube, and the solution was boiled at 120°C. After cooling, two drops of hydrogen peroxide were added, and the solution was again boiled at 120° C. After cooling, all the solutions were made up to 10 ml using double distilled water. After thoroughly mixing the solution, 1 ml from each tube was pipetted and diluted with 9 ml of double distilled water. Then, finally, the solution was filtered using 42-grade filter paper before doing the analysis.

3.3.2.6 Photographing

The naiads were photographed using a Stereo Microscope (Zeiss Discovery V20 Stereo Microscope attached to a Zeiss 506 camera). Separate images of the naiads from early to final instars were taken from all the experimental groups and the mophological changes were observed (Fig. 3.10, 3.11, 3.12).

3.3.3 Predatory potential

Establishment of *C. quinquefasciatus* larval colonies: The egg rafts of *C. quinquefasciatus* were collected from the cement tanks filled with water, dry leaves, and fresh papaya leaves to attract the mosquitoes. The collected eggs were then transferred to plastic trays filled with 3 L of water. The trays were kept inside the greenhouse to prevent other mosquitoes from laying their eggs in the trays. The eggs were hatched within 2 days after oviposition. Powdered dog biscuits and fish food were added to the larval trays as food. Fourth, instar larvae were used to study the predatory potential of *P.flavescens*.

The final naiad instar of *P. flavescens* reared under different SNCs (SNC 1, SNC 2, and SNC 3) was used to conduct the experiments on predatory potential. Fourth instar larvae of *C. quinquefasciatus* reared in the laboratory conditions were used to assess the predatory potential of *P. flavescens*. One individual from each group was introduced into separate plastic bowls with 500 ml of water and was starved for 24 hours before each predatory response trial (Figure 3.1). One hundred mosquito larvae (4^{th} instar) were introduced into each bowl. New batches of mosquito larvae were introduced into the bowls, which showed above 50% predation to maintain the same density of prey density throughout the experiment. The number of live mosquito larvae was counted at 1-hour intervals until 6 hours to record the consumption rate. Ammonia excretion in each bowl was also measured during the experiment using the ammonia meter (LAQUA PC2000 pH/Ion meter, HORIBA), Japan.

SPSS software was used for all the statistical analysis. The significance of ammonia and nitrate in the rearing experiment and the predation rates of *P. flavescens* were statistically evaluated using One-Way ANOVA. The pairwise comparison test was performed using Sidak and Tukey's test. The consumption rate of mosquito larvae by the naiads of *P. flavescens* was calculated by counting the live mosquito larvae remaining in each bowl. The measurements of the selected naiad traits were measured using ImageJ software.

3.4 RESULTS

3.4.1 Embryonic development of *P. flavescens*

Newly laid eggs of *P. flavescens* are oval-shaped with a small nipple-shaped micropylar apparatus at the anterior region of the egg with a length of 0.029 ± 0.003 mm in length, the site of sperm entry (Fig. 3.2). The eggs were white and transparent soon after oviposition, but the colour changed to yellowish-brown after a few hours. The whole surface of the egg is covered with very minute pores (Fig. 3.2: 3). The embryonic development of the *P. flavescens* took about 6-7 days to complete, and the length and width of the egg increase in size as the embryo develops (Fig. 3.1).

STAGE 1

The eggs of *P. flavescens* were elliptical, with a length of 0.484 ± 0.016mm and a width of 0.319 ± 0.008 mm. The egg is covered with a gelatinous substance of 0.069 ± 0.011mm thick. At this stage, the yolk is uniformly distributed throughout the egg. The colour of the eggs changed to yellowish-brown after 7-10 h (Fig. 3.3: 5).

STAGE 2

Within 24 hours after oviposition, this stage of embryonic development starts. This stage is easily distinguishable by looking at the structure of the yolk. The grainy yolk was divided into yolk spherules; we could see many grainy yolks inside every yolk spherule (Fig.3.3: 7).

STAGE 3

This stage occurs 24-48 hours after oviposition. The yolk near the posterior pole of the egg was consumed for the formation of cells, and we can see a small translucent germ band in that region (Fig. 3.3: 8,9). The presence of a germ band denotes the onset of stage 3. The size of the eggs was 0.498 ± 0.013mm long and 0.347 ± 0.009mm in width. 0.12 ± 0.015mm was the thickness of the jelly coat at this stage (Fig. 3.3: 10). Posterior blastoderm cells gave rise to the germ anlage, which grew towards the anterior region of the egg by crossing the equator but never reached the anterior pole. Different-sized germ bands can be seen in the posterior region of the eggs. After germ band proliferation and elongation blastokinesis occurs. Anatrepsis (germband penetration into the yolk mass) occurs at this stage. Differentiation of the embryo starts now. Body segmentation, abdomen elongation, and appendage formation all started at this stage. Anterior segments of the embryo are formed first, and all other segments are formed afterward.

STAGE 4

Stage 4 is the beginning of katatrepsis and occurs 24-48 hours. after oviposition. At this stage, the eggs were 0.495 ± 0.016mm long and 0.378 ±

0.010mm in width. The penetrated embryo will now come out from the yolk mass, which is called early katatrepsis. The head region of the embryo now faces the posterior pole of the egg (Fig. 3.3: 11). The anterior and posterior axes of the embryo and egg are reversed. This early katatrepsis of blastokinetic movement lasted for only a few hours.

STAGE 5

This embryonic developmental stage occurred immediately after the early katatrepsis. The last step of blastokinetic movement (final katatrepsis) happened at this stage. The embryo rotates 180° at this final katatrepsis. Now, the anteroposterior axes of both the embryo and egg showed similar orientation; the head region of the embryo now faced the anterior pole of the egg (Fig. 3.3: 12). All eggs attained this orientation 72 h after oviposition. Rudiments of antennae, labium, maxillae, mandible, labrum, and three pairs of legs are visible through the egg at this stage and the remaining egg was fully enclosed with the yolk.

STAGE 6

The onset of this embryonic developmental stage was the discolouration of the eyespots and proctodaeum as orange-brown (Fig. 3.4: 13, 14). At this stage, the size of the eggs was 0.527 ± 0.025mm in length and 0.400 ± 0.008mm in width. The abdominal tip of the embryo was positioned like a capital J at the posterior pole of the egg.

STAGE 7

The seventh stage of development occurred between 96-144 hours. The length and width of eggs at this stage were 0.520 ± 0.016mm and 0.399 ± 0.010mm. The egg was enclosed with an almost fully developed embryo. The embryo encloses most of the yolk mass, and only a small amount was left in the thoracic region of the embryo. The head region, mouthparts, legs, and abdomen were easily distinguishable. The proximally fused labial appendage was seen on the embryo's ventral surface. The orange-brown eyespots changed to dark reddish-brown at this developmental stage. The embryo shows minor muscular movements and slowly

changes its position within the egg. In some eggs, the dorsal side of the embryo was positioned upward and the ventral side downward (dorsum-up position), but in some eggs, the ventral side of the embryo was positioned upward and the dorsal side downward (venter-up position), and some of them were in an intermediate position (Fig. 3.4: 15-18)

STAGE 8

This final embryonic developmental stage of *P. flavescens* occurred 144 hours after oviposition. The egg size at this stage became 0.546 ± 0.12mm and width 0.411 ± 0.008mm. The yolk was completely enclosed into the embryo, and the egg was now occupied by the fully developed embryo, which resembles a dragonfly's naiads with an almost transparent body. A tiny pointed egg tooth was present at the central portion of the head between the eyes, and some prominent spines were seen on the frontal region above the labrum. During hatching, these frontal spine and egg teeth help the pre-larva rupture the egg chorion. A pair of antennae and their segments were visible in the head region. The three pairs of legs were seen as a coiled mass inside the egg. The abdomen at the posterior region of the egg was bent towards the anterior pole, and the ten abdominal segments were distinguishable. A pair of cerci was seen at the tip of the tenth abdominal segment. The fully developed embryo which look exactly like the dragonfly naiad, can be called pre-larvae (Fig. 3.4: 19-21). Most of the embryos at this final stage were seen in the ventral-up position (the ventral side of the embryo faces up); only a few were in the intermediate or dorsum-up position. The thickness of the jelly coat was reduced compared to the newly laid eggs and became tinner and tighter to form egg clutches (Fig. 3.5).

EGG HATCHING

With the help of the egg tooth and frontal spines present in the head region of the final embryo, the pre-larva emerged from the egg by severing the eggshell. About 70% of pre-larva emerged on day 6; more than 30% of emergence was recorded on day seven. The head of the naiad emerged first, then the thorax, and finally, the abdomen by peristaltic movement. The embryonic cuticle layer was shed

during emergence with the help of the distal part of the embryo. The newly emerged naiad body is whitish and transparent (Fig. 3.4: 22-24). They started their active movement within a few minutes after emergence and showed cannibalism from day one (first instar naiad).

3.4.2 Post-Embryonic Development of *P. flavescens*

We successfully established a laboratory-rearing system for *P. flavescens* with very low or no naiad cannibalism. The naiads from all four groups were monitored throughout the experiment and early development was found in SNC 1 naiads. The newly emerged first instar naiads were usually in the non-feeding stage and normally utilise the retained yolk in their midgut for nutrition, which lasts only a few hours. The newly emerged bodies of the naiads were whitish and transparent but became darker in later instars.

3.4.2.1 External features of dragonfly naiads.

The body of dragonfly naiads has been divided into the head, thorax, and abdomen.

1. Head

The head region bears the compound eyes, ocelli, antennae, and the mouthparts. The compound eyes are made with numerous ommatidia. The number of ommatidia increases during naiad development, and the size of the eyes also increases. No ocelli were seen at the early stages of the naiads but they were visible at the dorsal frons region of the head in the later instars. The antennal segments increase in number as the naiad develops and seven antennal segments are seen in the later naiad instars. Dragonflies are mandibulate insects and the mouth parts consist of a labrum, mandibles, maxillae, hypopharynx and labium. The protractile, prey-capturing labium is unique to dragonfly naiads.

2. Thorax

The thorax consists of prothorax and fused pterothorax, it has three pairs of legs and wing sheaths. The pterothorax has meso and metathoracic legs and two

wing sheaths. The wing sheaths are not present in the early instars of dragonfly naiads. Then, it appears as small wing buds in the pterothorax.

3. Abdomen

The abdomen has ten segments. The eighth and ninth abdominal segments have a pair of posterolateral spines. These spines appear on the naiad body in its early instars. The posterolateral spines in the ninth abdominal segment appear first and then in the eighth. The tenth abdominal segment bears the anal appendages; it consists of an epiproct, a pair of cerci, and a pair of paraprocts (Fig. 3.6).

3.4.2.2 Naiad stages

The naiad instars of dragonflies vary even within the dragonfly species. So instead of classifying the *P. flavescens* naiads into different instars, we classified the final instar as F-0 (= Final) and the other as F -1 (F minus 1), F -2 (F minus 2), F -3 (F minus 3), etc. The final instars of *P. flavescens* naiads were classified based on their wing sheath length and head width. The wing sheath length and head width ratio were plotted against the number of days, and it revealed three clear clouds of point and two overlapping clouds (Fig. 3.7). Each cloud indicates the different instars, F0, F-1, and F-2. F-3 and F-4 instars were difficult to discriminate from the plot due to the overlapping of the two instars at some points. The wing sheath length and head width ratios of the F-0 instar ranged from 1.07 -1.26. The wing sheath length of the naiads of *P. flavescens* was more significant than the head width in the F-0 instar. The ratio for F-1 ranged from 0.63-0.89, and that of the F-2 instar was between 0.36-0.48. The ratios of F-3 overlapped with the F-4 ratio, and it was not easy to separate them based only on the wing sheath and head width ratios. So, for classifying them, we also considered other features, like the position of the tip of both the wing sheaths.

Variations in the duration of naiad instars

Observations and imaging of the naiad development were started at the beginning of the wing development. Wing bud formation (fig. 3.8A), formation of lateral spines in the 8^{th} and 9^{th} abdominal segments, appearance of black dots and

markings on the abdomen, ocelli indication by markings, and eye enlargement are some of the major developments noticed during the early naiad instars. During the 7th instar, the wing pad arises from the wing bud, and from the 8th instar, we started photographing the naiads from all four experimental groups. The duration of the naiads from the first instar to the F-3 instar was short, and it took about 12 days to attain the F-3 instar. In all four experimental groups, there was no significant variation in the duration of naiad instars up to the F-4 instar.

F-4 and F-3 instar

In the F-4 instar, the naiad's forewing cases extend to the thorax's posterior end, and the hindwing extends to the first abdominal segment (fig. 3.8B). The naiads from all the experimental groups attained F-4 instar in 10 days**.** Within two days, the naiads moult to the F-3 instar, where the forewings extend over the first abdominal segment, and the hindwings extend over the second (fig. 3.8C).

F-2 and F-1 instar

On the 14th day of the naiad development, moulting was observed in the SNC 1 naiads to F-2 instar, and no moulting was found in other groups. The appearance of middorsal hooks in the abdominal segments S3 and S2 (fig. 3.8D, 3.8E) was noticed in the F-2 instar naiad. The hindwing reaches the third abdominal segment, and the forewing reaches the second abdominal segment in the early stages of the F-2 instar and later it exceeds the third and second abdominal segments. Also, we can easily distinguish the anal loop region of the hindwings at this stage. On day sixteen, all groups were moulted to the F-2 instar, and after 2 days, they moulted to F-1 instars except the control group naiads. We noticed 3 middorsal hooks (figure 3.8F) on the naiad's abdominal segments S2, S3, and S4, and the wing sheaths exceed the 4th abdominal segment.

Final instar (F-0)

Morphological changes in *P. flavescens* during the final instar.

At this stage, the wing sheath completely covers the first few abdominal segments (S1-S4), so from this stage onwards, it was difficult to see the middorsal line and hooks. Some changes in the shape of compound eyes have also been observed at this stage.

F-0 instar naiads have been classified into three stages (Table 3.1).

1. Stage 1
2. Stage 2
3. Stage 3

Table 3.1: Different stages of F-0 instar of *P. flavescens* naiads

Stage 1	Stage 2	Stage 3
The tip of the forewing is not visible, hidden under the hindwing.	The tip of the forewing is visible but not fully.	The forewing is completely visible.
The wing sheaths are flat.	The wing sheaths are flat.	The wing sheaths appear swollen.
No pigmentation on the wing sheaths.	No pigmentation on the wing sheaths.	Black dots and pigmentations appear on the wing sheaths.
The compound eyes expand towards the midline of the head region.	The compound eyes start expanding posteriorly and the boundary of expansion is visible.	The compound eyes become larger and appear darker.

The SNC 1 naiads reached the final instar on the 21st day, but the naiads of the other groups (SNC 2, 3, and control) were found to be in the F-1 instar on the 24th day. SNC 1 shows faster development (1 instar difference) than the other groups. They were in stage 1 of the F-0 instar. At this stage, the tip of the forewing sheath of the naiad is found hidden under the hindwing (Fig. 3.9G). The wing sheaths were flat, and no pigmentation was observed on the wings. During stage 1,

the wing sheaths completely cover the first few abdominal segments, so, the middorsal hooks of the abdominal segments S2, S3, and S4 are not visible from this stage. The compound eyes expand towards the midline of the head region (Fig. 3.9A, B, C), and the ocelli gradually get pigmented.

Stage 1 SNC 1 naiad develop into stage 2 of the final instar. At this stage, the tip of the forewing was visible (Fig. 3.9H) and the compound eyes now start expanding posteriorly. This expansion of the compound eye and its boundary is distinguishable (Fig. 3.9D). We can also see specific markings on the ocelli (Fig. 3.9D).

On day 28, the SNC 1 naiads reached stage 3 of the final instar. SNC 2 naiads moult to stage 1 of the F-0 instar, and the other groups (SNC 3 and control group) remain in the F-1 instar. At this stage, the forewing was completely visible (Fig. 3.9I), and the compound eyes expanded posteriorly (Fig. 3.9E). The ocelli get pigmented more. In the late phase of stage 3, just before the emergence, we can see darkened areas and dark spots on the wings (Fig. 3.9I). The compound eyes expand more and are coloured like the eyes of an adult dragonfly. The ocelli region was covered with many hairs (Fig. 3.9F). After two days, the SNC 1 naiads first reached the late F-0 stage 3 and emerged on the next day (31st day). SNC 2 naiads emerged after the emergence of the SNC 1 naiads, then the SNC 3 naiad and the control group naiads emerged on the 42nd day. In addition to that a significant morphological developmental variation were also observed in head (Fig. 3.10), thorax (Fig. 3.11), and abdomen (Fig. 3.12).

The adult emergence was mainly observed in the early morning. Before emergence, the final instar naiads moved outside the water and climbed into the offered wooden sticks and nets in the trays. The attachment of naiads to the emerging substrates is very important. If it fails, then the naiads cannot go through the emergence process, and they will die. Many naiads move towards the stick's tip for attachment, mainly using their claws to interlock with the substrates. The Odonate exuviae attaches to the substrates for several weeks or months.

3.4.2.3 Comparison of different traits of *P. flavescens* naiads

Eight different *P. flavescens* naiad traits, total naiad length, length of the abdomen, width of the abdomen, S8 spine length, S9 spine length, epiproct length, width of the head region, and wing sheath length (Fig. 3.13) were measured and compared between experimental groups and the control group. The measurements were taken until the first emergence of the adult happened in each experimental group. The size of the SNC 1 naiads was found to be larger than other groups, but no significant size variation was observed. The first adult emergence date was found to be different in all four experimental groups; the SNC 1 naiads emerged first, then SNC 2, SNC 3, and finally the control group naiads.

The average length of the final instar naiad was about 20.43 mm in SNC 1 and in the control group, the average length was about 18.76 mm. The average length of eight traits (Fig. 3.14, 3.15) increased faster in the SNC 1 naiads than in SNC 2, but it was almost similar in SNC 3 and control group naiads. This increase in length was due to the faster moulting of SNC 1 naiads. This group moulted to the final instar after the 21st day and thus showed a sudden length change after the 20th days (Fig. 3.14, 3.15).

3.4.2.4 Estimation of ammonia and nitrate in the naiad culture

Ammonia and nitrate content in the naiad culture was estimated throughout the experiment in five-day intervals. Experimental group-wise and day-wise comparisons of ammonia and nitrate levels were statistically analyzed using one-way ANOVA. Insignificant ($p > 0.05$) differences were observed in all four experimental groups. The ammonia content in the experimental groups never exceeded 2 ppm (Fig. 3.16), and the nitrate level was always found to be below 3 ppm (Fig. 3.16). SNC 1 showed the comparatively highest concentration of ammonia (1.955 ± 0.058) and nitrate (2.461 ± 0.301) in the water, but gradually, its concentration decreased below zero ppm in all the experimental groups after a few days. The between-group comparison was analyzed using Tukey's test, and no significant ($p < 0.05$) differences were obtained in the ammonia and nitrate.

3.4.2.5 Inductively Coupled Plasma Mass Spectrometry (ICPMS) analysis

The elemental composition of the *P. flavescens* naiad culture water has been estimated through the ICPMS analysis. The concentration of some of the elements like magnesium, potassium, and sodium has been observed to be higher in the SNC 1 naiad culture water (Fig. 3.17). A significant difference was observed in the SNC 1 naiad culture when compared to the other groups.

3.4.3 Predatory potential of *P. flavescens* naiads on *C. quinquefasciatus* larvae

In the laboratory, *P. flavescens* nymphs showed an effective predation on *C. quinquefasciatus* mosquito larvae. The consumption rate of mosquito larvae by the naiads of *P. flavescens* was observed to be high in all four groups during the first hour, and only a low intake was observed during the subsequent hours. Among the four groups, SNC 1 naiads showed the highest predation of (87.5 ± 8.96) mosquito larvae within 6 hours, followed by SNC 2 (78.33 ± 8.89), SNC 3 (61.33 ± 5.74), and control group (53.67 ± 5.38) respectively (Fig. 3.18A).

ANOVA was used to determine the predatory efficacy between the four experimental groups and no significant differences in the predation rate were found. We also observed ammonia excretion in each group in a one-hour interval. Relatively high ammonia excretion was noticed in SNC 1 naiads with mosquitoes. No significant differences were noticed in ammonia excretion by different experimental groups (Fig. 3.18B)

3.5 DISCUSSION

3.5.1 Embryonic development

The embryonic developmental study of the migratory dragonfly species, *P. flavescens* was carried out without any preparation or dissection of the embryo from the egg. Their eggs are oval/spheroid, which facilitates a quick sinking of the egg in the water soon after oviposition, and this helps to avoid egg predation by some aquatic animals (Andrew, 2011). The eggs of dragonflies get fertilized as they pass

through the female's vagina during oviposition, and immediately after oviposition, embryogenesis begins (Resh & Carde, 2009).

The eggshell of odonates consists of mainly three layers: the exochorion, endochorion, and the innermost vitelline envelope (Suhling et al., 2015). The eggs of dragonflies are covered with a thick chorion and are filled with yolk and cytoplasm. This yolk is the source of nutrition for embryonic development (Ando & Watanabe, 1995). Egg morphology of different species of dragonflies has been studied, especially the vitelline and chorionic layer organization (Miller, 1987; Andrew & Tembhare, 1995; Andrew, 2002). The eggs of *P. flavescens* were initially white and transparent after oviposition, gradually the colour changed to brown, and were found to be covered with a semitransparent jelly coat. The expansion of the exochorion forms this transparent and sticky jelly-like structure (Andrew et al., 2011); at the same time, the endochorion tears and the vitelline membrane expresses on the surface of the egg, the vitelline envelope undergoes a darkening process (Gaino et al., 2008). However, in some libellulid dragonflies like *P. flavescens,* this endochorion is unsculptured, and this endochorion undergoes a darkening process from yellow to brown (Trueman, 1991; Andrew, 2011). This jelly coat has been reported in many libelluloid species (Miller, 1987; Ivey et al., 1988; Andrew & Tembhare, 1995; Andrew, 2002). This jelly coat helps in plastron respiration, as in *Brachythemis lacustris* (Kirby, 1889), and helps in holding the egg clutch together. Some tiny particles in the water will stick to the jelly coat and form a protective camouflage (Corbet, 1999). In *P. flavescens,* this jelly coat helps attach eggs to the control group substratum, and this coat gets thinner towards the end of embryonic development.

A small nipple-shaped micropylar apparatus is present in the anterior apical region of the *P. flavescens* egg. This is the site of sperm entry. This micropylar apparatus comprises a small sperm storage chamber (atrium) and a median projecting stalk with a pair of subterminal orifices (Andrew, 2011). The micropylar apparatus of *P. flavescens* is not always present on the anterior apical center of the egg, it may show some positional deviations. The embryonic development of long-

germ insects is comparatively faster than the intermediate or short-germ types (Davis & Patel, 2002). The embryonic development of dragonflies is intermediate germ type (Sander, 1976). In such embryonic development, the anterior germ anlage divides first and forms the anterior segments (protocephalon), and all other segments are formed successively (Sander, 1996). *P. flavescens* took about 6-7 days to complete their embryonic development, and egg length and width gradually increased during its development. The egg size increases to a maximum when the embryonic eye spots appear, and no change in the size occurs after this (Kormondy, 1959). Katatrepsis occurs midway through embryonic development in all odonates (Ando, 1962). The same was observed in the *P. flavescens*.

At the seventh stage of embryonic development in *P. flavescens*, a slight stretch of yolk mass is observed above the embryo's thoracic region just before the final enclosure of the yolk mass. A small pointed egg tooth was also noticed in the head region of the embryo. The egg tooth is formed in the embryonic cuticle of the pre-larva in pterygote insects, and this tooth gets shed during hatching along with the embryonic cuticle. Thus, this egg tooth will not persist in the larval forms of pterygote insects. Nevertheless, in some apterygote insects, this egg tooth is formed in the larval cuticle and thus persists in the first larval instar (Konopova & Zrzavy, 2005). After hatching, the embryonic cuticle is seen as a white layer inside the eggshell in *P. flavescens*. All embryos attain a venter-up position just before hatching, which is a gravity-dependent rotation (Miyakawa, 1987).

P. flavescens lay eggs in clusters; we found some variations in the hatching time. Meanwhile, the eggs well spread in a petri dish showed no such variations (Gayathri et al., 2023). The eggs laid by a single female can show variations in their development rates, these variations are more significant in females that deposit egg-string or egg clusters (Corbet, 1962). The *Tetragoneuria cynosure* eggs show variation in the hatching time, in which the innermost eggs in the string do not develop as fast as others (Kormondy, 1959).

The eggs of *P. flavescens* took 6-7 days to hatch at room temperature 26 ± 1° C. Odonata's egg development is influenced by environmental factors like water

temperature (Ichikawa et al., 2017) and water pH (Punzo, 1988). The effect of different temperatures on *P. flavescens* eggs was studied by Ichikawa et al. (2017). They found that the hatching time of the eggs at high water temperatures (35° and 30° C) was about 5 days. However, the egg stage duration increased with declining water temperature. The critical water temperature for *P. flavescens* was found to be approximately 14.3° C.

3.5.2 Laboratory rearing of *P. flavescens*

SNC's successfully established a cannibalism-free, fast, and healthy laboratory-rearing technique for *P. flavescens.* Cannibalism is the best physiological option for organisms as it provides high nutrition and also helps to reduce the number of competitors (Polis, 1981). However, under laboratory conditions, the dispersal of naiads is limited in the tanks or containers, and the cannibalism rate will be very high compared to its control group habitat. Thus, for the successful mass-rearing of dragonflies under laboratory conditions, it is necessary to reduce their cannibalism from a physiological point of view. To reduce cannibalism and for the healthy growth of dragonfly naiads, they must be given timely and instar-specific food (Sathe, 2013). Even minimal size differences in naiads from the same egg clutch can lead to cannibalism (Anholt, 1994). We provided special nutrients as an extra source of nutrition for the naiads. Different compositions of special nutrients and sufficient prey were given to the naiads to reduce the nutrient deficiency. We experimentally proved that the effective management of nutrient deficiency reduced the dragonfly naiad's cannibalistic behaviour and increased survival rate. In each experimental group, the cannibalism was quantified by counting the number of missing naiads on every tenth day. We observed the culture daily but never noticed any control group death of the naiad; thus, reducing the number of naiads indicates cannibalism. All parameters except the composition of special nutrients were different in the four experimental groups. The cannibalism rate was low (below 10%) in SNC 1 compared to the control group dragonfly naiads. This indicates that SNC plays an important role in reducing cannibalism.

The wing sheaths only appear on the naiads during their development when stadium 5-7, and this part of the naiad is the fastest growing part compared to the growth rate of the head width (Corbet, 1999). In the case of *P. flavescens,* these wing sheaths were first detected in its sixth instar, and they first appeared as tiny buds in the thoracic region.

The availability of food directly influences the development of dragonfly naiad. The time naiads spent in each instar decreased with increased food availability (Wissinger, 1988). The instar duration of the naiads was found to decrease with an increase in the SNC content in the water. SNC was thought to increase the naiad's metabolic activity, leading to their early emergence. The number of naiad moults was the same in all the groups, but the duration of time spent by naiad in each instar was different in the four experimental groups. In all four experimental groups, the duration of each instar up to F-4 was the same, but some variation in the instar duration was noticed from the F-3 instar. The SNC 1 naiad spent the least time in the F-3 instar and they moulted to the F-2 instar first. In SNC 2, 3, and control groups the duration between instars was similar up to the F-2 instar, but from the F-1 instar, control group naiads started spending more time in between instars. Increased metabolic activities in the SNC naiad groups help to reduce the duration between instars, leading to the early emergence of the adults.

The naiads cultured in SNC molted slightly larger than the control group. These results indicate that the naiad groups in the SNC 1 were grown in a nutrient-rich environment and thus their development was faster than in other groups. The control group naiads may have experienced nutrient deficiency, which might be the reason for comparatively slow development. The nutritional conditions of the last instar dragonfly naiads might be carried over into the imago, which may influence its physiological state and cause variation in physical stamina (Whedon, 1942). The environmental conditions of the naiads affect the size of adult dragonflies (Minot et al., 2019). In adult dragonflies, large size increases lifetime reproductive success in both sexes (Sokolovska et al., 2000). The success rate of predation is significant for the fitness of adult dragonflies. The naiads of Odonata stop feeding before

emergence due to the reorganization of the labium, and the naiad's alimentary canal gradually becomes empty (Whedon, 1942). They emerge with empty guts and minimal fat but gain body mass rapidly during adulthood (Anholt et al., 1991). The adult dragonfly gains body mass after emergence through prey capture, which, directly influences the fecundity of female dragonflies, and in males, the predation rate increases flight muscle mass, which is correlated with reproductive success (Anholt et al., 1991). The SNC 1 naiads were found to be comparatively larger than the control group naiads. The adults who emerged from SNC 1, 2, and 3 were found to be larger than the control group. Their high flight muscle activities and larger wing size will help to increase their predatory potential. Flight muscle activity and wings are essential for migratory species like *P. flavescens*. After emergence, they increase their body mass before reaching maturity. Increased flight muscle mass helps to enhance the flying ability (Anholt et al., 1991). The naiads that emerged from SNCs were believed to capture more prey and increase their flight muscle mass, which helps to enhance the gliding and flying ability of the *P. flavescens*.

The *P. flavescens* completes the egg and naiad development phase of its life cycle in less than 51 days (Hawking & Ingram, 1994). We provided some emergence supports like sticks and nets in the culture trays when the naiads attained the final instar. Before emergence, the naiads stopped feeding prey, and their wing sheaths became swollen. Some of the naiads were found to emerge on the provided sticks and nets but some of them escaped from the culture trays and emerged outside the trays, that is, the naiads moved some distance away from the trays before emergence. Some dragonfly species crawl long distances before emergence, and thus, some of the specimens may lost, putting a screen top will help avoid this movement (Tennessen, 2019). In our experiment, the first emergence of *P. flavescens* occurred in SNC 1, and it took about 31 days for emergence after hatching. However, the emergence in the control group happened on the 42nd day after hatching. The first emergence of adult dragonflies between the control group and SNC 1 was about 11 days.

The SNC 1 naiads had higher melanisation than the other groups. Density-dependent positive correlation with melanisation/immunity was observed in dragonfly naiads (Murray et al., 2019). In many arthropods, Melanin is an essential chemical for wound healing (Theopold et al., 2004). We assume that the high melanisation in the SNC 1 naiads was due to the high density because cannibalism was comparatively less in SNC 1 from the initial days, leading to the high density. This makes the SNC 1 naiads more immunogenic towards infections and wound healing. This helps to increase the naiad survival rates in the laboratory.

Ilahi et al. (2019) studied the sensitivity of the naiads of Odonata to inorganic nutrient pollutants and found that *P. flavescens* is highly resistant to increasing water levels of ammonia and nitrate. Their study shows that the LC_{50} value of ammonia for *P. flavescens* was 740.3 ppm and 1353.1 ppm for nitrate. In our experiment, the ammonia and nitrate levels never exceeded 2 ppm, indicating culture system water quality was good. Thus, any mortality of the naiads observed in the control group was not due to the poor water quality.

3.5.3 Predatory potential

Many previous works on predatory potential studies of odonate naiads on mosquito larvae suggest that they are one of the potential biocontrol resources. Sebastian et al. (1980) successfully biocontrol *Aedes mosquitoes* using *Libellula* naiads as predators, and the study was conducted in the laboratory and field conditions. Augmentative release of dragonfly nymphs *Crocothemis servilla* in water reservoirs has reduced *A. aegypti* mosquito larvae (Sebastian et al., 1990). Lamptey and Brandl (2018) conducted a field experiment to determine the predatory potential of dragonfly naiads on mosquito larvae in their control group environment, and their result indicates that increasing the colonization of water bodies by *Bradinopyga strachani* is the best strategy for controlling the mosquito populations. The naiads of the *P. flavescens* grown in SNCs are more voracious and active predators of the mosquito larvae. The density of prey or predator influences the predatory potency of dragonfly naiads; the rate of predation increases with an increase in prey density and size of the dragonfly naiad and is inversely proportional to the space (Shad &

Andrew, 2013; Miura & Takahashi, 1988). The predatory potential of *P. flavescens* naiads on the mosquito larvae was evaluated in the laboratory, and we maintained a density of one hundred mosquito larvae in each bowl throughout the experiment to record the exact predation rate. Samanmali et al. (2018) tested the larvicidal potential of five dragonfly naiads over *A. aegypti* larvae, and they recommended *P. flavescens* and *Ana. Indicus* are potential predators for field trials in biological control of dengue outbreaks via suppression of *A. aegypti* larvae. The study conducted by Ilahi et al. (2019) with six Odonata species also recommends *P. flavescens* as a potential predator. The nymphs of *Bradinopyga geminata* show maximum predation on the first instar larvae of *C. quinquefasciatus* (Shad & Andrew, 2013). We checked the consumption rate of *P. flavescens* naiads on the fourth instar larvae of *C. quinquefasciatus*, and the result showed maximum predation.

The longevity of dragonfly naiads, their predatory ability, trophic position, and habitat sharing with mosquito larvae are some of the factors that help them to act as a potential biological control agent (Chatterjee et al., 2007). Many field and laboratory studies have reported a reduction in the population of mosquitoes by dragonfly naiads (Witzig et al., 1986). Many studies showed that dragonflies can control Aedes, *Culex*, and *Anopheles* mosquito species, the artificial rearing of these predators and releasing for biocontrol is an appropriate measure for vector control worldwide (Vatandoost, 2021). Controlling mosquitoes using control group predators like dragonflies can be feasible in habitats such as paddy fields and wetlands (Saha et al., 2012). *C. quinquefasciatus* mosquitoes are major filariasis vectors that cause other mosquito-borne diseases (Negi & Verma, 2018); their larval habitat is diverse, including wetlands and rice fields (Jacob et al., 2006). Many Odonata species, like *P. flavescens,* naiad habitat includes wetlands and rice paddy fields. As both the *culex* mosquito larvae and the naiads of Odonata share some common habitats, we can use the naiads of Odonata as potential biocontrol agents.

3.6 KEY FINDINGS

- We standardised the protocol for induced oviposition of *P. flavescens* in laboratory conditions.
- The egg stage duration of *P. flavescens* was found to be 6-7 days.
- An increase in egg size was noticed during embryonic development.
- A difference in hatching time was observed in eggs that were laid in clusters. Innermost eggs in the cluster show some delay in hatching.
- As a good bioindicator, these embryonic developmental studies of dragonflies can be used in climate change and water quality checking because water quality and climate change directly affect the embryonic development of Odonates.
- A mass-rearing technique of dragonflies in laboratory conditions was developed with controlled cannibalism.
- SNCs can be used as an additional nutrient source for the successful mass-rearing of Odonates in the laboratory.
- Dragonflies are a potential biocontrol agent of many pests and vectors, we can utilize this rearing technique in future Integrated Pest Management.
- We have also recorded different morphological changes in the *P. flavescens* naiads, which helps other researchers to conduct more studies on the post-embryonic development of the wandering glider *P. flavescens.*
- In this study, we examined the predation efficacy of the *P. flavescens* naiads, and our results show that dragonfly naiads are good predators of mosquito larvae. Moreover, as both these insects share some common habitats like wetlands and paddy fields, we recommend *P. flavescens* as a promising biocontrol agent for mosquito larvae, *C. quinquefasciatus*.

3.7 REFERENCES

Akram, W., & Ali-Khan, H. A. (2016). Odonate nymphs: generalist predators and their potential in the management of dengue mosquito, *Aedes aegypti* (Diptera: Culicidae). *Journal of Arthropod-Borne Diseases*, 10(2), 252-257.

Akre, B. G., & Johnson, D. M. (1979). Switching and sigmoid functional response curves by damselfly naiads with alternative prey available. *Journal of Animal Ecology*, 48 (3), 703–720. https://doi.org/10.2307/4191

Ando, H. (1962). The comparative embryology of Odonata with special reference to a relic dragonfly *Epiophlebia Superstes* Selys. *Japan Society for the Promotion of Science*, 3, 189–201.

Ando, H., & Watanabe, Y. (1995). Embryonic development of *Epiophlebia superstes. Insectarium*, 32(4), 92-98.

Andrew, R. J. (2002). Egg chorionic ultrastructure of the dragonfly *Tramea virginia* (Rambur) (Anisoptera: Libellulidae). *Odonatologica*, 31(2), 171-175.

Andrew, R. J. (2009). Fine structure of the egg chorion in two anisopteran dragonflies from central India (Libellulidae). *Odonatologica*. 38(4), 359-363.

Andrew, R. J., & Foerster, S. (2015). Egg shell ultrastructure of the dragonfly, *Micrathyria dictynna* Ris (Anisoptera: Libellulidae). *Zoologischer Anzeiger – A Journal of Comparative Zoology*, 254, 15-17. https://doi.org/10.1016/j.jcz.2014.09.003

Andrew, R. J., & Tembhare, D. B. (1992). Surface ultrastructure of the egg chorion in the dragonfly, *Ictinogomphus rapax* (Rambur) (Odonata: Gomphidae). *International journal of Insect Morphology and Embryology,* 21(4), 347-350. doi: 10.1016/0020-7322(92)90029-m

Andrew, R. J., Verma, P., & Rathodi, M. K. (2011). Post Ovipositional Changes in the Egg Chorionic Ultrastructure of the Dragonfly *Pantala flavescens* (Fabricius) (Insecta: Odonata: Anisoptera). *Biological Forum – An International Journal*, 3(2), 22-24.

Andrew, R.J., & Tembhare, D. B. (1995). Ultrastructural post-oviposition changes in the egg chorion of the dragonfly, *Zyxomma petiolatum* rambur (Odonata: Libellulidae). *International journal of Insect Morphology and Embryology,* 24(2), 235-238.

Anholt, B. R. (1994). Cannibalism and early instar survival in a larval damselfly. *Oceologia*, 99, 70-65. DOI: 10.1007/BF00317083

Anholt, B. R., Marden, J. H., & Jenkins, D. M. (1991). Patterns of mass gain and sexual dimorphism in adult dragonflies (Insecta: Odonata). *Canadian Journal of Zoology*, 69(5), 1156-1163. https://doi.org/10.1139/z91-164

Augustine, B., Eo, J., Kim, M. H., Kim, M. K., Choi, S. K., Yeob, S. J., … & Eric, O. D. (2021). Effects of temperature and water management in rice fields on larval growth of *Pantala flavescens* (Odonata: Libellulidae). *Korean Journal of Environmental Biology*, 39(4), 536-541. https://doi.org/10.11626/KJEB.2021.39.4.536

Baker, L. B. (1981). Behavioural interactions and use of feeding areas by nymphs of *Coenagrion resolution* (Coenagrionidae: Odonata). *Oceologia*, 49(3), 353-358. DOI: 10.1007/BF00347597

Benke, A. C. (1970). A method for comparing individual growth rates of aquatic insects with special reference to the Odonata. *Ecology*, 51(2), 328-331. doi:10.2307/1933673

Bradshaw, W. E., & Holzapfel, C. M. (2007). Evolution of animal photoperiodism. *Annual Review of Ecology, Evolution, and Systematics*, 38, 1–25.

Buskirk, J. V. (1989). Density-dependent cannibalism in larval dragonflies. *Ecology*, 70(5), 1442-1449. https://doi.org/10.2307/1938203

Busse, S., Buscher, T. H., Heepe, L., & Gorb, S. N. (2019). Adaptations of dragonfly larvae and their exuviae (Insecta: Odonata), attachment devices and their crucial role during emergence. *Journal of Insect Physiology*, 117. https://doi.org/10.1016/j.jinsphys.2019.103914

Chatterjee, S. N., Ghosh, A., & Chandra, G. (2007). Eco-friendly control of mosquito larvae by *Brachytron pratense* nymph. *Journal of Environmental Health*, 69(8), 44-49.

Christudhas, A., & Mathai, M. T. (2014). Genetic variation of a migratory dragonfly characterized with random DNA markers. *Journal of Entomology and Zoology studies*, 2(2), 182-184.

Corbet, P. S. (1962). *A Biology of Dragonflies,* London: Witherby.

Corbet, P. S. (1980). Biology of Odonata. *Annual Review of Entomology*, 25, 189-217. https://doi.org/10.1146/annurev.en.25.010180.001201

Corbet, P. S. (1999). *Dragonflies: Behaviour and Ecology of Odonata*, Harley: Colchester.

Corbet, P.S., Suhling, F., & Soendgerath, D. (2006). Voltinism of Odonata: a review. *International journal of Odonatology*, 9(1), 1–44. https://doi.org/10.1080/13887890.2006.9748261

Davis, G. K., & Patel, N. H. (2002). Short, long, and beyond: Molecular and embryological approaches to insect segmentation. *Annual Review of Entomology*, 47, 669–699.

Donoughe, S., & Extavour, C. G. (2016). Embryonic development of the cricket *Gryllus Bimaculatus*. *Developmental Biology*, 411, 140–156.

Ellis, M. R., & Ladeau, S. (2013). Influence of dragonfly larvae on mosquito development and survival. Cary Institute of Ecosystem Studies.

Gaino, E., Piersanti, S., & Rebora, M. (2008). Egg envelope synthesis and chorion modification after oviposition in the dragonfly *Libellula depressa* (Odonata, Libellulidae). *Tissue and Cell*, 40, 317-324. DOI: 10.1016/j.tice.2008.02.005

Gayathri M., Anand, P. P., & Shibu Vardhanan, Y. (2023). Visualisation of early embryos of the wandering glider, *Pantala flavescens* (Fabricius, 1798) (Odonata: Libellulidae), *Aquatic Insects*, 44(4), 297-309. https://doi.org/10.1080/01650424.2023.2202182

Goretti, E., Ceccagnoli, D., Porta, G. L., & Giovanni, M. V. D. (2001). Larval development of *Aeshna cyanea* (Muller, 1764) (Odonata: Aeshnidae) in Central Italy. *Hydrobiologia*, 457, 149-154.

Gossum, H. V., Sanchez, R., & Rivera, A. C, (2003). Observations on rearing damselflies under laboratory conditions. *Animal Biology*, 53(1), 37–45. http://dx.doi.org/10.1163/157075603769682567

Gresens, S. E., Cothran, M. L., & Thorp, J. H. (1982). The Influence of Temperature on the Functional Response of the Dragonfly *Celithemis fasciata* (Odonata: Libellulidae). *Oecologia,* 53, 281-284.

Hawking, J. H., & Ingram, B. A. (1994). Rate of larval development of *Pantala flavescens* (Fabricius) at its southern limit of range in Australia (Anisoptera: Libellulidae). *Odonatologica,* 23(1), 63-68

Hinton, H. E. (1981). *Biology of Insect Eggs*. 486-494. doi:10.1016/b978-1-4832-8401-9.50019-2

Holzmann, K. L., Charrier, C., & Johansson, F. (2022). Weak effects on growth and cannibalism under fluctuating temperatures in damselfly larvae. *Scientific Reports*, 12(1), 12910. https://doi.org/10.1038/s41598-022-17192-1

Hopper, K. R., Crowley, P. H., & Kielman, D. (1996). Density dependence, hatching synchrony, and within-cohort cannibalism in young dragonfly larvae. *Ecology,* 77, 191–200. http://dx.doi.org/10.2307/2265668

Hottenbacher, N., & Koch, K. (2006). Influence of egg size on egg and larval development of *Sympetrum striolatum* at different prey availability (Odonata: Libellulidae). *International Journal of Odonatology*, 9(2), 165-174. http://dx.doi.org/10.1080/13887890.2006.9748275

Hudson, J., & Berrill, M. (1986). Tolerance of low pH exposure by the eggs of Odonata (dragonflies and damselflies). *Hydrobiologia*, 140, 21-25.

Hyeun-Ji, L., & Johansson, F. (2015). Compensating for a bad start: compensatory growth across life stages in an organism with a complex life cycle. *Canadian Journal of Zoology*, 94, 41-47. doi.org/10.1139/cjz-2015-0157

Ichikawa, Y., Yokoi, T., & Watanabe, M. (2017). Thermal factors affecting egg development in the wandering glider dragonfly, *Pantala flavescens* (Odonata: Libellulidae). *Applied Entomology and Zoology*, 52(1), 89-95. DOI 10.1007/s13355-016-0457-9

Ilahi, I., Yousafzai, A. M., Attaullah, M., Haq, T. U., Ali, H., Rahim, A., … & Ahmad, B. (2019). The role of odonate nymphs in ecofriendly control of mosquitoes and sensitivity of odonate nymph to inorganic nutrient pollutants. *Applied Ecology and Environmental Research*, 17(3), 6171-6188.

Ivey, R. K., Bailey, J. C., Stark, B. P., & Lentz, D. L. (1988). A preliminary report of egg chorion features in dragonflies (Anisoptera). *Odonatologica*, 17(4), 393-399.

Jacob, B.G., Shililu, J., Muturi, E. J., Mwangangi, J. M., Muriu, S. M., Funes, J., Githure, J., … & Novak, R. J. (2006). Spatially targeting *Culex quinquefasciatus* aquatic habitats on modified land cover for implementing an integrated vector management

(IVM) program in three villages within the Mwea Rice Scheme, Kenya. *International Journal of Health Geographics*, 5(1), 18. DOI: 10.1186/1476-072X-5-18

Johansson, F. (1993). Intraguild predation and cannibalism in odonate larvae: Effects of foraging behaviour and zooplankton availability. *Oikos,* 66, 80–87. http://dx.doi.org/10.2307/3545198

Johnson, C. (1965). Mating and oviposition of damselflies in the laboratory. *Canadian Journal of Entomology*, 97, 321–326. http://dx.doi.org/10.4039/Ent97321-3

Jose, J., & Chandran, A. V. (2020). *Introduction to Odonata with identification keys for dragonflies & damselflies commonly found in Kerala*. Society for Odonate Studies. DOI: 10.13140/RG.2.2.35429.32486

Kenny, L.P., & Burne, M. R. (2001). *A Field Guide to the Animals of Vernal Pools*. Westborough, MA, Control group Heritage and Endangered Species Program.

Koch, K. (2015). Influence of temperature and photoperiod on embryonic development in the dragonfly *Sympetrum striolatum* (Odonata: Libellulidae). *Physiological Entomology*, 40, 90-101. DOI: 10.1111/phen.12091.

Konopova, B., & Zrzavy, J. (2005). Ultrastructure, development, and homology of insect embryonic cuticles. *Journal of Morphology*, 264, 339–362.

Kormondy, E. J. (1959). The systematics of Tetragoneuria, based on ecological, life history, and morphological evidence (Odonata: Corduliidae). *Miscellaneous Publications, Museum of Zoology, University of Michigan*, 107, 1–79.

Krull, W. H. (1929). The Rearing of Dragonflies from Eggs. *Annals of the Entomological Society of America*, 22, 651-658.

Kumar, R., Muhid, P., Dahms, H. U., Tseng, L. C., & Hwang, J. S. (2008). Potential of three aquatic predators to control mosquitoes in the presence of alternative prey: a comparative experimental assessment. *Marine and Freshwater Research*, 59, 817-835.

Lamptey, D. A., & Brandl, R. (2018). Effect of a dragonfly (*Bradinopyga strachani* Kirby, 1900) on the density of mosquito larvae in a field experiment using mesocosms. *Web Ecology*, 18, 81-89. https://doi.org/10.5194/we-18-81-2018

Lee, S. E., Kim, J. E., & Lee, H. S. (2001). Insecticide resistance in increasing interest. *Journal of Applied Biochemistry,* 44(3), 105-112.

Lerum, J. E. (1968). The Postemhryonic Development of the Compound Eye and Optic Ganglia in Dragonflies. *Proceedings of the lowa Academy of Science*, 75(1), 416-432. https://scholarworks.uni.edu/pias/vol75/iss1/56

Locklin, J. L., Huckabee, J. S., & Gering, E. J. (2012). A method for rearing large quantities of the damselfly, *Ischnura ramburii* (Odonata: Coenagrionidae), in the laboratory. *Florida Entomologist*, 95(2), 272–276. http://dx.doi.org/10.1653/024.095.0205

Lutz, P. E. (1974). Effects of temperature and photoperiod on larval development in *Tetragoneuria cynosure* (Odonata: Libellulidae). *Ecology*, 55, 370-377.

Mandal, S. K., Ghosh, A., Bhattacharjee, I., & Chandra, G. (2008). Biocontrol efficiency of odonate nymphs against larvae of the mosquito, *Culex quinquefasciatus* Say, 1823. *Acta Tropica*, 106(2), 109-114.

Masumoto, M., & Machida, R. (2006). Development of embryonic membranes in the silverfish *Lepisma saccharina Linnaeus* (Insecta: Zygentoma, Lepismatidae). *Tissue & Cell*, 38, 159–169.

Mataba, G. R., Clark, N. W., Kweka, E. J., Munishi, L., Brendonck, L., & Vanschoenwinkel, B. (2023). Interactive effects of dragonfly larvae and *Bacillus thuringiensis* var. *israelensis* on mosquito oviposition and survival. *Ecosphere*, 14(9), DOI: 10.1002/ecs2.4653

May, M. L. (1995). Comparative notes on micropyle structure in cordulegastroid and libelluloid Anisoptera. *Odonatologica*, 24(1), 53-62.

Miller, P. L. (1987). Oviposition behaviour and eggshell structure in some libellulid dragonflies, with particular reference to *Brachythemis lacustris* (Kirby) and *Orthetrum coerulescens* (Fabricius) (Anisoptera). *Odonatologica,* 16(4), 361-374.

Miller, P. L. (1992). The effect of oxygen lack on egg hatching in an Indian dragonfly, *Potamarcha congener*. *Physiological Entomology*, 17(1), 68-72.

Minot, M., Gall, M.L, & Huste, A. (2019). Biometry of the large dragonfly *Anax imperator* (Odonata: Aeshnidae): A study of traits from larval development to adults. *European Journal of Entomology*, 116, 269-280. doi: 10.14411/eje.2019.031

Miura, T., & Takahashi, R.M. (1988). A laboratory study of predation by damselfly nymphs, *Enallagmacivile*, upon mosquito larvae, *Culex tarsalis. Journal of the American Mosquito Control Association*, 4(2), 129-131.

Miyakawa, K. (1987). Position of germ rudiment and rotation of embryo in eggs of some dragonflies (Odonata). *Anthropod Embryology Society Japan*, 1, 125–149.

Miyakawa, K. (1990). Rotation of embryo in eggs of Petaluridae, Gomphidae, and Corduliidae, in connection, with types of oviposition, egg shape, and germ band (Odonata, Anisoptera). *Japanese Journal of Entomology*, 58, 447–463.

Moirangthem, B. D., Singh, S. N., & Singh, D. C. (2018). Comparative studies of three potent bioagent against mosquito larvae. *International Journal of Mosquito Research*, 5(6), 10-14.

Murray, R. L., Tah, S., Koprivnikar, J., Rowe, L., & Mccauley, S. J. (2019). Exposure to potentially cannibalistic conspecifics induces an increased immune response. *Ecological Entomology.* DOI: 10.1111/een.12806

Murugan, K., Dinesh, D., Kumar, P. J., Panneerselvam, C., Subramaniam, J., Madhiyazhagan, P., … & Benelli, G. (2015). *Datura metel*-synthesized silver nanoparticles magnify predation of dragonfly nymphs against the malaria vector *Anopheles stephensi*. *Parasitology Research*, 114, 4645-4654.

Nasrabadi, M., Azarm, A., Molaeezadeh, M., Bozorgomid, F., Shahidi, F., & Vatandoost, H. (2022). Use of aquatic insects for biological control of mosquitoes (Diptera;

Culicidae), vectors of different diseases. *Journal of Marine Science Research and Oceanography*, 5(4), 247-252.

Negi, C., & Verma, P. (2018). Review on *Culex quinquefasciatus*: Southern house mosquito. *International Journal of Life-Sciences Scientific Research,* 4(1), 1563-1566.

Okude, G., Fukatsu, T., & Futahashi, R. (2021). Comprehensive comparative morphology and developmental staging of final instar larvae toward metamorphosis in the insect order Odonata. *Scientific Reports,* 11, 5164. https://doi.org/10.1038/s41598-021-84639-2

Okude, G., Futahashi, R., Tanahashi, M., & Fukatsu, T. (2017). Laboratory rearing system for *Ischnura senegalensis* (Insecta: Odonata enables detailed description of larval development and morphogenesis in dragonfly. *Zoological Science,* 34, 386–397. https://doi.org/10.2108/zs170051

Panfilio, K. A. (2008). Extraembryonic development in insects and the acrobatics of blastokinesis. *Developmental Biology*, 313, 471–491.

Piersanti, S., Rebora, M., Salerno, G., Cordero-Rivera, A, & Frati, F. (2015). A method for rearing a large number of damselflies (*Ischnura elegans*, Coenagrionide) in the laboratory. *International Journal of Odonatology,* 18(2), 125-136. http://dx.doi.org/10.1080/13887890.2015.1015179

Polis, G. A. (1981). The evolution and dynamics of intraspecific predation. *Annual Review of Ecology, Evolution, and Systematics,* 12, 225-251. https://www.jstor.org/stable/2097111

Pritchard, G., Harder, L. D., & Mutch, R.A. (1996). Development of aquatic insect eggs in relation to temperature and strategies for dealing with different thermal environments. *Biological Journal of the Linnean Society,* 58(2), 221–244. https://doi.org/10.1111/j.1095-8312.1996.tb01432.x

Punzo, F. (1988). Effects of low environmental pH and temperature on hatching and metabolic rates in embryos of *Anax junius* Drury (Odonata: Aeshnidae) and the role of hypoxia in the hatching process. *Comparative Biochemistry and Physiology Part C: Comparative Pharmacology*, 91(2), 333–336.

Resh, V. H., & Carde, R. T. (Eds). (2009). *Encyclopedia of Insects.* (2nd ed). Academic Press is an imprint of Elsevier.

Rice, T.M. (2008). A review of methods for maintaining Odonate larvae in the laboratory, with a description of a new technique. *Odonatologica*, 37(1), 41-54

Rodrigues, M. E., Roque, F. D. O., Ferreira, R. G., Saito, V. S., & Samways, M. J. (2018). Egg-laying traits reflect shifts in dragonfly assemblages in response to different amount of tropical forest cover. *Insect Conservation and Diversity*, 12(3), 231-240. https://doi.org/10.1111/icad.12319

Rowe, R. J. (1980). Territorial behaviour of a larval dragonfly *Xanthocnemis zealandica* (McLachlan) (Zygoptera: Coenagrionidae). *Odonatologica*, 9(4), 285-292.

Rowe, R. J. (1991). Larval development and emergence in *Hemianax papuensis* (Burmeister) (Odonata: Aeshnidae). *Journal of the Australian Entomological Society*. 30, 209-215.

Saha, N., Aditya, G., Banerjee, S., & Saha, G. K. (2012). Predation potential of odonates on mosquito larvae: Implications for biological control. *Biological control*, 63(1), 1-8. http://dx.doi.org/10.1016/j.biocontrol.2012.05.004

Sahlen, G. (1994). Ultrastructure of the eggshell of *Aeshna juncea* (Odonata: Aeshnidae). *International Journal of Insect Morphology and Embryology*, 23(4), 345-354.

Sahlen, G., & Suhling, F. (2002). Relationships between egg size and clutch size among European species of Sympetrinae (Odonata: Libellulidae). *International Journal of Odonatology*, 5(2), 181-191.

Samanmali, C., Udayanga, L., Ranathunge, T., Perera, S. J., Hapugoda, M., & Weliwitiya, C. (2018). Larvicidal potential of five selected dragonfly nymphs in Sri Lanka over *Aedes aegypti* (Linnaeus) larvae under laboratory settings. *BioMed Research International*, 1-10. https://doi.org/10.1155/2018/8759459

Sander, K. (1976). Specification of the basic body pattern in insect embryogenesis. *Advances in Insect Physiology*, 12, 125–238.

Sander, K. (1996). Pattern formation in insect embryogenesis: The evolution of concepts and mechanisms. *International Journal of Insect Morphology and Embryology*, 25, 349–367.

Sathe, T. V & Shinde, K. P. (2016). *Dragonflies and pest management*. New Delhi, Daya Publishing House.

Sathe, T. V. (2013). *Dragonflies production technology*. New Delhi, Daya Publishing House.

Sebastian, A., Sein, M. M., Thu, M. M., & Corbet, P. S. (1990). Suppression of *Aedes aegypti* (Diptera: Culicidae) using augmentative release of dragonfly larvae (Odonata: Libellulidae) with community participation in Yangon, Myanmar. *Bulletin of Entomological Research*, 80, 223-232. DOI:10.1017/S0007485300013468

Sebastian, A., Thu, M. M., & Sein, M. M. (1980). The use of dragonfly nymphs in the control of *Aedes aegypti*. *The Southeast Asian Journal of Tropical Medicine and Public Health*, 11(1), 104-107.

Shad, A., & Andrew, J. (2013). A study on the predatory potency of dragonfly, *Bradinopyga geminata* nymphs over the immature stages of the filarial vector, *Culex quinquefasciatus* Say. *International Journal of Current Microbiology and Applied Sciences,* 2(4), 172-182.

Sherk, T. E. (1977). Development of the compound eyes of dragonflies (odonata). I. Larval compound eyes. *Journal of Experimental Zoology*, 201(3). 391-416. https://doi.org/10.1002/jez.1402010307

Sherk, T. E. (1978). Development of the compound eyes of dragonflies (Odonata) II. development of the larval compound eyes. *Journal of Experimental Zoology*, 203(1), 47-59. https://doi.org/10.1002/jez.1402030106

Sih, A., Crowley, P., McPeek, M., Petranka, J., & Strohmeier, K. (1985). Predation, competition, and prey communities: A review of field experiments. *Annual Review of Ecology and Systematics*, 16, 269-311. https://doi.org/10.1146/annurev.es.16.110185.001413

Singh, R. K., Dhiman, R. C., & Singh, S. P. (2003). Laboratory studies on the predatory potential of dragonfly nymphs on mosquito larvae. *Journal of communicable diseases*, 35(2), 96-101.

Sokolovska, N., Rowe, L., & Johansson, F. (2000). Fitness and body size in mature odonates. *Ecological Entomology*, 25(2), 239-248.

Stav, G., Blaustein, L., & Margalit, Y. (2005). Individual and interactive effects of a predator and controphic species on mosquito populations. *Ecological Applications*, 15(2), 587-598. https://doi.org/10.1890/03-5191

Subramanian, K. A. (2005). *Dragonflies and Damselflies of Peninsular India A Field Guide* (1st ed.). Project Lifescape. Indian Academy of Sciences, Bangalore, India.

Suhling, F., Sahlén, G., Gorb, S., Kalkman, V.J., Dijkstra, K-D.B., & van Tol, J. (2015). Order Odonata. In: Thorp, J., Rogers, D.C. (Eds.), Ecology and General Biology: Thorp and Covich's Freshwater Invertebrates, (pp. 893-932). Amsterdam: Academic Press.

Tennessen, K. (2019). *Dragonflies Nymphs of North America: An identification guide*. Springer. https://doi.org/10.1007/978-3-319-97776-8_2

Tennessen, K. J. (2019). Methods for collecting, rearing and preserving dragonflies. *Dragonfly Nymphs of North America*, 579-590. https://doi.org/10.1007/978-3-319-97776-8_13

Theopold, U., Schmidt, O., Soderhall, K., & Dushay, M. S. (2004). Coagulation in arthropods: defence, wound closure and healing. *Trends in Immunology,* 25(6), 289-94. doi: 10.1016/j.it.2004.03.004

Tillyard, R. J. (1917). *The Biology of Dragonflies (Odonata or Paraneuroptera)*, USA: Cambridge University Press.

Travis, J., Keen, W. H., & Juilianna, J. (1985). The role of relative body size in a predator prey relationship between dragonfly naiads and larval anurans. *Oikos*, 45 (1), 59–65. https://doi.org/10.2307/3565222

Trueman, J. W. H. (1991). Egg chorionic structures in Corduliidae and Libellulidae (Anisoptera). *Odonatologica*, 20, 441-452.

Ubhi, R., & Matthews, P. G. D. (2018). The transition from water to air in aeshnid dragonflies is associated with a change in ventilatory responses to hypoxia and hypercapnia. *Journal of Insect Physiology*, 106(3), 172-178. http://dx.doi.org/10.1016/j.jinsphys.2017.09.010

Vantandoost, H. (2021). Review: Dragonflies as an important aquatic predator insect and their potential for control of vectors of different diseases. *Journal of Marine Science*, 3(2), 13-20. DOI: https://doi.org/10.30564/jms.v3i3.3121

Venkatesh, A., & Tyagi, B. K. (2013). Predatory potential of *Bradinopyga geminate* and *Ceriagrion coromandelianum* Larvae on dengue vector *Aedes aegypti* under controlled conditions (anisoptera: libellulidae; zygoptera: coenagrionidae; diptera: culicidae). *Odonatologica*, 42(2), 139-149.

Waringer, J. (1983). A study on embryonic development and larval growth of *Sympetrum danae* (Sulzer) at two artificial ponds in Lower Austria (Anisoptera: Libellulidae). *Odonatologica*, 12(4), 331-343.

Weis, A. E., Abrahamson, W. G., & Andersen, M. C. (1992). Variable selection on eurosta's gall size, I: the extent and nature of variation in phenotypic selection. *Evolution; International Journal of Organic Evolution*, 46(6), 1674-1697. https://doi.org/10.1111/j.1558-5646.1992.tb01161.x

Weterings, R., Umponstira, C., & Buckley, H. L. (2015). Predation rates of mixed instar Odonata naiads feeding on *Aedes aegypti* and *Armigeres moultoni* (Diptera: Culicidae) larvae. *Journal of Asia-Pacific Entomology*, 18, 1-8. http://dx.doi.org/10.1016/j.aspen.2014.10.008

Whedon, A. D. (1942). Some observations on rearing Odonata in the laboratory. *Annals of the Entomological Society of America,* 35(3), 339-342. https://doi.org/10.1093/aesa/35.3.339

Wissinger, S. A. (1988). Effects of food availability on larval development and inter-instar predation among larvae of *Libellula lydia* and *Libellula luctuosa* (Odonata: Anisoptera). *Canadian Journal of Zoology*, 66, 543-549. https://doi.org/10.1139/z88-080

Witzig, J. F., Huner, J. V., & Avault, J. W. (1986). Predation by dragonfly naiads *Anax junius* on young crawfish *Procambarus clarkia*. *Journal of the World Aquaculture Society*, 17(1-4), 58-63.

Chapter 4

Isolation, Sequencing, and Molecular Structural Characterisation of Wing Resilin of Wandering Glider, *Pantala flavescens* (Libellulidae)

CONTENTS

LIST OF FIGURES

LIST OF TABLES

4

Isolation, Sequencing, and Molecular Structural Characterisation of Wing Resilin of Wandering Glider, *Pantala flavescens* (Libellulidae)

4.1 INTRODUCTION

The wings of Odonates are a corrugated network of veins interconnected by thin membranes (Appel & Gorb, 2011). The longitudinal veins of dragonflies are connected to the cross veins to form vein joints, and the thickness of the longitudinal veins varies from the wing base to the tip (Wootton & Newman, 1986; Jongerius & Lentink, 2010). These tubular wing veins are the central structural unit of the wing and act as cantilever beams (Marrocco et al., 2010). Several wing vein joints in Odonata, have been observed with different geometries and material compositions (Appel & Gorb, 2014). Different parts of the wings of dragonflies have different functions. The wing structure and function are mainly assisted by the costa, pterostigma, and by the nodus (Marrocco et al., 2010)

Elastomeric proteins are seen in many organisms, such as elastin and fibrillin in vertebrates, abductin in molluscs, wheat gluten, and insect resilin (Shewry et al., 2004). The rubber-like protein resilin was first identified by Weis-Fogh (1960) in the wing hinge ligament of the locust *Schistocerca grigaria* and the elastic tendons of the dragonfly *Aeshna grandi,* and it is mainly found in the insect cuticle. This rubber-like protein can be stretched to over 300% of the resilin's original length (Andersen & Weis-Fogh, 1964; Elvin et al., 2005). Later this resilin protein was discovered in many other organs of insects also, like in the feeding pump of *Rhodnius prolixus* (Bennet-Clark, 1963), the salivary pump of assassin

bugs (Edwards, 1960), in the jumping system of fleas (Bennet-Clark & Lucey, 1967) and the sound-producing organs of some insects like moths and cicades (Fonseca & Bennet-Clark, 1998). In dragonflies and locusts, this resilin is mainly seen in the wings, which beat at a frequency of 15-5-Hz (Jensen & Weis-Fogh, 1962).

The resilin protein shows structural diversity as in dragonfly tendons, this resilin is a pure polymer, whereas in cockroach tarsal pads, fruit fly wing hinges, and locust pre-alar arms this, protein can be seen as a composite of chitin and resilin (Elliot et al., 1965). The level of disorder in resilin protein is very high and is highly unstructured with little or no secondary structures like α-helices or β-sheets (Kappiyoor et al., 2011; Petrenko, 2010). Any deformation will cause a decrease in conformational entropy, which produces elastic force in the resilin (Weis-Fogh, 1961).

The resilin gene of *Drosophila melanogaster* was identified by Ardell and Andersen (2001). The resilin sequence of *D. melanogaster* consists of three central regions with a signal peptide sequence at the N-terminal domain. The three main domains include the N-terminal elastic domain (exon 1), the chitin-binding domain (exon 2), and the C-terminal elastic domain (exon 3) (Figure 4.1). This exon 1 (PSSSYGAPGGGNGGR) and exon 2 (GYSGGRPGGQDLG) have many repetitive sequences that give elastic properties to the resilin protein (Lyons et al., 2009; Qin et al., 2009). There is only a single exon in the dragonflies that is homologous to exon 1 of the other insect's resilin gene, and there is no chitin-binding domain in the dragonfly's resilin gene (King, 2010).

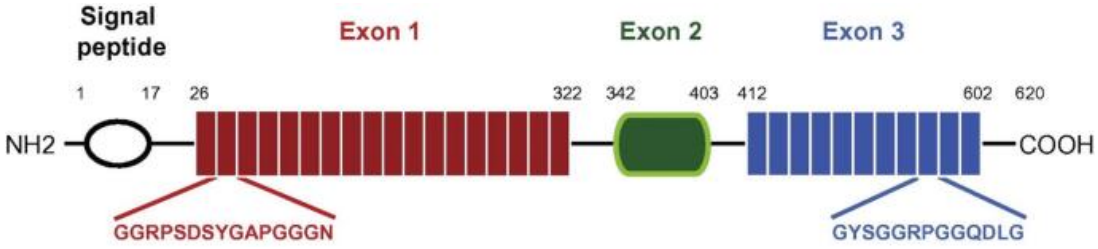

Figure 4.1: Resilin protein. Exons in resilin where exon-1 is known as N-terminal elastic repeat and exon-3 is known as C-terminal elastic repeat. Exon 2 is known as ChBD, which binds the chitin and helps the process of construction of the cuticle composite. (Source: Doi: 10.1002/adfm.202215162)

The polypeptide chains of resilin protein are linked together by covalent cross-links, the fully cross-linked protein is called resilin, and incompletely cross-linked proteins are called pro-resilin (Andersen, 2010). The resilin protein has a high proportion of amino acids glycine and proline, which makes the resilin a more flexible and disordered protein (Ardell & Andersen, 2001; Andersen, 2003; Willis, 2010). Proline forms Poly-proline (PPII) structures and will inhibit the formation of hydrogen-bonded secondary structures (Rauscher et al., 2006). In contrast, the absence of a side chain in glycine makes them more flexible, and this ordered nature is entropically unfavourable (Cheng et al., 2010). The unstructured resilin protein's secondary structure is in dynamic equilibrium between β-turn and PPII and β-strands conformations (Bochicchio et al., 2008). The resilin protein has a unique amino acid sequence and it differs from other elastomeric proteins like collagen, elastin, and silk fibroin (Kovalev et al., 2018).

The structural protein resilin is present throughout the insect cuticle, and this protein in the wing vein joints gives flexibility to the wings during flapping flight (Weis-Fogh, 1960; Gorb, 1999; Ma et al., 2015). This resilin protein helps to increase flexibility, improve efficiency, reduce stress, and store elastic energy, and this resilin helps the wings to return to their original position after elastic deformation (Chapman, 1998; Mistick et al., 2016; Mountcastle & Combes, 2013; Gorb, 1999; Michels et al., 2016; Rajabi et al., 2016). In dragonflies and damselflies, this resilin protein helps generate flexibility in the wing vein joints (Gorb, 1999; Appel & Gorb, 2011; Donoughe et al., 2011). The rubber-like properties, low stiffness, high fatigue lifetime, and high resilience (Weis-Fogh, 1960; Weis-Fogh, 1961; Gosline et al., 2002) of resilin make them an appropriate candidate for biomaterial applications, especially in some highly repetitive movement occurring areas, like in the joints, muscles, vocal folds, etc (Li et al., 2011; Lv et al., 2010). Even though the resilin-filled areas of the vein joints are very tiny, they play a significant role in bending shapes and give flexibility to the whole wing (Donoughe et al., 2011; Mountcastle & Combes, 2011).

The amino acids dityrosine and trityrosine give autofluorescence properties to the resilin protein (Andersen, 1964; Andersen & Weis-Fogh, 1964). The fluorescent microscope having a 4'6-diamino-2-phenylindole (DAPI) filter with excitation 321-378 and emission 420-470 is very suitable for the resilin autofluorescence visualisation (Michel & Gorb, 2012). Strong autofluorescence is shown in the insect cuticle at different wavelengths ranging from blue-green area to deep-red, whereas autofluorescence of resilin is at a very narrow band of wavelengths (Andersen, 1964; Stanislav, 1999). So, immune labelling and other treatments are unnecessary for the resilin protein (Stanislav, 1999).

The dragonfly *P. flavescens* (Libellulidae), the wandering glider or globe skimmer, is widely distributed and are long-distance migratory species (Christudhas & Mathai, 2014). In this study, we describe the distribution of resilin in different vein joints of the dragonfly *P. flavescens,* and isolated, sequenced, and characterised the resilin protein. Homology modeling was used to create the three-dimensional protein structure of the resilin from *P. flavescens*. We have also validated the model and checked the resilin protein properties.

4.2 REVIEW OF LITERATURE

Weis-Fogh (1960, 1961) pioneered studies on insect resilin in the cap tendon cuticle of *Aeshna cyanea*. Baumler and Busse (2019) studied resilin in the cap tendons of the Odonata, its distribution, biomechanical importance, and other functions related to its flight performance. Bailey and Weis-Fogh (1961) first studied the amino acid composition of the resilin protein.

Gorb (1999) studied the wing vein joints of the damselfly *Enallagma cyathigerum* and revealed the presence of resilin in the flexible vein joints. Appel and Gorb (2011) compared the distribution of resilin in different wing vein joints of the dragonfly *Epiophlebia superstes* and found that the distribution differs between the dorsal and ventral sides of the wing. Stanislav (1999) conducted a detailed study on the wing vein mobile joints of the damselfly *Enallagma cyathigerum* and revealed the presence of resilin in the mobile joints. The ultrastructure of the wing veins of dragonflies *Sympetrum vulgatum* and *Matrona basilaris* has been studied by

Appel et al. (2015), and their study revealed that resilin is also present in the internal cuticle layer of the veins. The function and diversity of resilin and cuticular spikes in the wings of dragonflies and damselflies have been studied by Donoughe et al. (2011). Fouziyah et al. (2014) studied the morphological and mechanical characteristics of the hindwing nodus of some Libellulid dragonflies, and they also studied the resilin in the nodus of the hindwing. Rajabi et al. (2016) studied the mechanical properties of the wing vein joints in dragonflies and the role of resilin in the vein joints. Rajabi et al. (2018) conducted a detailed study on the micro-morphological differences in the wings of perchers and flier dragonfly species from the family Libellulidae. Also, they compared the role of resilin in the nodus of both the forewing and hindwing. Marrocco et al. (2010) conducted a detailed study to understand the effect of resilin joints on the structural dynamics of the dragonfly wing. Noorhidayah et al. (2018) studied the morphological and mechanical properties of the resilin vein joints of the damselfly. They used the techniques of laser scanning microscopy and scanning electron microscopy to understand the structure and function of the vein joints, and they also used atomic force microscopy to study the elasticity of different parts of the wings. Li et al. (2014) conducted a detailed study on the antifatigue properties of the wings of *P. flavescens.* Their study showed that the sandwich microstructure of the veins of dragonflies gives the wing more strength, flexibility, and toughness, which helps in load bearing during flight and also plays a vital role in the antifatigue properties of the wings. Hou et al. (2017) studied the role of soft vein joints with resilin in dragonfly flight.

Sebastian and Gorb (2018) studied the material composition of the damselfly naiads *Erythromma najas* mouthparts cuticle and its influence on biomechanics. Resilin was also found to be dominant in the membranous transition between the labrum and anteclypeus, and this resilin helps in the labrum's mobility and shock absorption (Sebastian & Gorb, 2018). Pikkarainen and Kulonen (1972) studied the relationship between different collagens, fibroin, elastin, and resilin.

Andersen (2004) studied the distribution of dityrosine and trityrosine content of resilin in different cuticular regions of the adult and nymphs of the desert

locust *Schistocerca gregaria* and found a variation in the distribution of the di- and trityrosine ratio in different cuticular regions. Lombardi and Kaplan (1992) isolated resilin from the cockroach, *Periplaneta americana,* and characterized the protein. Andersen et al. (2023) studied the distribution and abundance of resilin protein at different ages of the honey bees *Apis mellifera* and their study revealed higher levels of resilin at the pupal stage but observed a significant decline in the level of resilin with age. Huo and Zhong (2023) studied the resilin joints and resilin stripes in the honeybee wings and their influence on the mechanical properties of the wings. Ma et al. (2015) studied the different functions of resilin in the wings of honeybees, especially the role of resilin in the camber changes during flapping flight. The functional role of resilin in the wings of beetles *Pachnoda marginata* and *Coccinella septempunctata* was studied by Haas et al. (2000), and they found that resilin plays an important role in wing deformation during wing folding and flight. Neff et al. (2000) identified the presence of resilin in the legs of a cockroach, *Periplaneta americana* by UV illumination and histological staining using toluidine blue. They have also developed a new confirmation method for identifying resilin by altering the pH and causing changes in the UV fluorescence. Burrows et al. (2008) studied the role of resilin in the jumping of froghopper insects. Kovalev et al. (2018) determined the mechanical properties of resilin in compression, and they studied the viscoelastic response of the resilin through microindentation of the wing hinge of *Locusta migratoria.* Michels et al. (2012) study revealed the existence of the elastic protein resilin in the mandibles of the copepod *Centropages hamatus* that helps crush the mineralised shells of diatoms.

After the reporting of resilin gene CG15290 from the *D. melanogaster* (Ardell & Anderson, 2001) many recombinant proteins based on resilin sequences have been designed by researchers with additional biological characteristics. Zhao et al. (2023) successfully inserted the resilin protein from *D. melanogaster* into the silkworm, and their result showed that the resilin protein improves the mechanical properties of the silk. Resilin's properties, like the high-frequency responsiveness, can be utilised in treating vocal fold pathologies by developing resilin-based material (Li et al., 2011). Resilin-based hydrogels have been engineered by Li et al.

(2013) with many beneficial mechanical and cell adhesive properties. Using a *Drosophila* Anti-Rec 1 resilin antibody, Wong et al. (2012) studied the expression of resilin in the developing insect cuticle. This was the first study detecting the expression of resilin during embryogenesis.

Lyons et al. (2011) studied the functional and molecular characterisation of resilin from three different insects: a flea (*Ctenocephalides felis*), a buffalo fly (*Haematobia irritans exigua*), and a dragonfly (*Aeshna* sp.). Their study showed that resilin's gene and protein sequence is conserved in many regions, and cross-linked recombinant resilin proteins show similar mechanical properties in flying and jumping insects.

Elliott et al. (1965) studied the structure of resilin using X-ray diffraction and electron microscopy, revealing that the resilin protein is highly amorphous. Nairn et al. (2008) evaluated the structure and the secondary structure distribution of a synthetic resilin AN16, based on the repeat units of resilin from *Anopheles gambiae*. The structure and functions of the resilin from *Drosophila* were studied by Qin et al. (2012). They proposed a resilin model to explain the resilin elasticity and energy conservation mechanisms. Khandaker et al. (2016) have done the molecular modelling of the resilin protein from *D. melanogaster* to study the relationship between amino acid sequences and the elastomeric behaviour of the resilin. Woodrow et al. (2024) introduced a new methodology for identification of the resilin in the insect cuticle by using Raman spectroscopy and they used the desert locust *Schistocerca gregaria* as the model species. Qin et al. (2009) generated the recombinant full-length resilin of *D. melanogaster* and also characterised the resilin. Hu et al. (2010) studied the structure and elastic properties of full-length resilin protein by using Temperature-modulated Differential Scanning Calorimetry (TMDSC), Real-time Fourier Transform Infrared Spectroscopy (FTIR), synchrotron Real-time X-ray, and AFM.

4.3 MATERIALS AND METHODS

4.3.1 Sample collection and Morphological characterization

The adult *P. flavescens* were collected from Palakkad district, Kerala, India, and their wings were used for the resilin protein studies. The forewing and hindwings of *P. flavescens* have been taken for the studies. The dissected wings were cleaned with a fine brush to remove dust contamination. The wings were then placed in a clean slide, covered with a coverslip for examination under the microscope Zeiss Axio Scope A.1 Fluorescence microscopes with Axiocam 305 multi-chrome **CCD** camera. We used fluorescence microscopy to confirm resilin in the wings of *P. flavescens.* Fore and hind wing morphological variability was documented in light, fluorescence microscope (DAPI filter), and FTIR imaging. In this DAPI filter, the resilin regions of the wings displayed a blue autofluorescence. We have taken images of the same area of the wings using fluorescence bright-field microscopy. The fluorescence intensity of wing joints was also measured using the ImageJ tool.

4.3.2 The *P. flavescens* naiad culture

Eggs of the adult female *P. flavescens* were collected and cultured in the laboratory. Plastic trays (34 cm length, 26 cm breadth, and 5 cm height) with 5L capacities were used for culturing the naiads. The tray was filled with de-chlorinated tap water, and some small pebbles were added to make hiding places for the naiads. We used to change the water every fifth day without disturbing the naiads.

The early instars of naiads were fed daily with artemia, paramecium, and moina, the later instars were fed with mosquito larvae and blood worms. Paramecium was cultured in the laboratory by using dried banana leaf. The dried banana leaves were added into a glass beaker with one-litre of dechlorinated tap water. The beaker was closed with a muslin cloth to avoid the egg laying by other insects. One or two drops of milk were added to provide the required bacteria and small protozoans. The paramecium is reproduced by simple division, and a sufficient number of paramecia are produced on the fifth day. Artemia tablets were used for the

culture. For one artemia tablet, we used one litre of de-chlorinated tap water mixed with two tablespoons of salt and provided continuous aeration. Moina is a crustacean mainly used as a live fish food and is commercially available. Initial cultures of the moina were collected from a fish shop, and then we cultured them in cement tanks using fresh papaya leaves. Mosquito larvae culture was also maintained in the laboratory. The egg rafts of mosquitoes were collected from the cement tanks used for the moina culture. The tanks were filled with water, a few dry leaves, and one large papaya leaf, which attracted the mosquitoes. We changed the papaya leaves every third day before they started decaying. The collected egg rafts were then transferred to plastic trays filled with 3 L of water. The eggs were hatched within 2 days after oviposition. Powdered dog biscuits and fish food were added to the larval trays as food. Commercially available live blood worms were used to feed the later naiad instars of *P. flavescens*. This final instar naiads of *P. flavescens* were preserved and used for the resilin gene isolation.

4.3.3 Molecular characterization

4.3.3.1 Isolation of resilin

The last instar naiads of *P. flavescens* were stored in 75% alcohol for resilin gene isolation. We used entire specimens to isolate DNA, which was appropriately cleaned and transferred to a sterilised, clean, dry Eppendorf tube. DNA was extracted from the tissue by using Nucleospin® Tissue Kit (Macherey-Nagel) following the manufacturer's instructions as follows:

1. Cut 25mg tissue into small pieces and transfer it into a microcentrifuge tube.

2. Add 180µL Buffer T1 and 25 µL Proteinase K solution. Vertex well and ensure that the samples are entirely covered with lysis solution and incubate at 56^{o} C until complete lysis is obtained. Vertex occasionally occurs during incubation.

3. Vertex the samples and add 200 µL Buffer B3. Vertex vigorously and incubated at 70^{o} C for 10 min.

4. Add 210 µL ethanol (96-100%) to the sample and vertex.

5. For each sample, place one Nucleospin® Tissue column into a collection Tube. Apply the sample to the column -centrifuge for 1 Min at 11,000 xg. Discard the Collection Tube with flow through and place the column in a new collection Tube.

6. Add 500 µL Buffer BW-centrifuge for 1 min at 11.000 xg. Discard the flow-through and place the column back into the collection tube.

7. Add 600 µL Buffer B5 to the column and centrifuge for 1 min at 11,000 xg. Discard the flow-through and place the column back into the collection tube.

8. Centrifuge the column for 1 min at 11,000 xg

9. Place the Nucleospin® Tissue column into a 1.5ml microcentrifuge tube and add 100 µL Buffer BE. Incubate at room temperature for 1 min-centrifuge 1 min at 11,000 xg.

4.3.3.2 Agarose gel electrophoresis

To assess integrity, the extracted DNA was subjected to 0.9% Agarose gel electrophoresis, the gel imaging was done using the SynGene gel documentation system GBox F3, UK.

4.3.3.3 PCR amplification and sequencing

The extracted DNA was subjected to PCR amplification. PCR was performed in a reaction mixture containing 6.25µL master mix, 1.25µL forward and reverse primer, 1µL extracted DNA sample, and 3.25µL water. The total volume of the reaction mixture is 13 µL.

The Primer 3 Plus tool designs the primer for resilin amplification when performing PCR. The primer is designed based on the previously deposited resilin sequence.

The designed primer:

- Res-F: 5’ TCTCCAGTGCTTCGAGGATA 3’
- Res-R: 5’ GCGCTCCGTAACTAGATGAAA 3’

4.3.3.4 PCR amplification profile of Resilin

Table 4.1: PCR amplification profile

PCR conditions	Time	Conditions step	
94°C	5 min.	Initial denaturation	
94°C	30 Sec.	Denaturation	35 cycles
55°C	30 sec.	Annealing	
72°C	1 min.	Extension	
72°C	10 min.	Final extension	

The purified PCR products were sequenced from both ends using forward and reverse primer by Sanger’s dideoxy chain termination method (Sanger & Coulson, 1975) at Rajiv Gandhi Center for Biotechnology (RGCB), Trivandrum, Kerala, India.

4.3.3.5 Sequence quality checking

The quality of the chromatogram was checked and validated in MEGA X software. Forward and reverse primer sequences were removed to eliminate sequence ambiguity. The Resilin sequences obtained were multiple-aligned using ClustalW and the MEGA X tool. The aligned sequences have been translated to amino acids to assess for the presence of premature stop codons that indicate the presence of nuclear pseudogenes or sequencing errors. The final sequence’s FASTA formats were used to search for its similarity in NCBI BLAST.

4.3.4 Insilico analysis

4.3.4.1 Template-based molecular modeling: Homology modeling

The FASTA sequence of the protein is given as the input. A new threading algorithm, MUSTER, extends the previous sequence profile-profile alignment (PPA) method. It combines various sequence and structure information into single body terms which can be conveniently used in dynamic programming search: (1) sequence profiles; (2) secondary structures; (3) structure fragment profiles; (4) solvent accessibility; (5) dihedral torsion angles; (6) hydrophobic scoring matrix. The balance of weighting parameters is optimized by a grading search based on the average TM-score of 111 training proteins, which perform better than conventional optimisation methods based on the PROSUP database (Wu & Zhang, 2008).

The algorithm is tested on 500 non-homologous proteins independent of training sets. After removing the homologous templates with sequence identity to the target >30%, in 224 cases, the first template alignment has the correct topology with a TM-score >0.5. Even with a more stringent cut-off by removing the templates with a sequence identity >20% or detectable by PSIBLAST with an E-value <0.05, MUSTER can identify correct folds in 137 cases with the first model of TM- score >0.5. Depending on the homology cut-offs, MUSTER's average TM-score of the first threading alignments is 5.1-6.3% higher than that by PPA. This improvement is statistically significant by the Wilcoxon signed-rank test with a P-value <1.0, demonstrating additional structural information's effect on the protein fold recognitions (Wu & Zhang, 2008).

The best models were evaluated in PROCHCEK (Laskowski et al., 1993) & PDBsum server (Laskowski et al.,2005). PROCHECK evaluates the stereochemical quality of the model through the Ramachandran plot. Good quality models were selected by more than 90% of residues in the most favoured and additional allowed regions and visualized in PyMol and EzMol 2.1 (Reynolds et al., 2018).

4.3.4.2 Signal peptide prediction

Phobius was used to predict the resilin's signal peptide topology. In Phobius, a hidden Markov model that combines transmembrane topology and signal peptide Predictions. The method optimises between transmembrane segments and signal peptides and allows constrained and homology-enriched predictions. The Phobius web server provides an easy and accurate means to predict signal peptides and transmembrane topology from an amino acid sequence. The sequences were submitted in Fasta format and preferably uploaded as a file. The predictions are given either in 'short' – signal line text output or 'long' – UniProt feature table-styled output (Kall et al., 2007).

4.3.4.3 Chemical structural characterization

SAPS evaluates a wide variety of protein sequence properties using statistics. Properties considered include compositional biases, clusters, runs of charge and other amino acid types, different kinds and extents of repetitive structures, locally recurring motifs, and anomalous spacing between identical residue types (Madeira et al., 2019).

4.3.4.4 Physico-Chemical characterization

ExPASy ProtParam computes various physicochemical properties that can be deduced from a protein sequence. The parameters computed by ProtParam include the molecular weight, theoretical pI, amino acid composition, atomic composition, extinction coefficient, estimated half-time, instability index, aliphatic index, and grand average of hydropathicity (GRAVY). Extinction coefficient (EC) indicates how much light a protein absorbs at a specific wavelength. It is helpful to estimate this coefficient for following a protein's spectrophotometer when purifying it (Pace et al., 1995; Edelhoch, 1967; Gill & von Hippel, 1989). In-vivo half-life, it is predicted that half of the protein amount in a cell to disappear after its synthesis in the cell. ProtParam relies on the "N-end rule", which relates the half-life of a protein to its N-terminal residue identity. The rule was established from experiments that explored the metabolic fate of artificial beta-galactosidase proteins with different N-

terminal amino acids engineered by site-directed mutagenesis (Bachmair et al.,1986; Gonda et al., 1989; Varshavsky, 1997). The instability index (II) provides an estimate of the stability of the protein in a test tube. A protein whose instability index is smaller than 40 is predicted as stable; a value above 40 predicts that the protein may be unstable (Guruprasad et al., 1990). The aliphatic index (AI) of protein is defined as the relative volume occupied by aliphatic side chains (alanine, valine, isoleucine, and leucine) (Ikai, 1980). The grand average of hydropathy (GRAVY) value for a peptide or protein is calculated as the sum of all the amino acids' hydropathy values divided by the number of residues in the sequences (Kyte & Doolittle, 1982).

4.3.4.5 Solvent Accessible Surface Area (ASA) analysis

VADAR (Volume, Area, Di-hederal Angle Reporter) is a compilation of more than 15 different algorithms and programs for analyzing and assessing peptide and protein structures from their PDB coordinate data. The results have been validated through extensive comparison to published data and careful visual inspection. The VADAR web server supports the submitting of either PDB formatted files or PDB accession numbers. VADAR produces extensive tables and high-quality graphs for quantitatively and qualitatively assessing protein structures determined by X-ray crystallography, NMR spectroscopy, 3D-threading, or homology modelling. The server evaluates key structural parameters for individual residues and the complete protein. These include excluded volume, accessible surface area, backbone, side chain dihedral angles, secondary structure, hydrogen bonding partners, hydrogen bond energies, steric quality, solvation-free energy, and local and overall fold quality. These derived parameters can rapidly identify both general and residue-specific problems within newly determined protein structures (Willard et al., 2003).

4.4 RESULTS

4.4.1 Resilin in the vein joints of *P. flavescens*

We have taken images of different wing vein joints of the *P. flavescens* in light, and fluorescence microscopy (Fig. 4.3, 4.4), and FTIR imaging (Fig. 4.5). Wing resilin is present in the forewing and hindwing and the selected vein joints were documented. Fluorescence was found to be present only in the mobile joints of the wing vein where the longitudinal vein meets the cross vein and is not seen in the immobile joints (Fig. 4.3I, 4.3L, 4.4I, 4.4L). The longitudinal veins are more robust and thicker than the cross veins. Most of the resilin was noticed in the ventral side of the wings rather than the dorsal side. Compared to the forewing, a high level of resilin fluorescence was observed in the hindwings. The fluorescence intensity was found to be different in different areas of the wings of *P. flavescens*. Resilin fluorescence is also seen in the dorsal and ventral side of the nodus and the veins of the anal area of both the fore-and hindwings (Fig. 4.2).

Fluorescence intensity measurement

Five forewing and hindwing mobile joints, R1, R2, R3, R4, and R5 (Table 4.2, 4.3) were selected for the fluorescence intensity comparison (Fig. 4.3, 4.4). The hindwing showed the highest fluorescence intensity (Fig. 4.6B). The highest intensity area of the forewing and hindwing was found to be different. In the forewing, the R1 (nodus) shows the highest resilin fluorescence (Fig. 4.6A), whereas in the hindwings, the R2 (Posterior and proximal vertex of the subtriangle) shows the highest fluorescence (Fig. 4.6B).

Table 4.2: Forewing vein joints

R1	Nodus (N)
R2	The distal end of the anterior margin of the triangle (T)
R3	The posterior end of the triangle (T)
R4	The distal end of radial supplement (Rspl)
R5	Distal end of anterior media (MA)

Table 4.3: Hindwing vein joints

R1	Nodus (N)
R2	Posterior and proximal vertex of the sub-triangle (t)
R3	Distal vertex of sub-triangle (t)
R4	Basal end of anal vein (A3)
R5	Posterior end of first cross-vein between R2 & R3

4.4.2 Sequencing of resilin from *P. flavescens*

Partial resilin of the *P. flavescens* was isolated, sequenced, and characterised. The partial sequence contained 250 bp (Fig. 4.7). The nucleotide sequences were then converted into protein sequences (77 amino acids sequence). While blasting this *P. flavescens* sequence, it showed similarity with the resilin gene of the *Ladona fulva* and *Aeshna* sp. This protein sequence of the resilin was then used for further insilico analysis.

The amino acid sequence of the resilin from *P. flavescens*:

RRGNFARDMGGWERRVHGCCFVWSSKAQVAKKLGSRIGKVPESNMKCRLL
LEKASNGFNLLLDNGKLRNKIIHSFVK

We compared the resilin protein sequence of *P. flavescens* with two Anisopteran dragonfly species, *L. fulva* (Libellulidae) (Fig. 4.8) and *Aeshna* sp. (Aeshnidae) (Fig. 4.9). The resilin sequence showed similarities with both species. The *P. flavescens* resilin sequence showed more similarities with the exon region of the resilin sequence of *L. fulva.*

BLAST ® » **Global Alignment** » results for RID-Y8DBGSD5114

Job Title	tr|A0A8K0K0T6|A0A8K0K0T6_LADFU Pro-resilin... ...
RID	Y8DBGSD5114 Search expires on 03-04 15:31 pm
Program	Needleman-Wunsch alignment of two sequences
Query ID	lcl|Query_3883643 (amino acid)
Query Descr	tr|A0A8K0K0T6|A0A8K0K0T6_LADFU Pro-resilin OS=Ladona fulva OX=123851 GN=J437_LFUL006303 PE=4 SV=1 ...
Query Length	521
Subject ID	lcl|Query_3883645 (amino acid)
Subject Descr	PF ...
Subject Length	77

Descriptions

Description	Score	Percent Ident	Accession
PF	-459.0	3.00%	Query_3883645

Graphic Summary

Distribution of the top 1 Blast Hits on 1 subject sequences

Query

1 100 200 300 400 500

Alignments

Alignment view: Pairwise with dots for identities ☐ CDS feature Restore defaults

PF

Sequence ID: Query_3883645 Length: 77 Number of Matches: 1
Range 1: 1 to 77

NW Score	Identities	Positives	Gaps	Frame
-459	15/523(3%)	27/523(5%)	448/523(85%)	

```
Query  1    MLAMSALALLCVSAEPPVSNEYLPPNGGAGMYSNGLTGAISSSYGAPNGNGNGGNGGRPS  60
Query  61   STYGAPNGNGIGGNGLSSTYGAPNGNGLGGNGGLSSTYGAPNGNGFGGNGGRPSSTYGAP  120
Query  121  NGNGNGGNGLSSTYGAPNGNGGNGLSSTYGAPNGNGFGRNGGRPSSTYGAPNGNGLGG  180
Query  181  NGGRPSSTYGAPNGNGNGGRLSSTYGAPNGNGFGNGNGGRPSSTYGAPNGNSYNGNGG  240
Query  241  RPSSTYGAPNGNGLGGNGGRPSSTYGAPNGNGFGNGNGGRPSSTYGAPNGNGNGGNGGRP  300
Query  301  SSTYGAPNGNGYNGNGGRPSSTYGAPNGNGLSGNGGRLSSTYGAPNGNGFGGNGLSSTYG  360
Query  361  APNGNGIGNGNGRPSSTYGAPNGGNGGYAGRNGGYAGGNGGYANGNGGYAGGNGGYANGN  420
Sbjct  1    ------------------------------.R.NF.RDM..WERRVH.CC-----FVWSS  25
Query  421  GGYAGGNSGYAGGNGDEYSEPASYQFQYEVNDQEGTEFGHQEQREGDEAQGEYRVLLPDG  480
Sbjct  26   KAQVAKKL.SRI.KVP.SNMKCRLLLE--------------------K.SNGFNL..DN.  65
Query  481  --RROIVSYTADQQGYQPEIRYEDTGAGNGYGRGGNAGGQNGY  521
Sbjct  66   KL.NK.IHSFVK------------------------------  77
```

Figure 4.8: protein blast of *P. flavescens* resilin with *Ladona fulva*

BLAST ® » **Global Alignment** » results for RID-Y8D650G1114

Job Title	tr|G4Y9J5|G4Y9J5_9ODON Resilin isoform ...
RID	Y8D650G1114 Search expires on 03-04 15:28 pm
Program	Needleman-Wunsch alignment of two sequences
Query ID	lcl|Query_3776819 (amino acid)
Query Descr	tr|G4Y9J5|G4Y9J5_9ODON Resilin isoform B OS=Aeshna sp. REL-2011 OX=1095469 PE=2 SV=1 ...
Query Length	477
Subject ID	lcl|Query_3776821 (amino acid)
Subject Descr	PF ...
Subject Length	77

Descriptions

Description	Score	Percent Ident	Accession
PF	-406.0	4.00%	Query_3776821

Graphic Summary

Distribution of the top 1 Blast Hits on 1 subject sequences

Query

1 90 180 270 360 450

Alignments

Alignment view: Pairwise | CDS feature | Restore defaults

PF

Sequence ID: Query_3776821 Length: 77 Number of Matches: 1

Range 1: 1 to 77

NW Score	Identities	Positives	Gaps	Frame
-406	21/477(4%)	28/477(5%)	400/477(83%)	

```
Query  1    MTSFRKGCFLGLLAVVALCSAEPPVGGSQSYLPPSSSYGAPSAGTGFGHGGGSPSQSYGA  60
            R+G F
Sbjct  1    ----RRGNF----------------------------------------------------  5

Query  61   PSFGGGSVGGGSHFGGGSHSGGGGGGYPSQSYGAPSRPSGSSFQAFGGAPSSSYGAPSSQ  120

Sbjct       ------------------------------------------------------------

Query  121  YGAPSGGGGSYAIQGGSFSSGGSRAPSQAYGAPSNNAGLSHQSQSFGGGLSSSYGAPSAG  180
              A   GG    + G  F
Sbjct  6    --ARDMGGWERRVHGCCFVWS-----------------------------------------  24

Query  181  FGGQSHGGGYSQGGNGGGHGGSSGGGYSYQSFGGGNGGGHGGSRPSSSYGAPSSSYGAPS  240

Sbjct       ------------------------------------------------------------

Query  241  GGKGVSGGFVSQPSGSYGAPSQSYGAPSRGGGHGGGSISSSYGAPSKGSGGFGGGSISSS  300

Sbjct       ------------------------------------------------------------

Query  301  YGAPSKGSVGGGVSSSYGAPAIGGGSFGGGSFGGGSFGGGSFGGGAPSSSYGAPSSSYSA  360
            SK  V   + S  G                                P S+         A
Sbjct  25   ----SKAQVAKKLGSRIGK-------------------------VPESNMKCRLLLEKA  54

Query  361  PSSSYGAPSKGSGGFGSSGGFSSFSSAPSSSYGAPSASYSTPSSSYGAPSSGGFGAGGGF  420
                          S GF+
Sbjct  55   -----------------SNGFNLLLD---------------------------------  63

Query  421  SSGGYSGGGGGYSSGGSGGFGGHGGSGGAGGYSGGGGYSGGGSGGGQKYDSNGGYVY  477
                                                  G  +       +V
Sbjct  64   ---------------------------------------------NGKLRNKIIHSFVK  77
```

Figure 4.9: protein blast of *P. flavescens* resilin with *Aeshna* sp.

```
CLUSTAL multiple sequence alignment by MUSCLE (3.8)


Resilin                          ----RR------------------------------------------------------
tr|G4Y9J5|G4Y9J5_9ODON           MTSFRKGCFLGLLAVVALC-SAEPPVGGSQSYLPP--------------SSSYGAPSAG
AEQ49438.1                       MTSFRKGCFLGLLAVVALC-SAEPPVGGSQSYLPP--------------SSSYGAPSAG
tr|A0A8K0K0T6|A0A8K0K0T6_LADFU   --------MLAMSALALLCVSAEPPV--SNEYLPPNGGAGMYSNGLTGAISSSYGAPN-G
NP_611157.1                      --MFKLLGLTLLMAMVVLG-RPEPPV---NSYLPP--------------SDSYGAP---


Resilin                          ---------------------GNFARD---------------------------------
tr|G4Y9J5|G4Y9J5_9ODON           TGFGHGGGSPSQSYGAPSFGGGSVGGG--SHFGGGSHSGGGGGGYPSQSYGAP--SRPSG
AEQ49438.1                       TGFGHGGGSPSQSYGAPSFGGGSVGGG--SHFGGGSHSGGGGGGYPSQSYGAP--SRPSG
tr|A0A8K0K0T6|A0A8K0K0T6_LADFU   NGNGGNGGRPSSTYGAPN-GNGIGGNGLSSTYGAPNGNGLGGNGGLSSTYGAP-----NG
NP_611157.1                      -GQSGPGGRPSDSYGAP--GGGNGGR------------------PSDSYGAPGQGQGQG
                                                  *  .

Resilin                          -----MGGWERRVHGCC------------------------------------------
tr|G4Y9J5|G4Y9J5_9ODON           SSFQAFGGAPSSSYGAP----------SSQYGAPSGG----------------------G
AEQ49438.1                       SSFQAFGGAPSSSYGAP----------SSQYGAPSGG----------------------G
tr|A0A8K0K0T6|A0A8K0K0T6_LADFU   NGFGGNGGRPSSTYGAPNGNGNGGNGLSSTYGAPNGNGNGGNGLSSTYGAPNGNGFGRNG
NP_611157.1                      QGQGGYAGKPSDTYGAPGGGNGNGGRPSSSYGAPGGG--------------------NG
                                       .*     :*.

Resilin                          -------------FVWSSKAQVAKKLGSRIGKV---------------------------
tr|G4Y9J5|G4Y9J5_9ODON           G----SYAIQGGSFSSGGSRAPSQAYGAPSNNAGLSHQSQSFGGGLSSSYGAP-SAGFGG
AEQ49438.1                       G----SYAIQGGSFSSGGSRAPSQAYGAPSNNAGLSHQSQSFGGGLSSSYGAP-SAGFGG
tr|A0A8K0K0T6|A0A8K0K0T6_LADFU   GRPSSTYGAPNGNGLGGNGGRPSSTYGAPNGNG------NGNGGRLSSTYGAPNGNGFGN
NP_611157.1                      GRPSDTYGAPGG----GNGGRPSDTYGAPGGGG------NGNGGRPSSSYGAP-GQGQGN
                                                  ..    :.  *:  .

Resilin                          ------------------------------------------------------------
tr|G4Y9J5|G4Y9J5_9ODON           QSHGGGYSQGGNGGGHGGSSGGGYSYQSFGGGNGGGHG--GSRPSSSYGA----------
AEQ49438.1                       QSHGGGYSQGGNGGGHGGSSGGGYSYQSFGGGNGGGHG--GSRPSSSYGA----------
tr|A0A8K0K0T6|A0A8K0K0T6_LADFU   GNGGRPSSTYGAPNGNSYNGNGGRPSSTYGAPNGNGLGGNGGRPSSTYGAPNGNGFGNGN
NP_611157.1                      GNGGRSSSSYGAPGG----GNGGRPSDTYGAPGGGN----GGRPSDTYGAPG----GGNN


Resilin                          ------------------------------------------------------------
tr|G4Y9J5|G4Y9J5_9ODON           QSHGGGYSQGGNGGGHGGSSGGGYSYQSFGGGNGGGHG--GSRPSSSYGA----------
AEQ49438.1                       QSHGGGYSQGGNGGGHGGSSGGGYSYQSFGGGNGGGHG--GSRPSSSYGA----------
tr|A0A8K0K0T6|A0A8K0K0T6_LADFU   GNGGRPSSTYGAPNGNSYNGNGGRPSSTYGAPNGNGLGGNGGRPSSTYGAPNGNGFGNGN
NP_611157.1                      GNGGRSSSSYGAPGG----GNGGRPSDTYGAPGGGN----GGRPSDTYGAPG----GGNN


Resilin                          ---------------------------------------------PESNMKCR--------
tr|G4Y9J5|G4Y9J5_9ODON           ---PSSSYGAPSG-GKGVSGGFVSQPSGSYGA-----------PSQSYGAP-SRGGGHG
AEQ49438.1                       ---PSSSYGAPSG-GKGVSGGFVSQPSGSYGA-----------PSQSYGAP-SRGGGHG
tr|A0A8K0K0T6|A0A8K0K0T6_LADFU   GGRPSSTYGAPNGNGNGGNGG---RPSSTYGAPNGNGYNGNGGRPSSTYGAPNGNGLSGN
NP_611157.1                      GGRPSSSYGAPGG-GNGG------RPSDTYGAPGGGNGNGSGGRPSSSYGAP-GQGQGGF
                                                                              *...  .

Resilin                          ------------------------------------------------------------
tr|G4Y9J5|G4Y9J5_9ODON           GGSISSSYGAPSK-----------GSGGFGGGSISSSYGAPSKGSV--GGG-VSSSYGAP
AEQ49438.1                       GGSISSSYGAPSK-----------GSGGFGGGSISSSYGAPSKGSV--GGG-VSSSYGAP
tr|A0A8K0K0T6|A0A8K0K0T6_LADFU   GGRLSSTYGAP------------NGNGFGGNGLSSTYGAPNGNGIGNGNGRPSSTYGAP
NP_611157.1                      GGRPSDSYGAPGQNQKPSDSYGAPGSGNGNGGRPSSSYGAPGSG----PGGRPSDSYGPP


Resilin                          ----------------------------------------------------------LLLE
tr|G4Y9J5|G4Y9J5_9ODON           AIGGGSFGG--------------------GSFGGGSFGGGSFGGGAPSSSYGAPSSSYSA
AEQ49438.1                       AIGGGSFGG--------------------GSFGGGSFGGGSFGGGAPSSSYGAPSSSYSA
tr|A0A8K0K0T6|A0A8K0K0T6_LADFU   NGGNGGYAGRNGGYAGGNGGYANGNGGYAGGNGGYANGNGGYAGGNSGYA-GGNGDEYSE
NP_611157.1                      ASGSGA----------------------GGAGGSGPGGADYDNDEPA-KYEFNYQVEDA


Resilin                          KAS----------------------------NGFNLL-----------------------
tr|G4Y9J5|G4Y9J5_9ODON           PSS-S------------YGAPSKGSGGFGSSGGFSSF---SSAPSSSYGAPSASYSTPSS
AEQ49438.1                       PSS-S------------YGAPSKGSGGFGSSGGFSSF---SSAPSSSYGAPSASYSTPSS
tr|A0A8K0K0T6|A0A8K0K0T6_LADFU   PASYQFQYEVNDQEGTEFGHQEQREGD-EAQGEYRVLLPDGRRQIVSYTADQQGYQ-PEI
NP_611157.1                      PSGLS------------FGHSEMRDGDF-TTGQYNVLLPDGRKQIVEYEADQQGYR-PQI
```

```
Resilin                          -------------------------------------LDNGKLRN--------------
tr|G4Y9J5|G4Y9J5_9ODON           SYGAP----------------------SSGGFGAGGGFSSGGYSG--------------
AEQ49438.1                       SYGAP----------------------SSGGFGAGGGFSSGGYSG--------------
tr|A0A8K0K0T6|A0A8K0K0T6_LADFU   RYEDT---------------------------GAGNGYGRGGNAG--------------
NP_611157.1                      RYEGDANDGSGPSGPGGPGGQNLGADGYSSGRPGNGNGNGNGGYSGGRPGGQDLGPSGYS
                                                                    . *   .

Resilin                          ------------------------------------------------------------
tr|G4Y9J5|G4Y9J5_9ODON           ---------GGGGYSSG-------GSGGFGG-----------------------------
AEQ49438.1                       ---------GGGGYSSG-------GSGGFGG-----------------------------
tr|A0A8K0K0T6|A0A8K0K0T6_LADFU   ---------GQNGY--------------------------------------------
NP_611157.1                      GGRPGGQDLGAGGYSNGKPGGQDLGPGGYSGGRPGGQDLGRDGYSGGRPGGQDLGASGYS


Resilin                          ------------------------------------------------------------
tr|G4Y9J5|G4Y9J5_9ODON           ----------------------HGGSGGAGGYSGG----------------------
AEQ49438.1                       ----------------------HGGSGGAGGYSGG----------------------
tr|A0A8K0K0T6|A0A8K0K0T6_LADFU   ------------------------------------------------------------
NP_611157.1                      NGRPGGNGNGGSDGGRVIIGGRVIGGQDGGDQGYSGGRPGGQDLGRDGYSSGRPGGRPGG


Resilin                          --------------------------------KIIHSFVK
tr|G4Y9J5|G4Y9J5_9ODON           -----------------GGYSGGGSGGGQKYDSNGGYVY
AEQ49438.1                       -----------------GGYSGGGSGGGQKYDSNGGYVY
tr|A0A8K0K0T6|A0A8K0K0T6_LADFU   ---------------------------------------
NP_611157.1                      NGQDSQDGQGYSSGRPGQGGRNGFGPGGQNGDNDGSGYRY
```

Figure 4.10: Multiple sequence alignment

4.4.3 Insilico analysis of *P. flavescens* resilin

4.4.3.1 Homology modeling of the sequenced resilin protein

The isolated partial sequence of the *P. flavescens* resilin protein consists of one beta-sheet, one beta-alpha beta unit, two beta-hairpins, one beta-bulge, four strands, one helix, and four beta turns.

4.4.3.2 Amino acid composition of resilin protein

A total 77 amino acids were present in the sequenced resilin protein of *P. flavescens* (Table 4.4). The primary amino acid compositions of resilin are Lysine (11.7%), Glycine (10.4%), Arginine (10.4%), and Leucine (10.4%).

Table 4.4: Amino acid composition of resilin

Amino acid	Number	Percentage composition
Ala (A)	4	5.2%
Arg (R)	8	10.4%
Asn (N)	6	7.8%
Asp (D)	2	2.6%
Cys (C)	3	3.9%
Gln (Q)	1	1.3%
Glu (E)	3	3.9%
Gly (G)	8	10.4%
His (H)	2	2.6%
Ile (I)	3	3.9%
Leu (L)	8	10.4%
Lys (K)	9	11.7%
Met (M)	2	2.6%
Phe (F)	4	5.2%
Pro (P)	1	1.3%
Ser (S)	6	7.8%
Thr (T)	0	0.0%
Trp (W)	2	2.6%
Tyr (Y)	0	0.0%
Val (V)	5	6.5%
Phl (O)	0	0.0%
Sec (U)	0	0.0%

4.4.3.3 Physiochemical characterization of resilin

The physicochemical properties of the resilin protein were studied using the Expasy Protparam server. The expected half-life of resilin is more than one hour in mammalian reticulocytes and two minutes in yeast and *Escherichia coli*. The molecular weight of the resilin protein is 8759.31, and the Isoelectric point (pI) is 10.75. other characteristic properties like the Instability Index (II), Aliphatic Index, and Grand Average of Hydropathicity (GRAVY) of the resilin protein are 31.62, 79.74, and -0.471. The resilin protein is highly stable because the Instability Index value is less than 40.

4.4.3.4 Quality of the protein

QMEAN Z-Scores were checked to check the quality of the resilin protein model. The resilin protein model's QMEAN score was compared with the QMEAN scores of the reference structures solved by X-ray crystallography from the Protein Data Bank (PDB), and the Z-score was calculated. The low-quality protein models are expected to have high negative QMEAN Z-score values, and they belong to the red regions in the colour gradient, but the suitable structures are mainly seen in the light red or blue region (Benkert et al., 2008; Benkert et al., 2011). The QMEAN Z-score value for the resilin protein model was found to be -2.66 (Fig. 4.11), indicating that it is a bad model, and this might be due to the unavailability of the previously deposited NMR-based or X-ray crystallography-based models of resilin protein.

4.4.3.5 Functional characterisation of resilin

Feature-Based Function Prediction (FFPred) server was used for the analysis of protein in biological process prediction, molecular function prediction, and cellular component prediction. By analysing the biological process (Table 4.5) of the resilin protein, it was found to participate in the regulation of the metabolic process (GO:0019222) and the cellular macromolecule biosynthetic process (GO:0034645). The resilin protein exhibits three major molecular functions (Table 4.6), including nucleic acid binding (GO:0003676) and organic cyclic compound binding (GO:0097159). This protein also acts as the structural constituent of ribosome

(GO:0003735). The cellular component prediction (Table 4.7) shows that the protein is mainly seen in the mitochondrion (GO:0005739) and its membrane (GO:0005743, GO:0031966).

Table 4.5: Biological process prediction. SVM reliability is regarded as High (H) when MCC, sensitivity, specificity, and precision are jointly above a given threshold (0.9). Otherwise, Reliability is indicated as Low (L).

GO term	Name	Prob	SVM Reliability
GO:0034645	cellular macromolecule biosynthetic process	0.959	H
GO:0019222	regulation of the metabolic process	0.930	H
GO:2001141	regulation of RNA biosynthetic process	0.929	H
GO:0051171	regulation of nitrogen compound metabolic process	0.924	H
GO:0006355	regulation of transcription, DNA-templated	0.923	H
GO:0010468	regulation of gene expression	0.912	H
GO:0051252	regulation of RNA metabolic process	0.907	H
GO:0044237	cellular metabolic process	0.972	L
GO:0008152	metabolic process	0.911	L
GO:0009058	biosynthetic process	0.905	L

Table 4.6: Molecular function prediction. SVM reliability is regarded as High (H) when MCC, sensitivity, specificity, and precision are jointly above a given threshold (0.9). Otherwise, Reliability is indicated as Low (L).

GO term	Name	Prob	SVM Reliability
GO:0003676	nucleic acid binding	0.989	H
GO:0003735	structural constituent of ribosome	0.935	H
GO:0097159	organic cyclic compound binding	0.914	L

Table 4.7: Cellular component prediction. SVM reliability is regarded as High (H) when MCC, sensitivity, specificity and precision are jointly above a given threshold (0.9). Otherwise, Reliability is indicated as Low (L).

GO term	Name	Prob	SVM Reliability
GO:0005743	mitochondrial inner membrane	0.980	H
GO:0031966	mitochondrial membrane	0.959	H
GO:0005739	mitochondrion	0.912	H
GO:0043229	intracellular organelle	0.957	L
GO:0005737	cytoplasm	0.922	L
GO:0043231	intracellular membrane-bounded organelle	0.901	L

4.4.3.6 Validation of resilin protein model

Ramachandra plot was used to check the model's stability. Above 90% of the amino acid residue were found to be occupied in the core or most favoured (91.7%) and additional allowed region (8.3%) of the Ramachandran plot, and no residues were found to be occupied in the disallowed region, which indicates that the resilin protein model is highly stable (Fig. 4.14).

4.4.3.7 Residue Properties of resilin

A high level of torsion and omega angle is observed in the analysis of residue properties of the resilin protein model (Fig. 4.15). Thus, this analysis revealed that the resilin model has a high level of flexibility.

4.4.3.8 Hydrophobicity of the protein

Most of the structure contains highly hydrophobic regions, and the remaining regions have moderate and neutral hydrophobic areas (Fig. 4.16). This indicates that the protein is hydrophobic.

4.4.3.9 Signal peptide prediction

Phobius software was used for verifying the signal peptide in the resilin protein model. The protein model of the partial sequence of resilin from *P. flavescens* doesn't contain any signal peptide region (Fig. 4.17A). However, in the

protein – protein net work interaction analysis clearly demonstrated the resilin protein interacted with several other functional proteins which were mainly connected to the cellular signally mechanisms (Fig. 4.17B).

4.4.3.10 Property characterization

The total accessible surface area (ASA) was found to be 5015 A°, exposed non-polar ASA was 515.7 A°, exposed polar ASA was 922.4 A°, and % side ASA hydrophobicity was 34.76 A° (Table 4.8).

Table 4.8: Accessible surface area of resilin

Property	Observed A°
Total ASA	5015.0
Exposed nonpolar ASA	515.7
Exposed polar ASA	922.4
% side ASA hydrophobic	34.76

4.5 DISCUSSION

4.5.1 Resilin in the wings of *P. flavescens*

In flying insects, resilin is mainly seen in the wing vein joints (Gorb,1999), veins, folding lines (Haas et al., 2000), internal cuticle layers of the veins (Appel et al., 2015), veins and membranes transition areas, wing and thorax connecting area, and in elastic tendons (Andersen & Weis-Fogh, 1964; Jakle et al., 2003). The presence of resilin in the internal cuticle layers of the wing veins of dragonflies prevents vein damage (Appel et al., 2015). In this study, we observed resilin in the vein joints, veins, and membrane transition areas of the *P. flavescens* wing. The veins of the anal region of both the hindwing and forewing showed the presence of resilin and were more prominent in the hindwings. The longitudinal veins of the leading edge of *P. flavescens* mainly bear pressure and have the strongest mechanical properties, which play the role of a girder and help reduce the wings' bending angle during flapping flight (Li et al., 2014). Our study observed resilin in the posterior end of some cross veins joining the leading-edge vein.

In dragonflies and damselflies, the wing vein joints have been divided into two, mobile and immobile joints. In the mobile joints, the longitudinal wing veins are elastically jointed with the cross veins, whereas in immobile joints, they are firmly jointed (Stanislav, 1999). The rotational stiffness of the wing vein joints with more resilin will be low, and such vein joints can deform more when a load is applied to an intact wing (Donoughe et al., 2011). These wing vein joints give flexibility to the insects (Newman, 1982) and contain resilin protein (Gorb, 1999). The mobile joints of dragonflies are generally single-sided (suborder Epiprocta). In such wings, the resilin is either seen dorsally or ventrally but not seen on both sides (Donoughe et al., 2011). In *P. flavescens,* we observed resilin present in both dorsal and ventral sides of the wing at some mobile joints, and present on both sides but in some joints, they are seen either ventrally or dorsally. Resilin was absent in the immobile joints of the *P. flavescens*. The abundance of resilin was found to be different in the vein joints of the wings, and this variation might be due to the specific functions of different areas of the wings during the flight of dragonflies. Variations in the distribution of resilin in the ventral or dorsal surface of the wings will influence the flight pattern of dragonflies between species (Mamat-Noorhidayah, 2018).

A high level of resilin has been observed in the nodus of both the forewing and hindwings of *P. flavescens,* and it is present on the dorsal and ventral surfaces of the wing. This nodus with high resilin plays an important role in enabling wing torsion (Donoughe et al., 2011). When compared to the percher dragonfly's active flier *P. flavescens* has a low level of resilin in the nodus that helps to reduce the flexibility, which in turn helps to reduce large displacement of the wing nodi and so the size of the knot-shaped protrusion on the nodus in *P. flavescens* is small compared to the percher dragonflies (Rajabi et al., 2017; Rajabi et al., 2018).

During aerial flight Odonata, wings and wing sclerites experience many non-natural impacts like displacement and deflection (Rajabi et al., 2017). In such situations, resilin absorbs the shock against the mechanical impacts on the wings (Weish-Fogh, 1960; Lyons et al., 2011) which helps in the uniform distribution of

the stress that reduces the risk of structural failure (Haas et al., 2000; Michels et al., 2012; Rajabi et al., 2017; Busse & Gorb, 2018; Rajabi et al., 2015; Manoonpong et al., 2016). As a long-distance migratory dragonfly species, *P. flavescens* might experience such mechanical impact on wings, and this resilin helps them to recover the structural failure. So, studies on resilin in migratory species are very important to understand how the resilin protein influences the flight of such long-distance migratory insects.

4.5.2 Resilin gene of *P. flavescens*

Ardell and Andersen, (2001) were the first to report the resilin gene CG15290 from *D. melanogaster*. Lyons et al. (2011) used a degenerate primer approach for the amplification of the resilin gene from fleas (*Ctenocephalides felis*), buffalo fly (*Haematobia irritans exigua*), and dragonfly (*Aeshna sp*.). In dragonflies (Anistoptera), the resilin gene sequence studies were conducted only in the *Aeshna* sp. (Aeshnidae) and in *L. fulva* (Libellulidae). This was the first study of the resilin gene of the wandering glider *P. flavescens*. In this study, we compared the partial sequence of *P. flavescens* resilin protein with the whole genome sequence of the *L. fulva* and with the isolated resilin sequence from the *Aeshna* sp. (1820 bp length). While blasting, *P. flavascens* resilin sequence showed lesser similarities with the *L. fulva* (521 aa) and *Aeshna* sp. (477 aa) because we have isolated only the partial sequence of the resilin protein. Thus, the sequence length is much less (77 aa). These length differences in the sequences might be the reason for the lesser similarities.

The insect resilin gene has both conserved and non-conserved domains, and the conserved domain participates in the cross-linking of tyrosine residues forming di- and tri-tyrosine, which influences the elastic properties of the resilin (Andersen, 1964; King, 2010). Thus, based on the functions of insects, the form of resilin also shows variations in the amino acid sequences, composition, and mechanical properties among insects so that each species has its form of resilin (King, 2010). In our study, the *P. flavescens* resilin sequence showed more similarities with the *L. fulva* than *Aeshna* sp. because *P. flavescens* and *L. fulva* are from the same family

Libellulidae. Further studies on this resilin gene of Odonata are necessary to understand more mechanical and functional properties of the resilin in dragonflies.

4.5.3 In silico analysis of resilin protein

In silico studies, it helps to understand proteins' structure, function, and mechanism of action (Agarwal et al., 2013). We created a model for resilin protein from *P. flavescens.* We validated and characterised the protein model, and then finally, we confirmed the protein as resilin.

The *D. melanogaster* gene product (CG15920) is hydrophobic only in the signal peptide region and in a very short region of residues (between 537 and 544). All other regions that is, the two flanking regions and the central regions, are mainly dominated by hydrophilic amino acids (Ardell & Andersen, 2001). The resilin protein mainly comprises polar amino acids and is hydrophilic (Charati et al., 2009). In our study, 52% of the total amino acids (77 aa) were polar amino acids, and 48% were non-polar amino acids. As the isolated resilin sequence length of *P. flavescens* is very less it is difficult to interpret the hydrophobicity of the resilin protein by looking at the amino acid composition. The amino acid glycine was found to be more in the resilin protein of *P. flavescens,* and the absence of a side chain in glycine makes them more flexible (Cheng et al., 2010).

The physiochemical characterisation and the Ramachandran plot of the resilin model showed that the protein is highly stable. The residue property analysis of the resilin revealed that the resilin model has high torsion and omega angle, giving the protein more flexibility. In this study, the QMEAN Z-score value of the resilin model was not satisfactory. We got a negative Z-score value (<-2), indicating that quality of the protein model is bad. Previously deposited NMR-based or X-ray crystallographic-based structure of the resilin was unavailable for comparison and this might be the major reason for the negative Z-score value of our resilin model. However, the resilin model would have been a good model if the templates were available for comparison.

The resilin gene product (CG15920) of *D. melanogaster* is 620 residues long, and it contains a short (17 residues) signal peptide region at the N-terminal of the resilin gene (Nielsen et al., 1997). The signal peptide prediction of the *P. flavescens* resilin model showed the absence of signal peptide in the protein. We have isolated only the partial sequence of the resilin protein with a concise length of amino acid sequences (77 aa), and we may have gotten the sequences away from the signal peptide region. This might be the reason for our study's absence of signal peptides.

The property characterisation of the resilin model showed that it has all the properties of a good protein. As all these characteristics match with the previously available resilin protein, we confirm the protein model as resilin. As this is the first study of the resilin protein from the wandering glider *P. flavescens,* more studies in the future are necessary to understand the mechanical and functional properties of resilin and its influence on the long-distance migration of *P. flavescens*.

4.6 KEY FINDINGS

- Resilin is present in the major vein junction of the fore and hindwing of the *P. flavescens*.
- More prominent resilin fluorescence was observed in the ventral region of the wings than in the dorsal regions.
- A higher level of resilin fluorescence was observed in the hindwings than in the forewings.
- Partial resilin of *P. flavescens* was isolated, sequenced, and characterized.
- This is the first study of resilin protein from the wandering glider *P. flavescens*.

4.7 REFERENCES

Agarwal, P., Thakur, Z., & Kulharia, M. (2013). Homology modeling and structural validation of tissue factor pathway inhibitor. *Bioinformation*, 9(16). DOI: 10.6026/97320630009808

Andersen S. O. (2004). Regional differences in degree of resilin cross-linking in the desert locust, *Schistocerca gregaria*. *Insect biochemistry and molecular biology*, 34(5), 459–466. https://doi.org/10.1016/j.ibmb.2004.02.006.

Andersen, S. O., & Weis-Fogh, T. (1964). Resilin: a rubber-like protein in arthropod cuticle. *Advances in Insect Physiology*, 2, 1–65

Andersen, S. O. (1964). The cross links in resilin identified as dityrosine and trityrosine, BioChem. *Biochimica et Biophysica Acta,* 93, 213-215.

Andersen, S. O. (2003). *Structure and function of resilin*. In: Shewry PR, Tatham AS, Bailey AJ (Eds) Elastomeric proteins: structures, biomechanical properties, and biological roles. Cambridge: Cambridge University Press.

Andersen, S. O. (2010). Studies on resilin-like gene products in insects. *Insect Biochemistry and Molecular Biology,* 40, 541–551

Andersen, S.O., & Weis-Fogh, T. (1964). Resilin. A rubber like protein in arthropod cuticle. In Advances in Insect Physiology; In J. W. L. Beament., J. E. Treherne., V. B. Wigglesworth (Eds). 2 (pp. 1-65). Cambridge, MA, USA: Academic Press.

Anderson, A., Keime, N., Fong, C., Kraemer, A., & Fassbinder-Orth, C. (2023). Resilin distribution and abundance in *Apis mellifera* across biological age Classes and Castes. *Insects*, 14(9), 764. https://doi.org/10.3390/insects14090764

Appel, E., & Gorb, S. N. (2011). Resilin-bearing wing vein joints in the dragonfly *Epiophlebia superstes*. *Bioinspiration and Biomimetics*, 6(4). DOI 10.1088/1748-3182/6/4/046006

Appel, E., & Gorb, S. N. (2014). *Comparative functional morphology of vein joints in Odonata*. In H. F. Paulus (Ed). Stuttgart: Schweizerbart Science Publishers.

Appel, E., Heepe, L., Lin, C. P., & Gorb, S. N. (2015). Ultrastructure of dragonfly wing veins: composite structure of fibrous material supplemented by resilin. *Journal of anatomy*, 227(4), 561–582. https://doi.org/10.1111/joa.12362

Ardell, D. H., & Andersen, S. O. (2001). Tentative identification of a resilin gene in Drosophila melanogaster. *Insect biochemistry and molecular biology*, 31(10), 965–970. https://doi.org/10.1016/s0965-1748(01)00044-3

Bailey, K., & Weis-Fogh, T. (1961). Amino acid composition of a new rubber-like protein, resilin. *Biochimica et Biophysica Acta*, 48, 452–459. doi:10.1016/0006-3002(61)90043-9

Baumler, F., & Busse, S. (2019). Resilin in the flight apparatus of Odonata (Insecta)-cap tendons and their biomechanical importance for flight. *Biology Letter,* 15, 20190127. http://dx.doi.org/10.1098/rsbl.2019.0127

Benkert, P., Biasini, M., & Schwede, T. (2011). Toward the estimation of the absolute quality of individual protein structure models. *Structural Bioinformatics*, 27(3), 343-350. doi: 10.1093/bioinformatics/btq662

Benkert, P., Tosatto, S.C.E., & Schomburg, D. (2008). QMEAN: A comprehensive scoring function for model quality assessment. *Proteins*, 71(1), 261-277.

Bennet-Clark, H. C. (1963). Negative pressures produced in the pharyngeal pump of the blood-sucking bug, *Rhodnius prolixus*. *Journal of Experimental Biology*, 40(1), 223-229.

Bennet-Clark, H. C., & Lucey, E. C. A. (1967). The jump of the flea: a study of the energetics and a model of the mechanism. *Journal of Experimental Biology*, 47(1), 59-76.

Bochicchio, B., Pepe, A., & T. A. M. (2008). Investigating by CD the molecular mechanism of elasticity of elastomeric proteins. *Chirality*, 20, 985-994.

Burrows, M., Shaw, S. R., & Sutton, G. P. (2008). Resilin and chitinous cuticle form a composite structure for energy storage in jumping by froghopper insects. *BMC biology*, 6, 41. https://doi.org/10.1186/1741-7007-6-41

Busse, S., & Gorb, S. N. (2018). Material composition of the mouthpart cuticle in a damselfly larva (Insecta: Odonata) and its biomechanical significance. *Royal Society Open Science*. 5, 172117. http://dx.doi.org/10.1098/rsos.172117

Chapman, R. F. (1998). *The Insects: Structure and Function*, (4th ed). Cambridge, UK: Cambridge University Press.

Charati, M. B., Ifkovits, J. L., Burdick, J. A., Linhardt, J. G., & Kiick, K. L. (2009). Hydrophilic elastomeric biomaterials based on resilin-like polypeptides. *Soft Matter*, 5(18), 3412-3416. DOI: 10.1039/b910980c.

Cheng, S., Cetinkaya, M., & Grater, F. (2010). How sequence determines elasticity of disordered proteins. *Biophysical Journal*, 99, 3863–3869.

Christudhas, A., & Mathai, M. T. (2014). Genetic variation of a migratory dragonfly characterized with random DNA markers. *Journal of Entomology and Zoology studies*, 2(2), 182-184.

Donoughe, S., Crall, J. D., Merz, R. A. & Combes, S. A. (2011). Resilin in dragonfly and damselfly wings and its implications for wing flexibility. *Journal of Morphology*, 272(12), 1409–1421. DOI: 10.1002/jmor.10992.

Edwards, J. S. (1960). *Predation and digestion in assassin bugs* (Doctoral dissertation, University of Cambridge).

Elliott, G. F., Huxley, A. F., & Weis-Fogh, T. (1965). On the structure of resilin. *Journal of Molecular Biology*, 13(3), 791-795.

Elvin, C. M., Carr, A. G., Huson, M.G., Maxwell, J. M., Pearson, R.D., Vuocolo, T., … & Dixon, N. E. (2005). Synthesis and properties of crosslinked recombinant pro-resilin. *Nature*, 437, 999.

Fauziyah, S., Alam, C., Soesilohadi, R. C., Retnoaji, B., & Alam, P. (2014). Morphological and mechanical characterisation of the hindwing nodus from the Libellulidae family of dragonfly (Indonesia). *Arthropod structure & development*, 43(5), 415–422. https://doi.org/10.1016/j.asd.2014.06.004

Fonseca, P. J., & Bennet-Clark, H. C. (1998). Asymmetry of tymbal action and structure in a cicada: a possible role in the production of complex songs. *Journal of experimental Biology*, 201(5), 717-730.

Gorb, S. N. (1999). Serial elastic elements in the damselfly wing: mobile vein joints contain resilin. *Naturwissenschaften,* 86(11), 552–555. DOI: 10.1007/s001140050674

Gosline, J., Lillie, M., Carrington, E., Guerette, P., Ortlepp, C., & Savage, K. (2002). Elastic proteins: biological roles and mechanical properties. *Philos Trans R Soc Lond B Biol Sci*. 357(1418), 121-32. doi: 10.1098/rstb.2001.1022.

Haas, F., Gorb, S. N., & Wootton, R. J. (2000). Elastic joints in dermapteran hind wings: materials and wing folding. *Arthropod Structure and Development*, 29, 137–146. doi:10.1016/S1467-8039(00)00025-6

Haas, F., Gorb, S., & Blickhan, R. (2000). The function of resilin in beetle wings. *Proceedings. Biological sciences*, 267(1451), 1375–1381. https://doi.org/10.1098/rspb.2000.1153

Hou, D., & Zhong, Z. (2023). Mechanical Behavior of Honeybee Forewing with Flexible Resilin Joints and Stripes. *Biomimetics,* 8, 451. https://doi.org/10.3390/biomimetics8060451

Hou, D., Zhong, Z., Yin, Y., Pan, Y., & Zhao, H. (2017). The Role of Soft Vein Joints in Dragonfly Flight. *Journal of Bionic Engineering*, 14, 738-745.

Hu, X., Qin, G., Cebe, P., & Kaplan, D. L. (2010). Structure and elasticity mechanism of full length resilin proteins. *Proceedings of the 2010 IEEE 36th Annual Northeast Bioengineering Conference (NEBEC),* 1-2. doi: 10.1109/NEBC.2010.5458182.

Jakle, B. (2003). *Resilin in insect flight systems*. Diploma Thesis University of Tubingen

Jensen, M., & Weis-Fogh, T. (1962). Biology and physics of locust flight V. strength and elasticity of locust cuticle. *Philosophical Transactions of the Royal Society of London,* 245: 137-169.

Jongerius, S. R., & Lentink, D. (2010). Structural analysis of a dragonfly wing. *Experimental Mechanics*. 50, 1323–34

Kappiyoor, R., Balasubramanian, G., Dudek, D. M., & Puri, I. K. (2011). Elastomechanical properties of resilin. *Soft Matter*, 7, 11006-11009.

Khandaker, M. S. K., Dudek, D. M., Beers, E. P., Dillard, D. A., & Bevan, D. R. (2016). Molecular modeling of the elastomeric properties of repeating units and building blocks of resilin, a disordered elastic protein. *Journal of the mechanical behavior of biomedical materials*, 61, 110–121. https://doi.org/10.1016/j.jmbbm.2016.01.017

King, R. (2010). *Dynamic Mechanical Properties of Resilin*. In Engineering Science & Mechanics, Virginia Polytechnic

Kovalev, A., Filippov, A., & Gorb, S. N. (2018). Slow viscoelastic response of resilin. *Journal of comparative physiology*. *A, Neuroethology, sensory, neural, and behavioral physiology*, 204(4), 409–417. https://doi.org/10.1007/s00359-018-1248-2

Li, L., Teller, S., Clifton, R. J., Jia, X., & Kiick, K. L. (2011). Tunable mechanical stability and deformation response of a resilin-based elastomer. *Biomacromolecules*, 12(6), 2302–2310. https://doi.org/10.1021/bm200373p

Li, L., Tong, Z., Jia, X., & Kiick, K. L. (2013). Resilin-like polypeptide hydrogels engineered for versatile biological functions. *Soft matter*, 9(3), 665–673. https://doi.org/10.1039/C2SM26812D

Li, X. J., Zhang, Z. H., Liang, Y. H., Ren, L. Q., Jie, M., & Yang, Z. G. (2014). Antifatigue properties of dragonfly *Pantala flavescens* wings. *Microscopy research and technique*, 77(5), 356–362. https://doi.org/10.1002/jemt.22352

Lombardi, E. C., & Kaplan, D. L. (1992). Preliminary characterization of resilin isolated from the cockroach, *Periplaneta americana*. *MRS Online Proceedings Library*, 292, 3–7. https://doi.org/10.1557/PROC-292-3

Lv, S., Dudek, D. M., Cao, Y., Balamurali, M. M., Gosline, J., & Li, H. (2010). Designed biomaterials to mimic the mechanical properties of muscles. *Nature*, 465(7294), 69–73. https://doi.org/10.1038/nature09024

Lyons, R. E., Wong, D. C., Kim, M., Lekieffre, N., Huson, M. G., Vuocolo, T., … & Elvin, C. M. (2011). Molecular and functional characterisation of resilin across three insect orders. *Insect biochemistry and molecular biology*, 41(11), 881–890. https://doi.org/10.1016/j.ibmb.2011.08.002.

Lyons, R.E., Nairn, K. M., Huson, M. G., Kim, M., Dumsday, G. & Elvin, C. M. (2009). Comparisons of recombinant resilin-like proteins: repetitive domains are sufficient to confer resilin-like properties. *Biomacromolecules*, 10, 3009–3014.

Ma, Y., Ning, J. G., Ren, H. L., Zhang, P. F., & Zhao, H. Y. (2015). The function of resilin in honeybee wings. *The Journal of experimental biology*, 218, 2136–2142. https://doi.org/10.1242/jeb.117325

Mamat-Noorhidayah., Yazawa, K., Numata, K., & Norma-Rashid, Y. (2018). Morphological and mechanical properties of flexible resilin joints on damselfly wings (*Rhinocypha* spp.). *PLoS ONE*, 13 (3), e0193147. https://doi.org/10.1371/journal.

Manoonpong, P., Petersen, D., Kovalev, A., Worgotter, F., Gorb, S. N., Spinner, M., & Heepe, L. (2016). Enhanced locomotion efficiency of a bio-inspired walking robot using contact surfaces with frictional anisotropy. *Scientific Reports*, 6, 39455. doi:10.1038/srep39455

Marrocco, J., Demasi, L., & Venkataraman, S. (2010). Investigating the structural dynamics implication of flexible resilin joints on dragonfly wings. *ACSESS Proc*. 10, 9.

Michels, J., & Gorb, S. N. (2012). Detailed three-dimensional visualization of resilin in the exoskeleton of arthropods using confocal laser scanning microscopy. *Journal of Microscopy,* 245, 1–16

Michels, J., Appel, E., & Gorb, S.N. (2016). Functional diversity of resilin in arthropoda. *Beilstein Journal of Nanotechnology*, 7, 1241–1259

Michels, J., Vogt, J., & Gorb, S.N. (2012). Tools for crushing diatoms – opal teeth in copepods feature a rubber-like bearing composed of resilin. *Scientific Reports*, 2, 465. https://doi.org/10.1038/srep00465

Mistick, E. A., Mountcastle, A. M., & Combes, S. A. (2016). Wing flexibility improves bumblebee flight stability. *Journal of Experimental Biology*. 219, 3384–3390.

Mountcastle, A. M., & Combes, S. A. (2013). Wing flexibility enhances load-lifting capacity in bumblebees. *Proceedings of the Royal Society B*. 280(1759), 20130531. http://doi.org/10.1098/rspb.2013.0531

Nairn, K. M., Lyons, R. E., Mulder, R. J., Mudie, S. T., Cookson, D. J., Lesieur, E., … & Elvin, C. M. (2008). A synthetic resilin is largely unstructured. *Biophysical journal*, 95(7), 3358–3365. https://doi.org/10.1529/biophysj.107.119107

Neff, D., Frazier, S. F., Quimby, L., Wang, R. T., & Zill, S. (2000). Identification of resilin in the leg of cockroach, *Periplaneta americana*: confirmation by a simple method using pH dependence of UV fluorescence. *Arthropod structure & development*, 29(1), 75–83. https://doi.org/10.1016/s1467-8039(00)00014-1

Newman, D. J. S. (1982). *The Functional Wing Morphology of Some Odonata.* Doctoral dissertation. Exeter: University of Exeter.

Nielsen, H., Engelbrecht, J., Brunak, S., & Von Heijne, G. (1997). Identification of prokaryotic and eukaryotic signal peptides and prediction of their cleavage sites. *Protein Engineering Design & Selection*, 10, 1–6.

Petrenko, R. (2010). *Computer simulations of resilin-like peptides*. Doctoral Dissertation, University of Cincinnati.

Pikkarainen, J., & Kulonen, E. (1972). Relations of various collagens, elastin, resilin and fibroin. *Comparative biochemistry and physiology B*, 41(4), 705–712. https://doi.org/10.1016/0305-0491(72)90083-1

Qin, G., Hu, X., Cebe, P., & Kaplan, D. L. (2012). Mechanism of resilin elasticity. *Natural Communications,* 3, 1003. https://doi.org/10.1038/ncomms2004

Qin, G., Lapidot, S., Numata, K., Hu, X., Meirovitch, S., Dekel, M., … & Kaplan, D. L. (2009). Expression, cross-linking, and characterization of recombinant chitin binding resilin. *Biomacromolecules*, 10(12), 3227–3234. https://doi.org/10.1021/bm900735g

Rajabi, H., Bazargan, P., Pourbabaei, A., Eshghi, S., Darvizeh, A., Gorb, S. N., … & Dirks, J. H. (2017). Wing cross veins: an efficient biomechanical strategy to mitigate fatigue failure of insect cuticle. *Biomechanics and Modeling in Mechanobiology*. 16, 1947–1955. doi:10.1007/s10237-017-0930-6

Rajabi, H., Darvizeh, A., Shafiei, A., Taylor, D., & Dirks, J. H. (2015). Numerical investigation of insect wing fracture behaviour. *Journal of Biomechanics*. 48, 89–94.

Rajabi, H., Ghoroubi, N., Darvizeh, A., Appel, E., & Gorb, S. N. (2016). Effects of multiple vein microjoints on the mechanical behaviour of dragonfly wings: numerical

modelling. *Royal Society Open Science*, 3, 150610. http://dx.doi.org/10.1098/rsos.150610

Rajabi, H., Ghoroubi, N., Stamm, K., Appel, E., & Gorb, S.N., (2017). Dragonfly wing nodus: a one-way hinge contributing to the asymmetric wing deformation. *Acta Biomaterialia*. 60, 330e338.

Rajabi, H., Schroeter, V., Eshghi, S., & Gorb, S. N. (2017). The probability of wing damage in the dragonfly *Sympetrum vulgatum* (Anisoptera: Libellulidae): a field study. *Biology Open,* 6, 1290–1293. doi:10.1242/bio.027078

Rajabi, H., Stamm, K., Appel, E., & Gorb, S. N. (2018). Micro-morphological adaptations of the wing nodus to flight behaviour in four dragonfly species from the family Libellulidae (Odonata: Anisoptera). *Arthropod structure & development*, 47(4), 442–448. https://doi.org/10.1016/j.asd.2018.01.003

Rauscher, S., Baud, S., Miao, M., Keeley, F. W., & Pomes, R. (2006). Proline and Glycine Control Protein Self-Organization into Elastomeric or Amyloid Fibrils. *Structure*, 4, 1667–1676.

Shewry, P. R, Tatham, A. S. & Bailey, A. J. (2004). *Elastomeric proteins: structures, biomechanical properties, and biological roles*. Cambridge: Cambridge University Press.

Stanislav, N. G. (1999). Serial elastic elements in the damselfly wing: mobile vein joints contain resilin. *Naturwissenschaften*, 86, 552-555.

Weis-Fogh, T. (1960). A rubber-like protein in insect cuticle. *Journal of Experimental Biology*. 37, 889–907.

Weis-Fogh, T. (1961). Thermodynamic properties of resilin, a rubberlike protein. *Journal of Molecular Biology*. 3(5), 520–531. https://doi.org/10.1016/S0022-2836(61)80018-1

Willis, J. H. (2010). Structural cuticular proteins from arthropods: annotation, nomenclature, and sequence characteristics in the genomics era. *Insect Biochemistry and Molecular Biology*, 40, 189–204

Wong, D. C., Pearson, R. D., Elvin, C. M., & Merritt, D. J. (2012). Expression of the rubber-like protein, resilin, in developing and functional insect cuticle determined using a *Drosophila* anti-Rec 1 resilin antibody. *Developmental dynamics*, 241(2), 333–339. https://doi.org/10.1002/dvdy.23724

Woodrow, C., Cullen, D. A., Montealegre-Z, F., & Gonzalez-Rodriguez, J. (2024). Non-invasive characterization of the elastic protein resilin in insects using Raman spectroscopy. *International journal of biological macromolecules*, 254, 127967. https://doi.org/10.1016/j.ijbiomac.2023.127967

Wootton, R. J., & Newman, D. J. S. (1986). An approach to the mechanics of pleating in dragonfly wings. *Journal of Experimental Biology*. 125, 361–72.

Zhao, S., Ye, X., Dai, X., Wang, X., Yu, S., & Zhong, B. (2023). *Drosophila melanogaster* resilin improves the mechanical properties of transgenic silk. *PLoS ONE*, 18(3), e0282533.

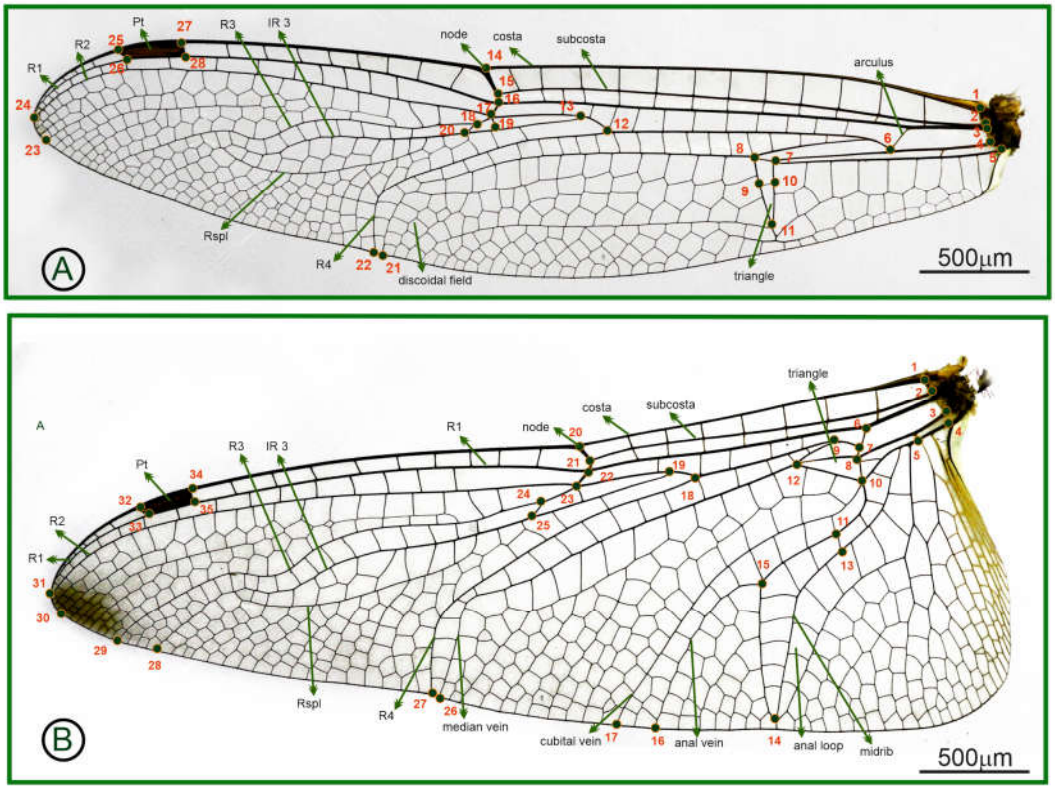

Figure 1.1: Wings of dragonfly with landmarks. (A) Forewing, (B) hindwing

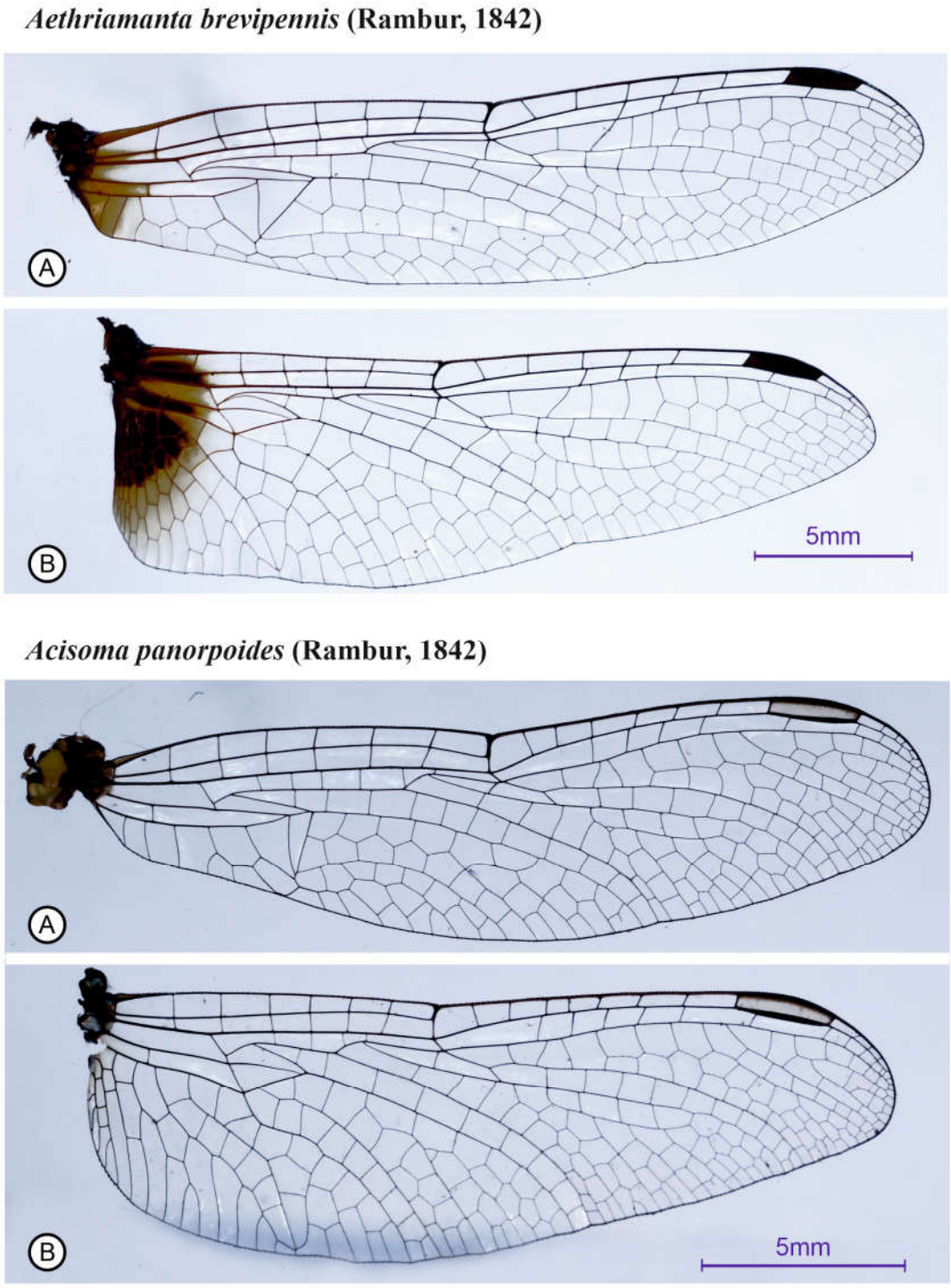

Figure 1.2: Wings of *Aethriamanta brevipennis* and *Acisoma panorpoides.* (A) forewing, (B) hindwing

***Brachythemis contaminata* (Fabricius, 1793)**

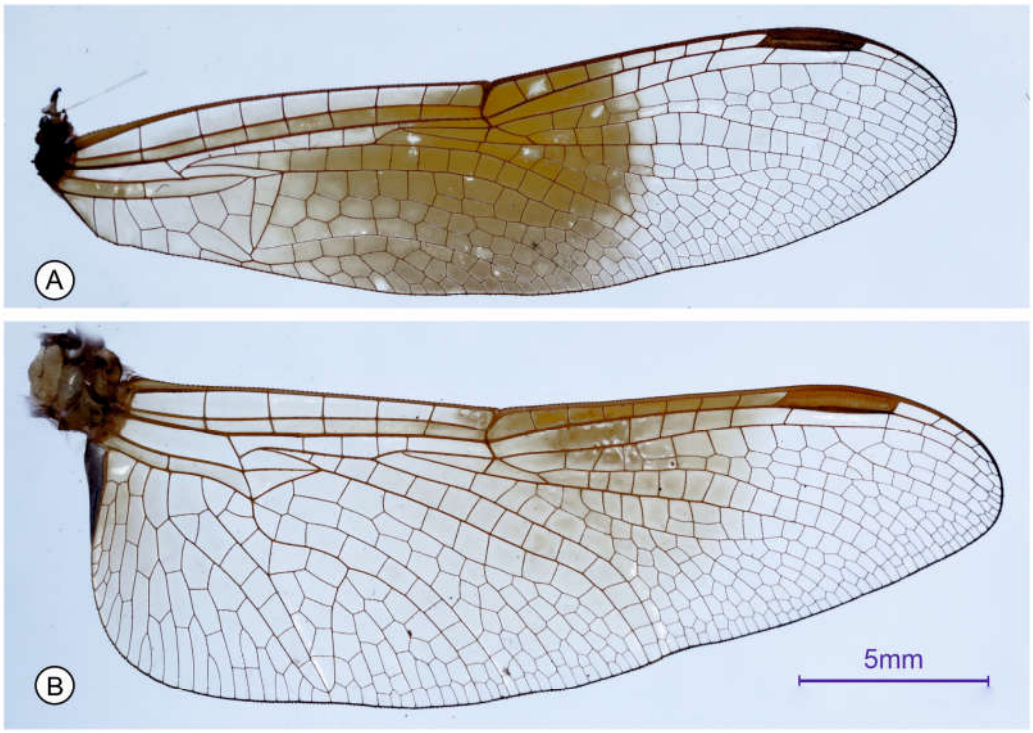

***Bradinopyga geminata*, (Rambur, 1842)**

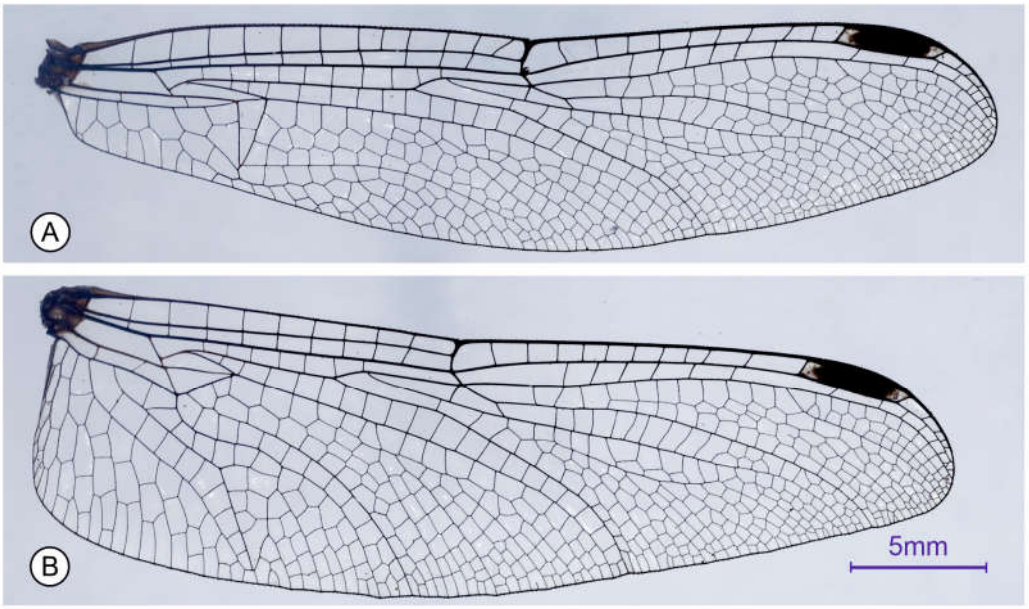

Figure 1.3: Wings of *Brachythemis contaminata* and *Bradinopyga geminata*. (A) forewing, (B) hindwing

***Crocothemis servilia* (Drury, 1770)**

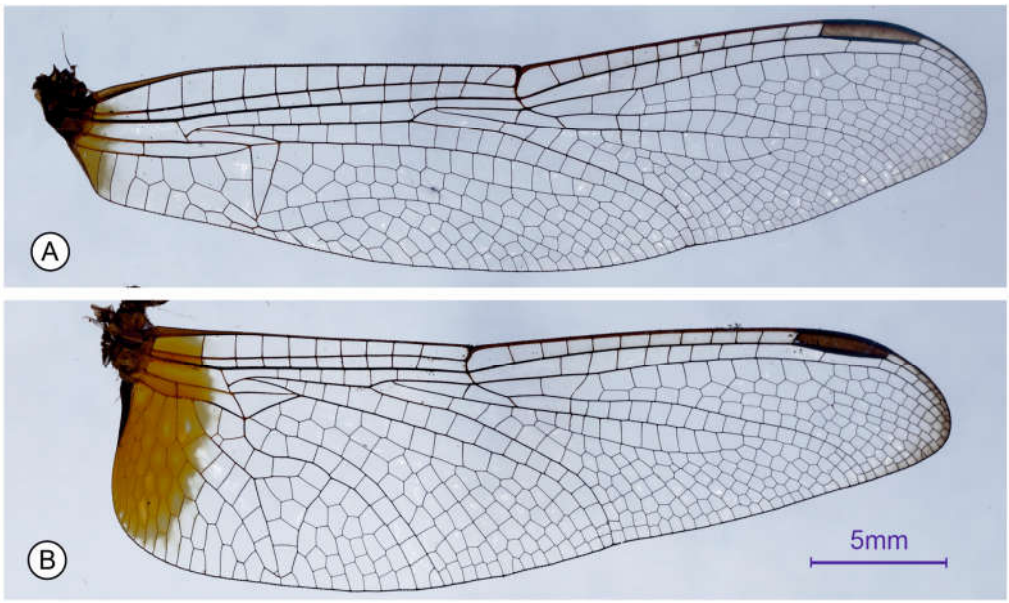

***Diplacodes trivialis* (Rambur, 1842)**

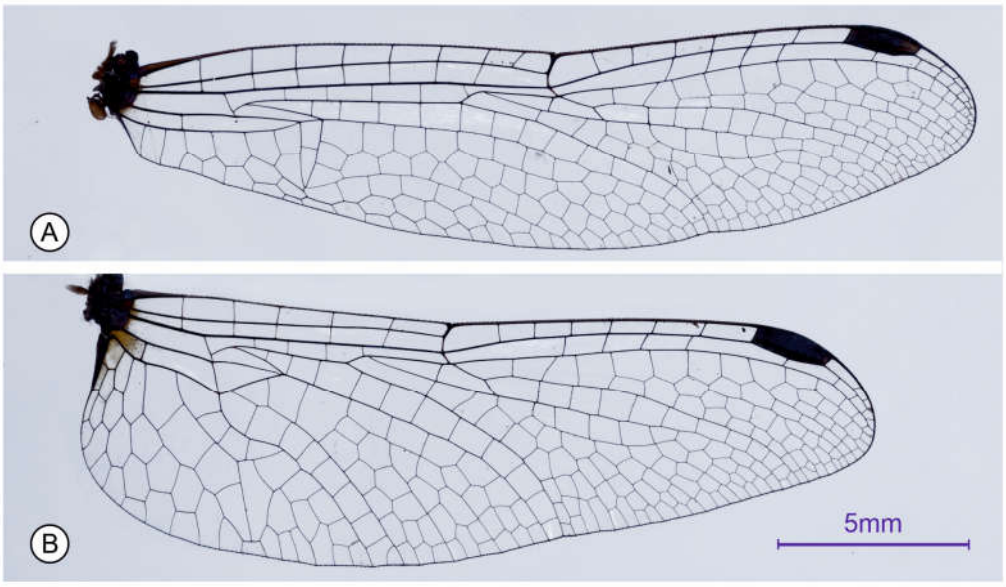

Figure 1.4: Wings of *Crocothemis servilia* and *Diplacodes trivialis*. (A) forewing, (B) hindwing

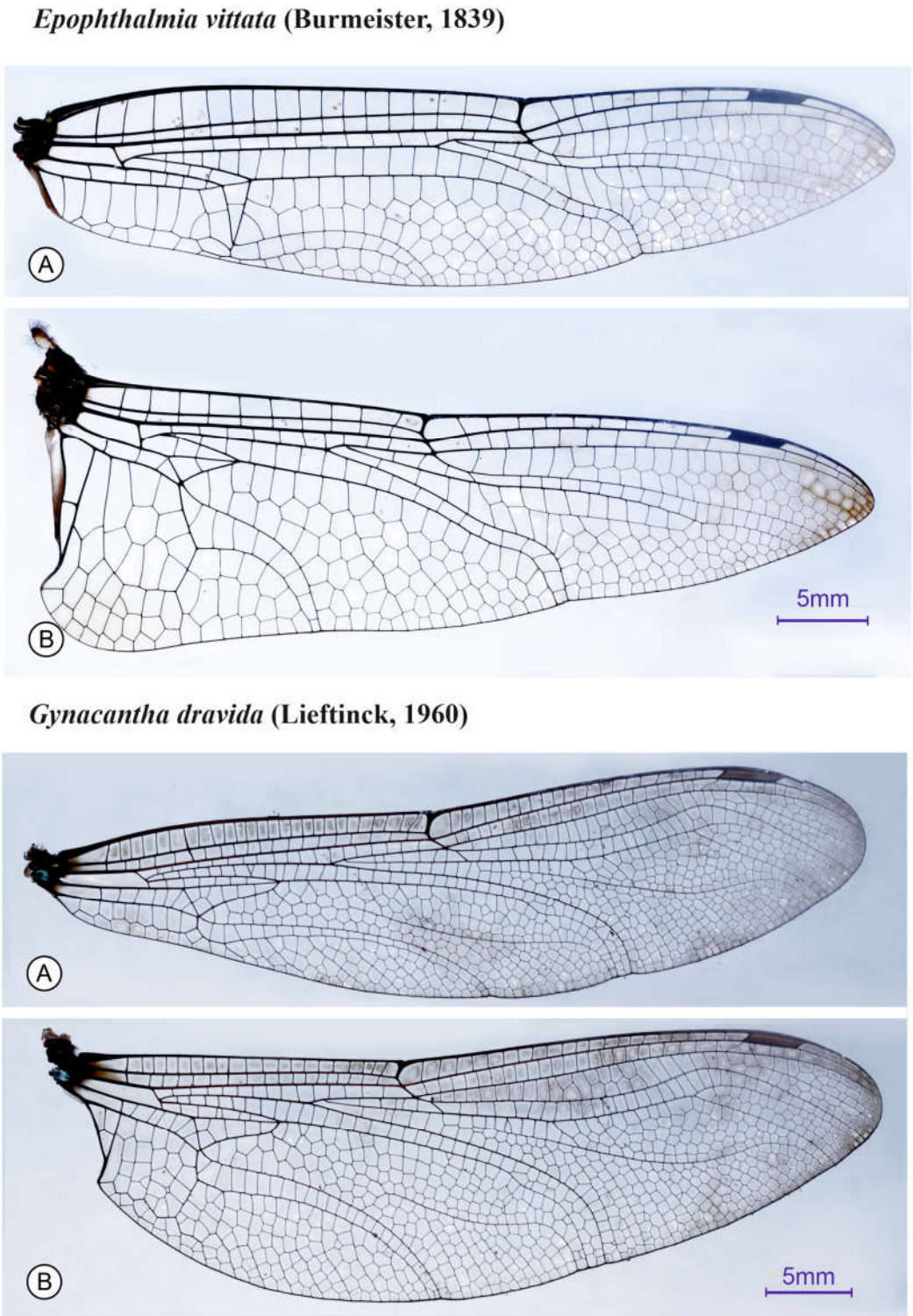

Figure 1.5: Wings of *Epophthalmia vittata* and *Gynacantha dravida*. (A) forewing, (B) hindwing

***Hylaeothemis apicalis* (Fraser, 1942)**

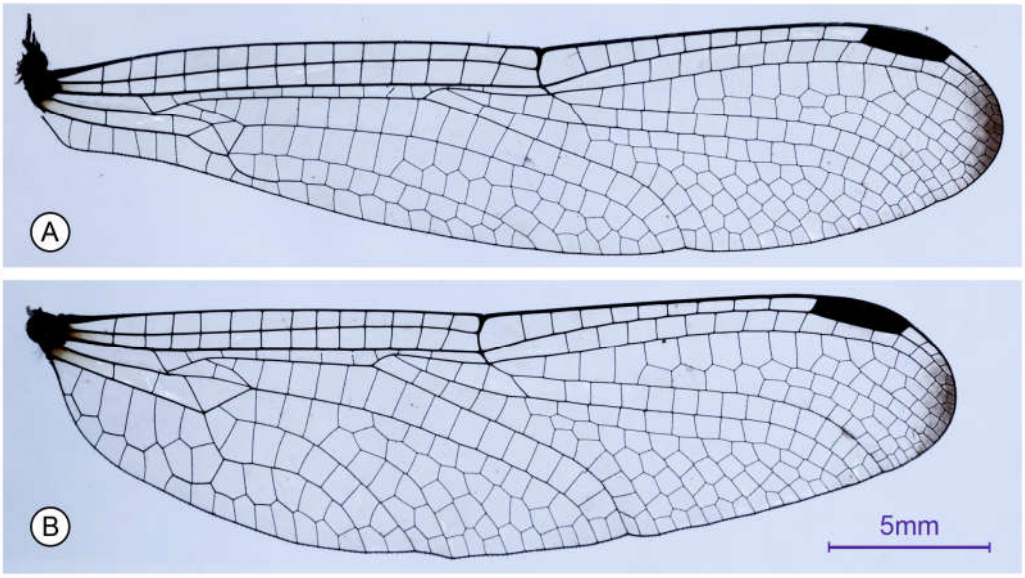

***Ictinogomphus rapax* (Rambur, 1842)**

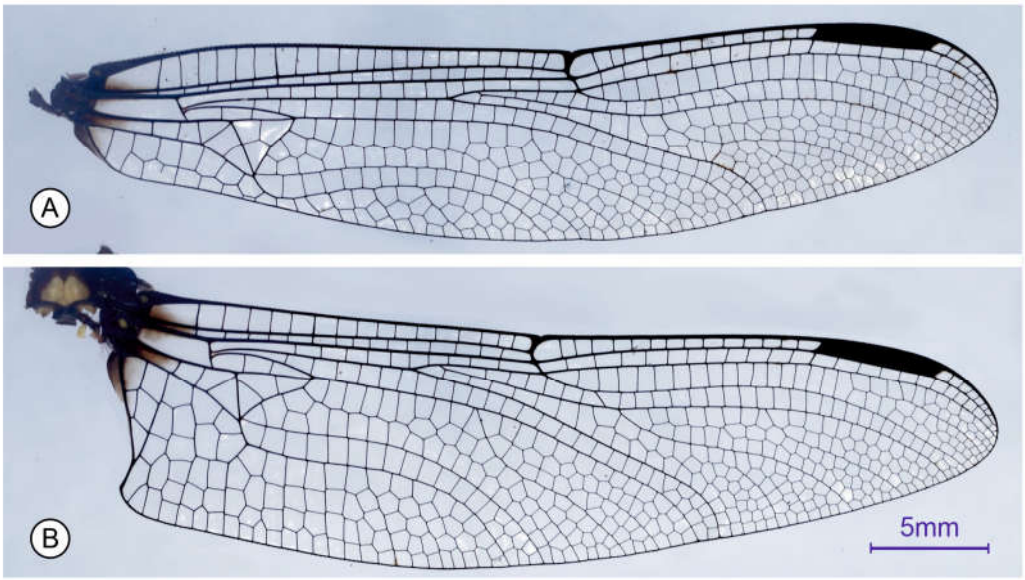

Figure 1.6: Wings of *Hylaeothemis apicalis* and *Ictinogomphus rapax*. (A) forewing, (B) hindwing

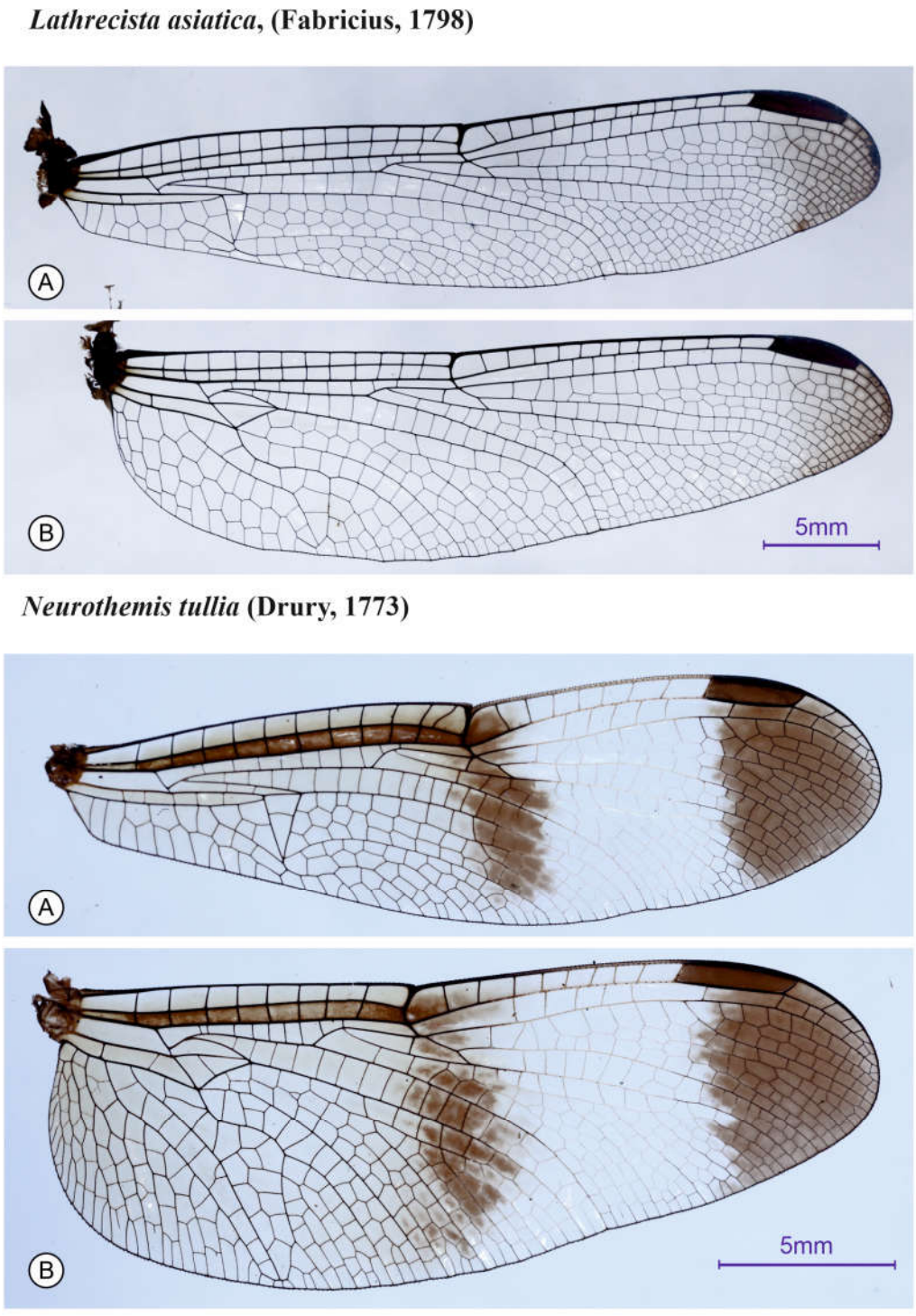

Figure 1.7: Wings of *Lathrecista asiatica* and *Neurothemis tullia*. (A) forewing, (B) hindwing

***Orthetrum glaucum* (Brauer, 1865)**

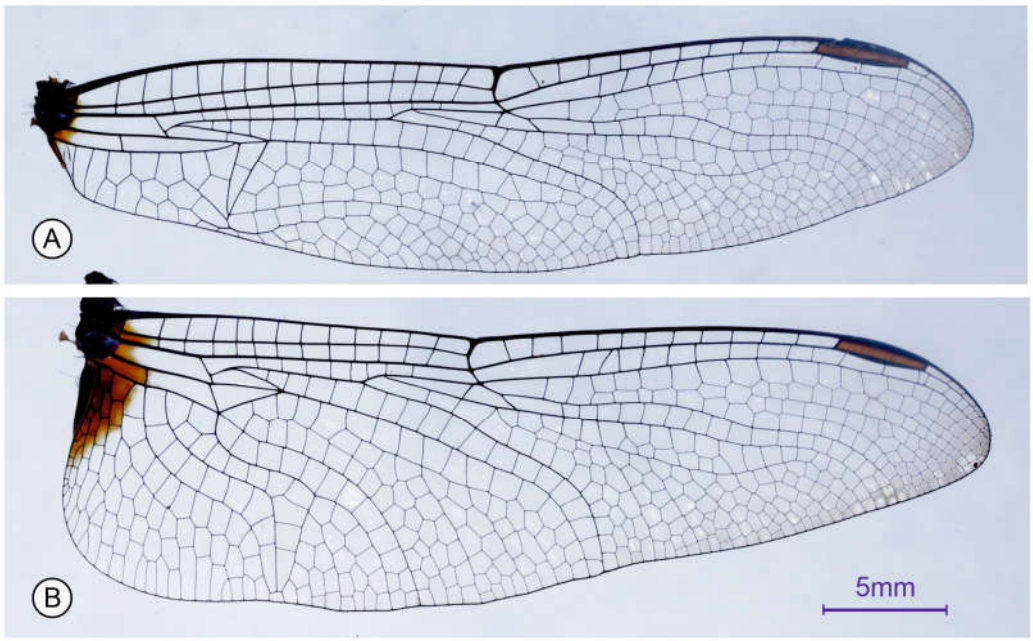

***Orthetrum luzonicum* (Brauer, 1868)**

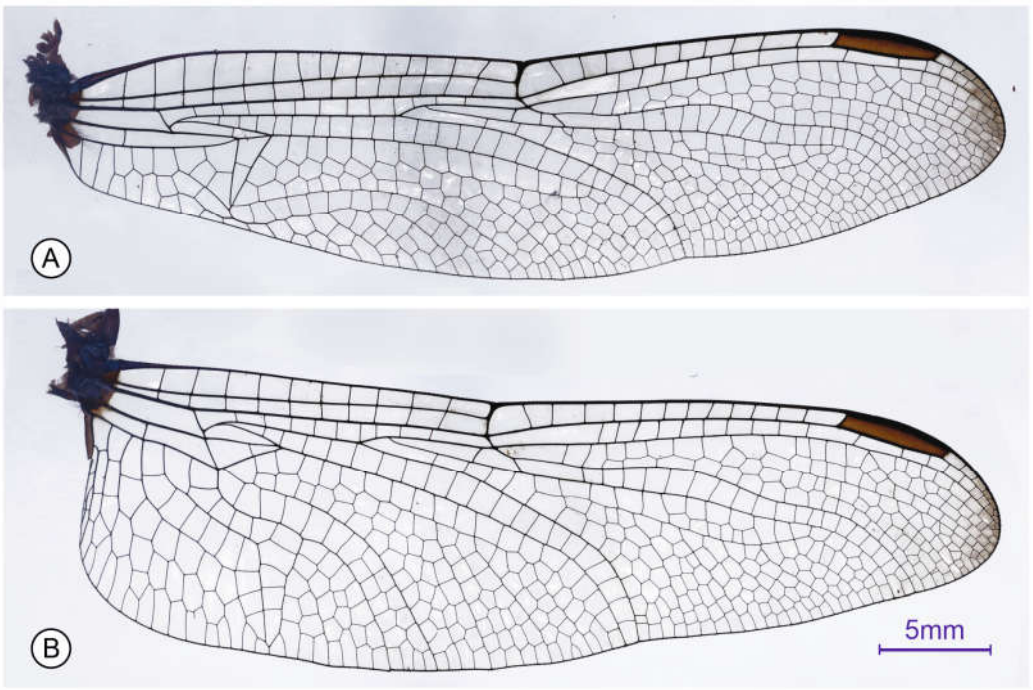

Figure 1.8: Wings of *Orthetrum glaucum* and *Orthetrum luzonicum*. (A) forewing, (B) hindwing

***Orthetrum pruinosum* (Burmeister, 1839)**

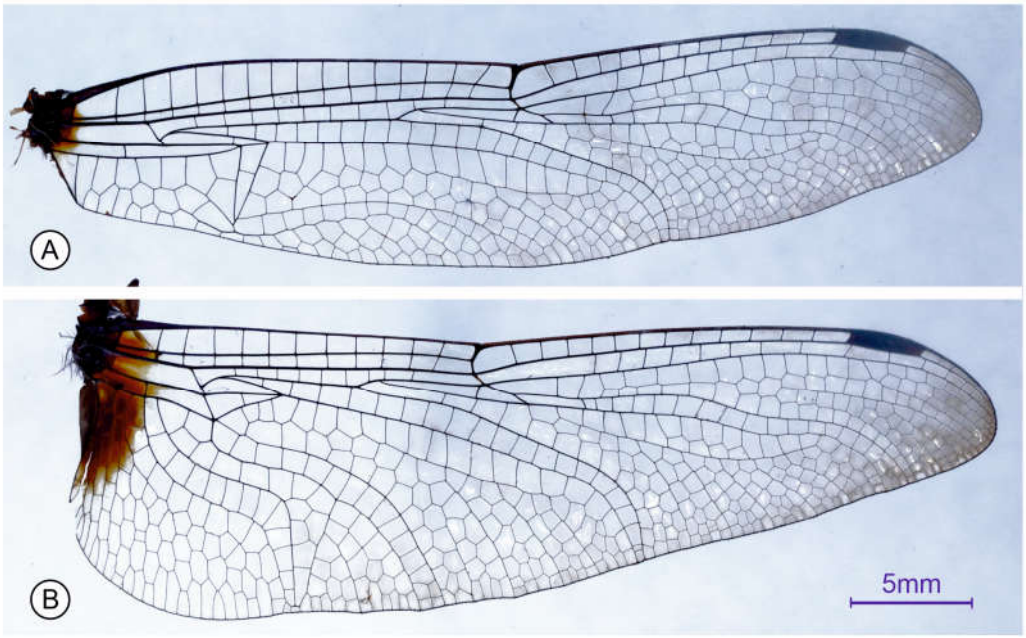

***Orthetrum sabina* (Drury, 1770)**

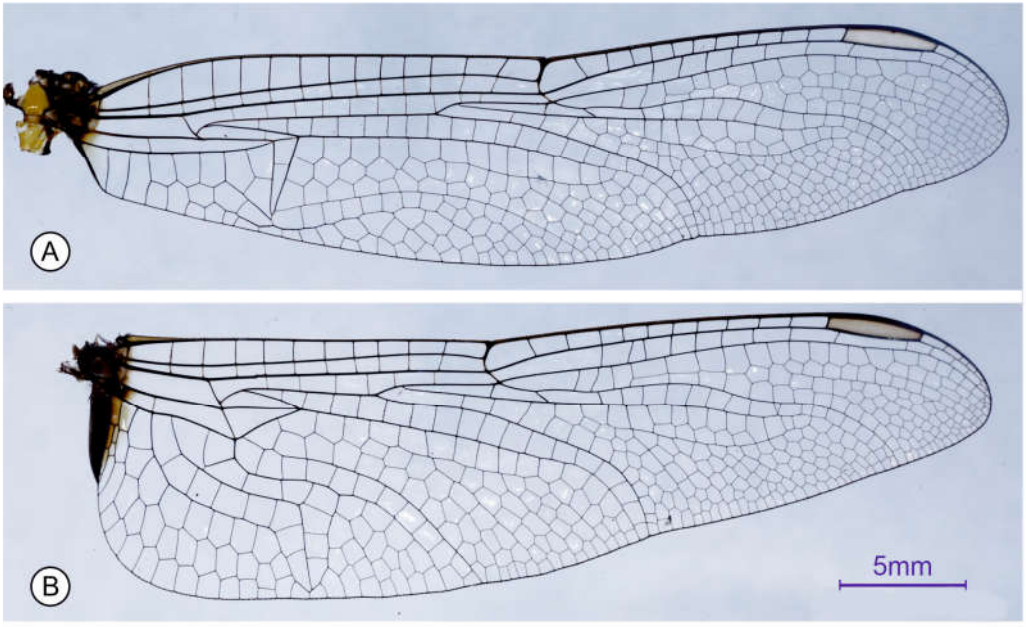

Figure 1.9: Wings of *Orthetrum pruinosum* and *Orthetrum sabina*. (A) forewing, (B) hindwing

***Potamarcha congener*, (Rambur, 1842)**

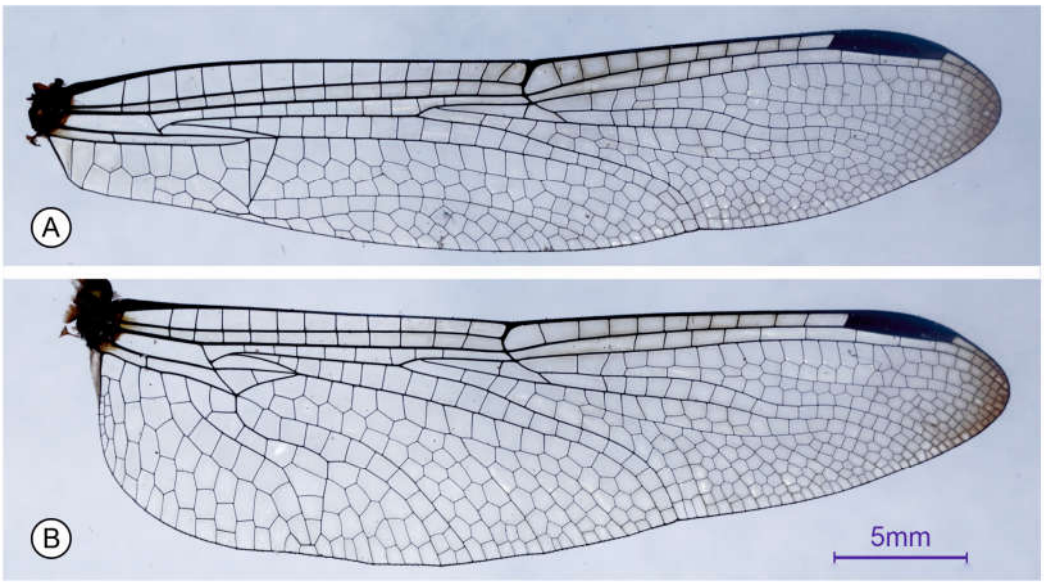

***Pantala flavescens* (Fabricius, 1798)**

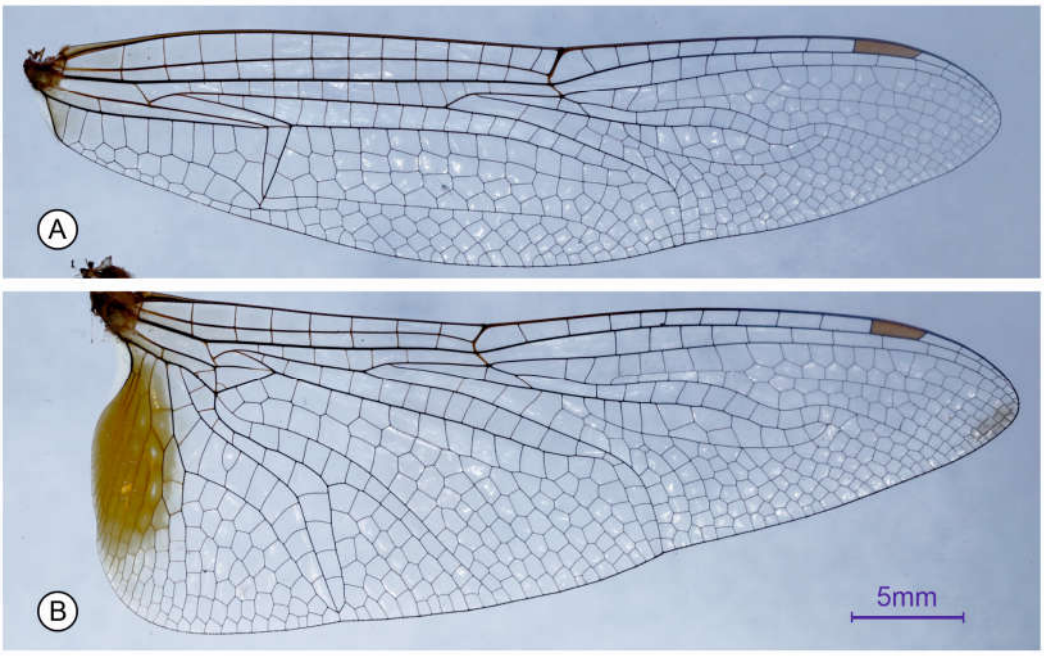

Figure 1.10: Wings of *Potamarcha congener* and *Pantala flavescens*. (A) forewing, (B) hindwing

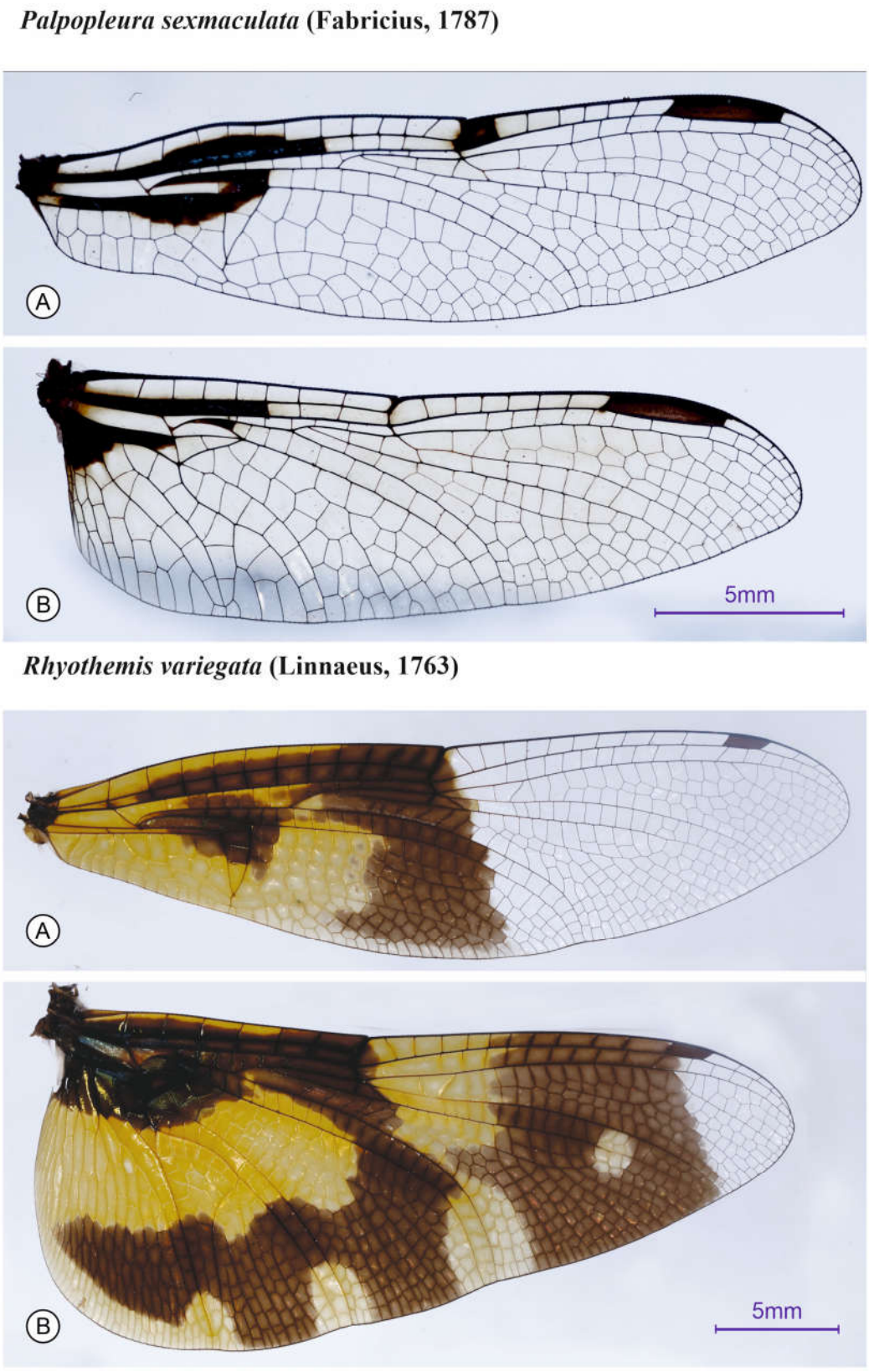

Figure 1.11: Wings of *Palpopleura sexmaculata* and *Rhyothemis variegata*. (A) forewing, (B) hindwing

***Trithemis aurora* (Burmeister, 1839)**

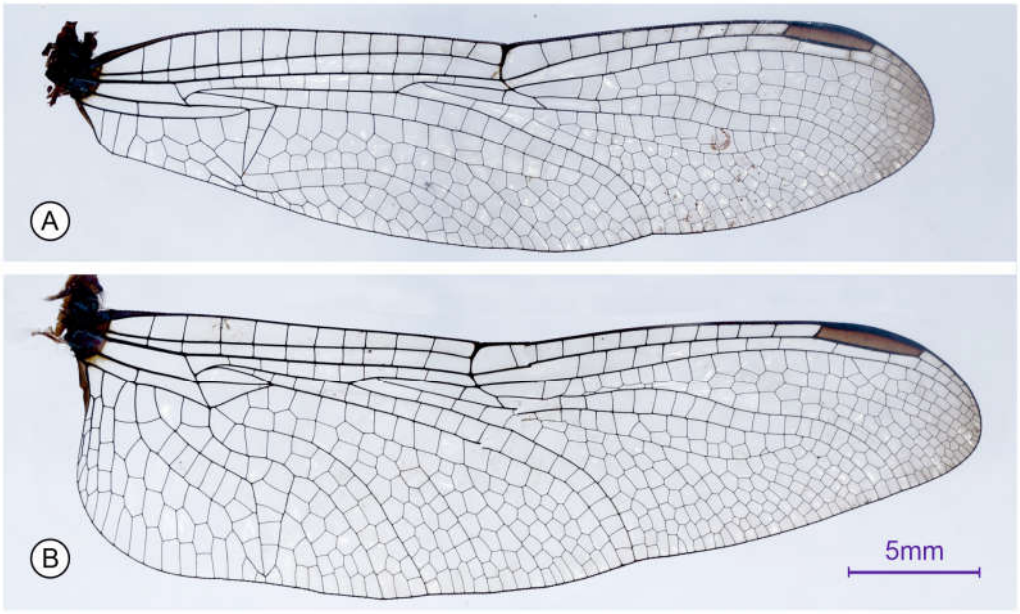

***Tramea basilaris* (Palisot de Beauvois, 1817)**

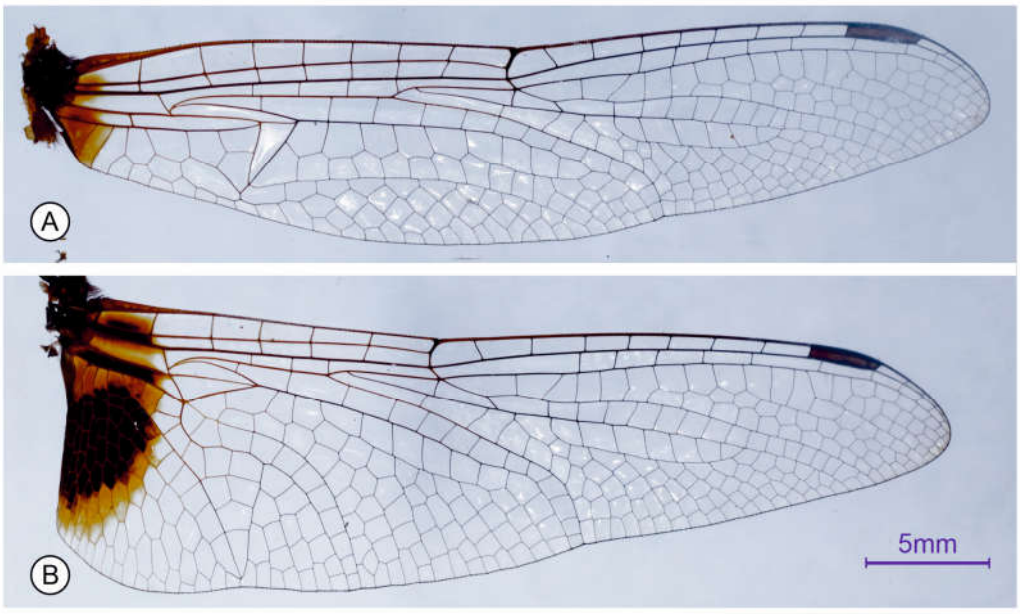

Figure 1.12: Wings of *Trithemis aurora* and *Tramea basilaris*. (A) forewing, (B) hindwing

***Trithemis festiva* (Rambur, 1842)**

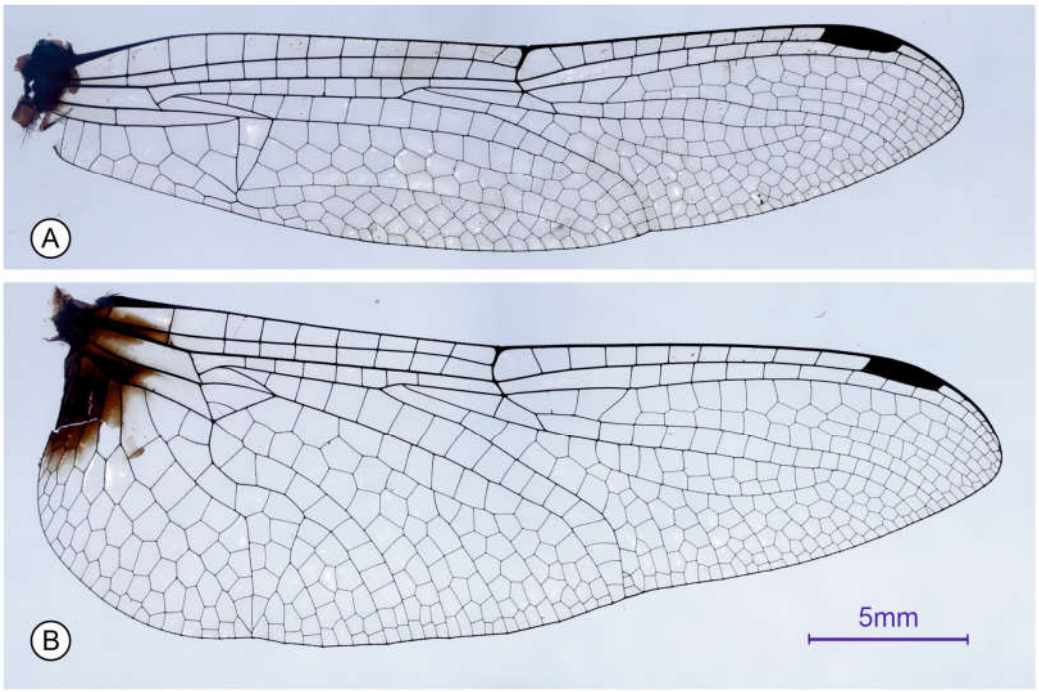

***Tramea limbata* (Desjardins, 1832)**

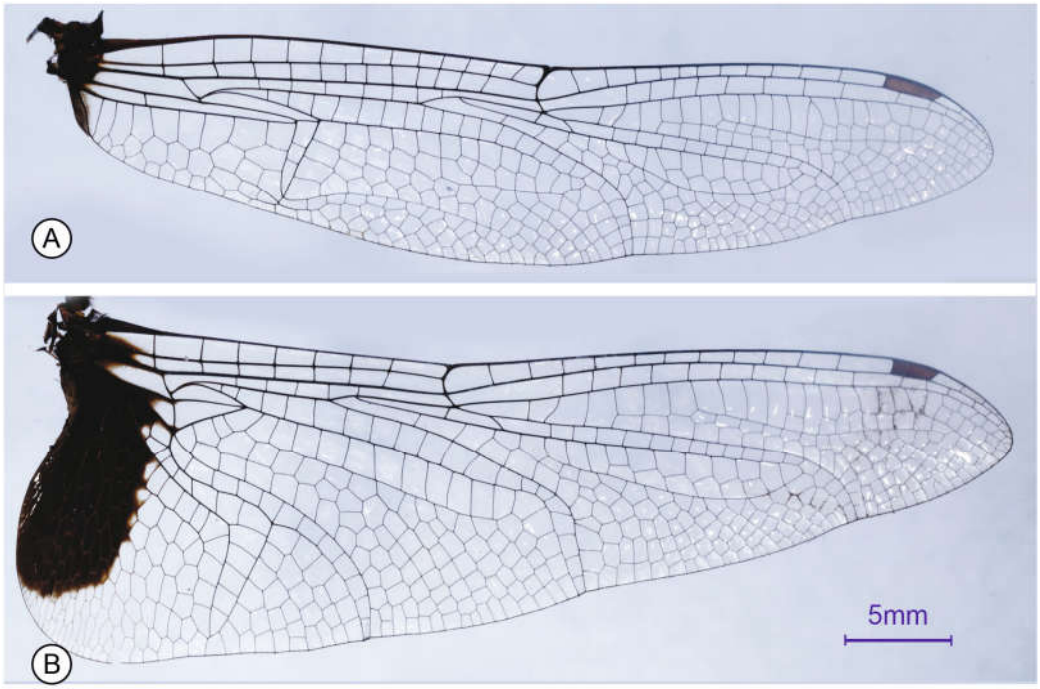

Figure 1.13: Wings of *Trithemis festiva* and *Tramea limbata*. (A) forewing, (B) hindwing

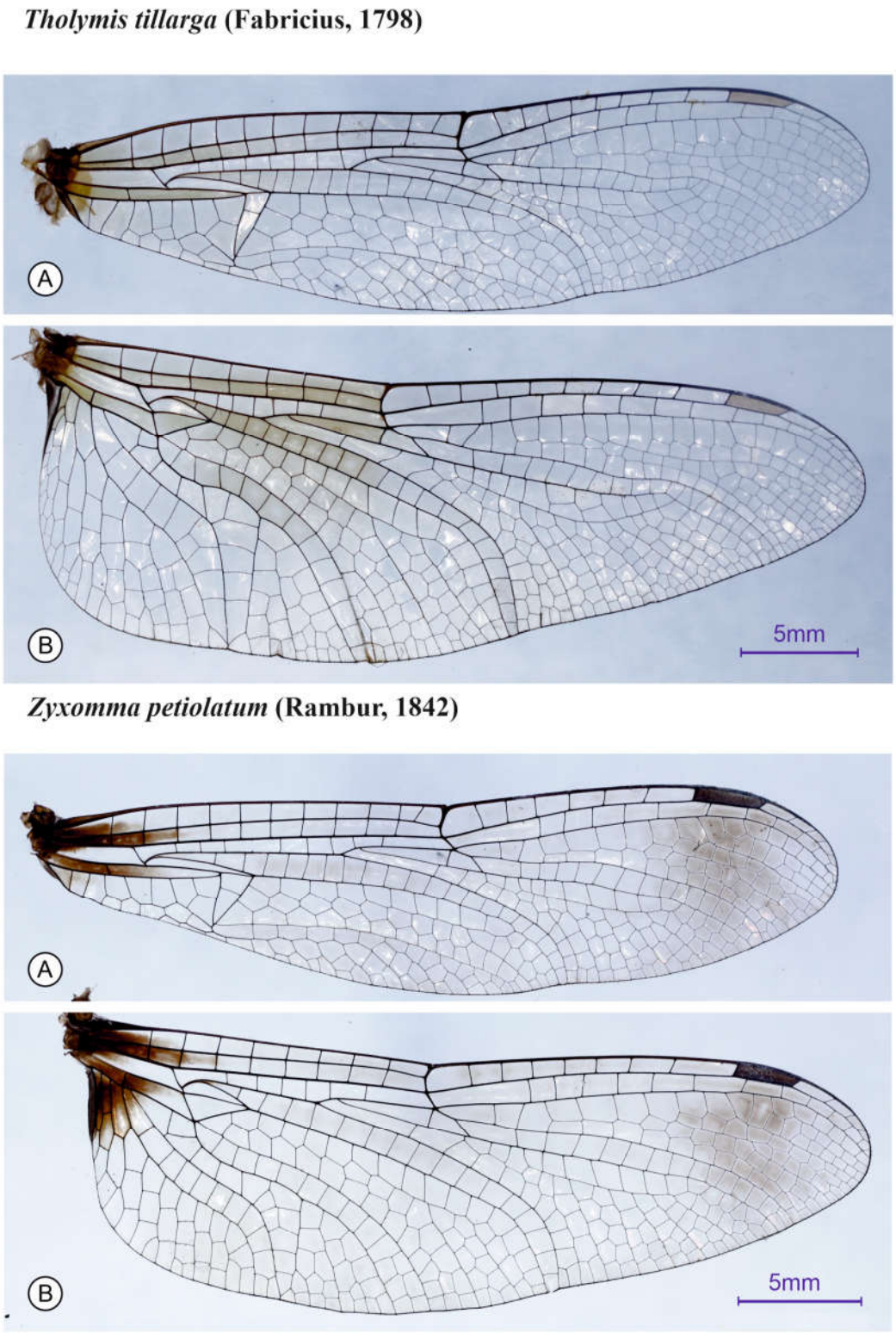

Figure 1.14: Wings of *Tholymis tillarga* and *Zyxomma petiolatum*. (A) forewing, (B) hindwing

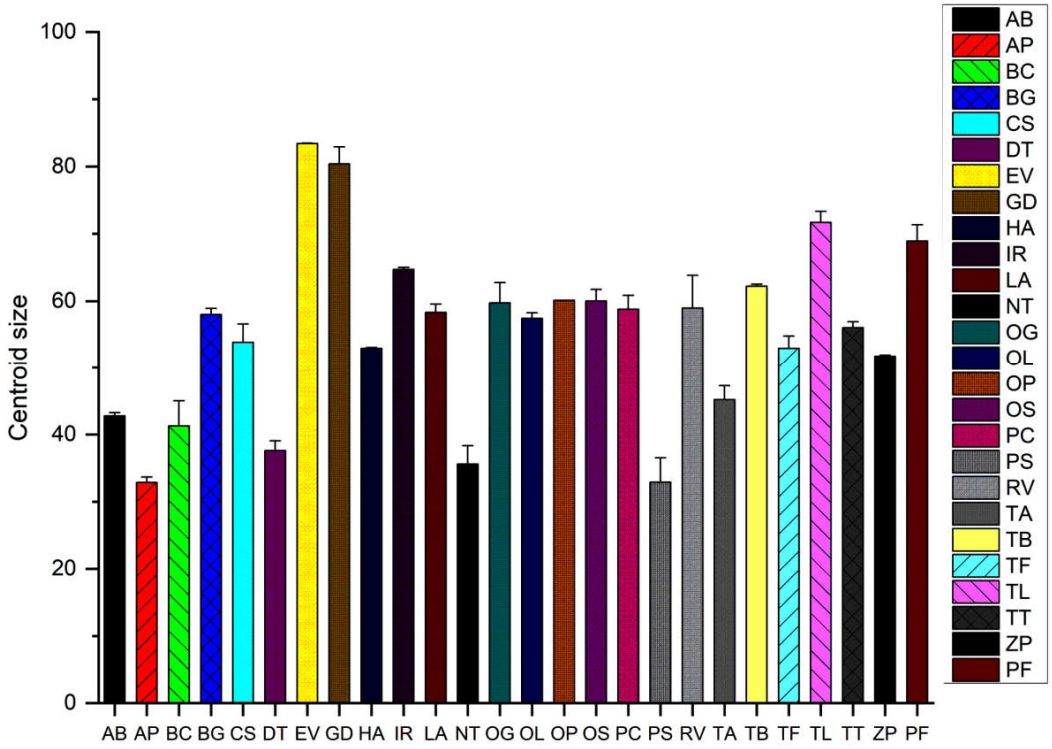

Figure 1.15: Centroid size analysis of forewing. AP - *Acisoma panorpoides;* AB - *Aethriamanta brevipennis;* BC - *Brachythemis contaminata;* BG - *Bradinopyga geminata;* CS - *Crocothemis servilia;* DT - *Diplacodes trivialis;* EV - *Epophthalmia vittata;* GD - *Gynacantha dravida;* HA - *Hylaeothemis apicalis;* IR - *Ictinogomphus rapax;* LA - *Lathrecista asiatica;* NT - *Neurothemis tullia;* OG - *Orthetrum glaucum;* OL - *Orthetrum luzonicum;* OP - *Orthetrum pruinosum;* OS - *Orthetrum sabina;* PS - *Palpopleura sexmaculata;* PC - *Potamarcha congener;* PF - *Pantala flavescens;* RV - *Rhyothemis variegata;* TT - *Tholymis tillarga;* TB - *Tramea basilaris;* TL - *Tramea limbata;* TA - *Trithemis aurora;* TF - *Trithemis festiva;* ZP - *Zyxomma petiolatum*

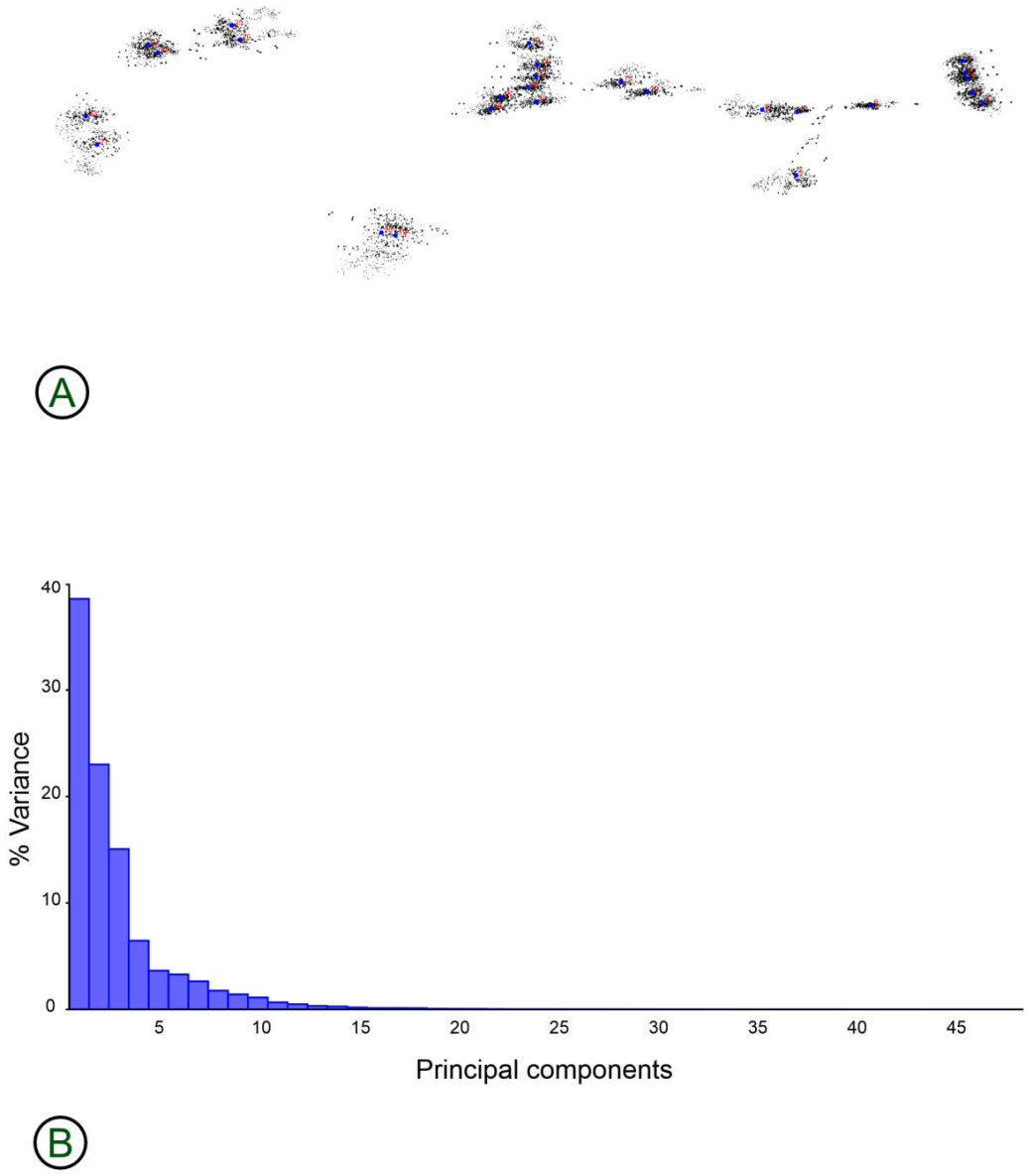

Figure 1.16: GPA and Percentage variance analysis in forewings

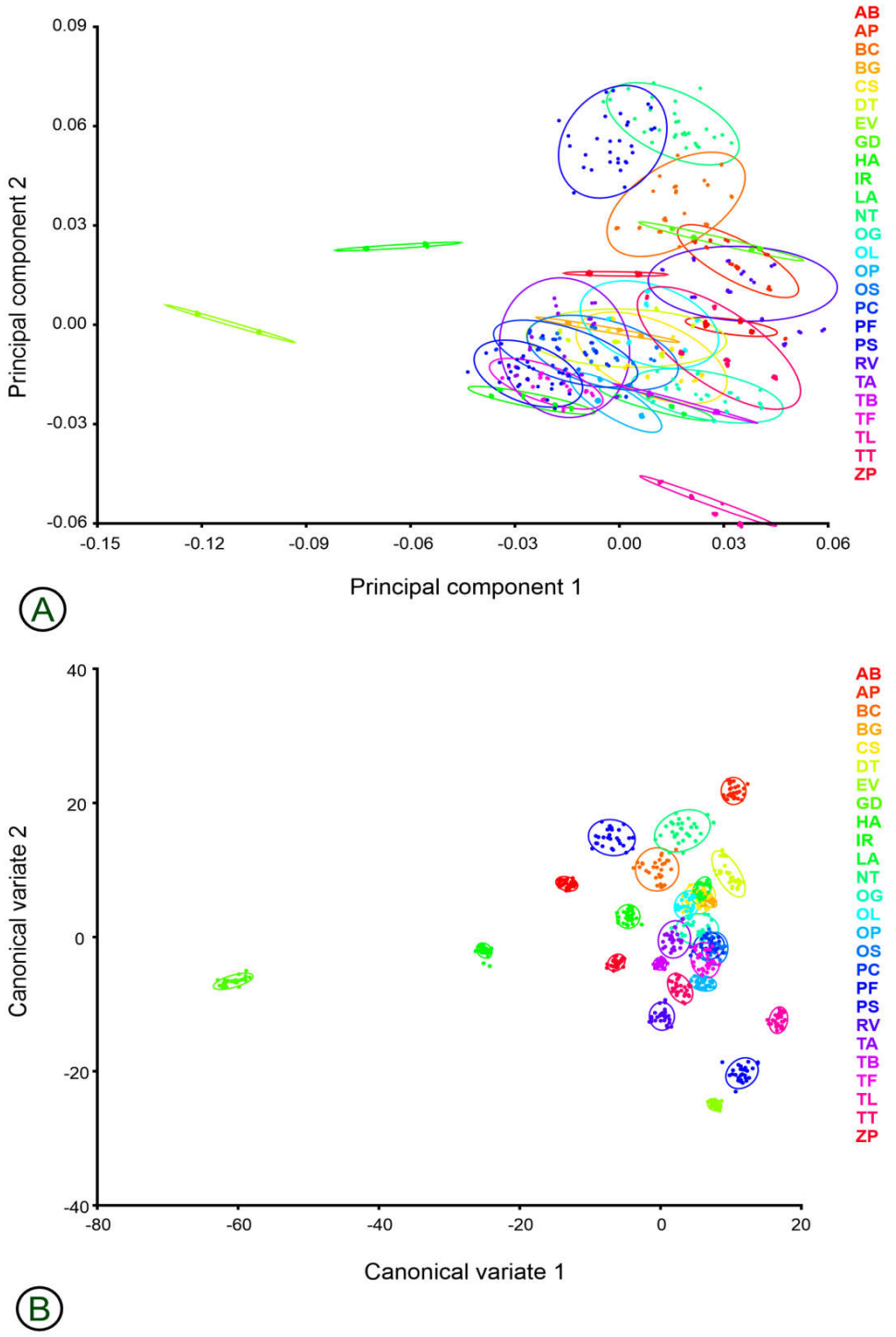

Figure 1.17: PC and CVA morphospace boundary analysis of forewings. (A) PC1 vs. PC2 morphospace analysis representing 60.24% of variance; (B) CVA morphospace analysis. AP – *A. panorpoides;* AB – *A. brevipennis;* BC – *B. contaminata;* BG – *B. geminata;* CS – *C. servilia;* DT – *D. trivialis;* EV – *E. vittata;* GD – *G. dravida;* HA – *H. apicalis;* IR – *I. rapax;* LA – *L. asiatica;* NT – *N. tullia;* OG – *O. glaucum;* OL – *O. luzonicum;* OP – *O. pruinosum;* OS – *O. sabina;* PS – *P. sexmaculata;* PC – *P. congener;* PF – *P. flavescens;* RV – *R. variegata;* TT – *T. tillarga;* TB – *T. basilaris;* TL – *T. limbata;* TA – *T. aurora;* TF – *T. festiva;* ZP – *Z. petiolatum*

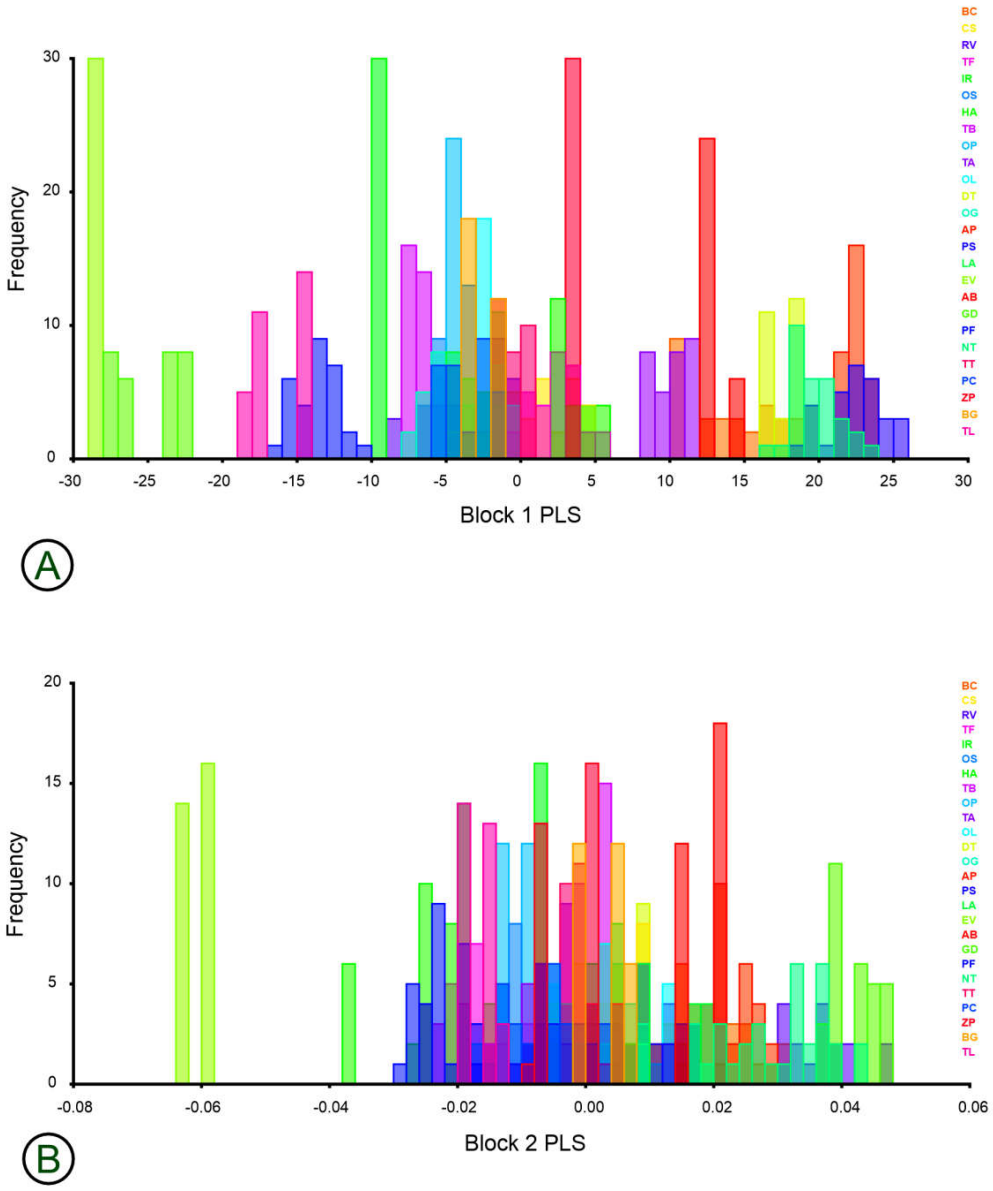

Figure 1.18: PLS analysis of forewing. (A) PLS analysis of forewing size; (B) PLS analysis of forewing shape. AP – *A. panorpoides;* AB – *A. brevipennis;* BC – *B. contaminata;* BG – *B. geminata;* CS – *C. servilia;* DT – *D. trivialis;* EV – *E. vittata;* GD – *G. dravida;* HA – *H. apicalis;* IR – *I. rapax;* LA – *L. asiatica;* NT – *N. tullia;* OG – *O. glaucum;* OL – *O. luzonicum;* OP – *O. pruinosum;* OS – *O. sabina;* PS – *P. sexmaculata;* PC – *P. congener;* PF – *P. flavescens;* RV – *R. variegata;* TT – *T. tillarga;* TB – *T. basilaris;* TL – *T. limbata;* TA – *T. aurora;* TF – *T. festiva;* ZP – *Z. petiolatum*

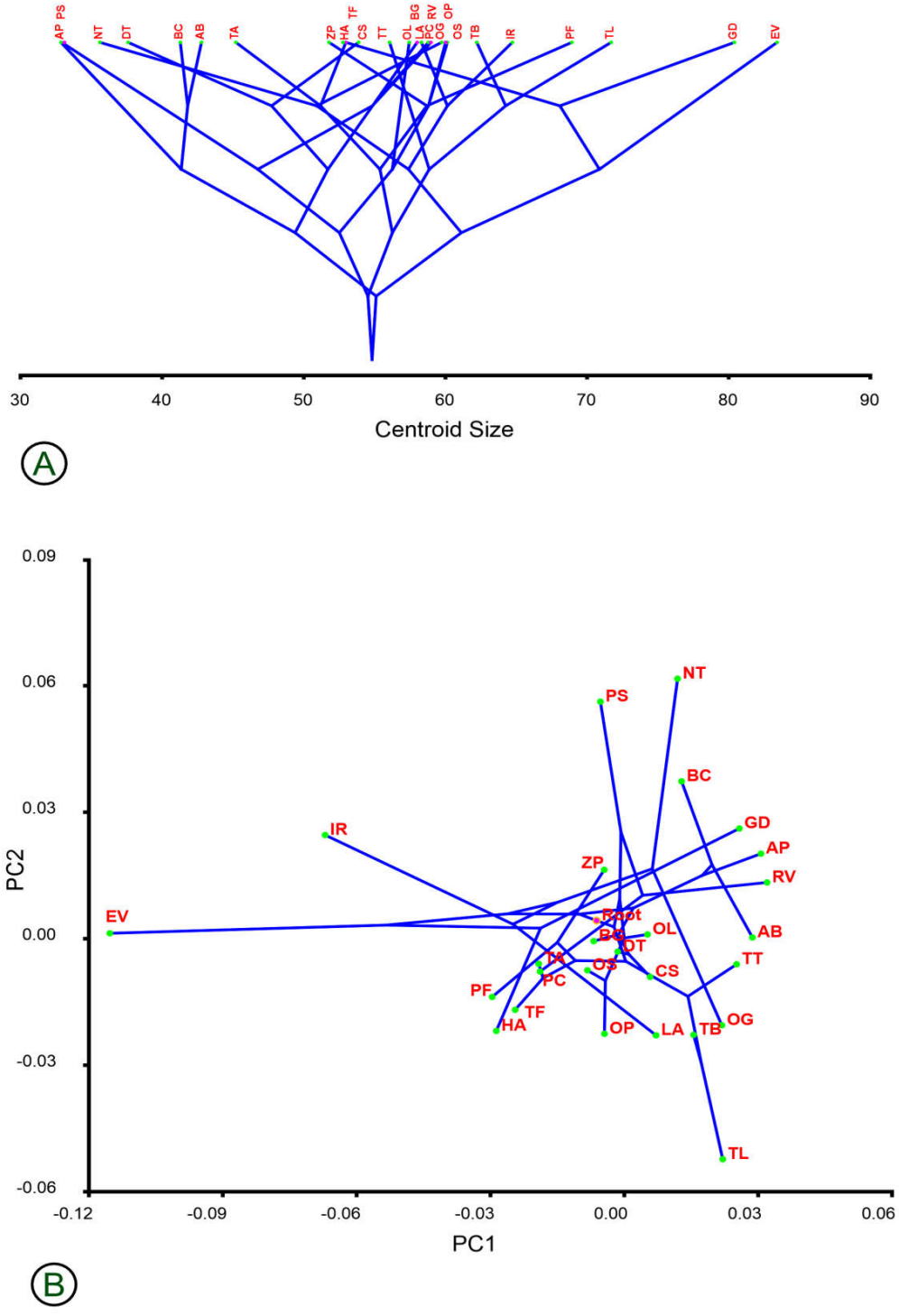

Figure 1.19: Phylogenetic analysis of forewings. (A) Size-based phylogenetic analysis of forewings; (B) Shape-based phylogenetic analysis of forewings. AP – *A. panorpoides;* AB – *A. brevipennis;* BC – *B. contaminata;* BG – *B. geminata;* CS – *C. servilia;* DT – *D. trivialis;* EV – *E. vittata;* GD – *G. dravida;* HA – *H. apicalis;* IR – *I. rapax;* LA – *L. asiatica;* NT – *N. tullia;* OG – *O. glaucum;* OL – *O. luzonicum;* OP – *O. pruinosum;* OS – *O. sabina;* PS – *P. sexmaculata;* PC – *P. congener;* PF – *P. flavescens;* RV – *R. variegata;* TT – *T. tillarga;* TB – *T. basilaris;* TL – *T. limbata;* TA – *T. aurora;* TF – *T. festiva;* ZP – *Z. petiolatum*

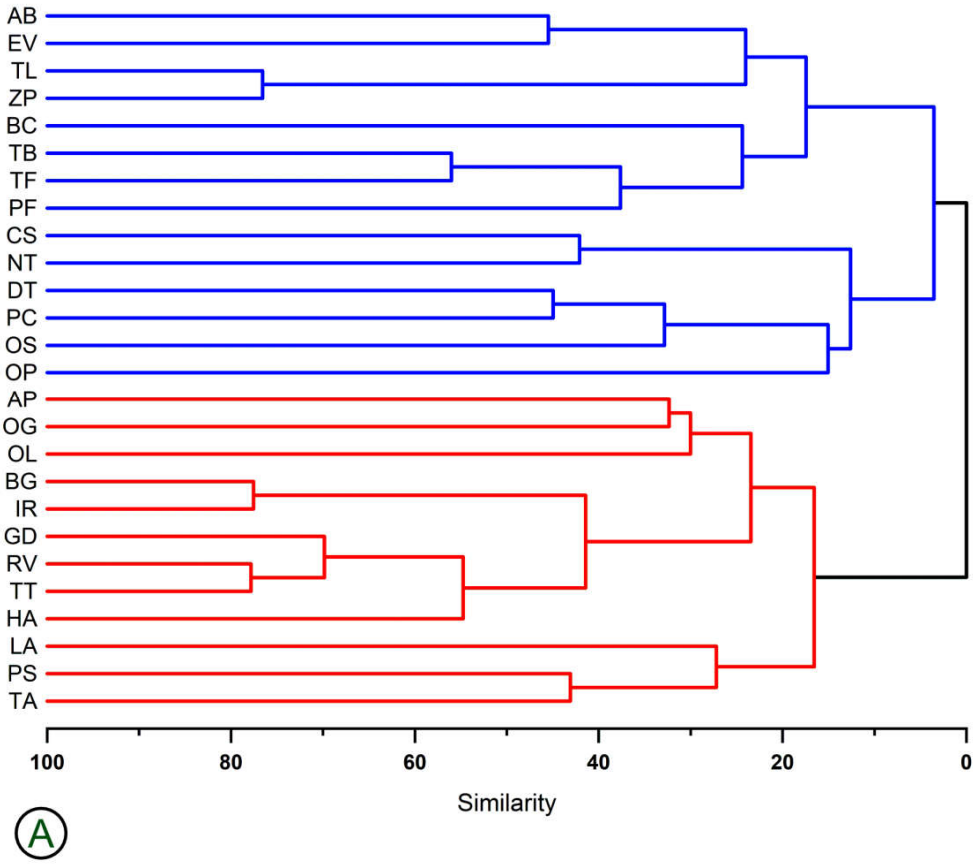

Figure 1.20: Hierarchical cluster dendrogram analysis of forewing. AP – *A. panorpoides;* AB – *A. brevipennis;* BC – *B. contaminata;* BG – *B. geminata;* CS – *C. servilia;* DT – *D. trivialis;* EV – *E. vittata;* GD – *G. dravida;* HA – *H. apicalis;* IR – *I. rapax;* LA – *L. asiatica;* NT – *N. tullia;* OG – *O. glaucum;* OL – *O. luzonicum;* OP – *O. pruinosum;* OS – *O. sabina;* PS – *P. sexmaculata;* PC – *P. congener;* PF – *P. flavescens;* RV – *R. variegata;* TT – *T. tillarga;* TB – *T. basilaris;* TL – *T. limbata;* TA – *T. aurora;* TF – *T. festiva;* ZP – *Z. petiolatum*

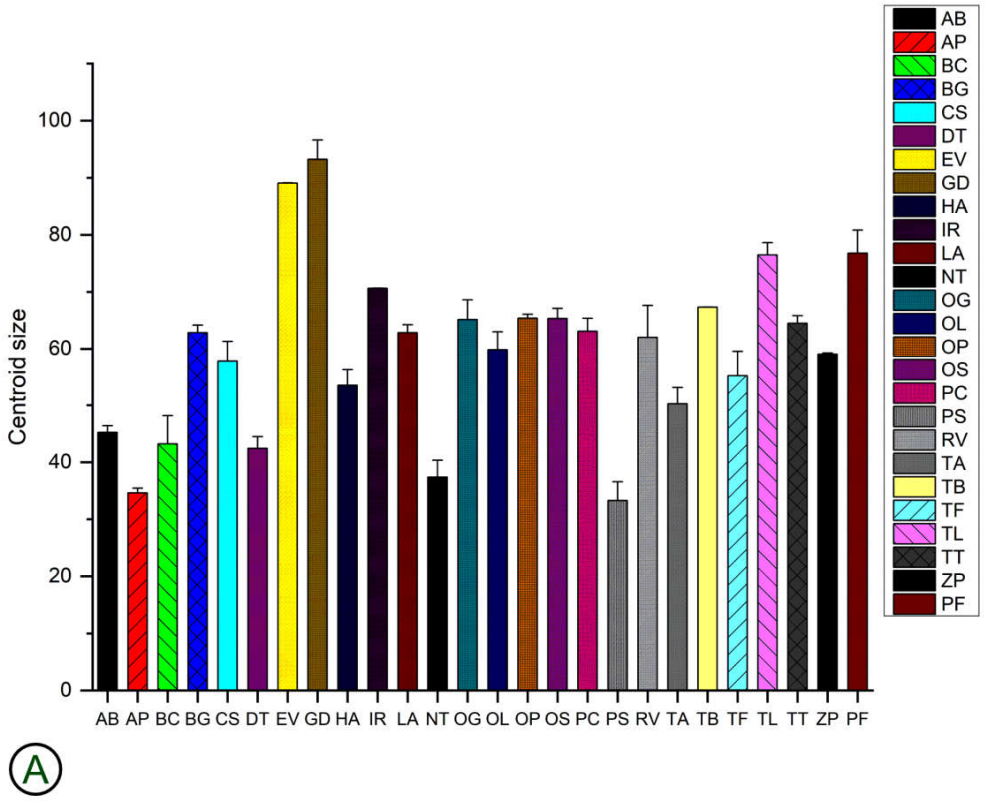

Figure 1.21: Centroid size analysis of hindwing. AP – *A. panorpoides;* AB – *A. brevipennis;* BC – *B. contaminata;* BG – *B. geminata;* CS – *C. servilia;* DT – *D. trivialis;* EV – *E. vittata;* GD – *G. dravida;* HA – *H. apicalis;* IR – *I. rapax;* LA – *L. asiatica;* NT – *N. tullia;* OG – *O. glaucum;* OL – *O. luzonicum;* OP – *O. pruinosum;* OS – *O. sabina;* PS – *P. sexmaculata;* PC – *P. congener;* PF – *P. flavescens;* RV – *R. variegata;* TT – *T. tillarga;* TB – *T. basilaris;* TL – *T. limbata;* TA – *T. aurora;* TF – *T. festiva;* ZP – *Z. petiolatum*

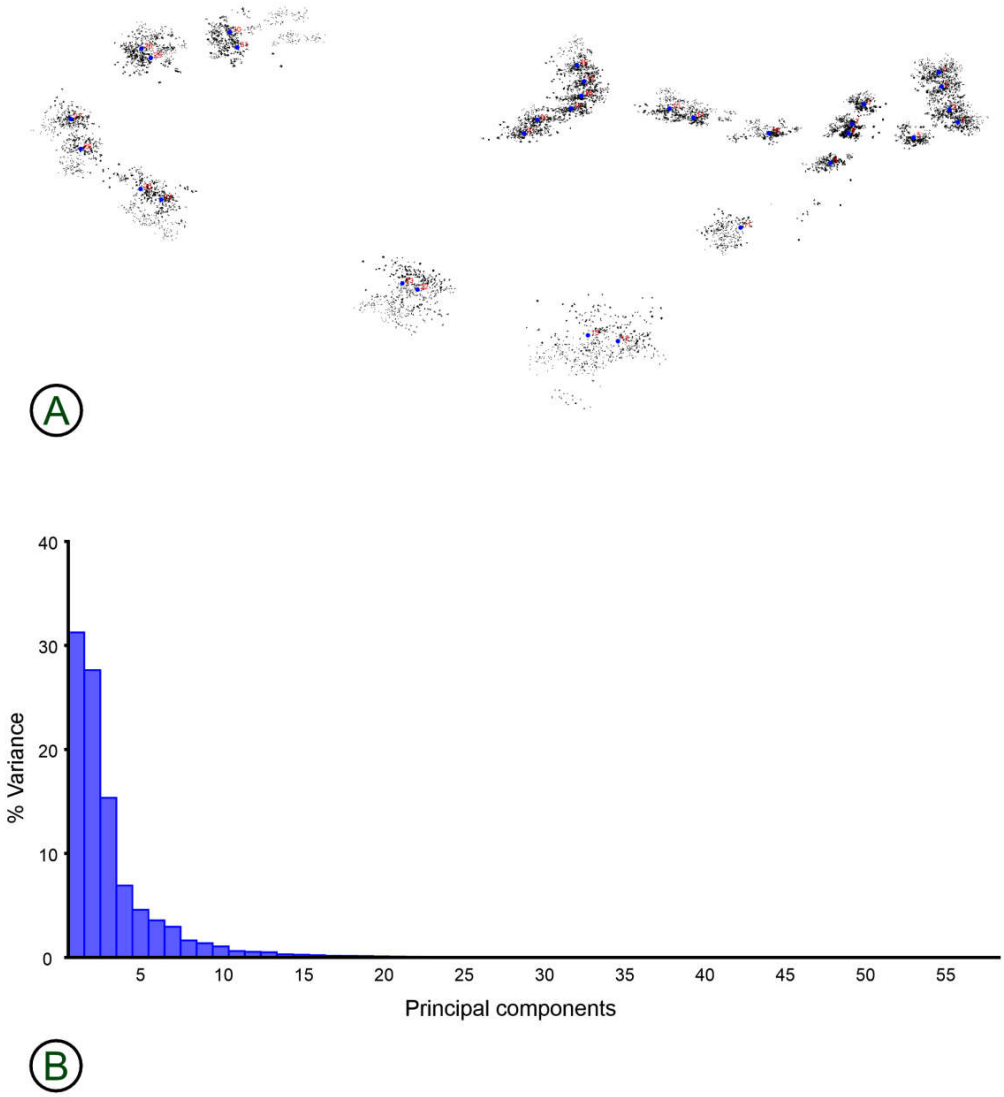

Figure 1.22: GPA and Percentage variance analysis in hindwings

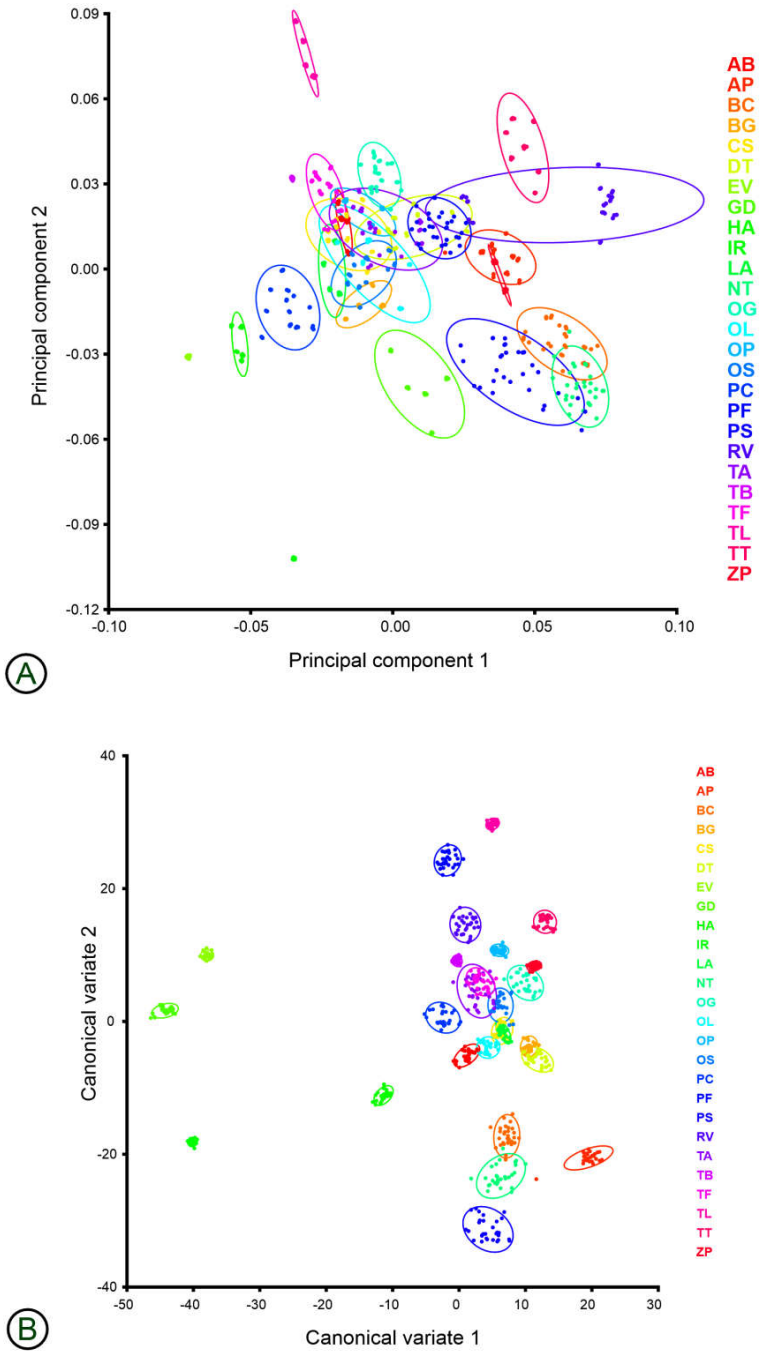

Figure 1.23: PC and CVA morphospace boundary analysis of hindwings. (A) PC1 vs. PC2 morphospace analysis representing 60.58% of variance; (B) CVA morphospace analysis. AP – *A. panorpoides;* AB – *A. brevipennis;* BC – *B. contaminata;* BG – *B. geminata;* CS – *C. servilia;* DT – *D. trivialis;* EV – *E. vittata;* GD – *G. dravida;* HA – *H. apicalis;* IR – *I. rapax;* LA – *L. asiatica;* NT – *N. tullia;* OG – *O. glaucum;* OL – *O. luzonicum;* OP – *O. pruinosum;* OS – *O. sabina;* PS – *P. sexmaculata;* PC – *P. congener;* PF – *P. flavescens;* RV – *R. variegata;* TT – *T. tillarga;* TB – *T. basilaris;* TL – *T. limbata;* TA – *T. aurora;* TF – *T. festiva;* ZP – *Z. petiolatum*

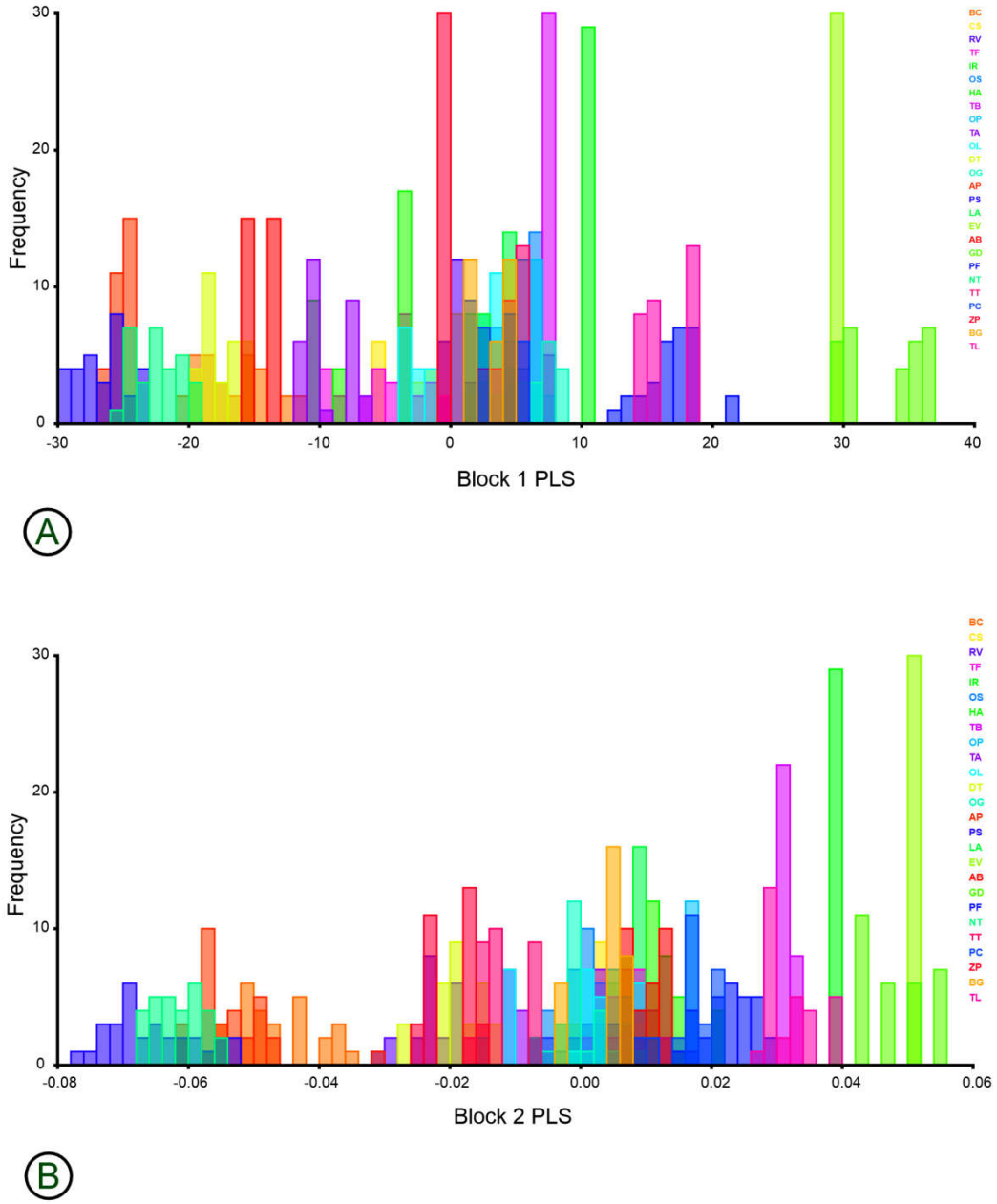

Figure 1.24: PLS analysis of hindwing. (A) PLS analysis of hindwing size; (B) PLS analysis of hindwing shape. AP – *A. panorpoides;* AB – *A. brevipennis;* BC – *B. contaminata;* BG – *B. geminata;* CS – *C. servilia;* DT – *D. trivialis;* EV – *E. vittata;* GD – *G. dravida;* HA – *H. apicalis;* IR – *I. rapax;* LA – *L. asiatica;* NT – *N. tullia;* OG – *O. glaucum;* OL – *O. luzonicum;* OP – *O. pruinosum;* OS – *O. sabina;* PS – *P. sexmaculata;* PC – *P. congener;* PF – *P. flavescens;* RV – *R. variegata;* TT – *T. tillarga;* TB – *T. basilaris;* TL – *T. limbata;* TA – *T. aurora;* TF – *T. festiva;* ZP – *Z. petiolatum*

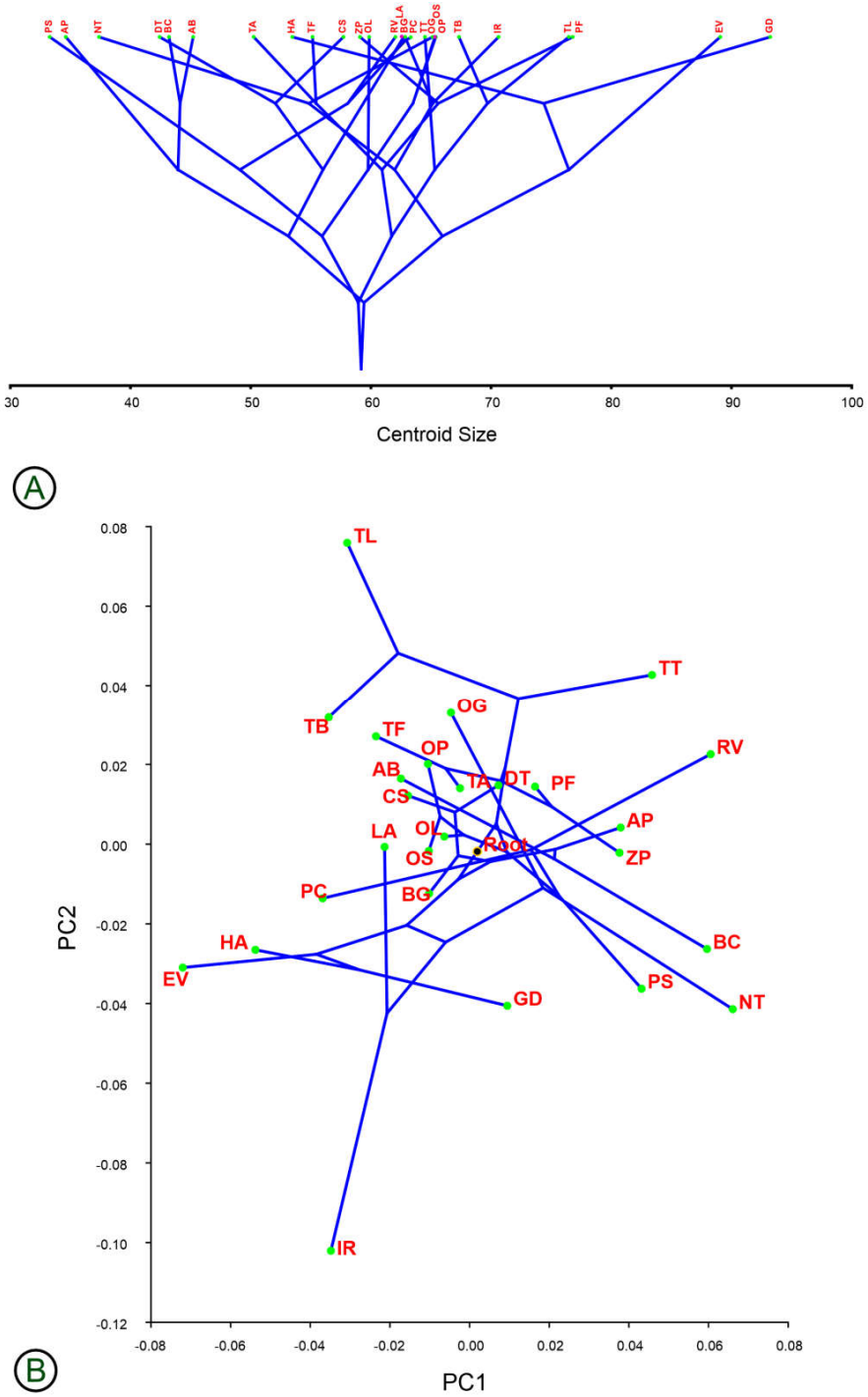

Figure 1.25: Phylogenetic analysis of hindwings. (A) Size-based phylogenetic analysis of hindwings; (B) Shape-based phylogenetic analysis of hindwings. AP – *A. panorpoides;* AB – *A. brevipennis;* BC – *B. contaminata;* BG – *B. geminata;* CS – *C. servilia;* DT – *D. trivialis;* EV – *E. vittata;* GD – *G. dravida;* HA – *H. apicalis;* IR – *I. rapax;* LA – *L. asiatica;* NT – *N. tullia;* OG – *O. glaucum;* OL – *O. luzonicum;* OP – *O. pruinosum;* OS – *O. sabina;* PS – *P. sexmaculata;* PC – *P. congener;* PF – *P. flavescens;* RV – *R. variegata;* TT – *T. tillarga;* TB – *T. basilaris;* TL – *T. limbata;* TA – *T. aurora;* TF – *T. festiva;* ZP – *Z. petiolatum*

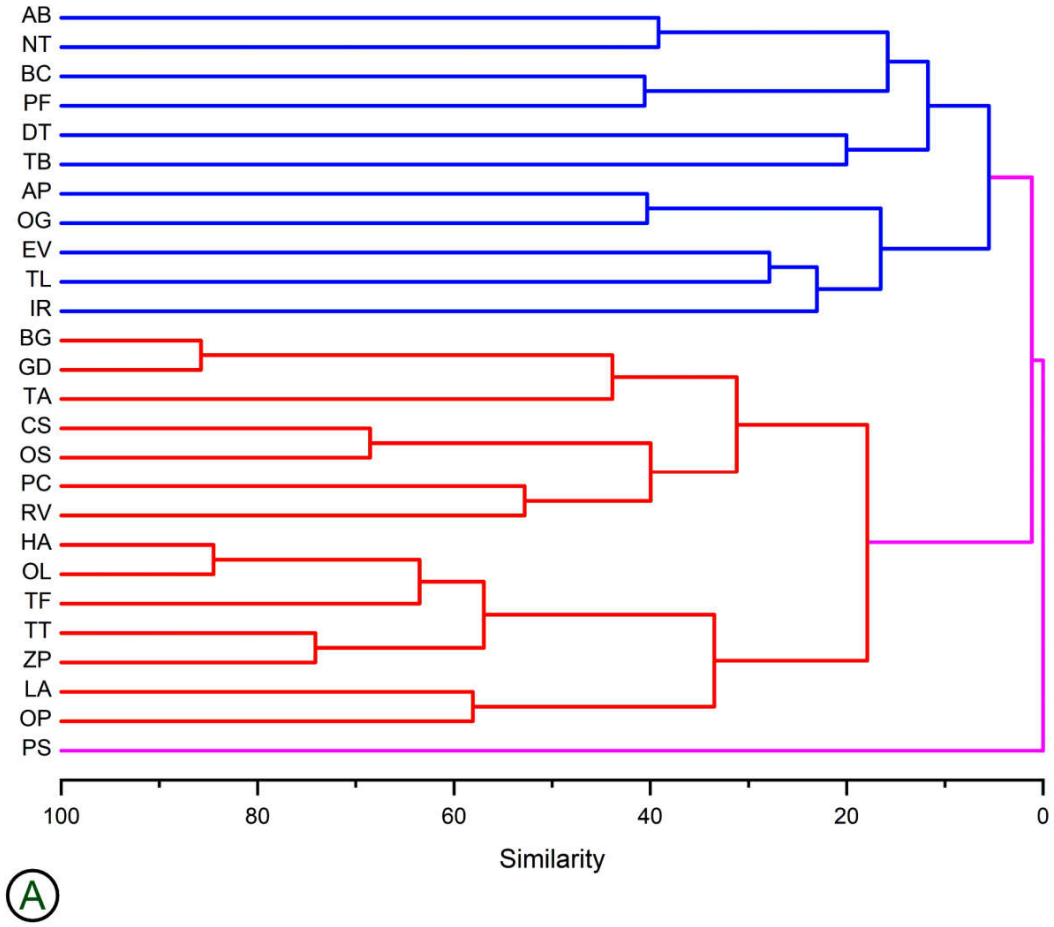

Figure 1.26: Hierarchical cluster dendrogram analysis of hindwing. AP – *A. panorpoides;* AB – *A. brevipennis;* BC – *B. contaminata;* BG – *B. geminata;* CS – *C. servilia;* DT – *D. trivialis;* EV – *E. vittata;* GD – *G. dravida;* HA – *H. apicalis;* IR – *I. rapax;* LA – *L. asiatica;* NT – *N. tullia;* OG – *O. glaucum;* OL – *O. luzonicum;* OP – *O. pruinosum;* OS – *O. sabina;* PS – *P. sexmaculata;* PC – *P. congener;* PF – *P. flavescens;* RV – *R. variegata;* TT – *T. tillarga;* TB – *T. basilaris;* TL – *T. limbata;* TA – *T. aurora;* TF – *T. festiva;* ZP – *Z. petiolatum*

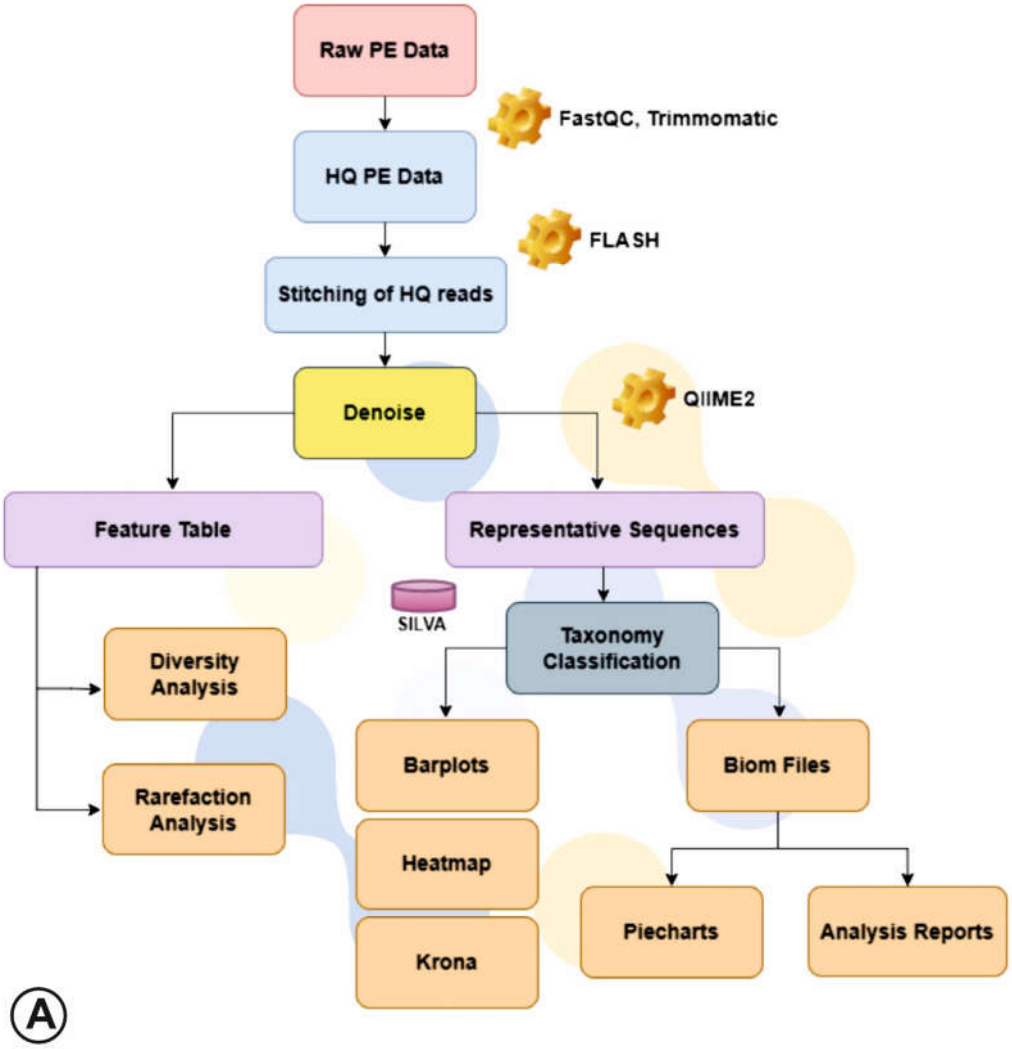

Figure 2.1: The bioinformatics analysis workflow

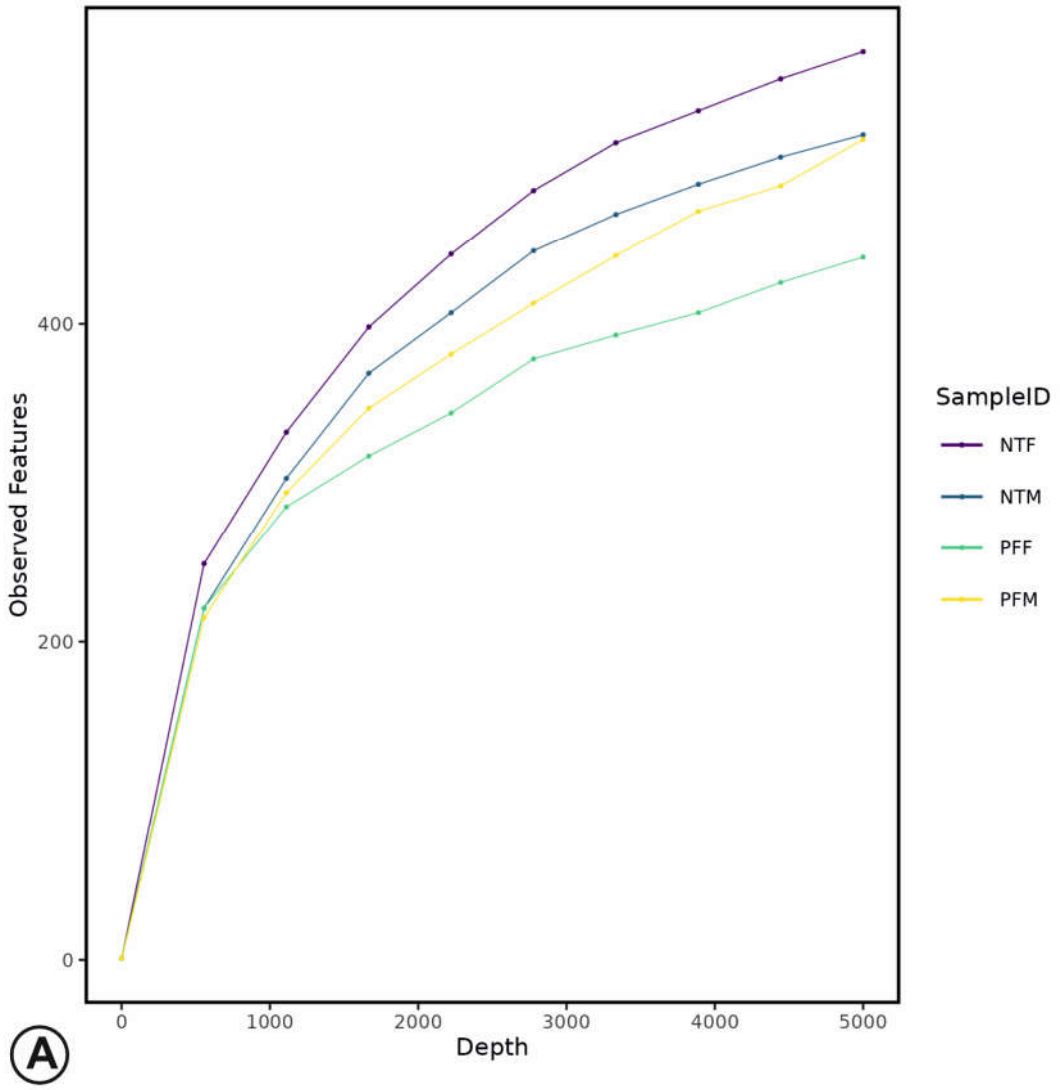

Figure 2.2: Rarefaction curve. the vertical axis displays the community's diversity, and the horizontal axis displays the number of sequences considered in the diversity calculation.

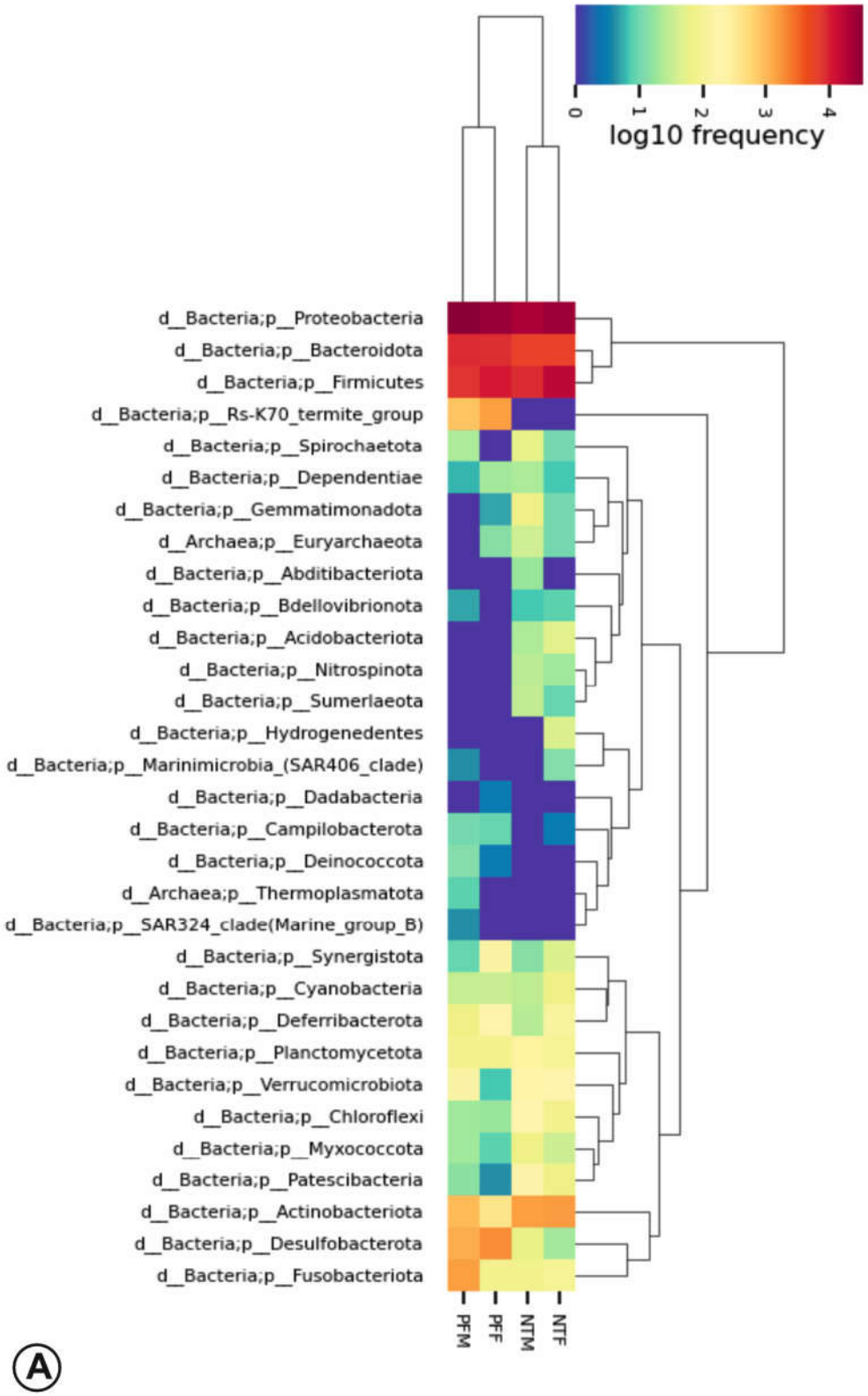

Figure 2.3: Abundance heatmap of dominant phylum. Red colour indicates a higher relative abundance of particular phyla in a sample, while Purple colour indicates a lower relative abundance of particular phyla.

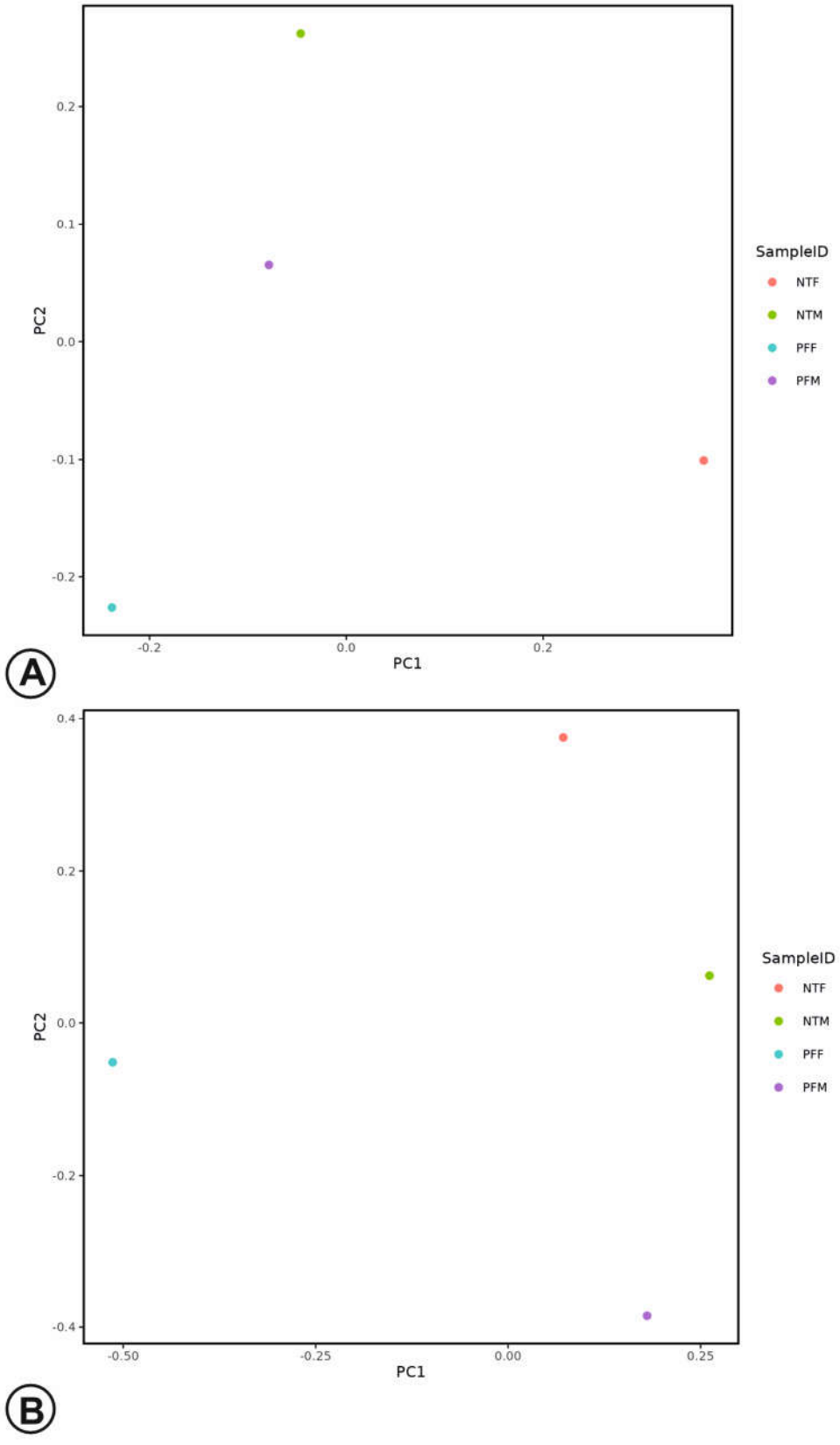

Figure 2.4: Principal Coordinate plot. (A) weighted Unifrac distances of the four samples, (B) unweighted Unifrac distances of the four samples

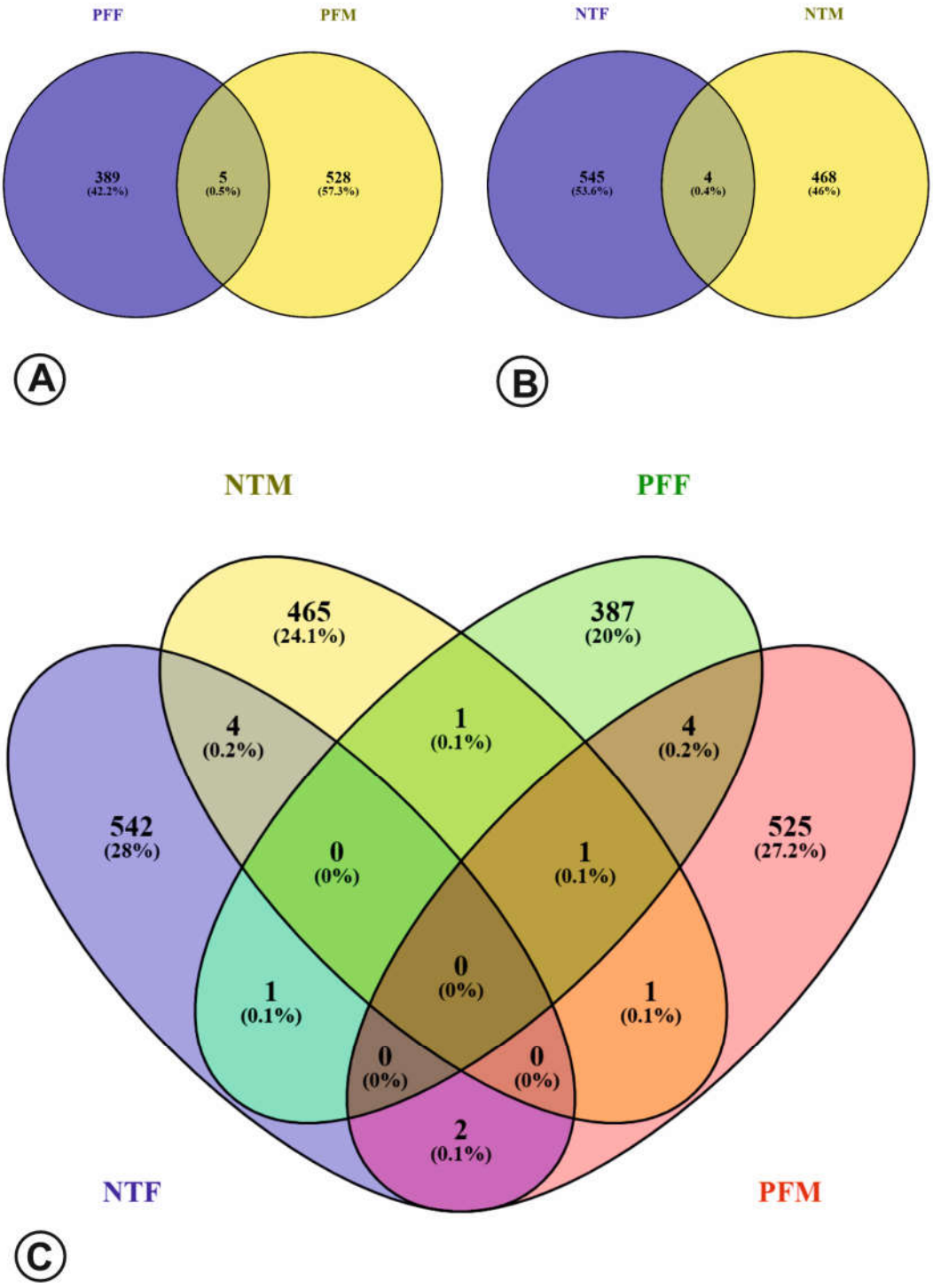

Figure 2.5: Venn diagram. (A) *P. flavescens* male and female, (B) *N. tullia* male and female, (C) Venn diagram showing the number and percentage of the 1933 OTUs observed in the four samples and from each combination of the four samples.

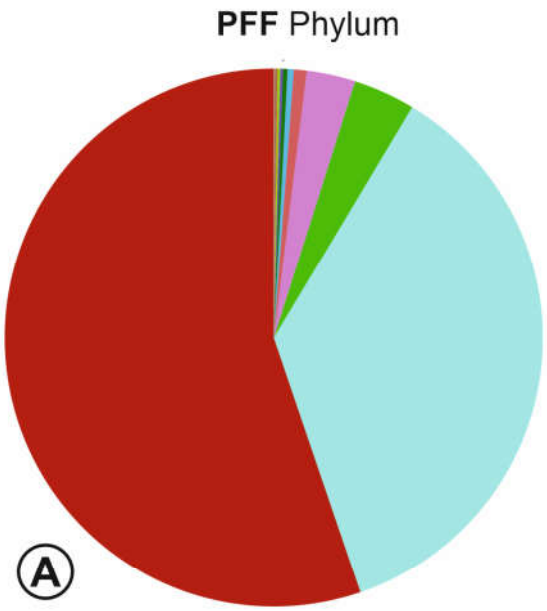

Legends	Taxonomy	Abundance
	p_Proteobacteria	55 .22%
	p_Firmicutes	19.8%
	p_Bacteroidota	16.37%
	p_Desulfobacterota	3.71%
	p_Rs-K70_termite_group	2.93%
	p_Actinobacteriota	0.77%
	p_Deferribacterota	0.37%
	p_Synergistota	0.27%
	p_Planctomycetota	0.16%
	p_Fusobacteriota	0.16%
	p_Cyanobacteria	0.06%
	p_Dependentiae	0.04%
	p_Chloroflexi	0.03%
	p_Euryarchaeota	0.03%
	p_Campilobacterota	0.02%
	p_Myxococcota	0.01%
	p_Verrucomicrobiota	0.01%
	p_Gemmatimonadota	0.01%
	p_Patescibacteria	0.01%
	Others	0.01%

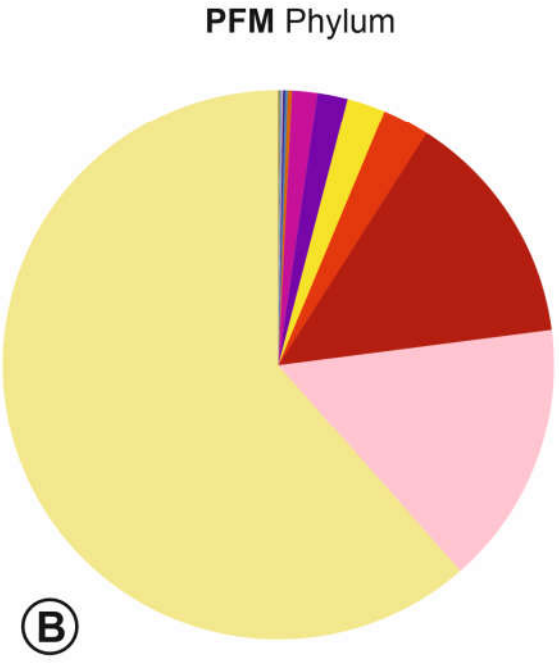

Legends	Taxonomy	Abundance
	p_Proteobacteria	61.48%
	p_Bacteroidota	15.56%
	p_Firmicutes	13.91%
	p_Fusobacteriota	2 .74%
	p_Desulfobacterota	2 .25%
	p_Actinobacteriota	1.77%
	p_Rs-K70_termite_group	1.49%
	p_Verrucomicrobiota	0.24%
	p_Planctomycetota	0.15%
	p_Deferribacterota	0.13%
	p_Cyanobacteria	0.05%
	p_Spirochaetota	0.04%
	p_Ch loroflexi	0.03%
	p_Myxococcota	0.03%
	p_Patescibacteria	0.03%
	p_Deinococcota	0.02%
	p_Campilobacterota	0.02%
	p_Synergistota	0.01%
	p_Thermoplasmatota	0.01%
	Others	0.03%

Figure 2.6: Pie chart of bacterial Phyla in *P. flavescens*. (A) PFF, (B) PFM

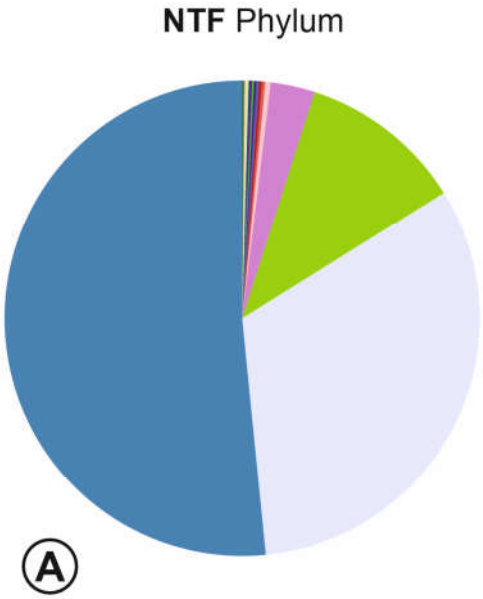

Legends	Taxonomy	Abundance
	p_Proteobacteria	51.59%
	p_Firmicutes	32.27%
	p_Bacteroidota	11.2%
	p_Actinobacteriota	3.02%
	p_Verrucomicrobiota	0.36%
	p_Deferribacterota	0.23%
	p_Fusobacteriota	0.19%
	p_Planctomycetota	0.18%
	p_Chloroflexi	0.16%
	p_Patescibacteria	0.13%
	p_Cyanobacteria	0.13%
	p_Acidobacteriota	0.1%
	p_Synergistota	0.09%
	p_Hydrogenedentes	0.09%
	p_Myxococcota	0.07%
	p_Desulfobacterota	0.04%
	p_Nitrospinota	0.03%
	p_Marinimicrobia_(SAR406_clade)	0.02%
	p_Spirochaetota	0.02%
	Others	0.08%

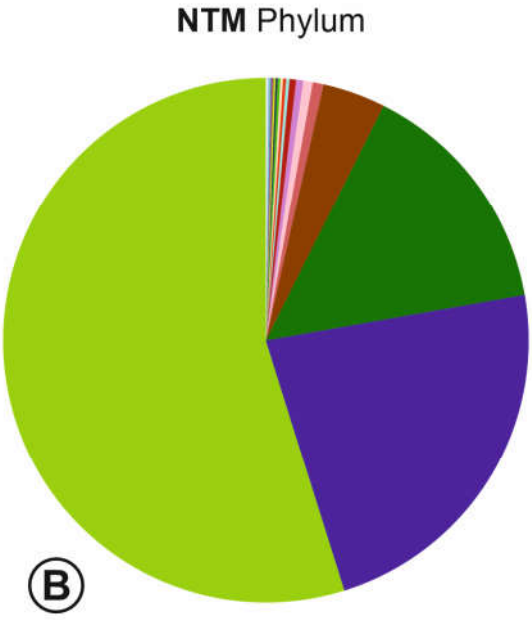

Legends	Taxonomy	Adundance
	p_Proteobacteria	54.84%
	p_Firmicutes	22.94%
	p_Bacteroidota	14.84%
	p_Actinobacteriota	3.86%
	p_Planctomycetota	0.67%
	p_Verrucomicrobiota	0.58%
	p_Chloroflexi	0.44%
	p_Patescibacteria	0.4%
	p_Fusobacteriota	0.21%
	p_Gemmatimonadota	0.18%
	p_Myxococcota	0.17%
	p_Desulfobacterota	0.16%
	p_Spirochaetota	0.14%
	p_Euryarchaeota	0.09%
	p_Sumerlaeota	0.08%
	p_Cyanobacteria	0.07%
	p_Nitrospinota	0.07%
	p_Deferribacterota	0.06%
	p_Acidobacteriota	0.06%
	Others	0.15%

Figure 2.7: Pie chart of bacterial Phyla in *N. tullia*. (A) NTF, (B) NTM

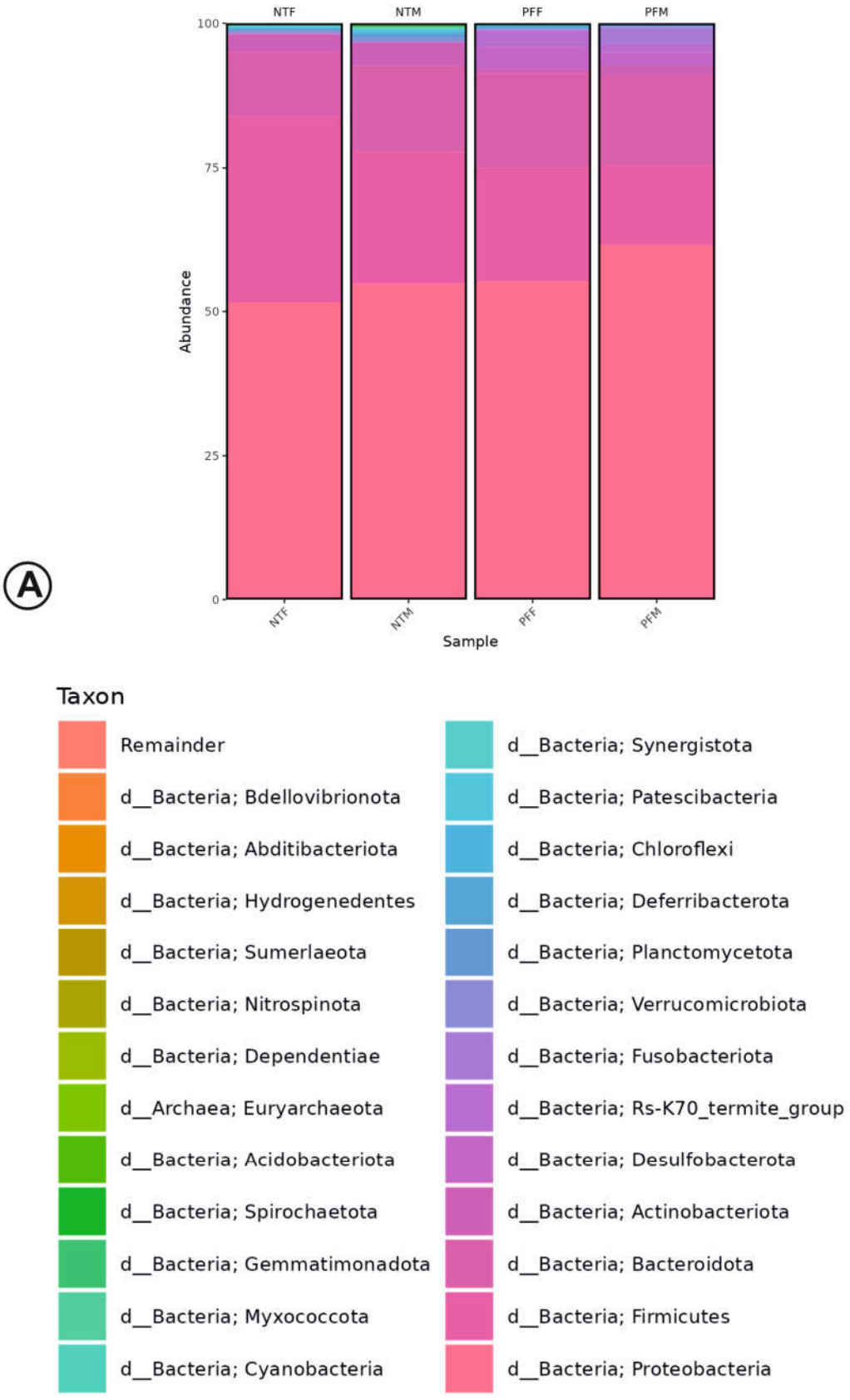

Figure 2.8: Bar plot of bacterial Phyla. Comparison of bacterial gut samples NTF, NTM, PFF, and PFM

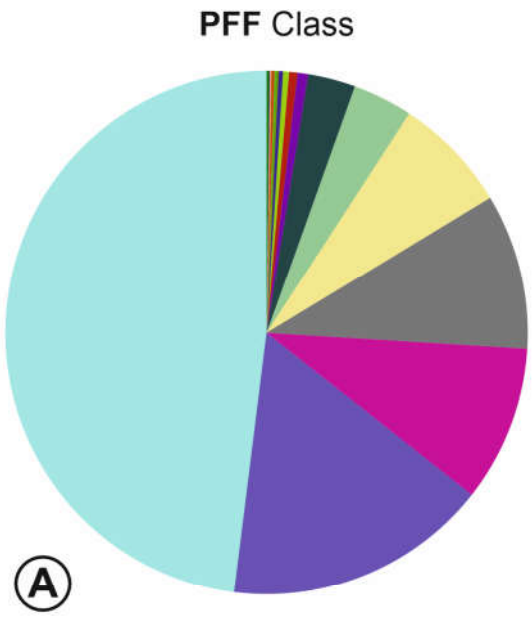

Legends	Taxonomy	Abundance
	c_ Gamma proteobacteria	48 .01%
	c_Bacteroidia	16.37%
	c_Bacilli	9.64%
	c_Clostridia	9.62%
	c_Alphaproteobacteria	7.15%
	c_Desulfovibrionia	3.71%
	c_Rs-K70_termite_group	2.93%
	c_Actinobacteria	0.66%
	c_ Negativicutes	0.52%
	c_Deferribacteres	0.37%
	c_Synergistia	0.27%
	c_Fusobacteriia	0.16%
	c_vadinHA49	0.1%
	c_Thermoleophilia	0.08%
	p_Proteobacteria;_	0.06%
	c_Cyanobacteriia	0.06%
	c_Planctomycetes	0.04%
	c_Babeliae	0.04%
	c_Acidimicrobiia	0.03%
	Others	0.17%

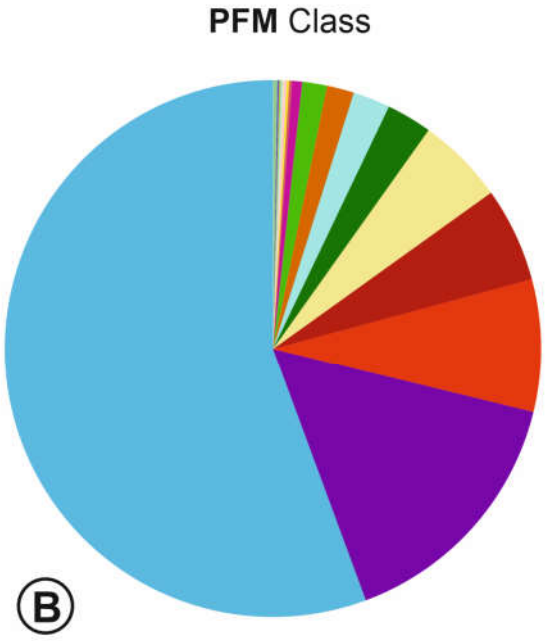

Legends	Taxonomy	Abundance
	c_ Gamma proteobacteria	55.64%
	c_Bacteroidia	15.56%
	c_Bacilli	8.0%
	c_Alphaproteobacteria	5.69%
	c_Clostridia	5.26%
	c_Fusobacteriia	2.74%
	c_Desulfovibrionia	2.24%
	c_Actinobacteria	1.64%
	c_Rs-K70_termite_group	1.49%
	c_ Negativicutes	0.61%
	c_ Chlamydiae	0.17%
	p_Proteobacteria;_	0.15%
	c_Deferribacteres	0.13%
	c_Planctomycetes	0.12%
	c_Coriobacteri ia	0.1%
	c_Verrucomicrobiae	0.08%
	c_Varn pirivibrionia	0.05%
	p_Firmicutes;_	0.04%
	c_ Spirochaetia	0.04%
	Others	0.26%

Figure 2.9: Pie chart of bacterial Class in *P. flavescens*. (A) PFF, (B) PFM

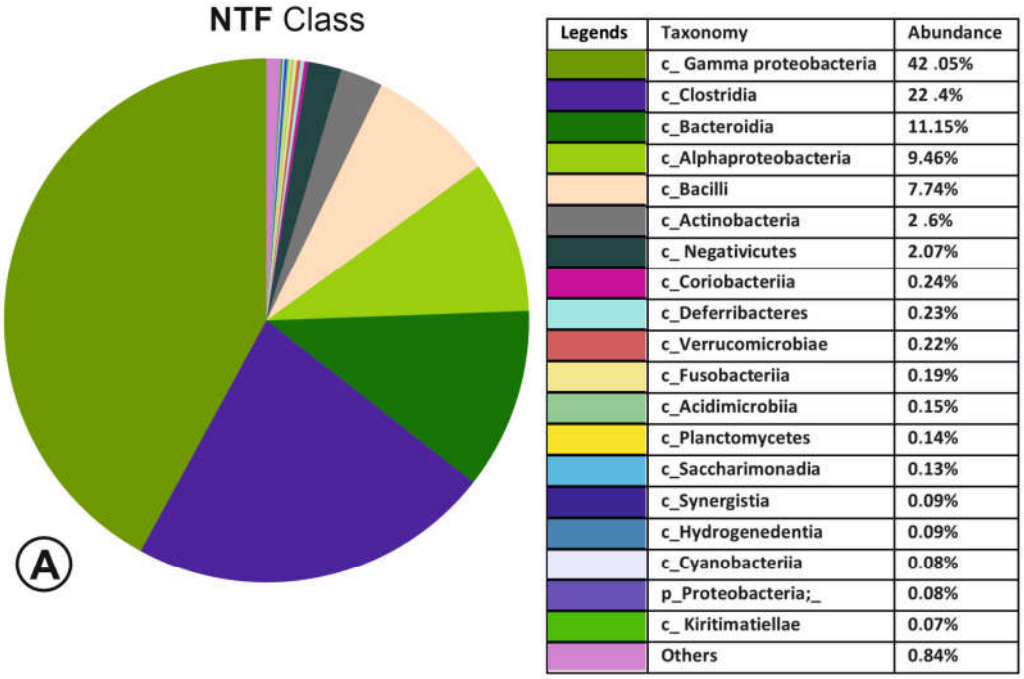

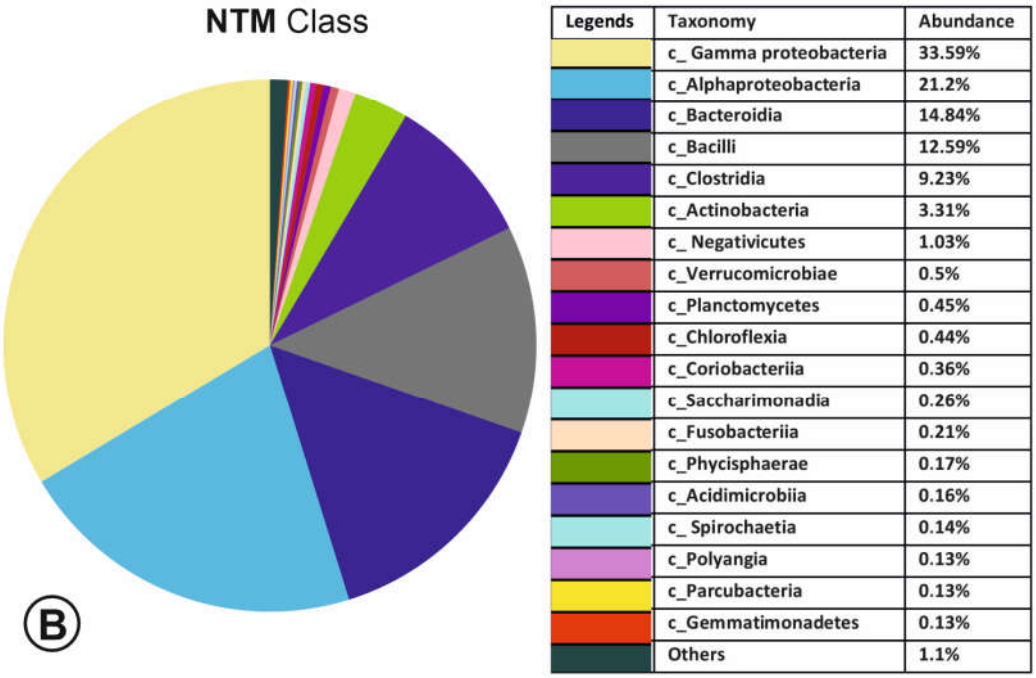

Figure 2.10: Pie chart of bacterial Class in *N. tullia*. (A) NTF, (B) NTM

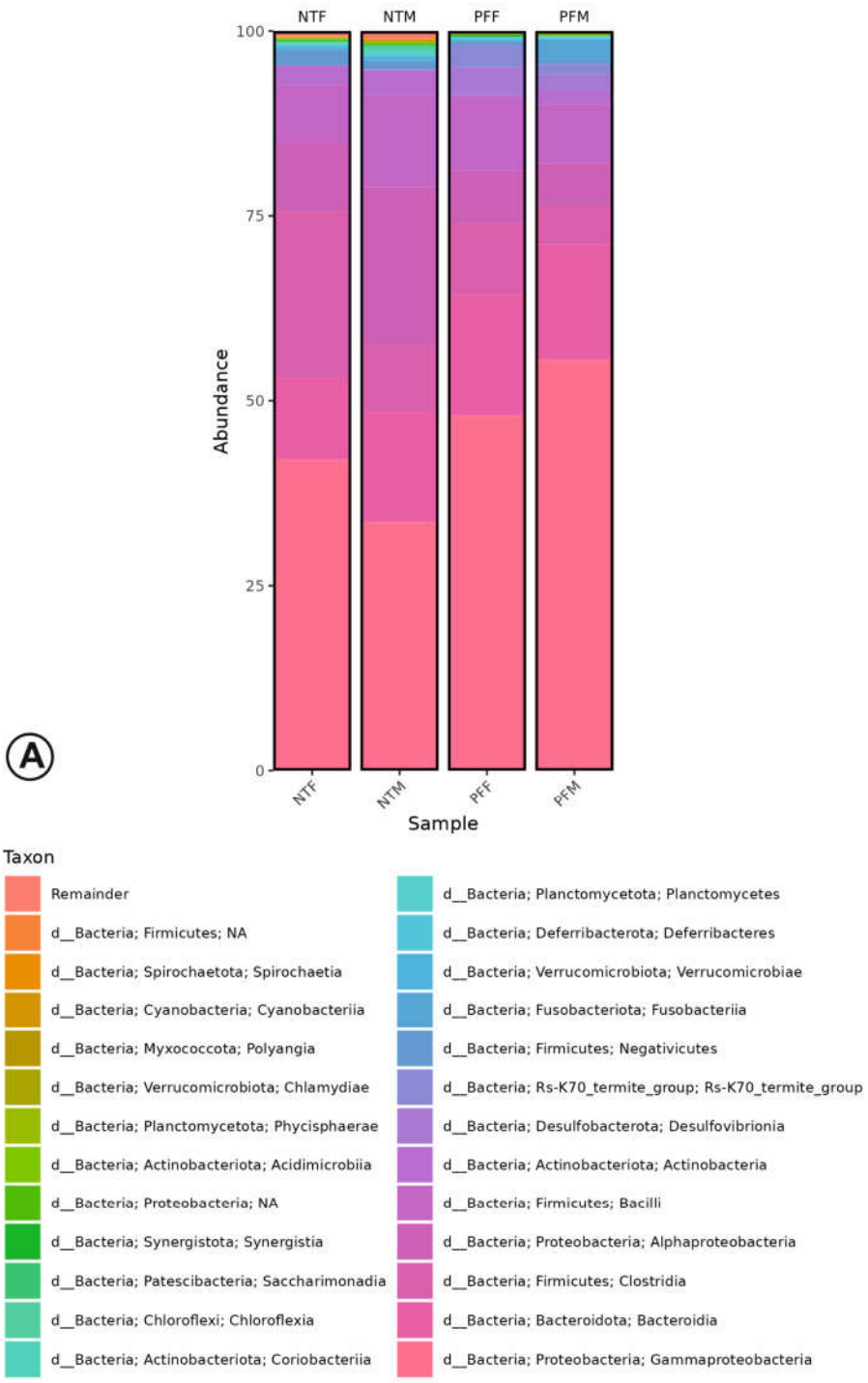

Figure 2.11: Bar plot of bacterial Class. Comparison of bacterial gut samples NTF, NTM, PFF, and PFM

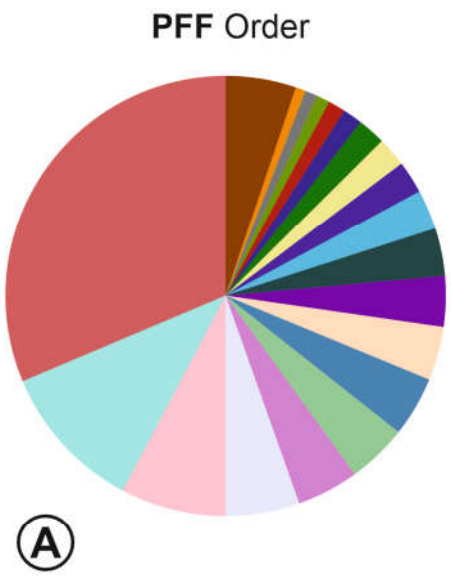

Legends	Taxonomy	Abundance
	o_Enterobacterales	31.35%
	o_Bacteroidales	10.92%
	o_Lactobacillales	7.74%
	o_Burkholderiales	5.42%
	o_Clostridiales	4.54%
	o_Pseudomonadales	4.41%
	o_Flavobacteriales	4.4%
	o_Cardiobacteriales	3.94%
	o_Desulfovibrionales	3.71%
	o_Acetobacterales	3.53%
	o_Rs-K70_termite_group	2.93%
	o_Rhizobiales	2.4%
	o_Oscillospirales	2.16%
	o_Peptostreptococca les-Tissierellales	2.05%
	o_Entomoplasmatales	1.44%
	o_Aeromonadales	1.27%
	o_Rickettsiales	0.96%
	c_Gammaproteobacteria ;_	0.92%
	o_Sphingobacteriales	0.74%
	Others	5.17%

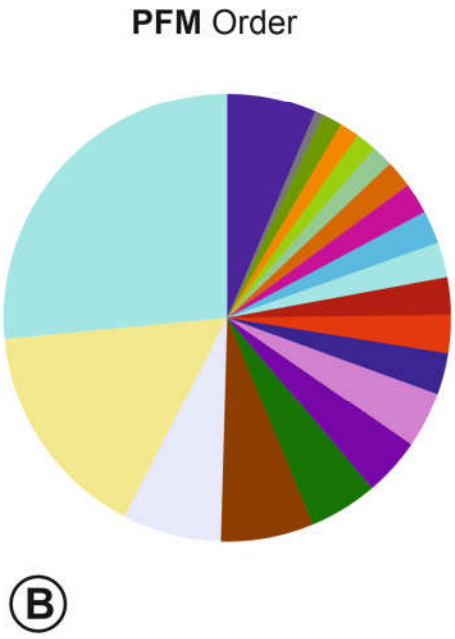

Legends	Taxonomy	Abundance
	o_Enterobacterales	26.51%
	o_Pseudomonadales	15.89%
	o_Bacteroidales	7.15%
	o_Lactobacillales	6.71%
	o_Flavobacteriales	4.96%
	o_Cardiobacteriales	4.17%
	o_Burkholderiales	4.09%
	c_Gammaproteobacteria ;_	2.99%
	o_Fusobacteriales	2.74%
	o_Sphingobacteriales	2.7%
	o_Rhizobiales	2.53%
	o_Oscillospirales	2.37%
	o_Desulfovibrionales	2.24%
	o_Acetobacterales	1.98%
	o_Xanthomonadales	1.56%
	o_Rs-K70_termite_group	1.49%
	o_Peptostreptococca les-Tissierellales	1.44%
	o_Micrococcales	1.43%
	o_Erysipelotrichales	0.62%
	Others	6.44%

Figure 2.12: Pie chart of bacterial Order in *P. flavescens*. (A) PFF, (B) PFM

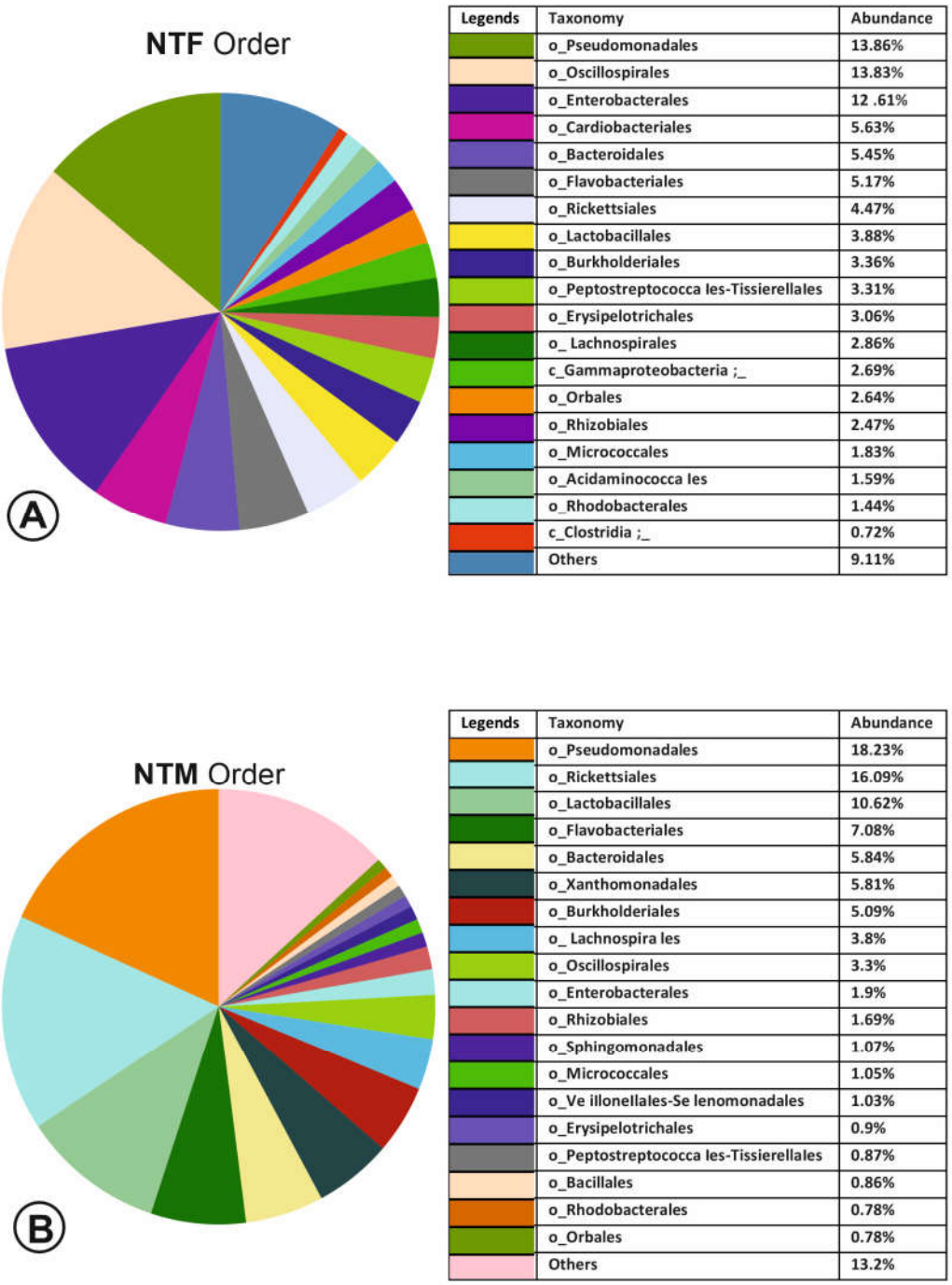

Legends	Taxonomy	Abundance
	o_Pseudomonadales	13.86%
	o_Oscillospirales	13.83%
	o_Enterobacterales	12 .61%
	o_Cardiobacteriales	5.63%
	o_Bacteroidales	5.45%
	o_Flavobacteriales	5.17%
	o_Rickettsiales	4.47%
	o_Lactobacillales	3.88%
	o_Burkholderiales	3.36%
	o_Peptostreptococca les-Tissierellales	3.31%
	o_Erysipelotrichales	3.06%
	o_ Lachnospirales	2.86%
	c_Gammaproteobacteria ;_	2.69%
	o_Orbales	2.64%
	o_Rhizobiales	2.47%
	o_Micrococcales	1.83%
	o_Acidaminococca les	1.59%
	o_Rhodobacterales	1.44%
	c_Clostridia ;_	0.72%
	Others	9.11%

Legends	Taxonomy	Abundance
	o_Pseudomonadales	18.23%
	o_Rickettsiales	16.09%
	o_Lactobacillales	10.62%
	o_Flavobacteriales	7.08%
	o_Bacteroidales	5.84%
	o_Xanthomonadales	5.81%
	o_Burkholderiales	5.09%
	o_ Lachnospira les	3.8%
	o_Oscillospirales	3.3%
	o_Enterobacterales	1.9%
	o_Rhizobiales	1.69%
	o_Sphingomonadales	1.07%
	o_Micrococcales	1.05%
	o_Ve illonellales-Se lenomonadales	1.03%
	o_Erysipelotrichales	0.9%
	o_Peptostreptococca les-Tissierellales	0.87%
	o_Bacillales	0.86%
	o_Rhodobacterales	0.78%
	o_Orbales	0.78%
	Others	13.2%

Figure 2.13: Pie chart of bacterial Order in *N. tullia*. (A) NTF, (B) NTM

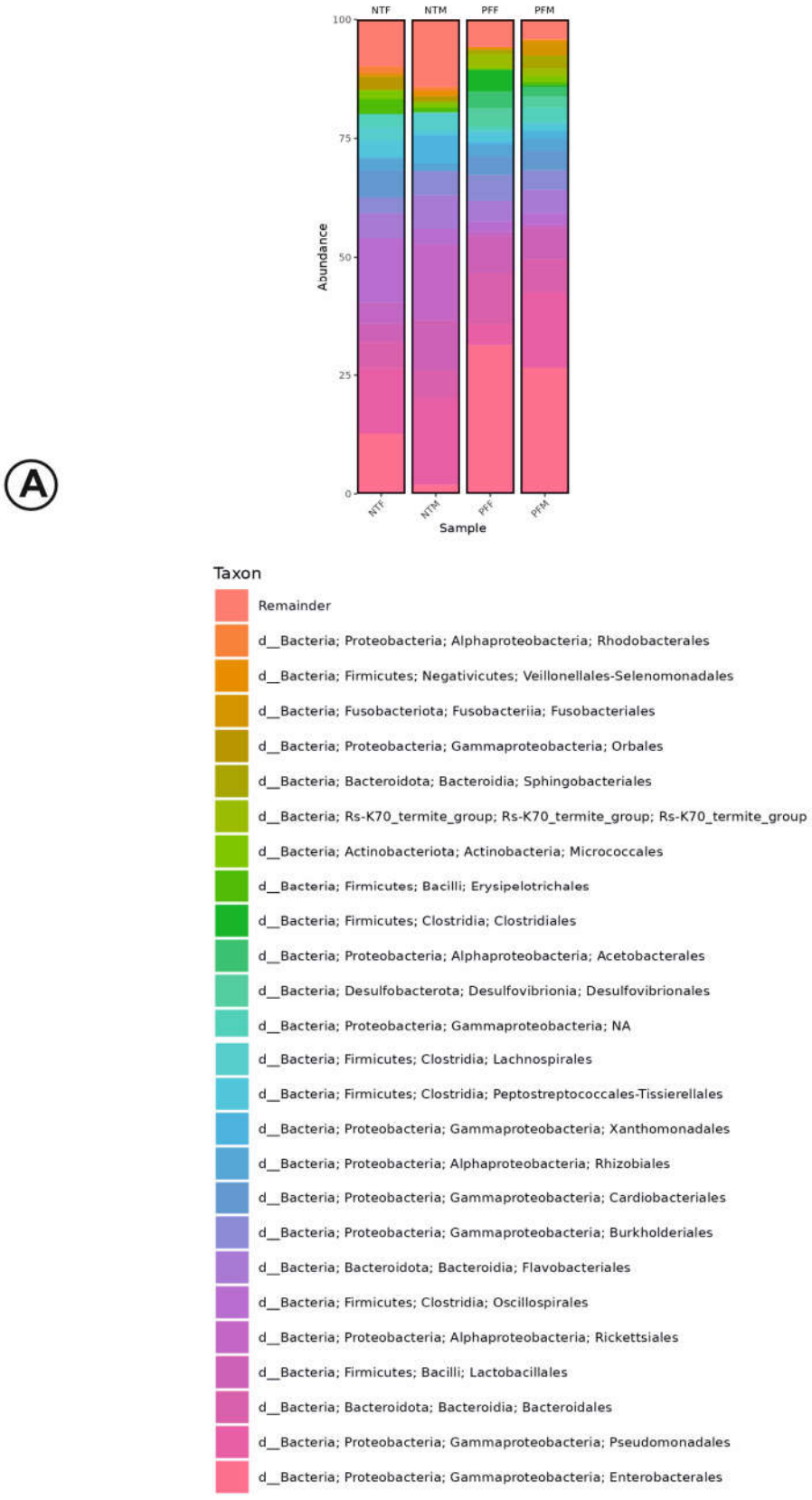

Figure 2.14: Bar plot of bacterial Order. Comparison of bacterial gut samples NTF, NTM, PFF, and PFM

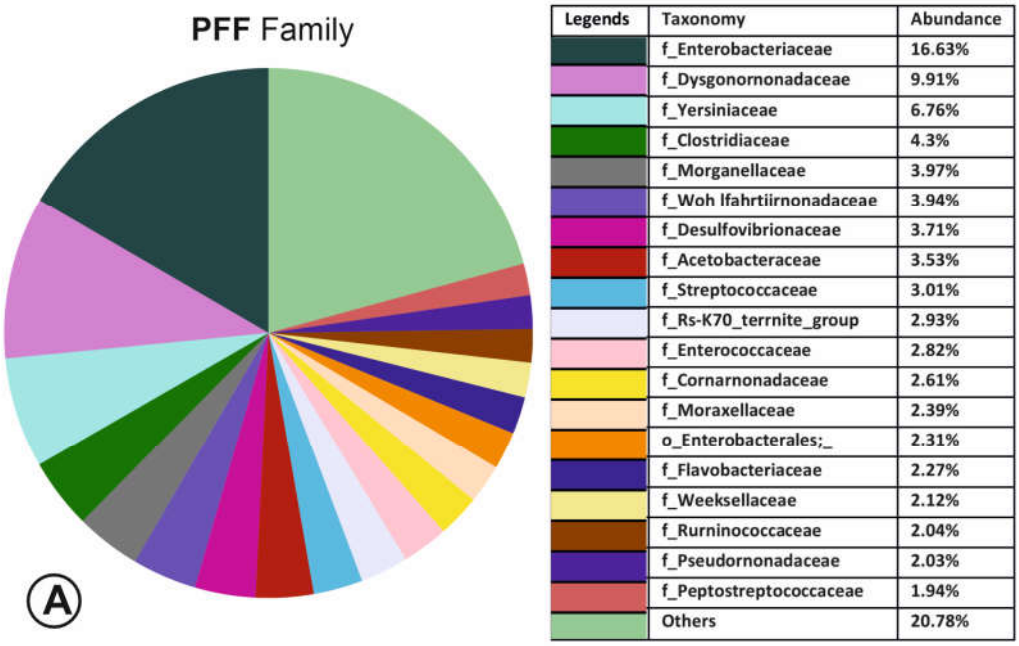

Legends	Taxonomy	Abundance
	f_Enterobacteriaceae	16.63%
	f_Dysgonornonadaceae	9.91%
	f_Yersiniaceae	6.76%
	f_Clostridiaceae	4.3%
	f_Morganellaceae	3.97%
	f_Woh lfahrtiirnonadaceae	3.94%
	f_Desulfovibrionaceae	3.71%
	f_Acetobacteraceae	3.53%
	f_Streptococcaceae	3.01%
	f_Rs-K70_terrnite_group	2.93%
	f_Enterococcaceae	2.82%
	f_Cornarnonadaceae	2.61%
	f_Moraxellaceae	2.39%
	o_Enterobacterales;_	2.31%
	f_Flavobacteriaceae	2.27%
	f_Weeksellaceae	2.12%
	f_Rurninococcaceae	2.04%
	f_Pseudornonadaceae	2.03%
	f_Peptostreptococcaceae	1.94%
	Others	20.78%

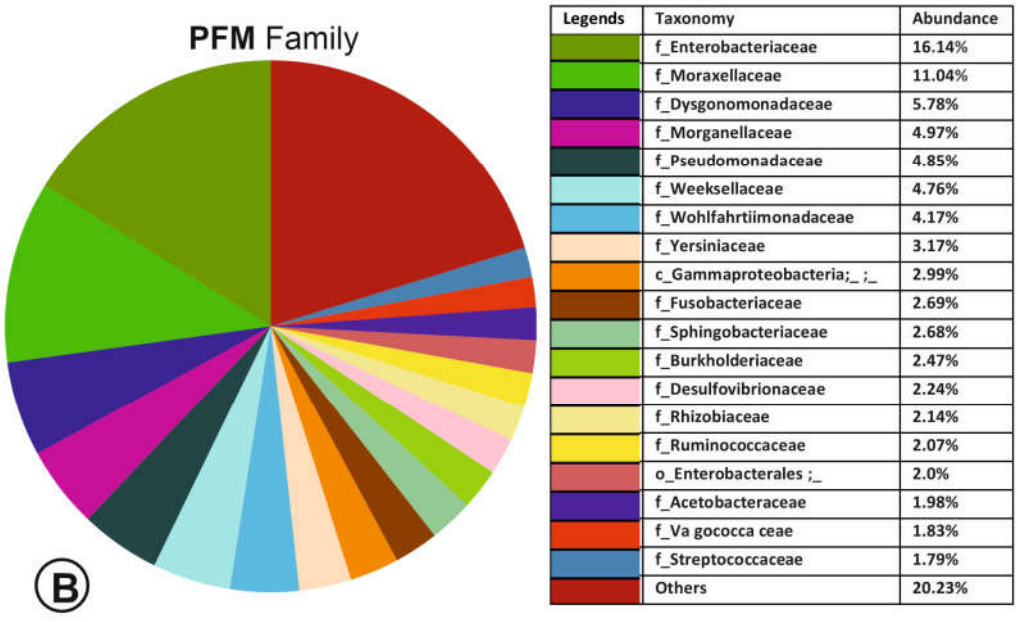

Legends	Taxonomy	Abundance
	f_Enterobacteriaceae	16.14%
	f_Moraxellaceae	11.04%
	f_Dysgonomonadaceae	5.78%
	f_Morganellaceae	4.97%
	f_Pseudomonadaceae	4.85%
	f_Weeksellaceae	4.76%
	f_Wohlfahrtiimonadaceae	4.17%
	f_Yersiniaceae	3.17%
	c_Gammaproteobacteria;_ ;_	2.99%
	f_Fusobacteriaceae	2.69%
	f_Sphingobacteriaceae	2.68%
	f_Burkholderiaceae	2.47%
	f_Desulfovibrionaceae	2.24%
	f_Rhizobiaceae	2.14%
	f_Ruminococcaceae	2.07%
	o_Enterobacterales ;_	2.0%
	f_Acetobacteraceae	1.98%
	f_Va gococca ceae	1.83%
	f_Streptococcaceae	1.79%
	Others	20.23%

Figure 2.15: Pie chart of bacterial Family in *P. flavescens*. (A) PFF, (B) PFM

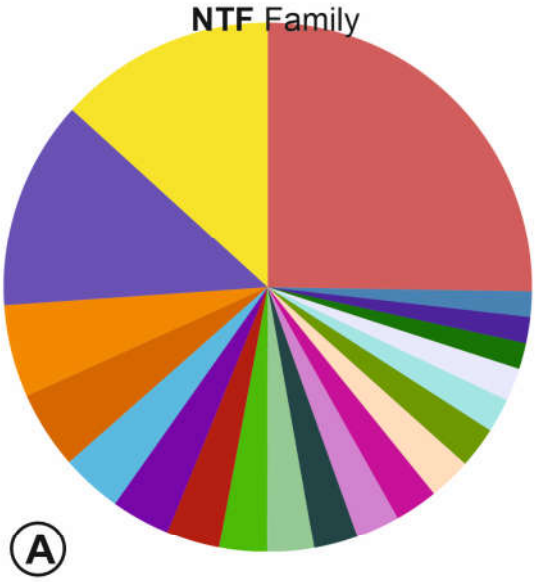

Legends	Taxonomy	Abundance
	f_Moraxellaceae	13.28%
	f_Rurninococcaceae	12.81%
	f_Woh lfahrtiirnonadaceae	5.63%
	f_Weeksellaceae	4.74%
	f_Morganellaceae	3.73%
	f_Yersiniaceae	3.61%
	f_Peptostreptococcaceae	3.25%
	f_Rickettsiaceae	2.92%
	f_Enterobacteriaceae	2.86%
	c_Garnrnaproteobacteria;_;_	2.69%
	f_Lachnospiraceae	2.68%
	f_Orbaceae	2.64%
	f_Dysgonornonadaceae	2.59%
	f_Erysipelotrichaceae	2.51%
	f_Burkholderiaceae	2.07%
	o_Enterobacterales;_	2.02%
	f_Microbacteriaceae	1.59%
	f_Acidarninococcaceae	1.59%
	f_Anaplasrnataceae	1.55%
	Others	25.25%

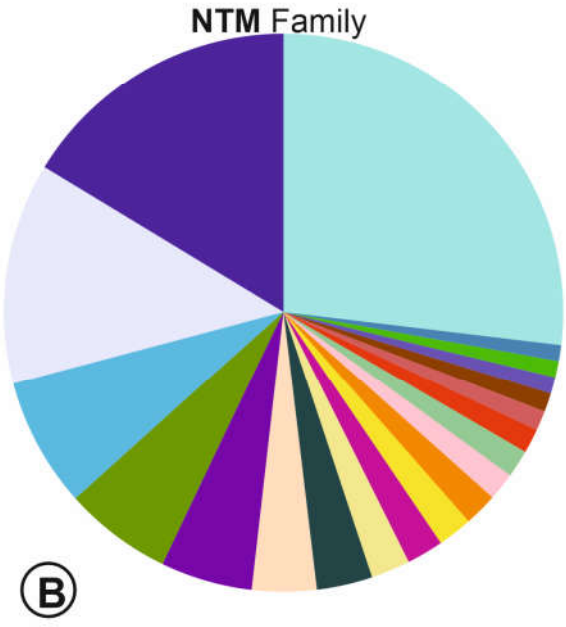

Legends	Taxonomy	Abundance
	f_Moraxellaceae	16.31%
	f_Anaplasmataceae	12.85%
	f_Enterococcaceae	7.49%
	f_Weeksellaceae	6.23%
	f_Rhodanobacteraceae	5.3%
	f_Lachnospiraceae	3.73%
	f_Rickettsiaceae	3.22%
	f_Prevotellaceae	2.26%
	f_Alcaligenaceae	2.12%
	f_Lactobacillaceae	2.0%
	f_Pseudomonadaceae	1.92%
	f_Oxalobacteraceae	1.6%
	f_Ruminococcaceae	1.59%
	f_Enterobacteriaceae	1.39%
	f_Bacteroidaceae	1.16%
	f_Sphingomonadaceae	1.07%
	f_Streptococcaceae	0.97%
	f_Burkholderiaceae	0.96%
	f_Rhizobiaceae	0.93%
	Others	26.9%

Figure 2.16: Pie chart of bacterial Family in *N. tullia*. (A) NTF, (B) NTM

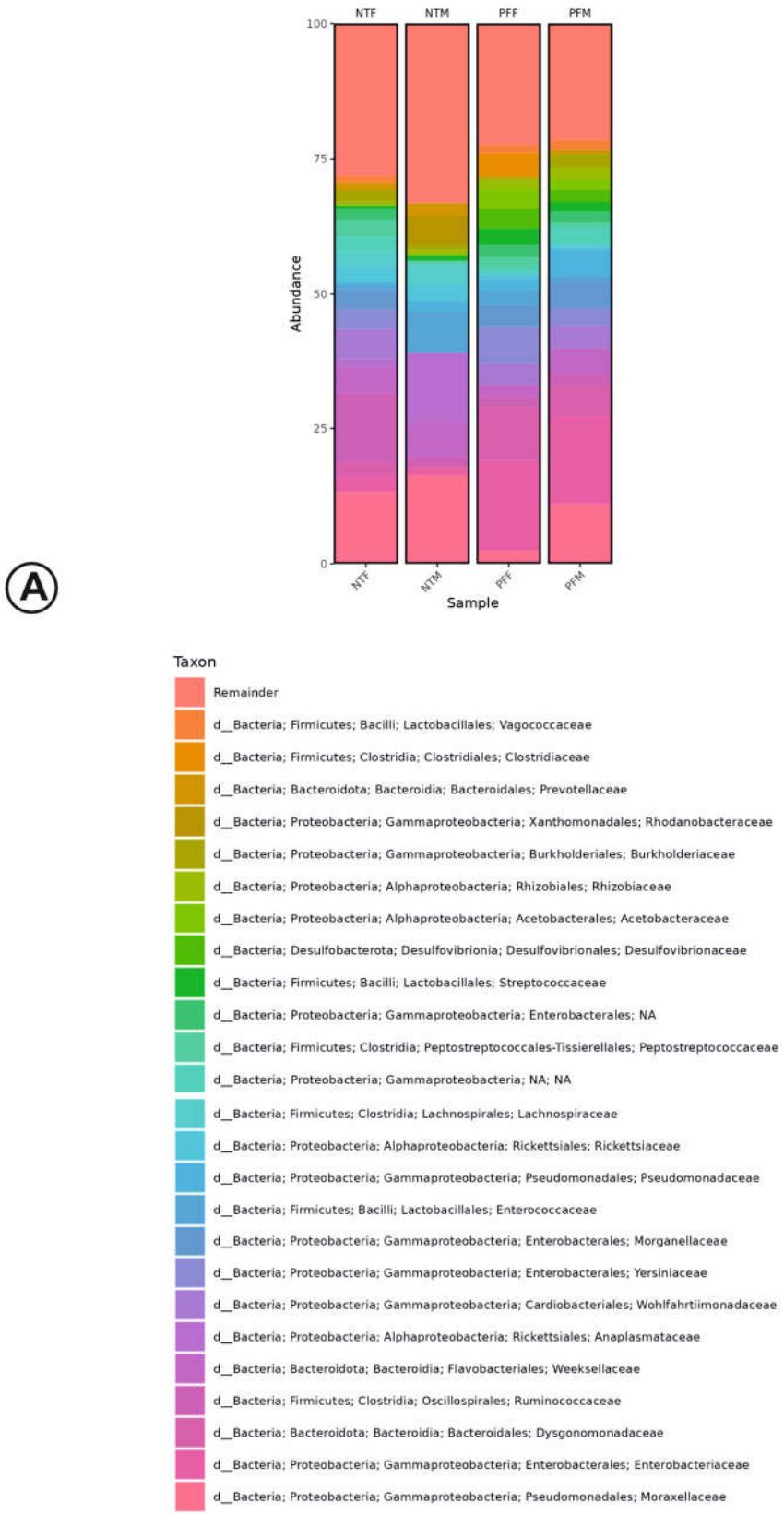

Figure 2.17: Bar plot of bacterial Family. Comparison of bacterial gut samples NTF, NTM, PFF, and PFM

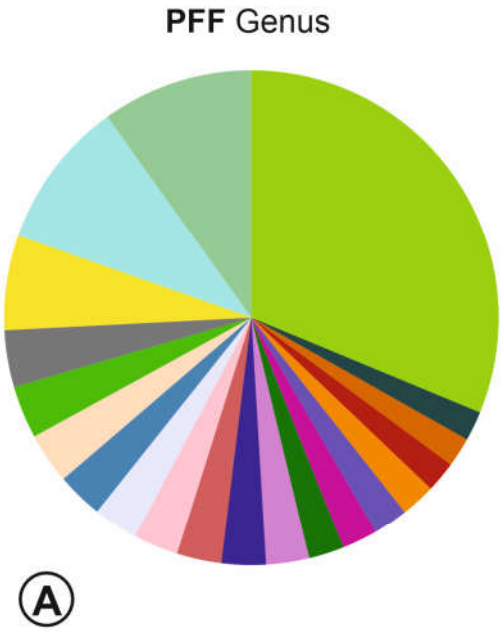

Legends	Taxonomy	Abundance
	g_Dysgonomonas	9.9%
	f_Enterobacteriaceae ;_	9.71%
	g_Serratia	6.19%
	g_Desulfovibrio	3.71%
	f_Clostridiaceae ;_	3.42%
	g_Pseudocitrobacter	3.31%
	f_Acetobacteraceae;_	3.02%
	f_Wohlfahrtiimonadaceae;_	2.93%
	g_Rs-K70_termite_group	2.93%
	g_Arsenophonus	2.92%
	g_Lactococcus	2.89%
	g_Enterococcus	2.82%
	o_Enterobacterales;_;_	2.31%
	g_Comamonas	2.31%
	g_Acinetobacter	2.27%
	g_Myroides	2.26%
	g_Pseudomonas	2.0%
	g_Enterobacter	1.93%
	g_Apibacter	1.92%
	Others	31.22%

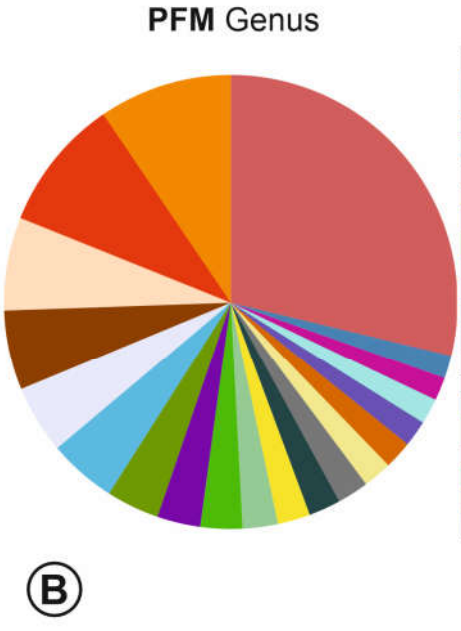

Legends	Taxonomy	Abundance
	g_ Escherichia-Shigella	9.51%
	g_Acinetobacter	9.42%
	f_Enterobacteriaceae ;_	6.62%
	g_Dysgonomonas	5.69%
	g_Arsenophonus	4.88%
	g_Pseudomonas	4.85%
	g_Apibacter	3.78%
	g_ Serratia	3.08%
	c_Gammaproteobacteria;_;_;_	2.99%
	g_Cetobacterium	2.52%
	g_ Wohlfahrtiimonas	2 .31%
	g_Burkholderia-Caballeronia-Paraburkholderia	2.27%
	g_Desulfovibrio	2.24%
	g_Sphingobacterium	2.05%
	o_Enterobacterales;_;_	2.0%
	f_Acetobacteraceae;_	1.86%
	g_ Vagococcus	1.83%
	g_uncultured	1.67%
	g_Allorhizobium-Neorhizobium-Pararhizobium-Rhizobium	1.64%
	Others	28. 77%

Figure 2.18: Pie chart of bacterial Genus in *P. flavescens*. (A) PFF, (B) PFM

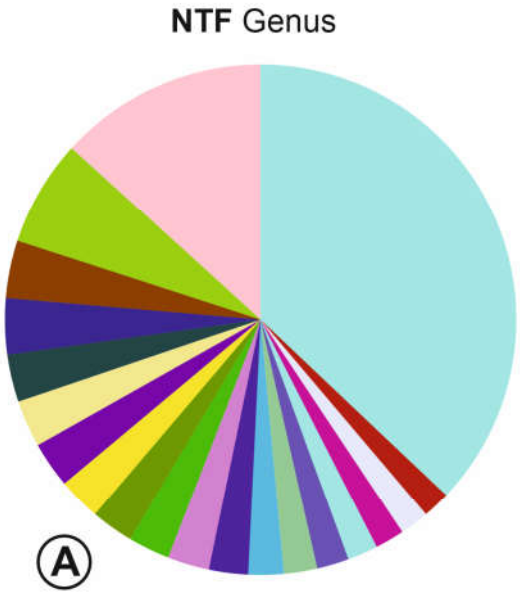

Legends	Taxonomy	Abundance
	g_Acinetobacter	13.24%
	g_Candidatus_ Soleaferrea	6.76%
	g_Arsenophonus	3.65%
	g_Serratia	3.55%
	f_Wohlfahrtiimonadaceae;_	2.99%
	f_Ruminococcaceae;_	2.97%
	g_Rickettsia	2.92%
	g_Apibacter	2.7%
	c_Gammaproteobacteria;_;_;_	2.69%
	g_Ignatzschineria	2.64%
	f_Orbaceae;_	2.64%
	g_Dysgonomonas	2.47%
	g_ZOR0006	2.23%
	g_Romboutsia	2.11%
	o_Enterobacterales;_;_	2.02%
	g_Enterobacter	1.92%
	g_uncultured	1.85%
	g_Chryseobacterium	1.84%
	g_uncultured	1.74%
	Others	37.06%

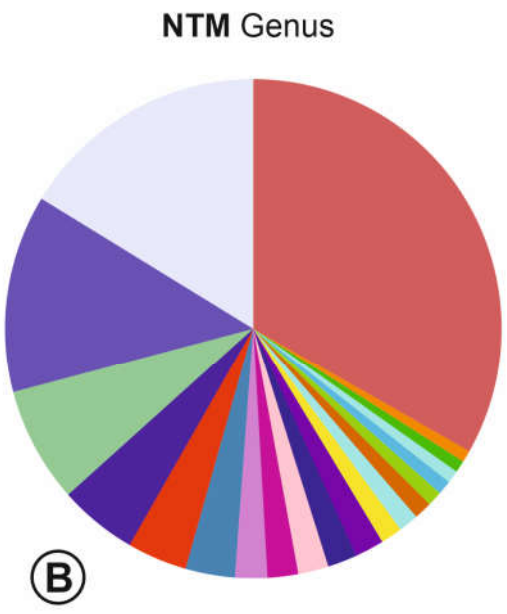

Legends	Taxonomy	Abundance
	g_Acinetobacter	16.27%
	g_Wolbachia	12.85%
	g_Enterococcus	7.49%
	f_Rhodanobacteraceae;_	5.09%
	g_Apibacter	3.9%
	g_Rickettsia	3.22%
	g_Prevotella	2.09%
	g_Lactobacillus	2.0%
	g_Chryseobacterium	1.98%
	g_Pseudomonas	1.91%
	f_Alcaligenaceae ;_	1.9%
	g_Janthinobacterium	1.4%
	f_Enterobacteriaceae ;_	1.3%
	g_Bacteroides	1.16%
	g_Streptococcus	0.97%
	f_Lachnospiraceae;_	0.91%
	g_Ralstonia	0.82%
	f_Orbaceae;_	0.78%
	g_[Ruminococcus]_torques_group	0.76%
	Others	33.2%

Figure 2.19: Pie chart of bacterial Genus in *N. tullia*. (A) NTF, (B) NTM

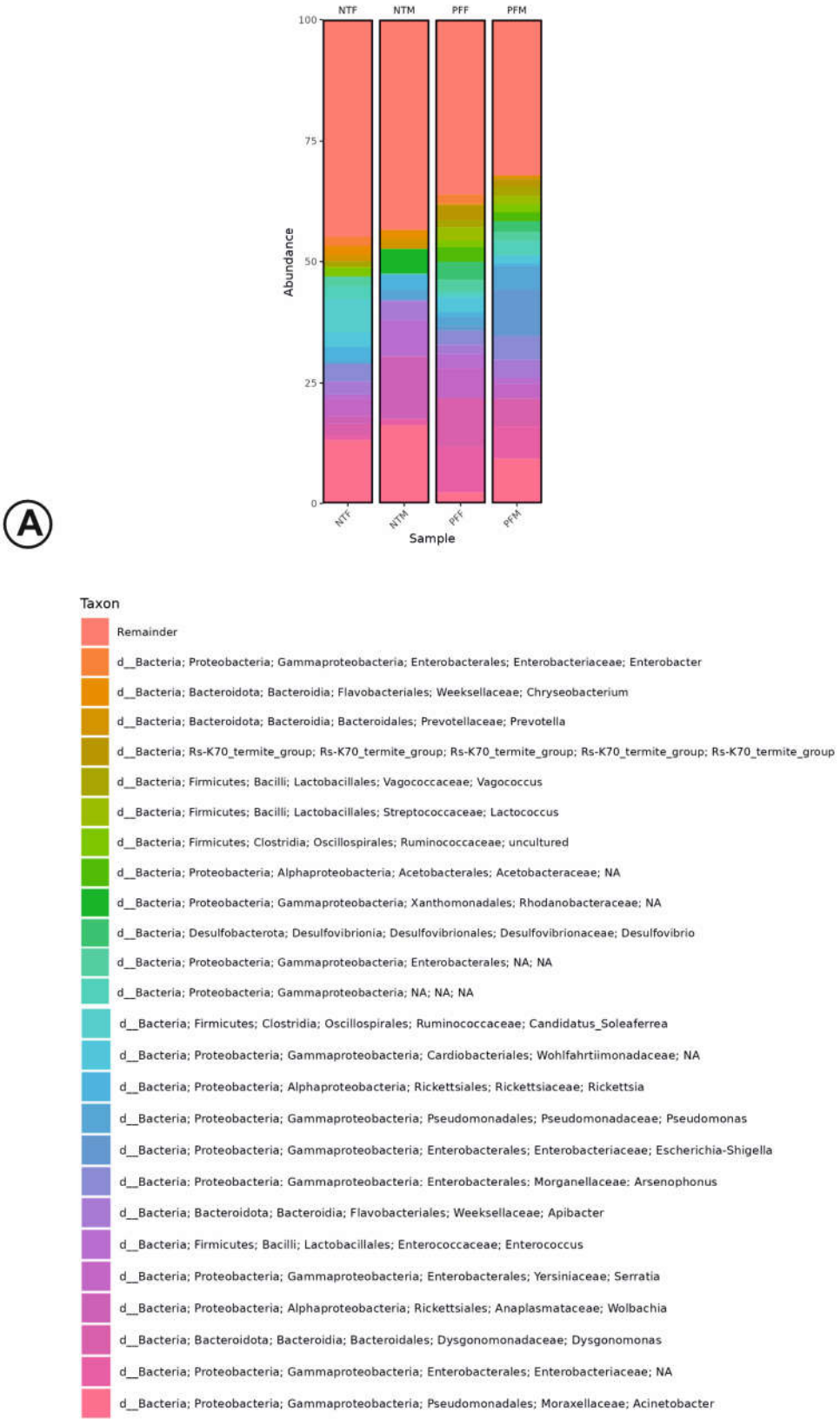

Figure 2.20: Bar plot of bacterial Genus. Comparison of bacterial gut samples NTF, NTM, PFF, and PFM

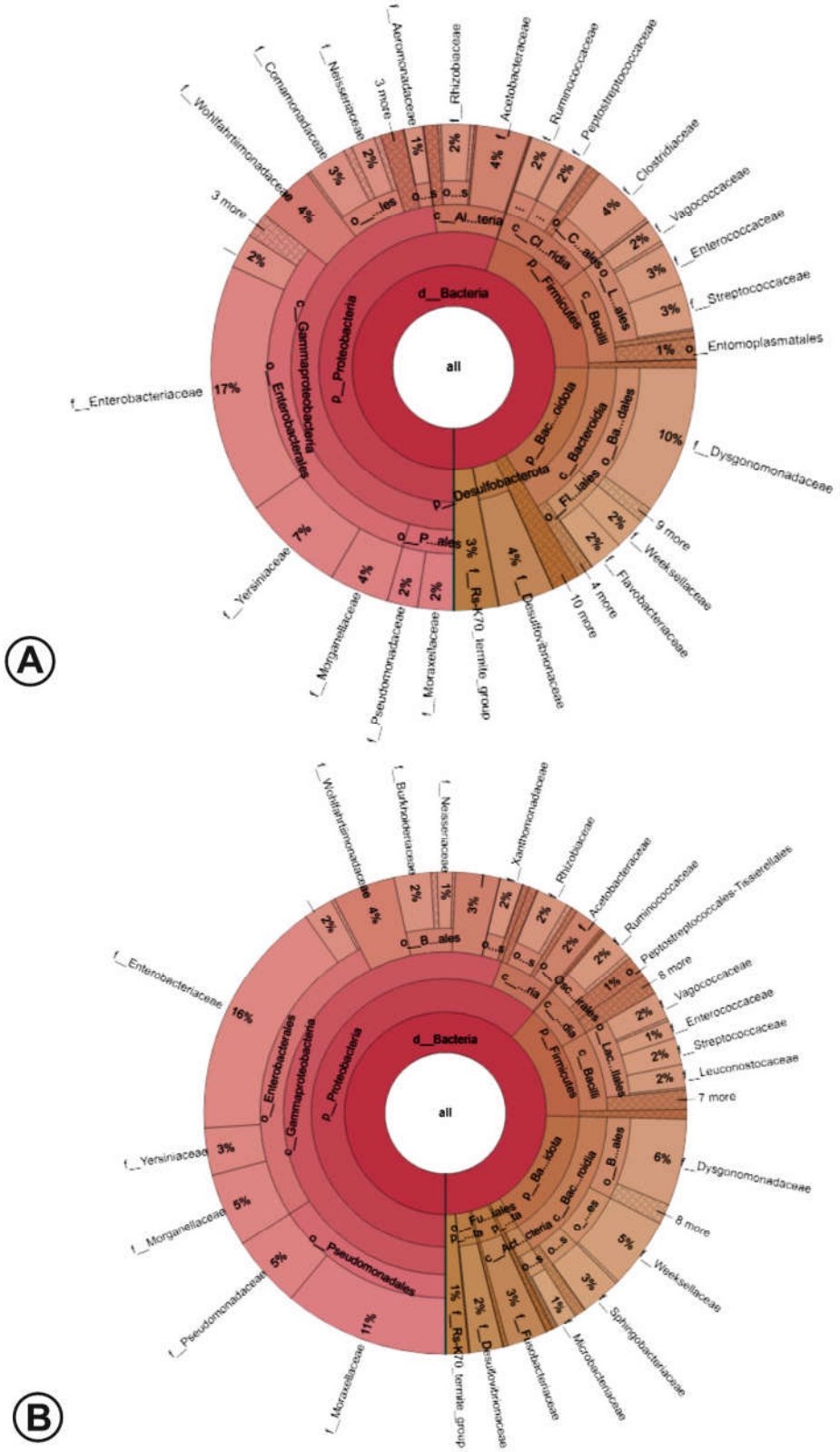

Figure 2.21: Krona chart of gut bacterial groups in *P. flavescens.* (A) PFF, (B) PFM

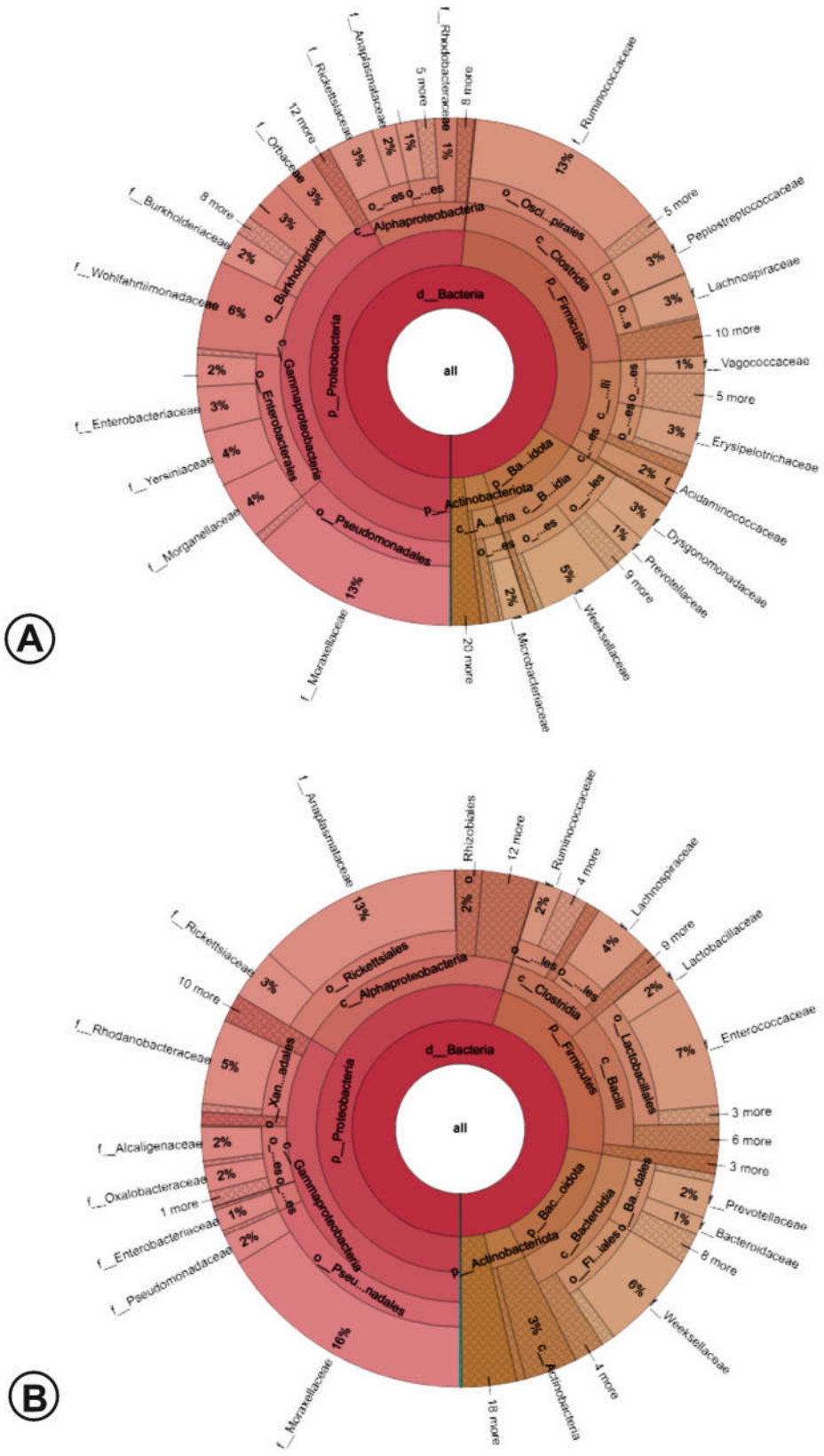

Figure 2.22: Krona chart of gut bacterial groups in *N. tullia*. (A) NTF, (B) NTM

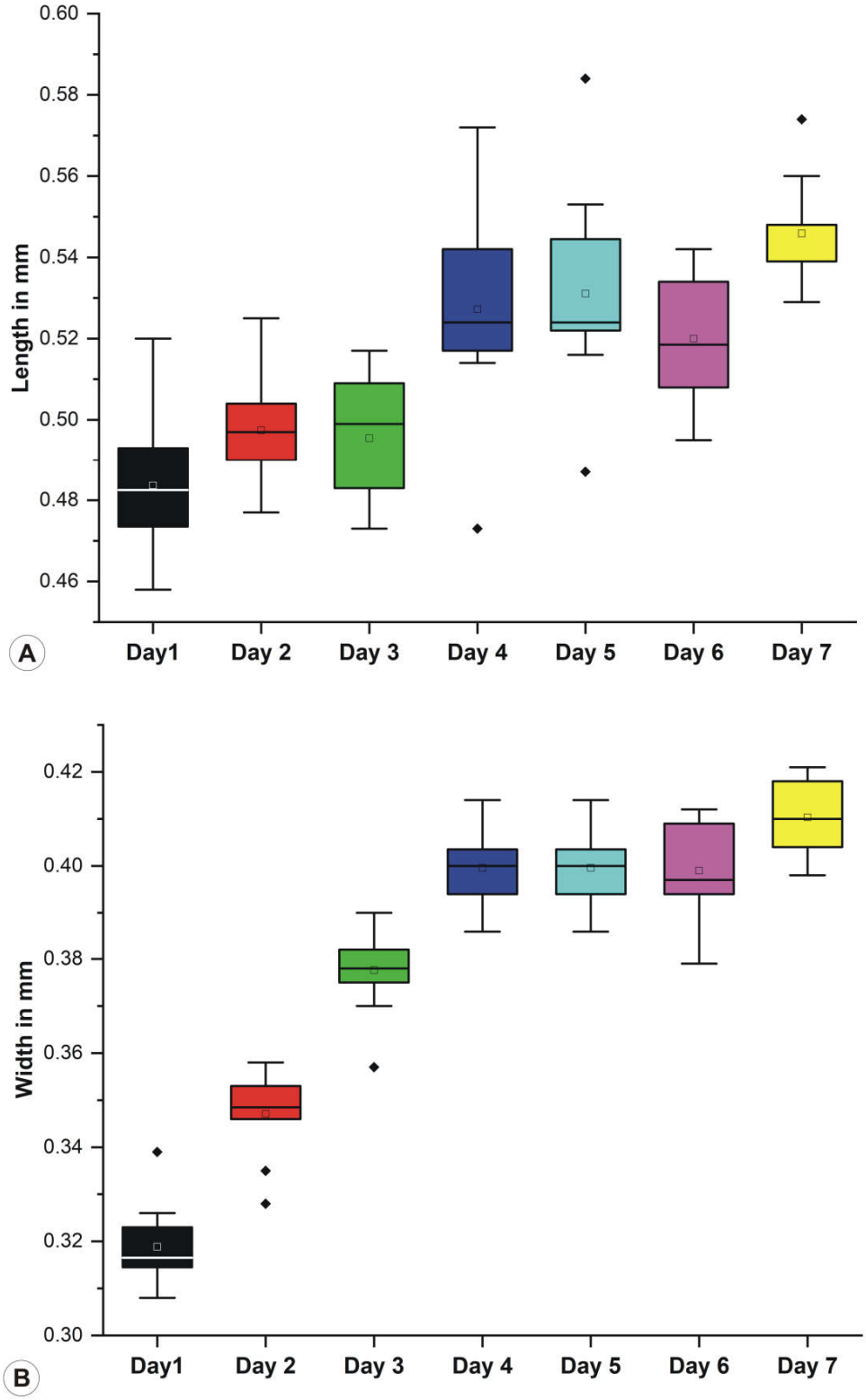

Figure 3.1: Graphical representation of size changes in *P. flavescens* egg. (A) Length of *P. flavescens* eggs, (B) width of *P. flavescens* eggs.

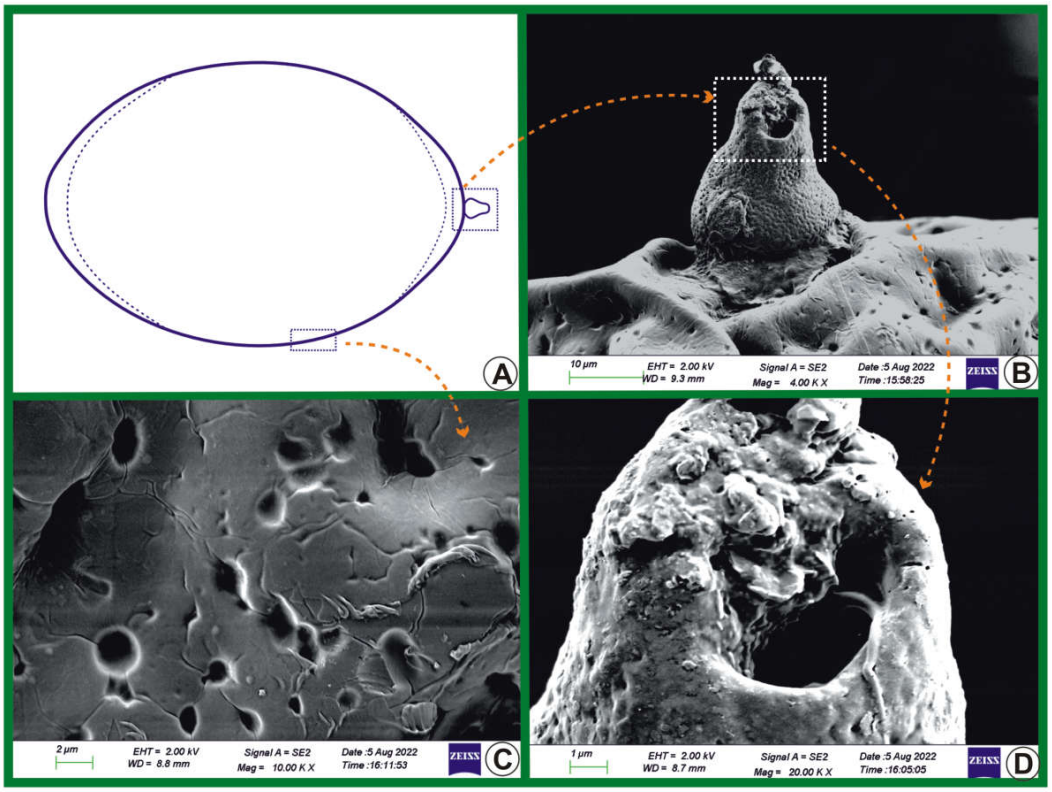

Figure 3.2: Illustration of eggs of *P. flavescens.* Scanning electron micrographs; (A) and (B) anterior end of egg showing micropyles and tiny pores, (C) egg surface showing small pores, (D) micropyle opening.

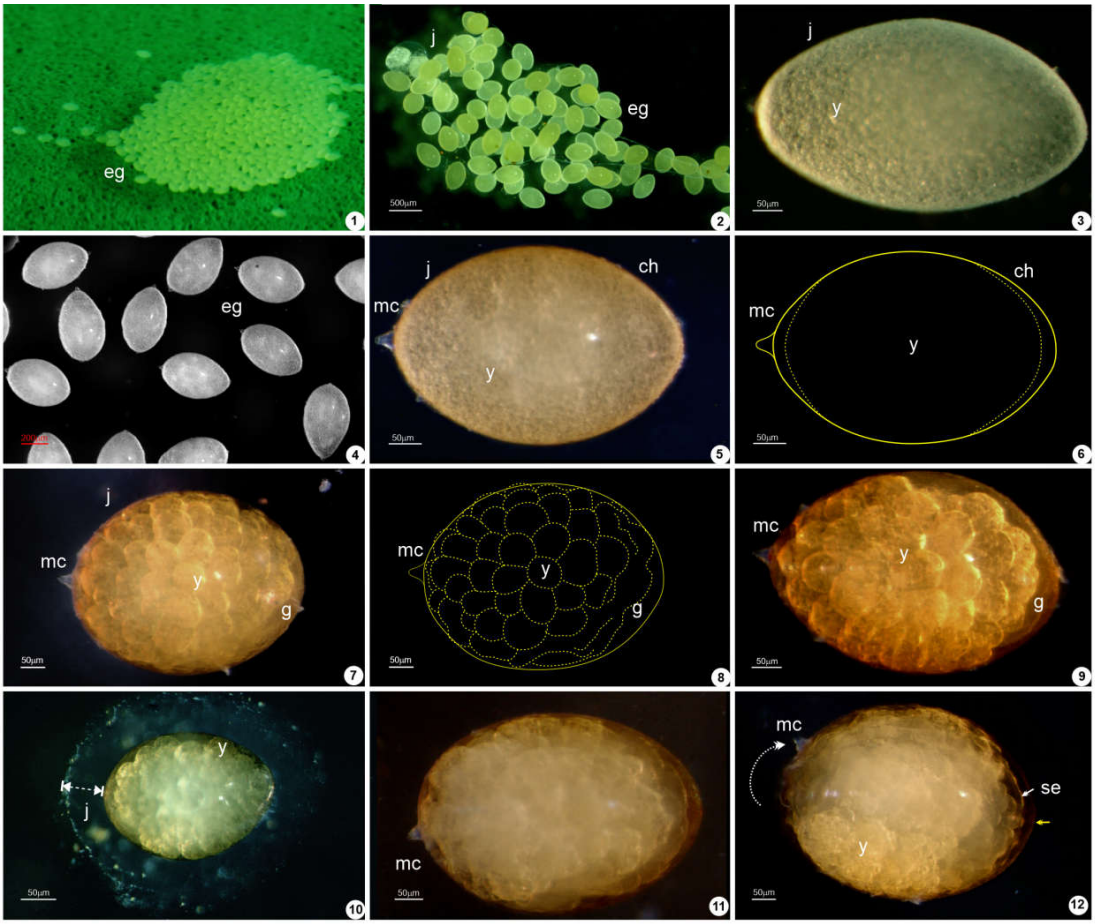

Figure 3.3: Embryonic development of *P. flavescens* 1. (1–6) stage 1; (7) stage 2, without germ band; (7–10) stage 3; (11–12) stage 4. eg: egg, j: jelly, y: yolk, mc: micropylar cone, ch: chorion, g: germ band, em: embryo, se: serosa.

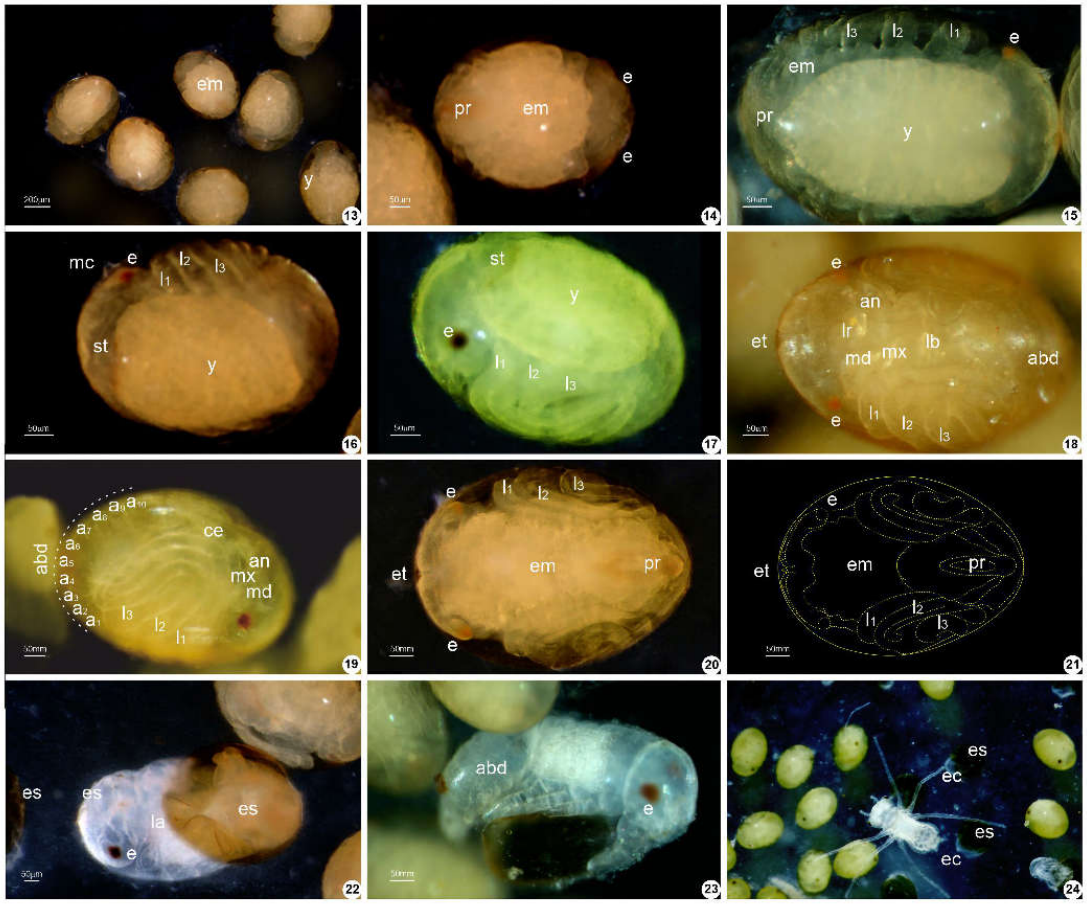

Figure 3.4: Embryonic development of *P. flavescens* 2. (13–14) stage 4; (15–17) stage 5; (18–21) stage 6; (22–23) hatching; (24) newly emerged larva. y: yolk, e: eye, pr: proctodaeum, em: embryo, l: leg, a: abdominal segment, abd: abdomen, an: antennae, ce: cercus, ec: embryonic cuticle, es: eggshell, et: egg tooth, ep: epiproct, fs: frontal spines, lb: labium, lr: labrum, la: larva, md: mandible, mx: maxillae, mc: micropylar cone, st: stomodaeum.

Figure 3.5. Different stages of the jelly coat in *P. flavescens* egg.

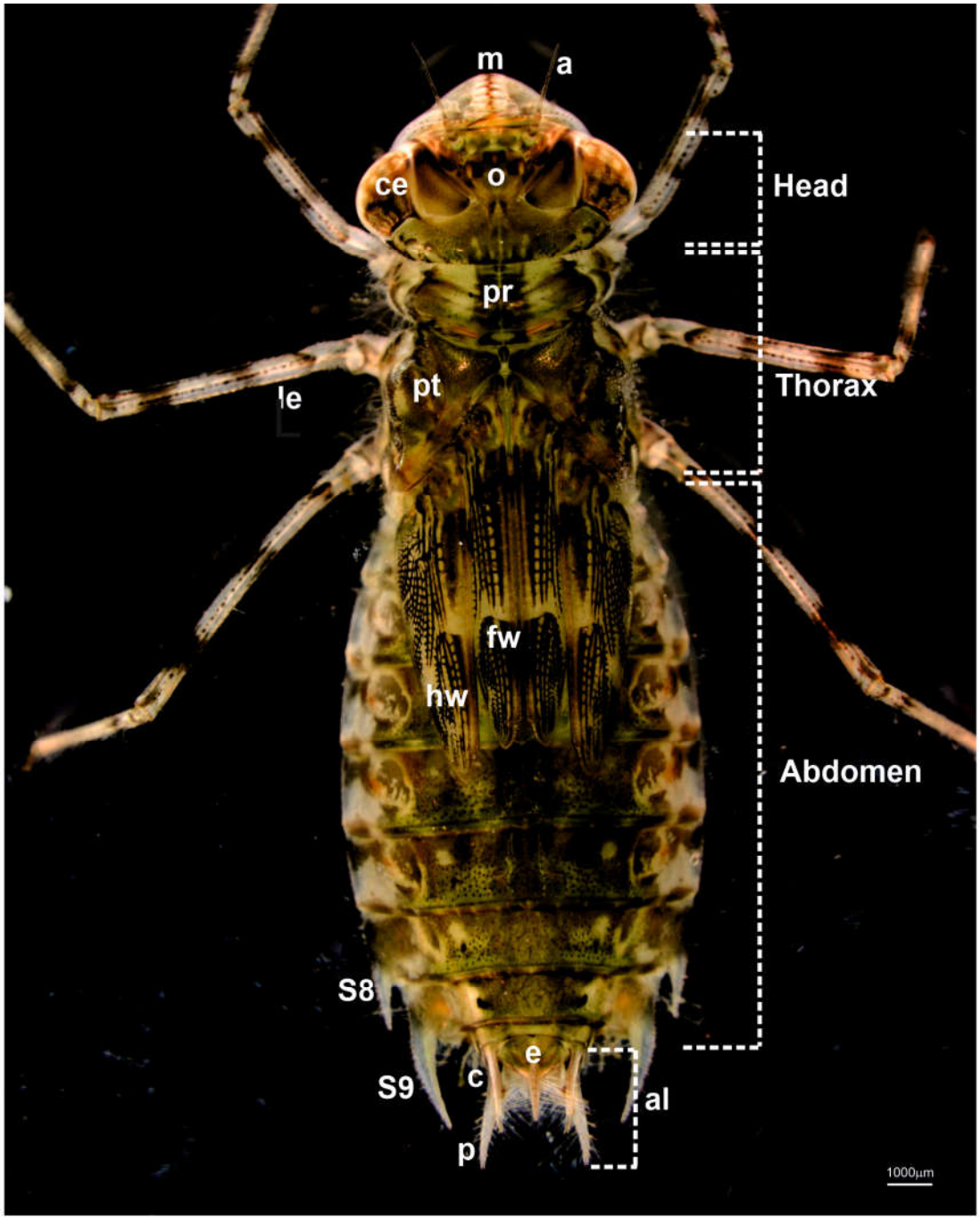

Figure 3.6: Naiad of *P. flavescens*. a: antennae, al: anal appendage, c: cerci, ce: compound eye, e: epiproct, hw: hindwing sheath, l: leg, m: mouthparts, o: ocelli, p: paraproct, pr: prothorax, pt: pterothorax, S8, S9: posterolateral spine of abdominal segments eight and nine

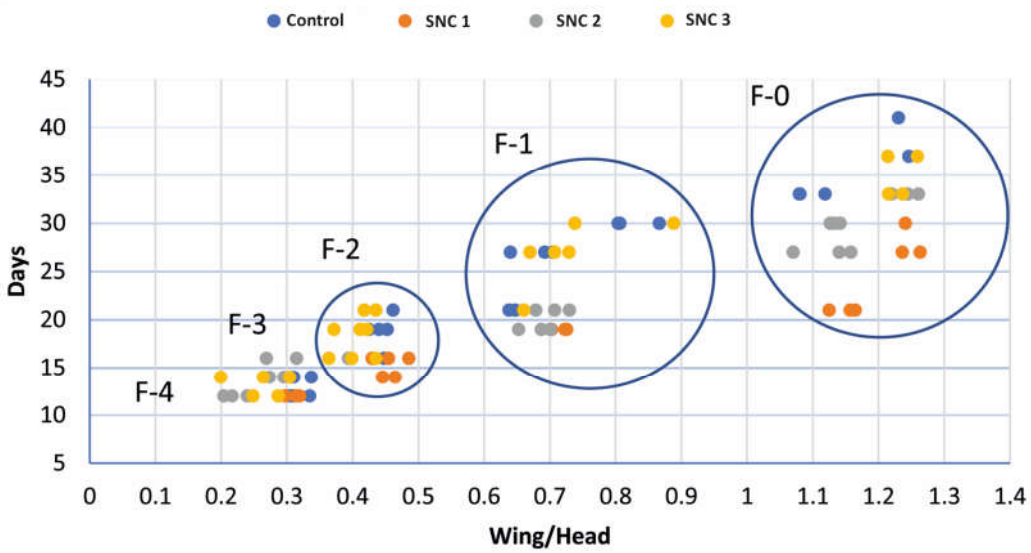

Figure 3.7: Graphical representation of different naiad instars of *P. flavescens*. Ratio of wing sheath length and head width plotted against the developmental days showing different naiad instars F-4, F-3, F-2, F-1, and F-0.

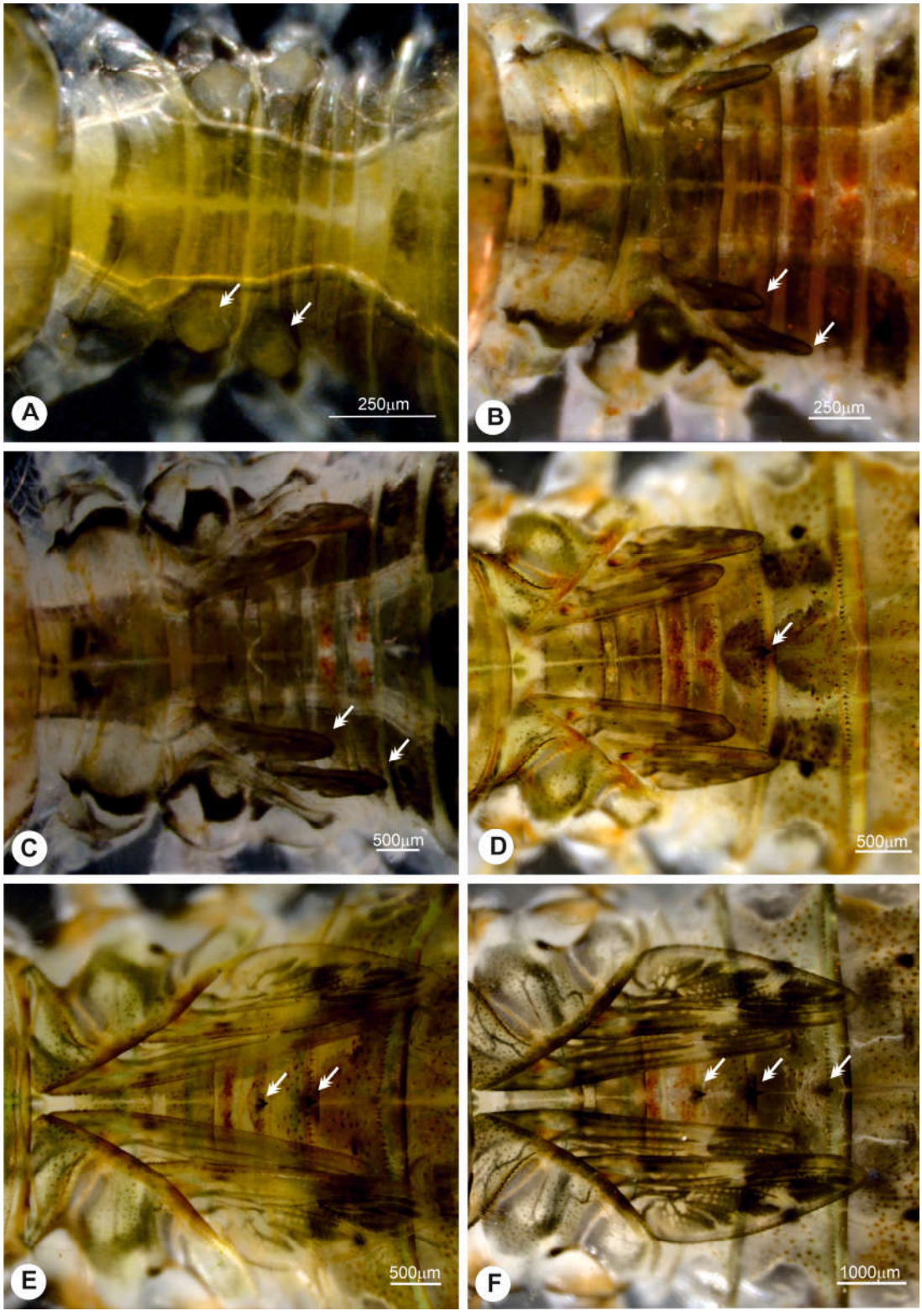

Figure 3.8: Morphological changes in the naiads. (A) wing bud, (B) wing sheath in the F-4 instar, (C) wing sheath in the F-3 instar, (D) appearance of middorsal hook on S3, (E) middorsal hooks on S2 and S3, (F) middorsal hooks on S2, S3, and S4

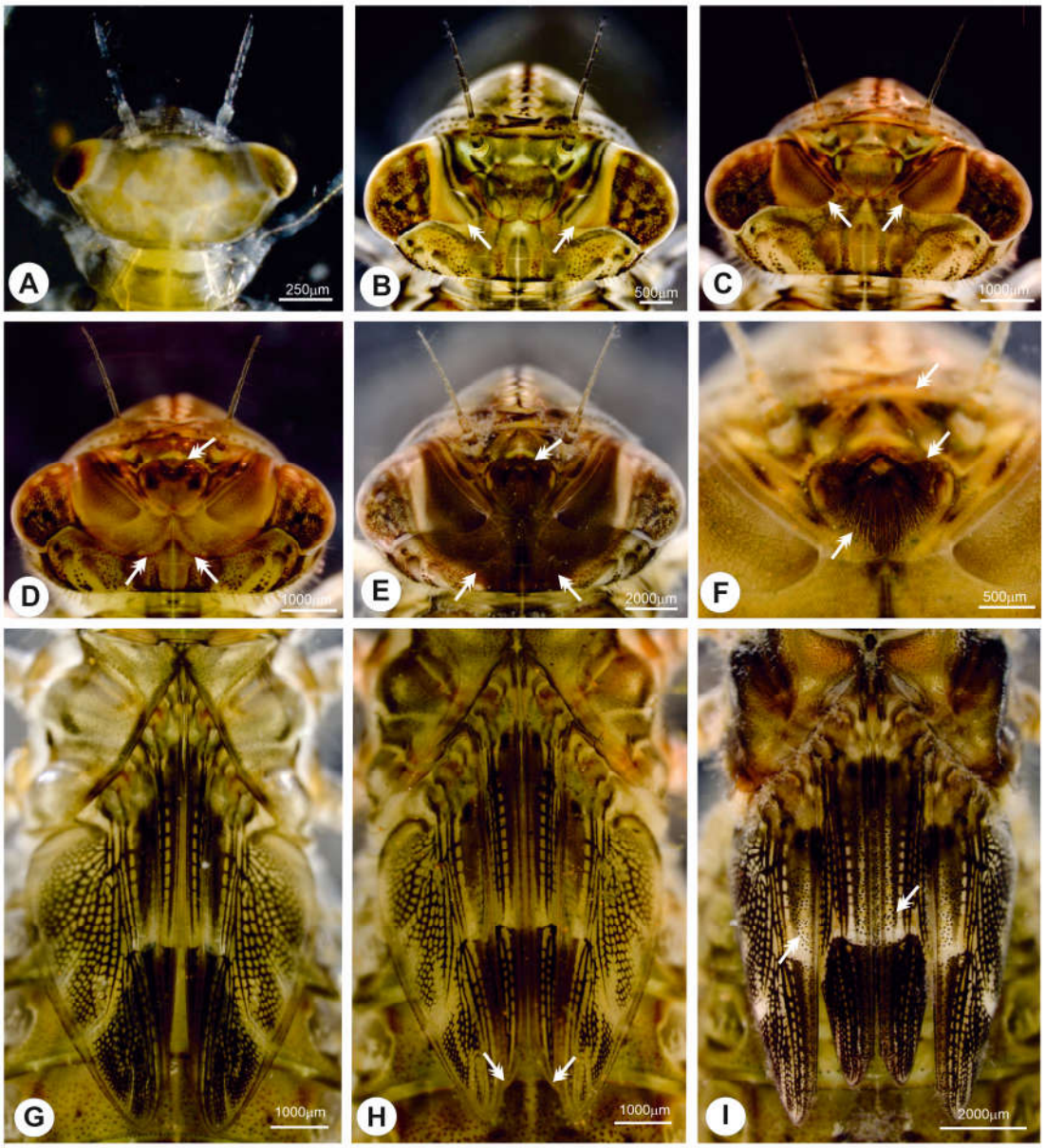

Figure 3.9: Morphological changes in the compound eye and wing sheath of final instar naiads. (A-F) morphological changes of the compound eyes in F-0 instar naiad: dorsal view of the head region showing different stages of F-0 instar. (B & C) stage 1 image shows the dorsal expansion of the compound eyes. (D) stage 2 image, the white arrowheads indicate the posterior expansion of the compound eyes. (E & F) stage 3 image, the white arrowheads indicate the hairs in the ocelli region. (G-I) developmental stages of the wing sheath in F-0 instar naiad, dorsal view of wing sheath of different stages of final instar larvae. (G) stage 1, (H) stage 2 image, white arrowheads indicate the wing tips, (I) stage 3 image in which the white arrowheads indicate the black dots on the wing sheaths

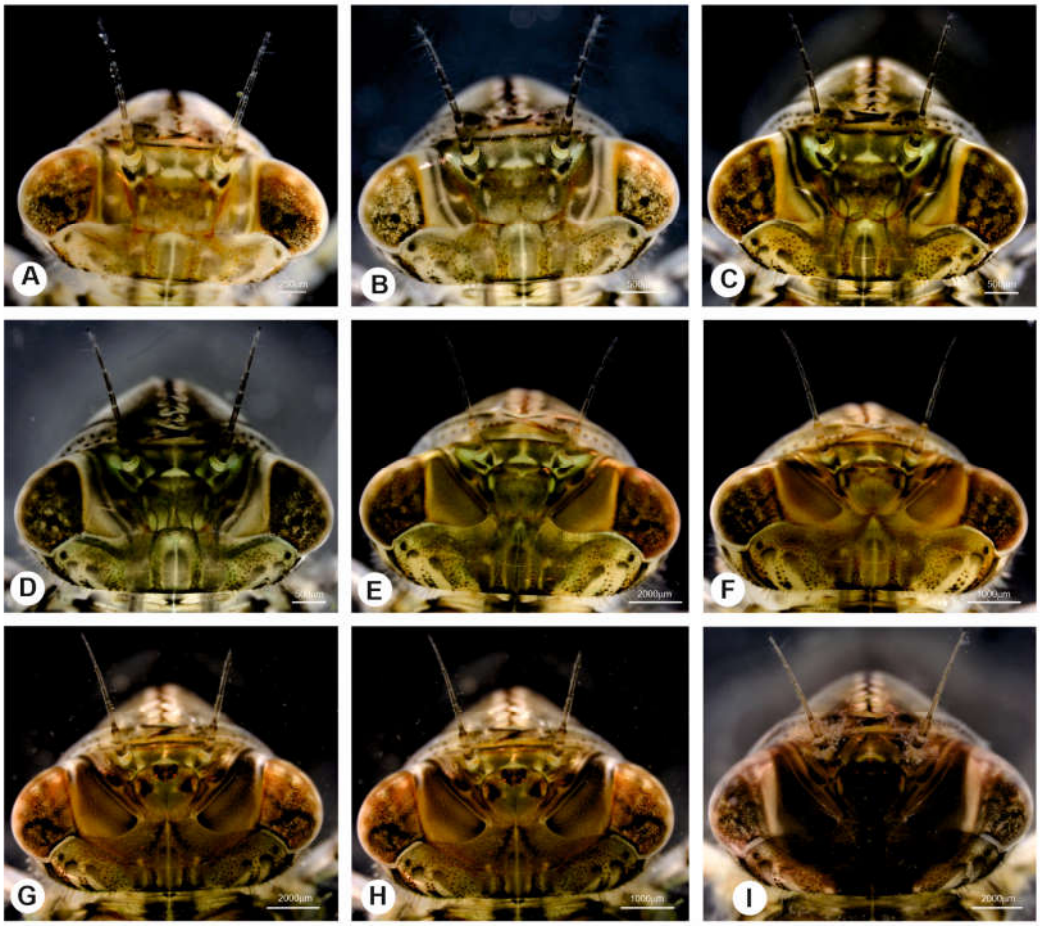

Figure 3.10: Major developmental changes in the head of *P. flavescens* naiads

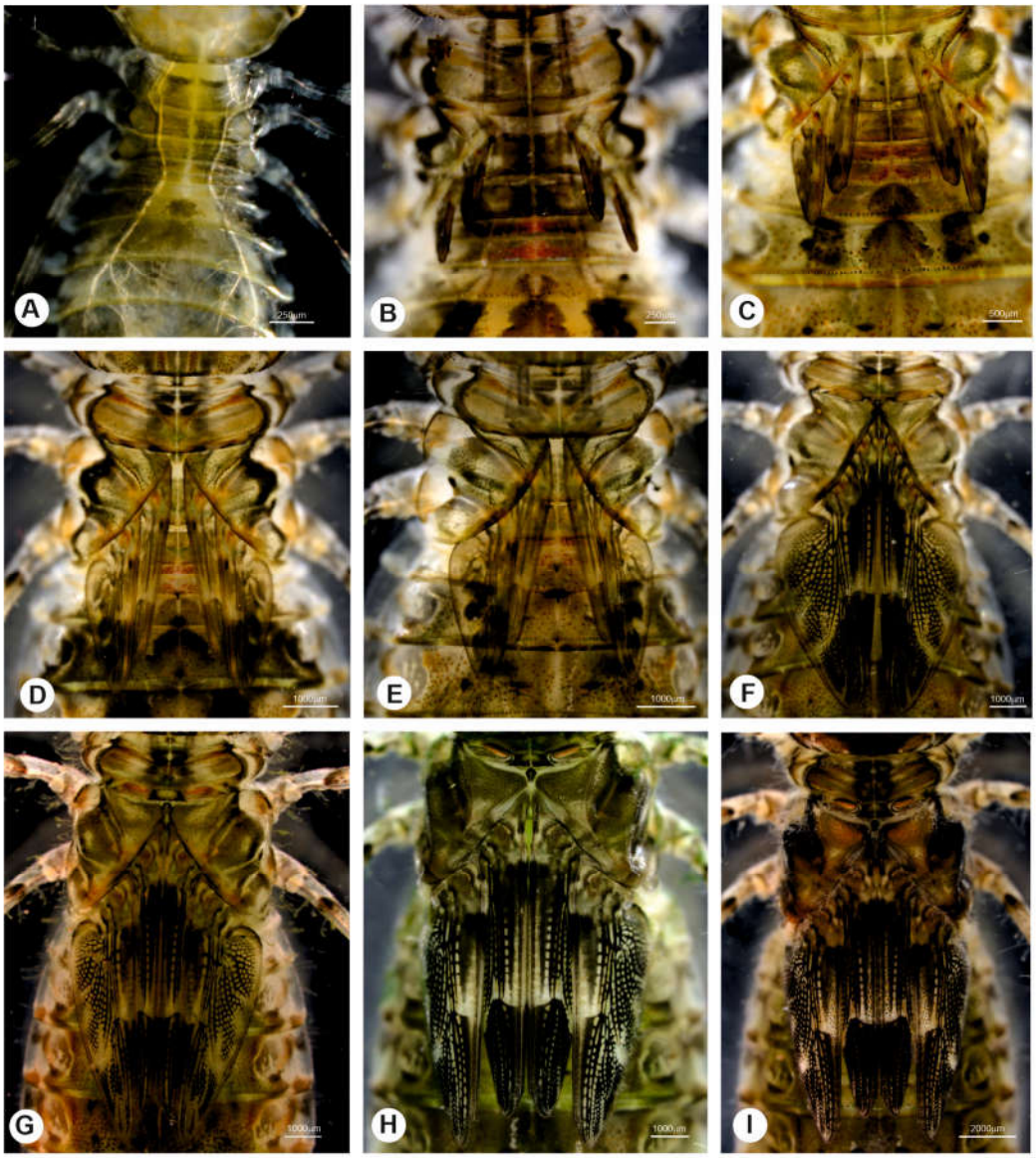

Figure 3.11: Major developmental changes in the thorax of *P. flavescens* naiads

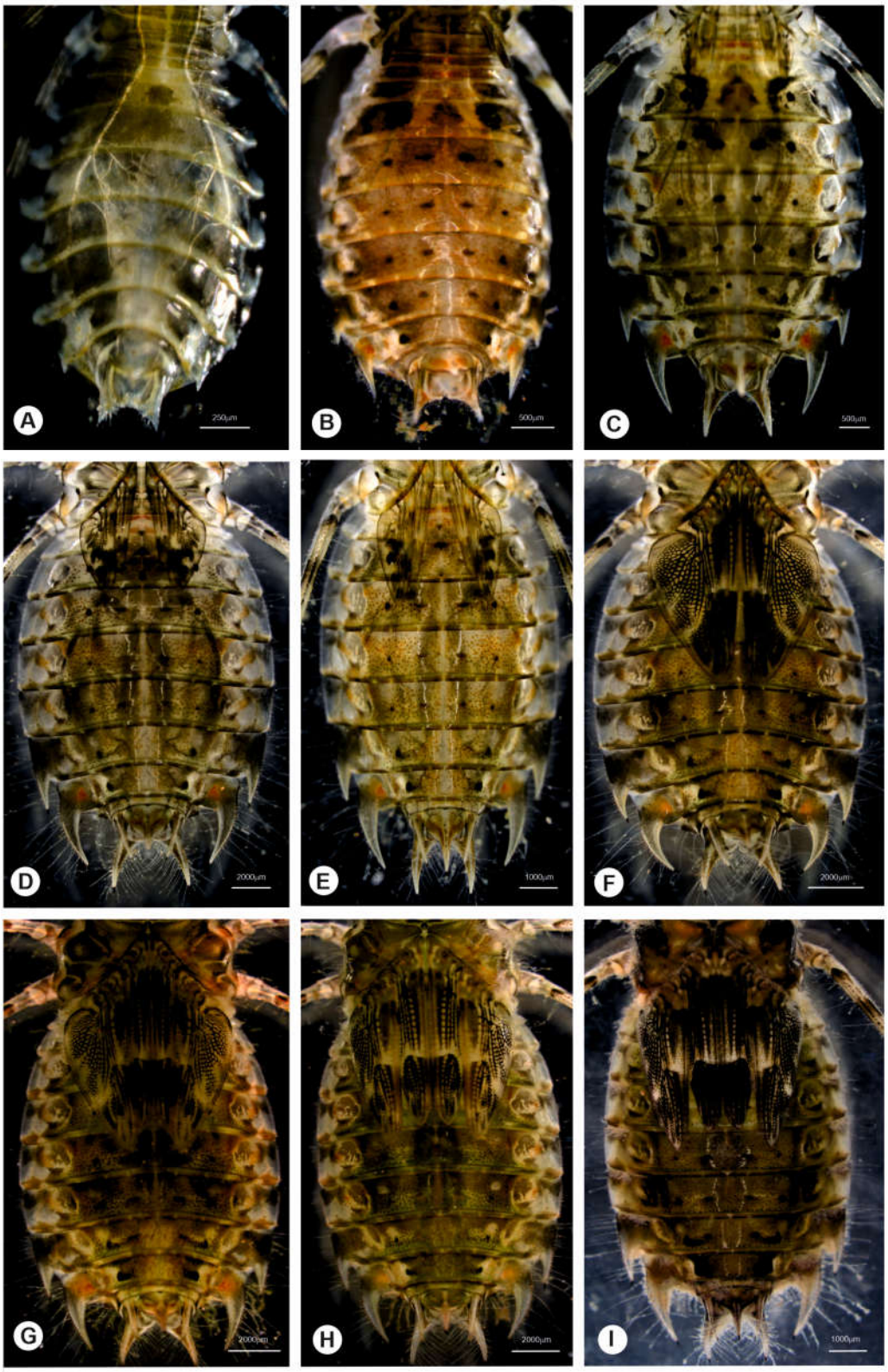

Figure 3.12: Major developmental changes in the abdomen of *P. flavescens* naiads

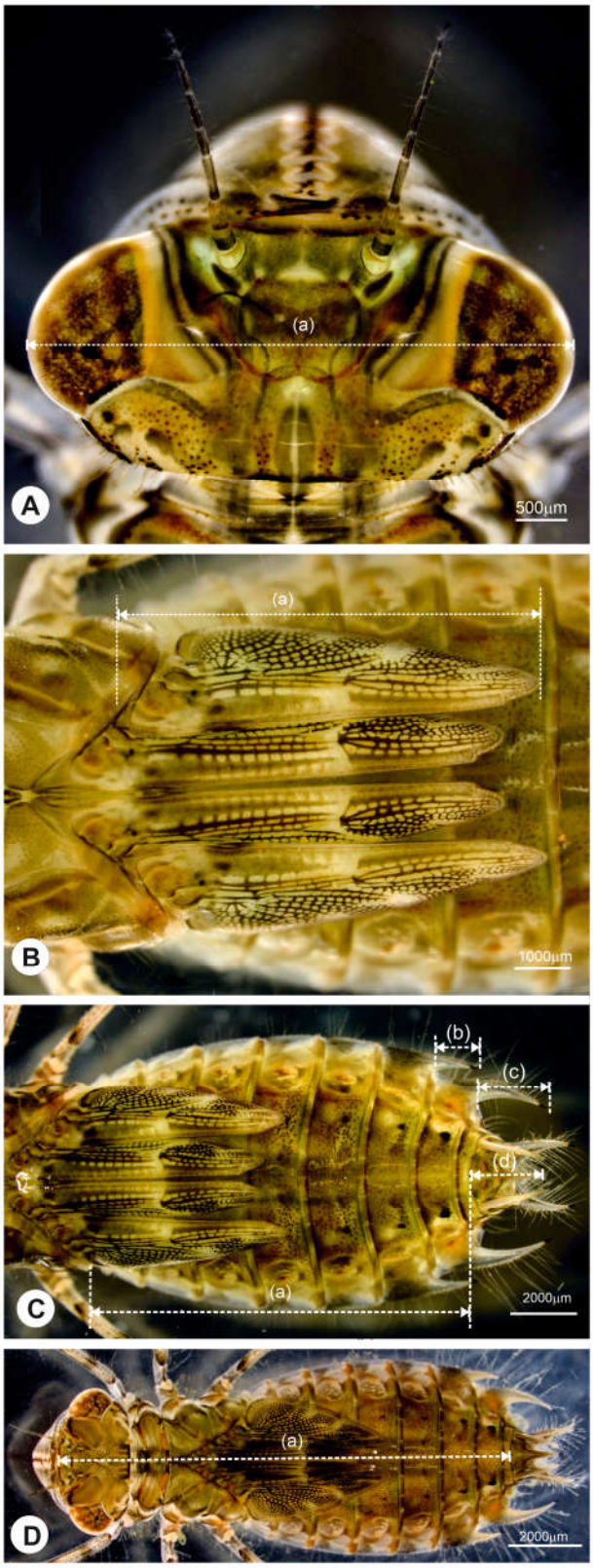

Figure 3.13: Different trait measurements of *P. flavescens* naiads. (A) Head width, (B) wing sheath length, (C) a: length of the abdomen, b: S8 spine length, c: S9 spine length, d: epiproct length, (D) total length

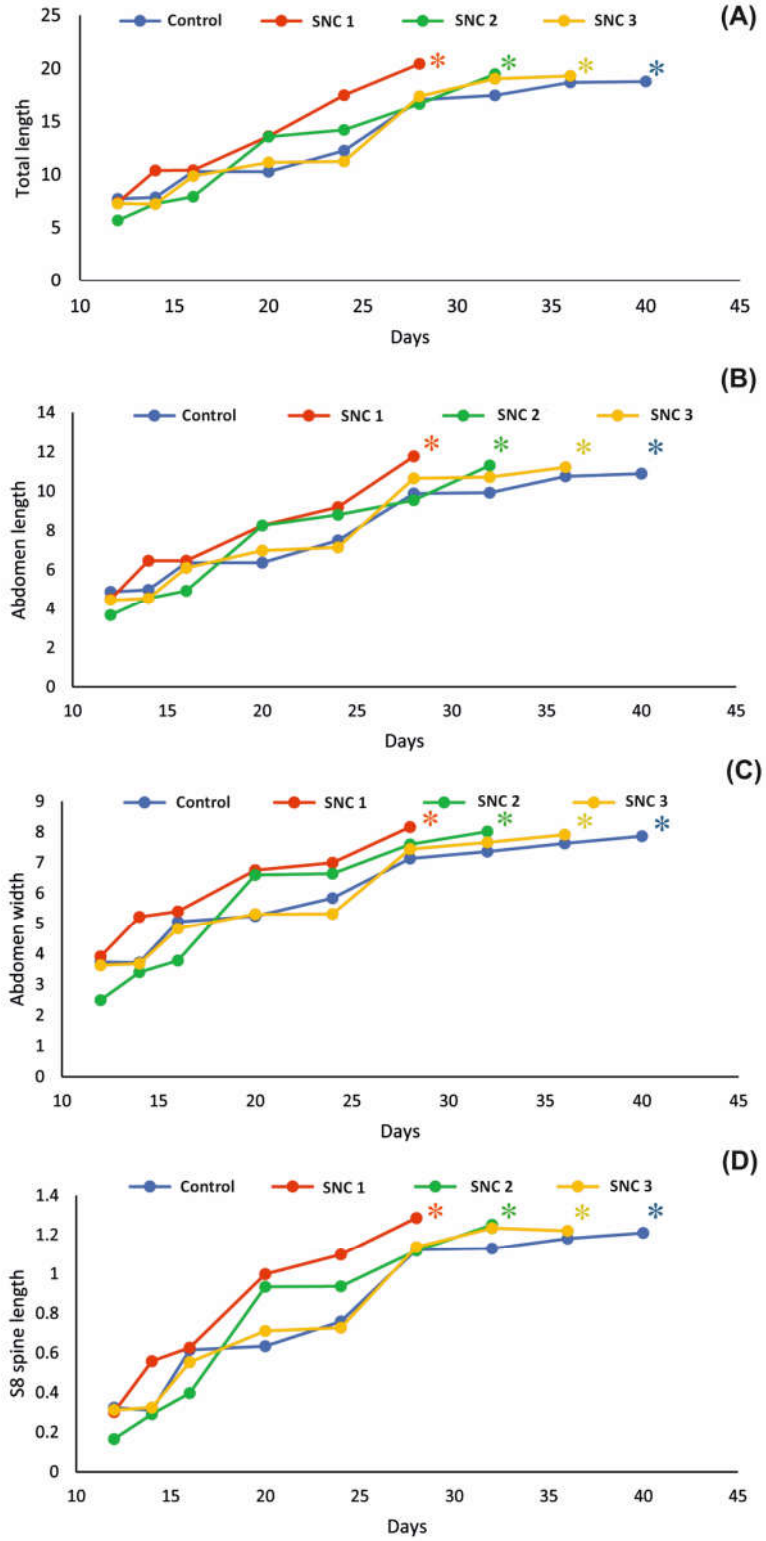

Figure 3.14: Graphical representation of different traits of naiads 1a. (A) total length of the larvae, (B) length of the abdomen, (C) abdomen width, (D) lateral spine length of eight abdominal segments (S8).

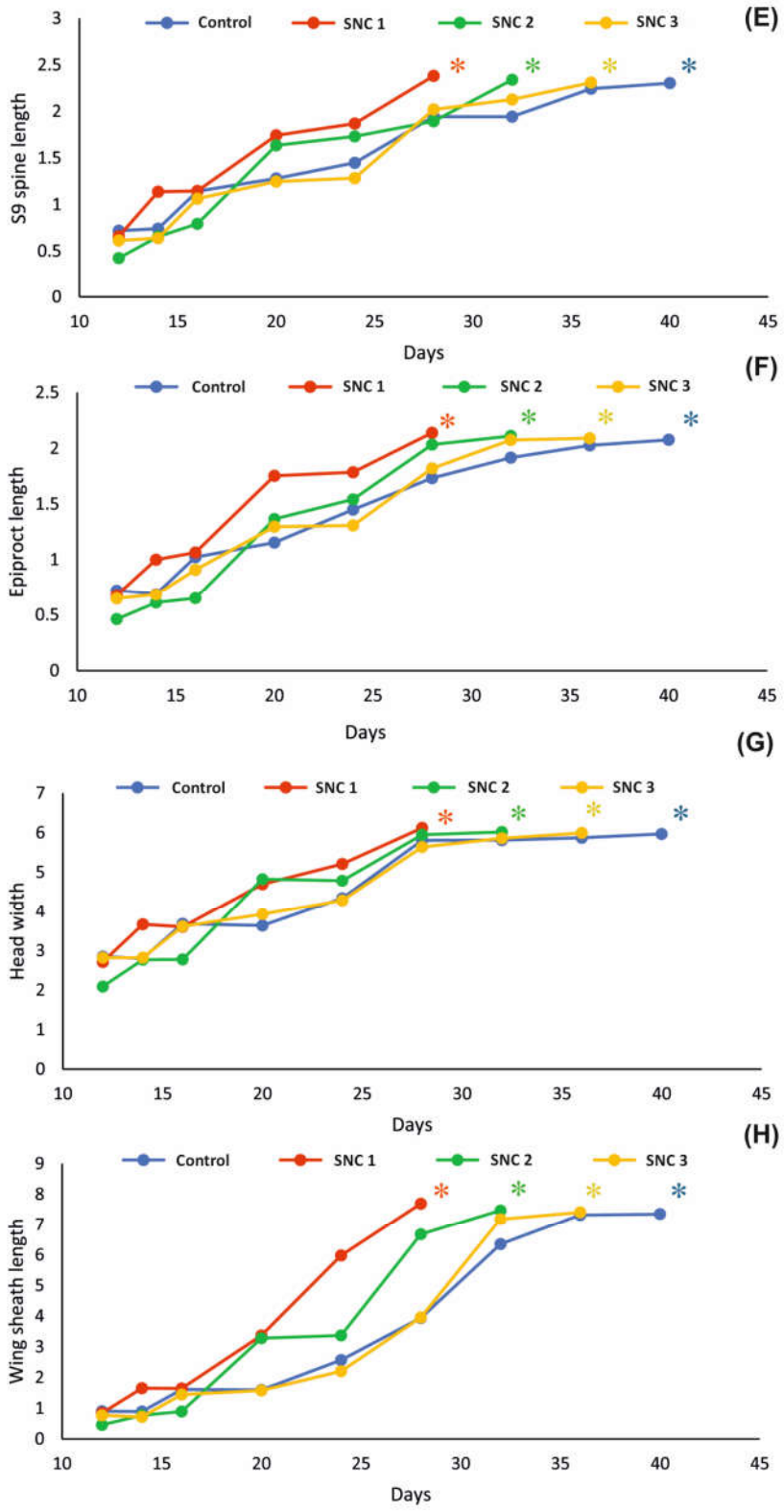

Figure 3.15: Graphical representation of different traits of naiads 1b. (E) Lateral spine length of ninth abdominal segment (S9), (F) epiproct length, (G) head width, (H) length of the wing sheath.

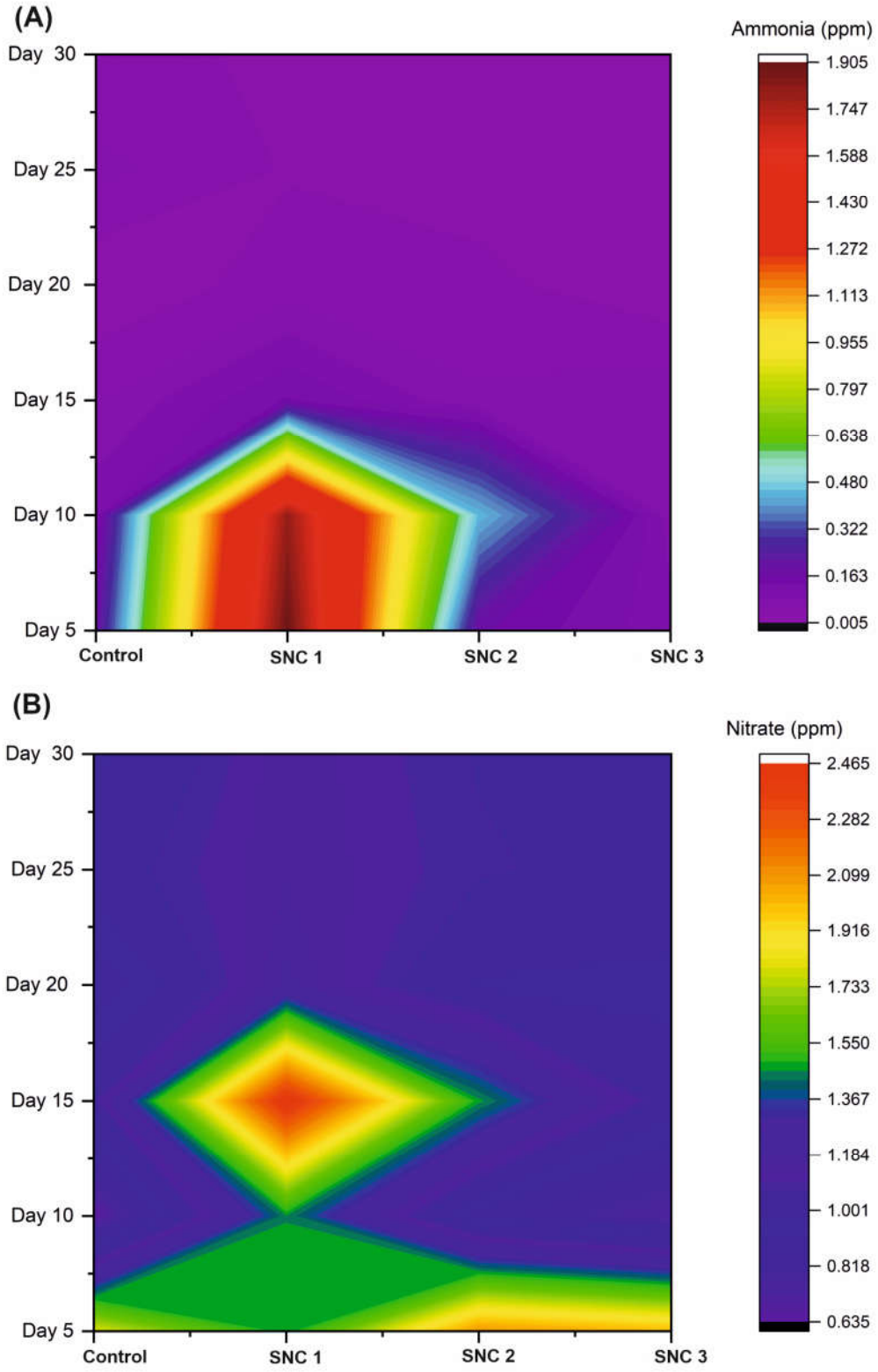

Figure 3.16: Graphical representation of ammonia and nitrate content. (A) ammonia in the water, (B) nitrate in the water

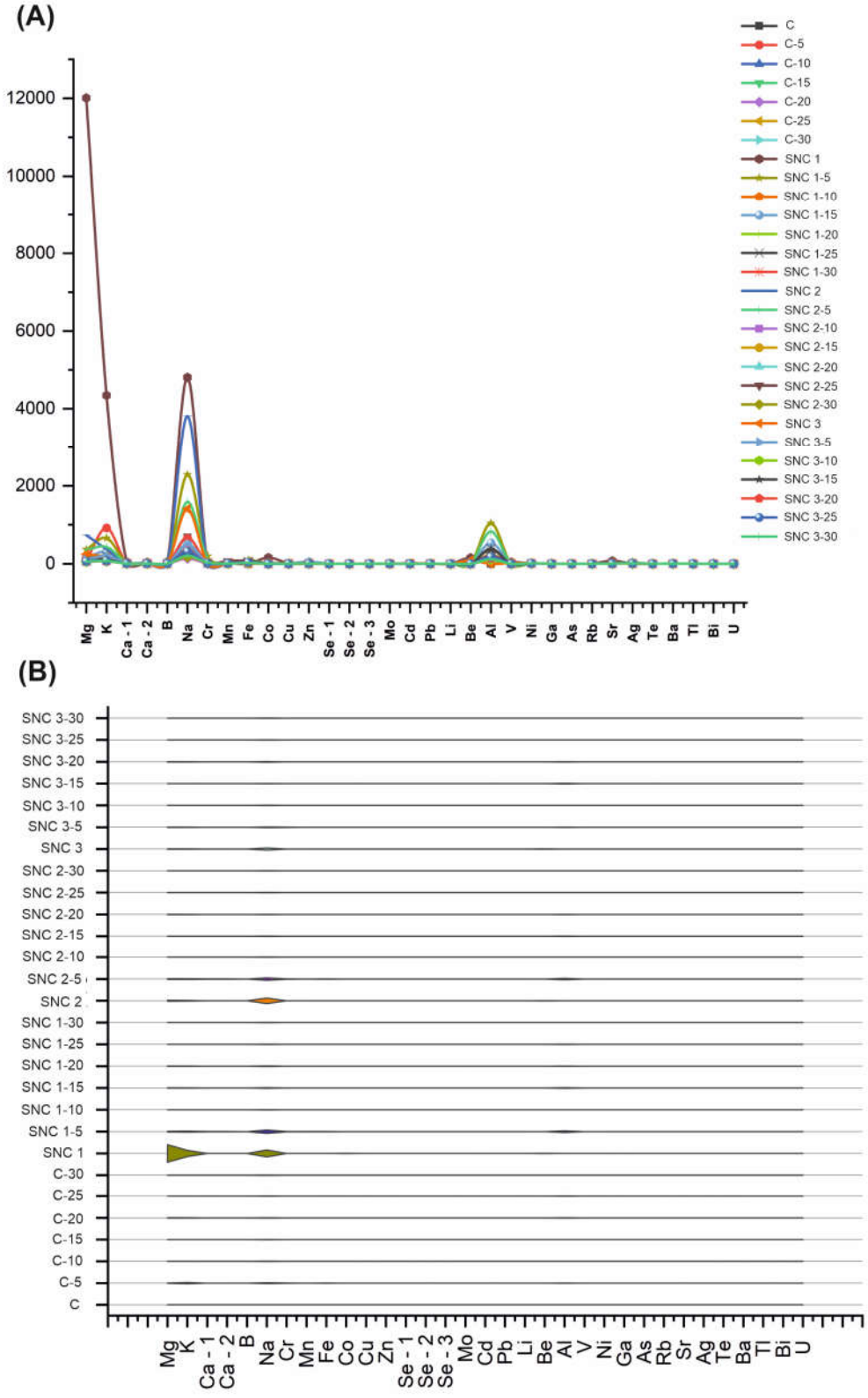

Figure 3.17: ICPMS analysis of the experimental groups

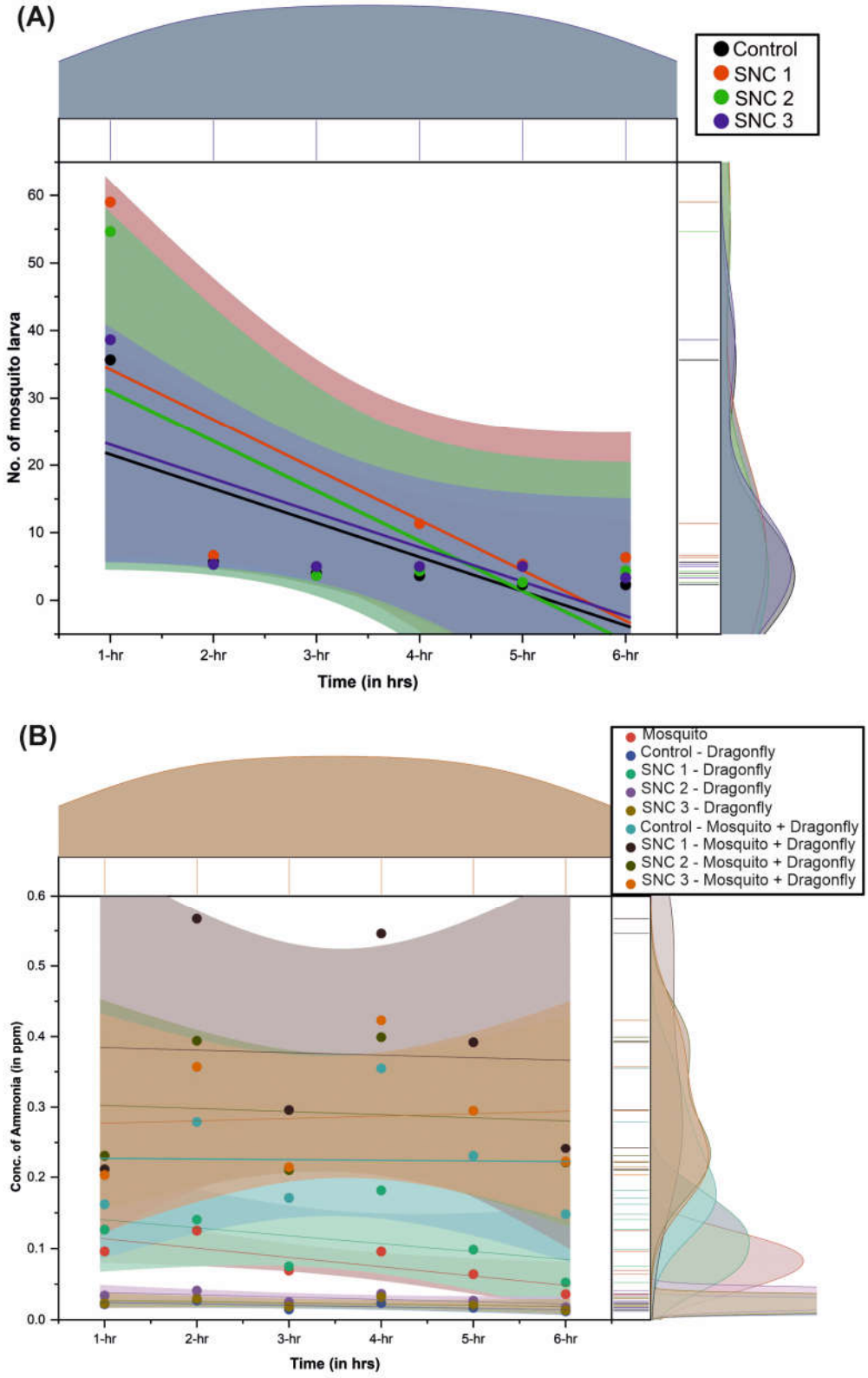

Figure 3.18: Predatory potential and ammonia excretion of different experimental groups. (A) predatory potential, (B) ammonia excretion.

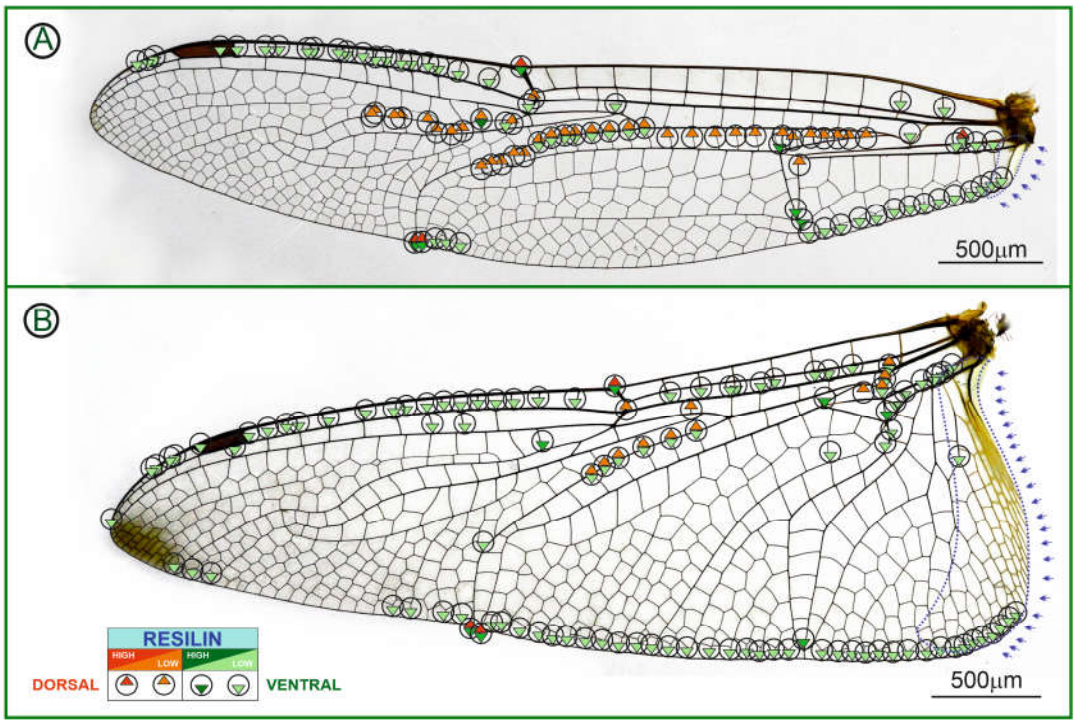

Figure 4.2: Resilin in the vein joints of the forewing and hindwing

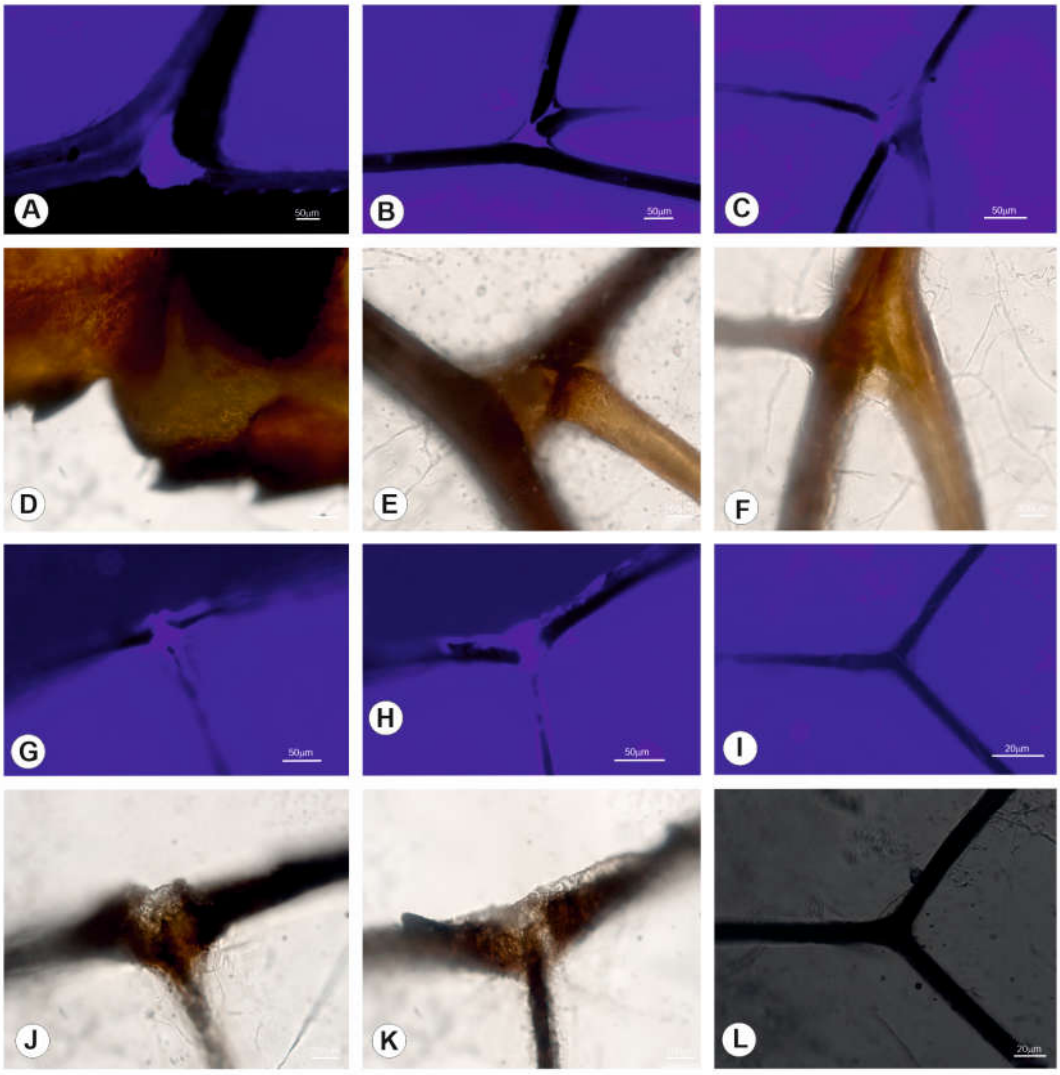

Figure 4.3: Forewing vein joints of *P. flavescens*. (A-H, J, K) mobile vein joints, (I, L) Immobile vein joints

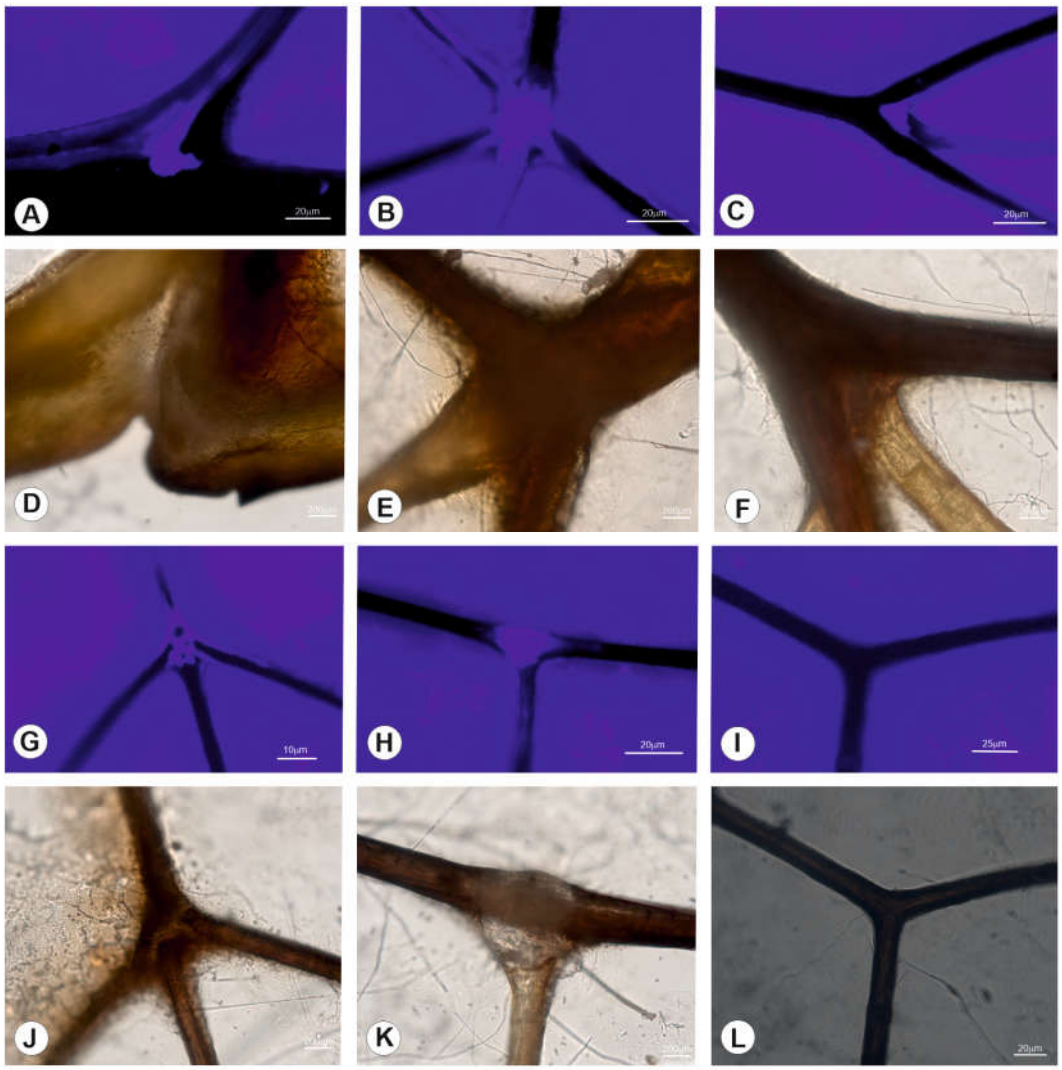

Figure 4.4: Hindwing vein joints of *P. flavescens*. (A-H, J, K) mobile vein joints, (I, L) Immobile vein joints

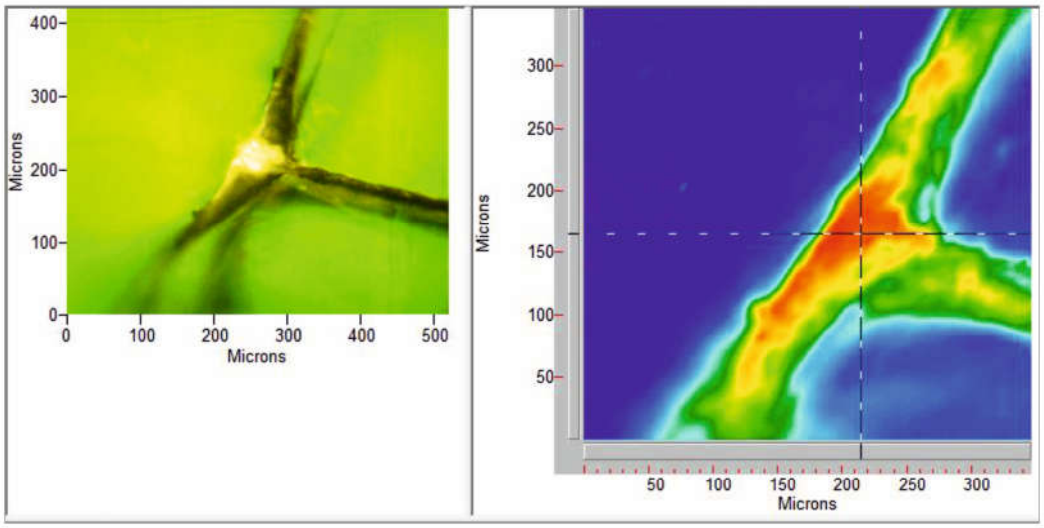

A

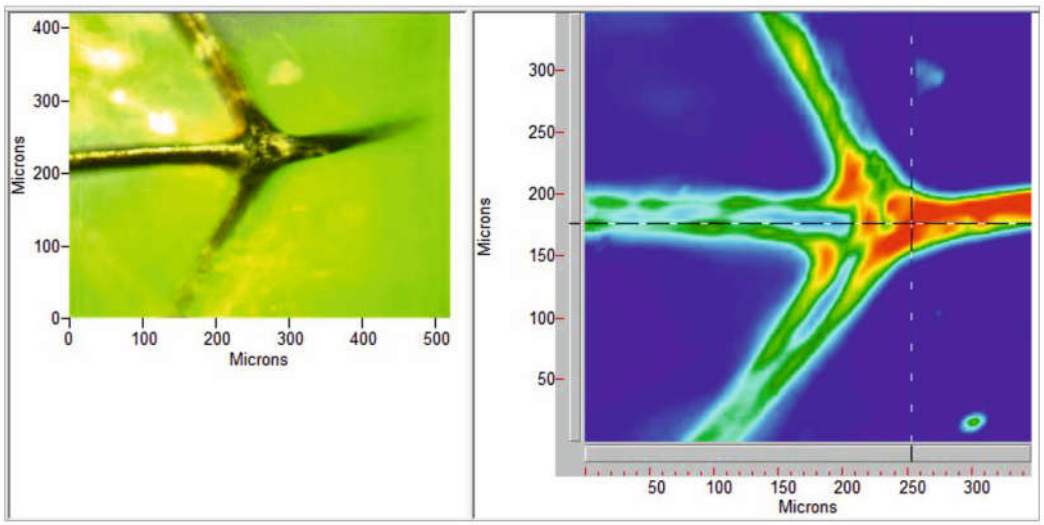

B

Figure 4.5: FTIR image of wing vein joints of *P. flavescens*. (A) forewing FTIR imaging, (B) hindwing FTIR imaging

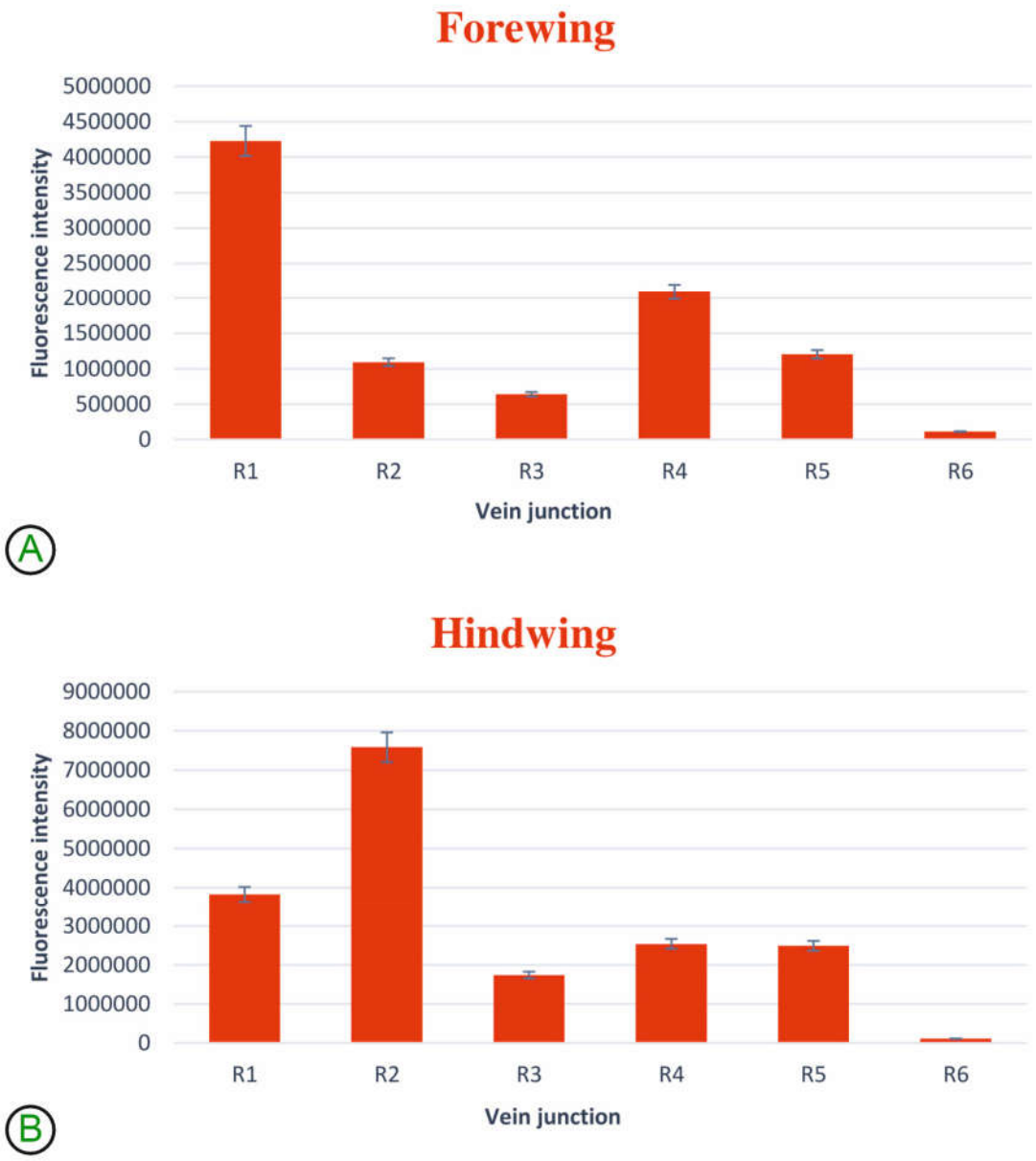

Figure 4.6: Fluorescence intensity plot. (A) Fluorescence intensity of forewing, (B) Fluorescence intensity of hindwing

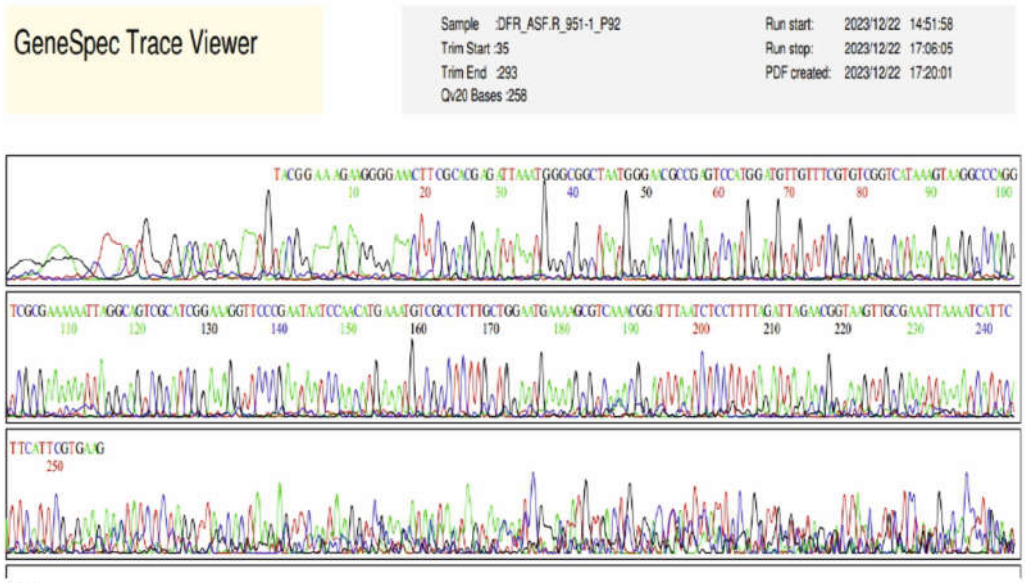

A

5'AGAAGGGGAAACTTCGCACGAGATTAAATGGGCGGCTAATGGGAACGCCGAGTCC
ATGGATGTTGTTTCGTGTGGTCATAAAGTAAGGCCCAGGTCGCGAAAAAATTAGGCA
GTCGCATCGGAAAGGTTCCCGAATAATCCAACATGAAATGTCGCCTCTTGCTGGAATG
AAAAGCGTCAAACGGATTTAATCTCCTTTTAGATTAGAACGGTAAGTTGCGAAATAAA
ATCATTCATTCATTCGTGAAGAA **3'**

B

C

Figure 4.7: Resilin protein sequence of *P. flavescens*. (A) electropherogram, (B) resilin DNA sequence, (C) Chromatogram

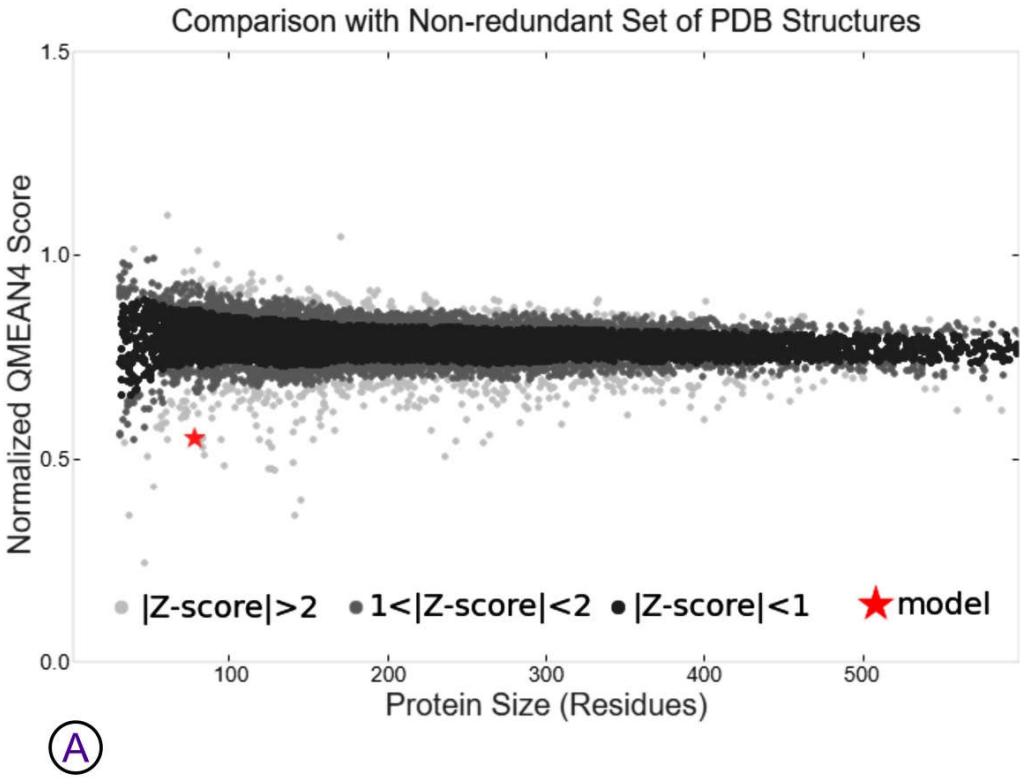

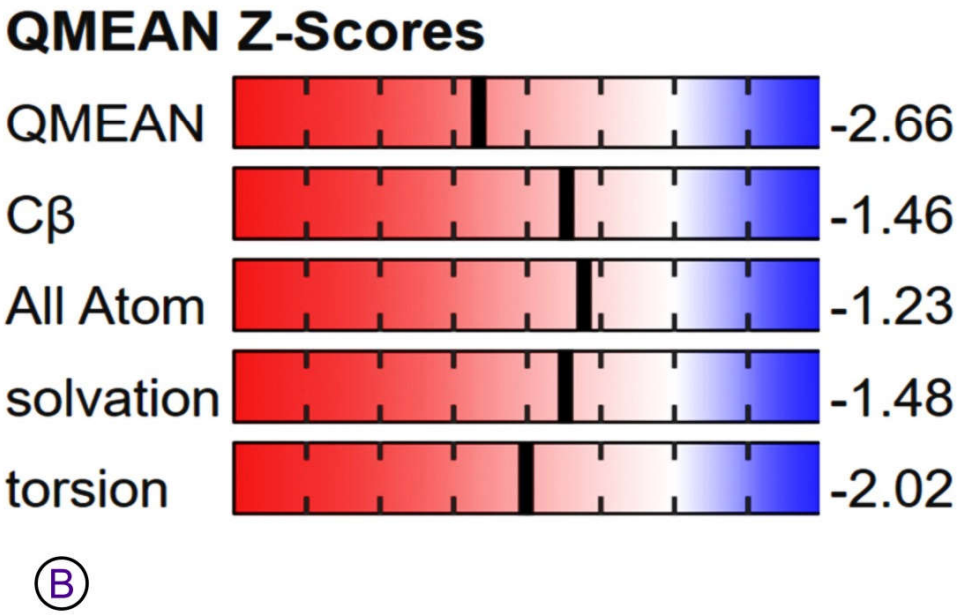

Figure 4.11: Structural validation of resilin protein model. (A) QMEAN score of structure of resilin protein model, (B) Graphical representation of the Z-Score

Figure 4.12: 3D structure of Resilin protein of *P. flavescens*

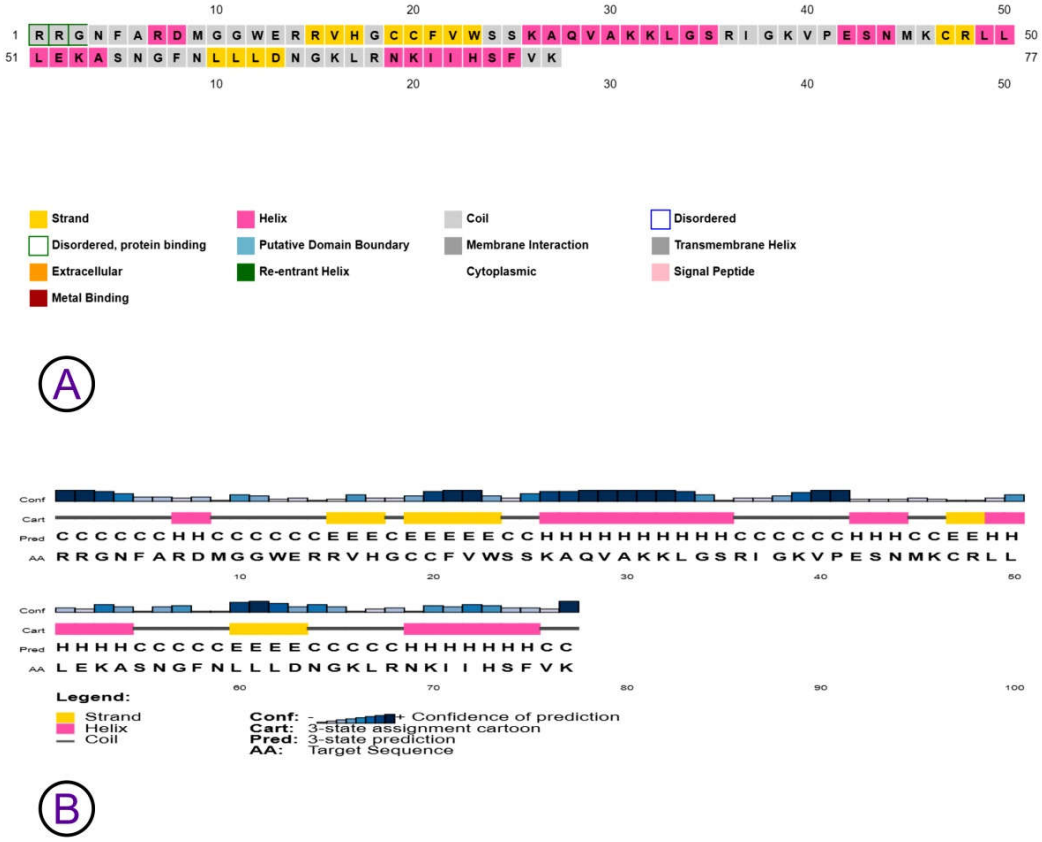

Figure 4.13: Amino acid sequence of the secondary structure of resilin protein. The yellow colour represents the strand, the pink colour represents the helix, and the grey colour represents the coil.

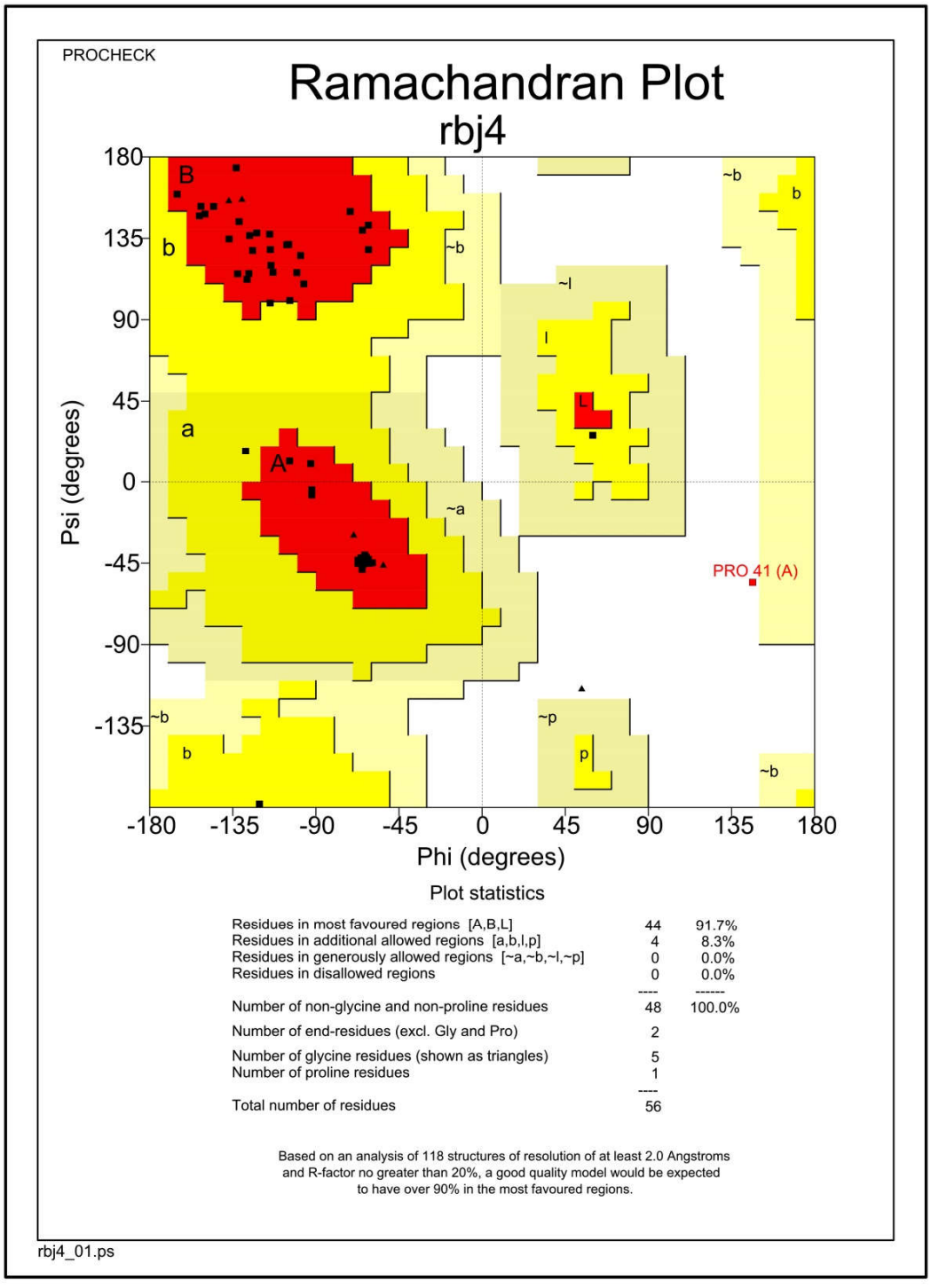

Figure 4.14: Ramachandran Plot analysis of Resilin protein

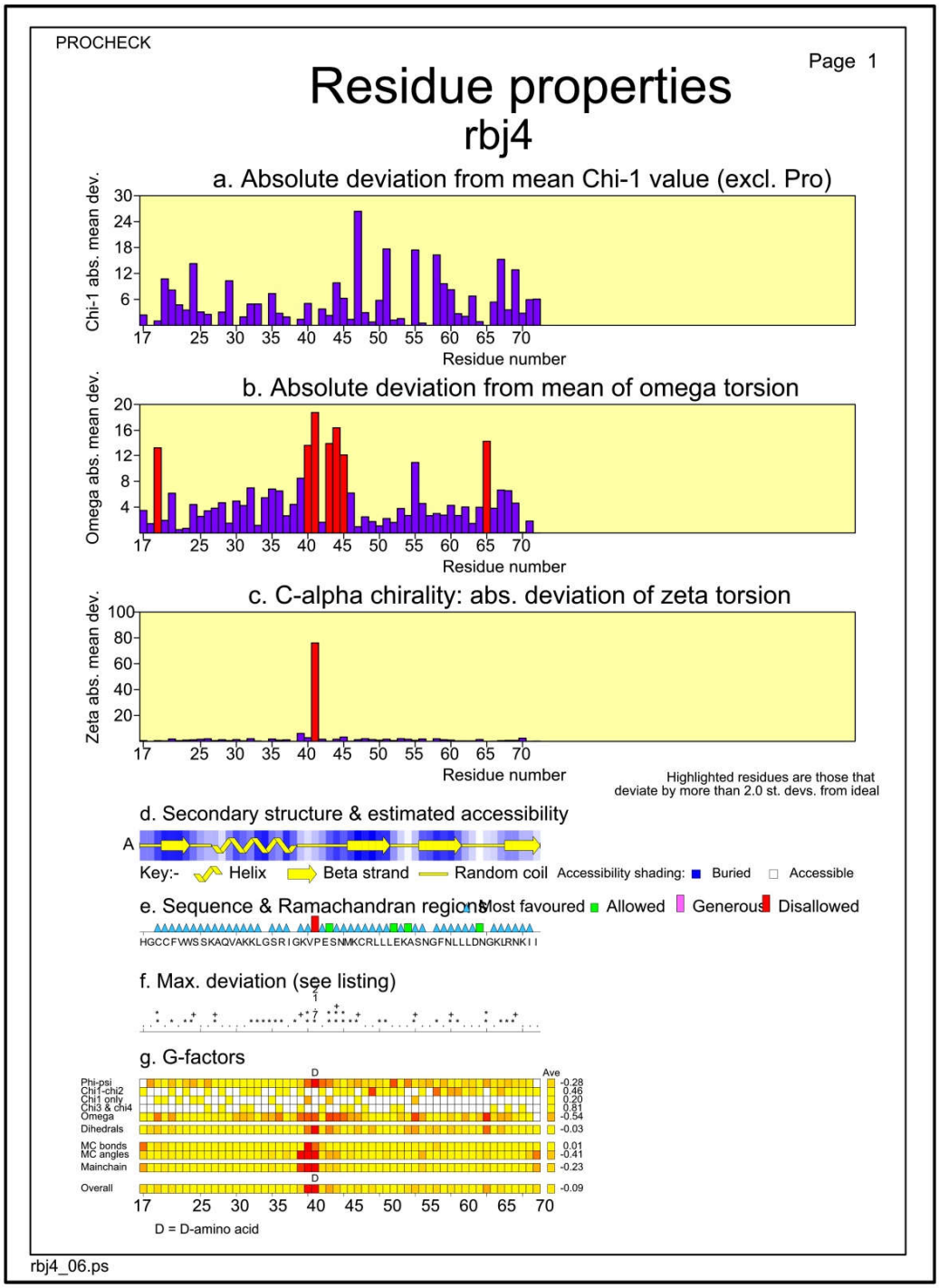

Figure 4.15: Residue properties of resilin

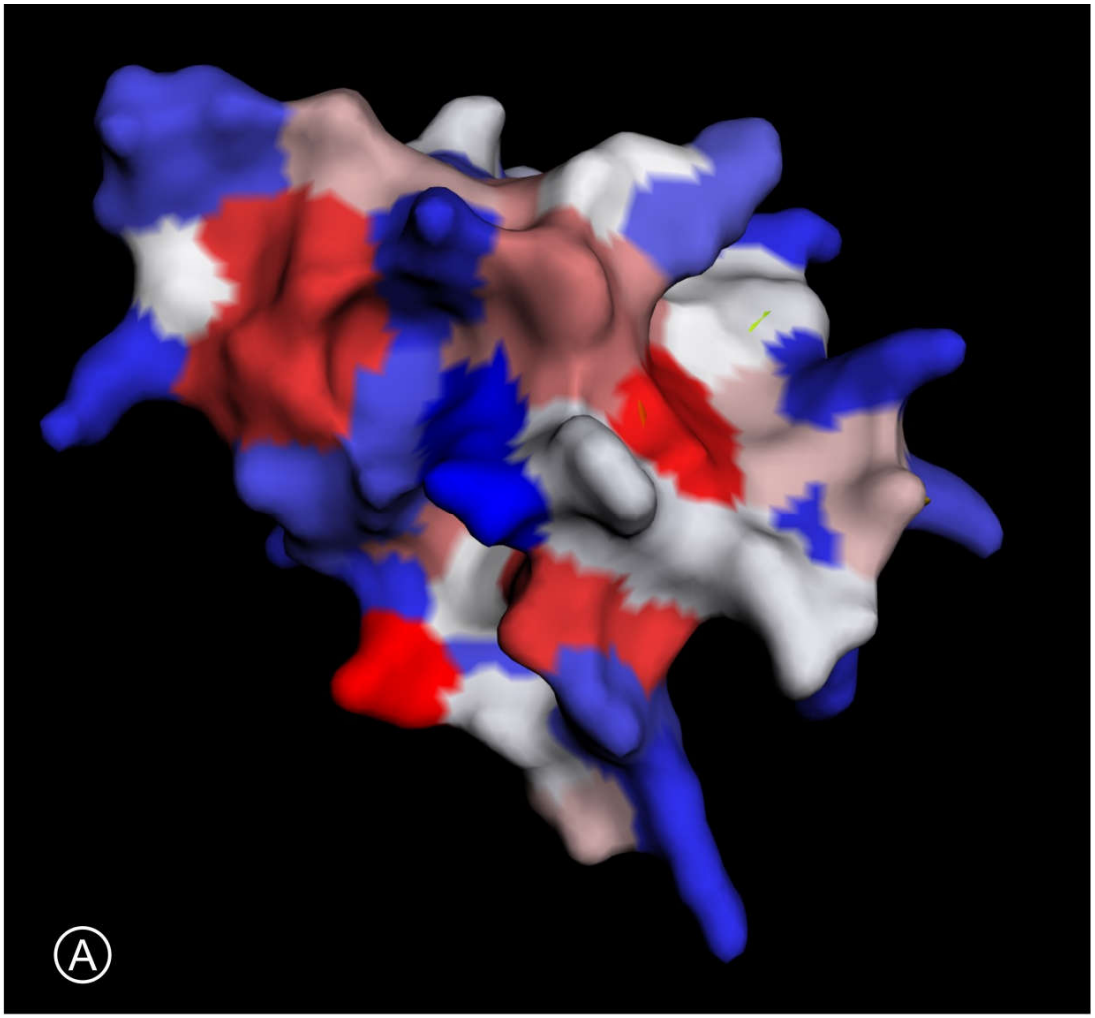

Figure 4.16: Hydrophobicity analysis of *P. flavescens* resilin protein model

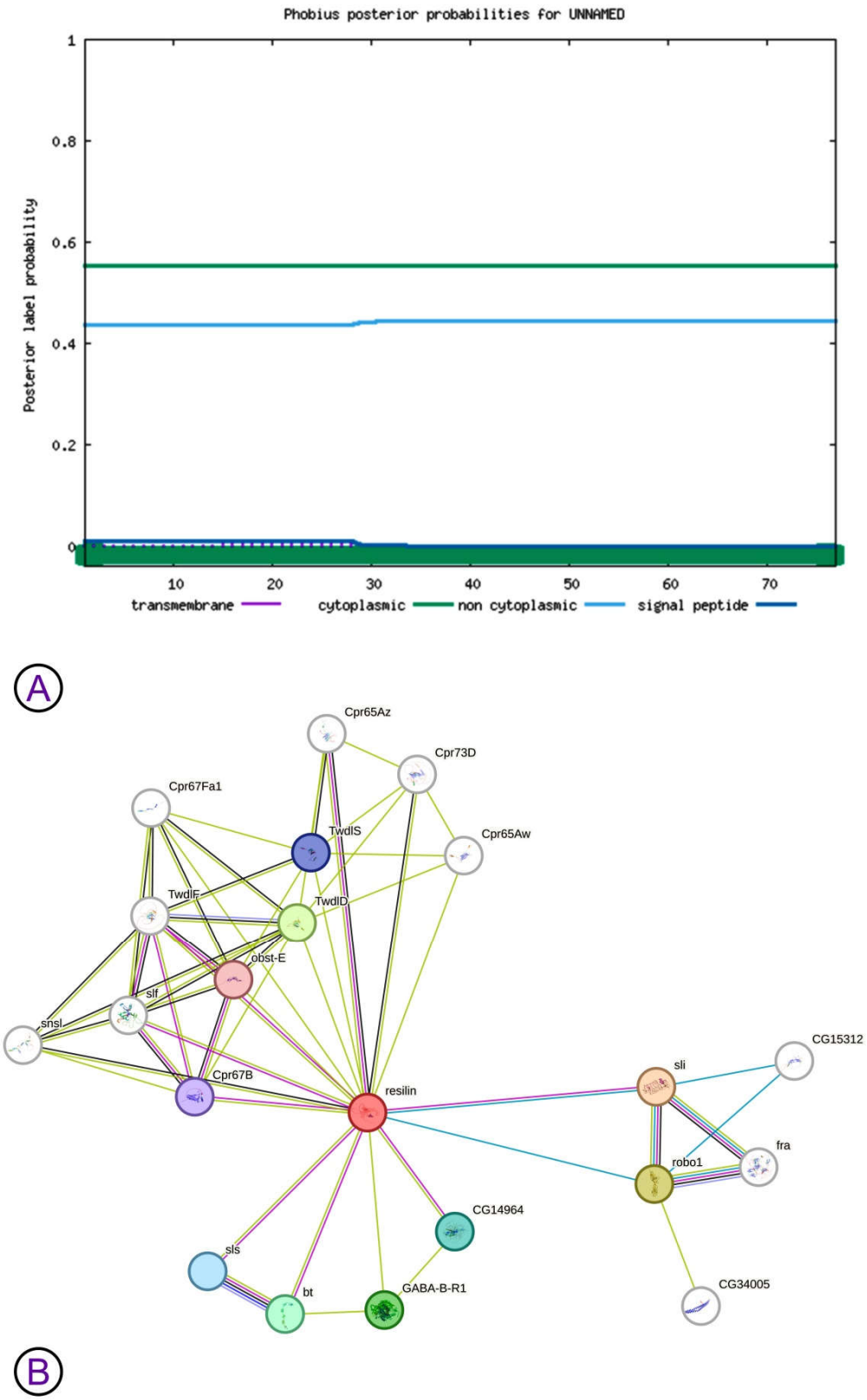

Figure 4.17(A) Signal peptide prediction of resilin model; (B) The STRING protein-protein interaction network with resilin protein

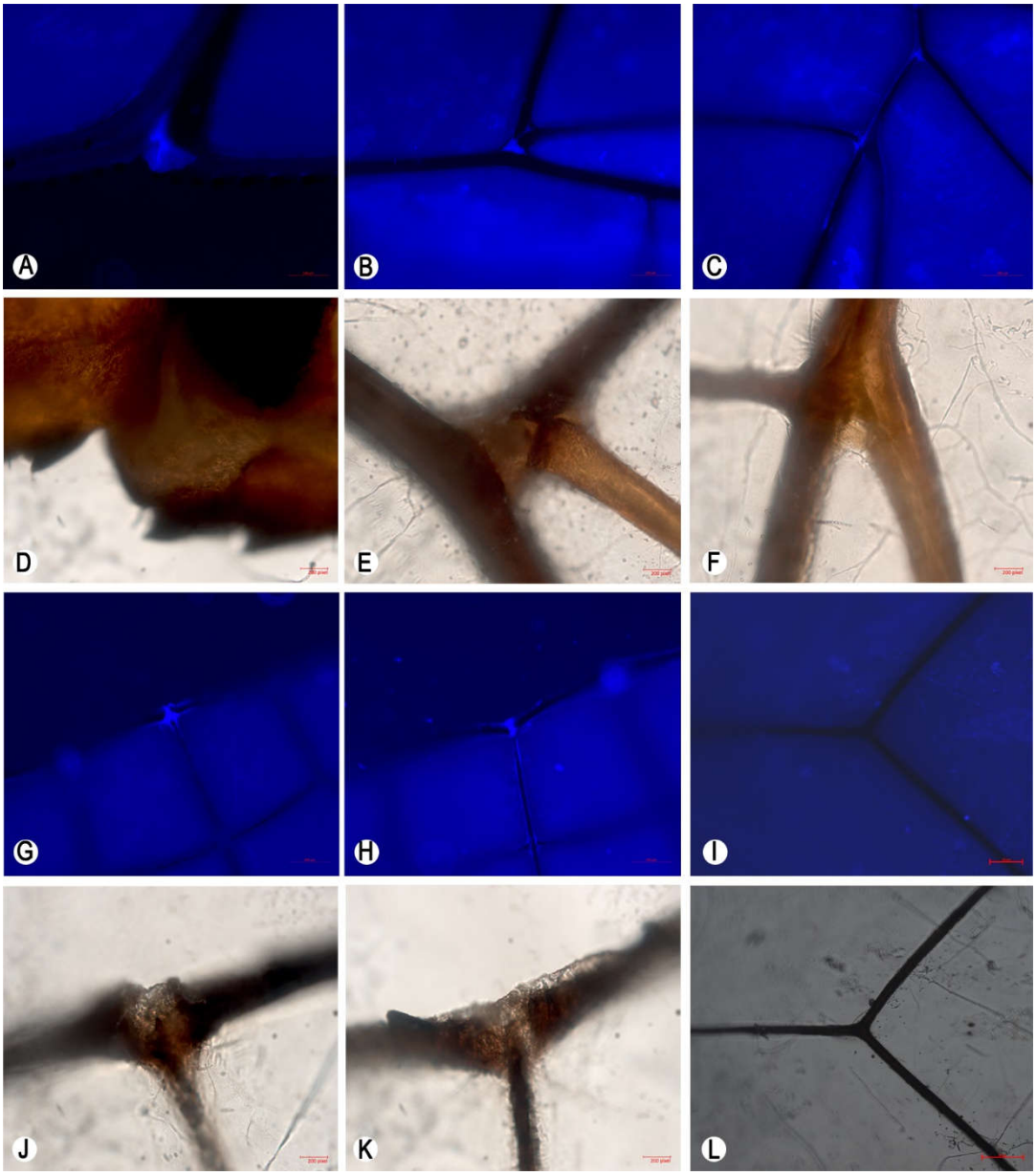

Figure 4.3: Forewing vein joints of *P. flavescens*. (A-H, J, K) mobile vein joints, (I, L) Immobile vein joints

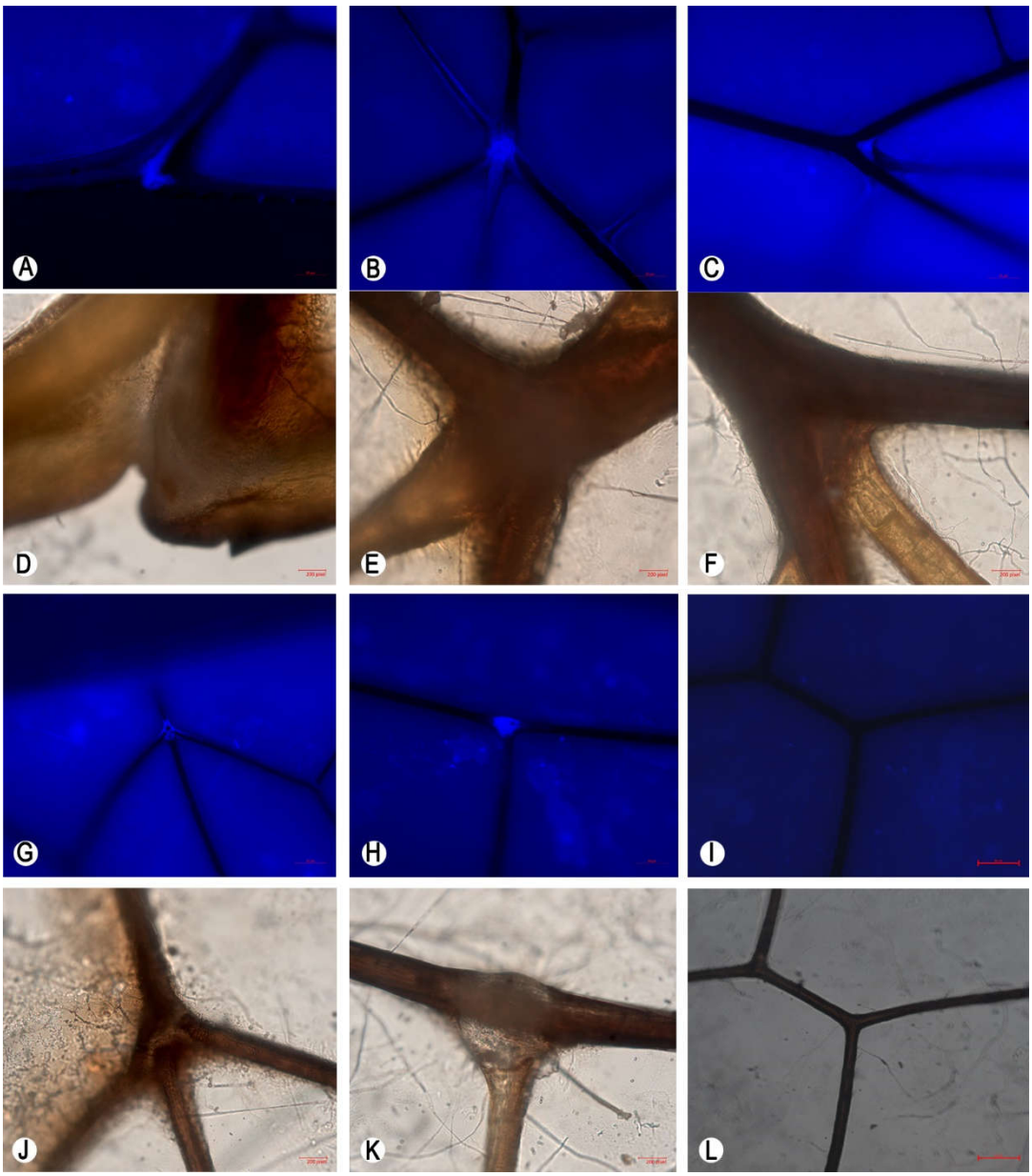

Figure 4.4: Hindwing vein joints of *P. flavescens*. (A-H, J, K) mobile vein joints, (I, L) Immobile vein joints

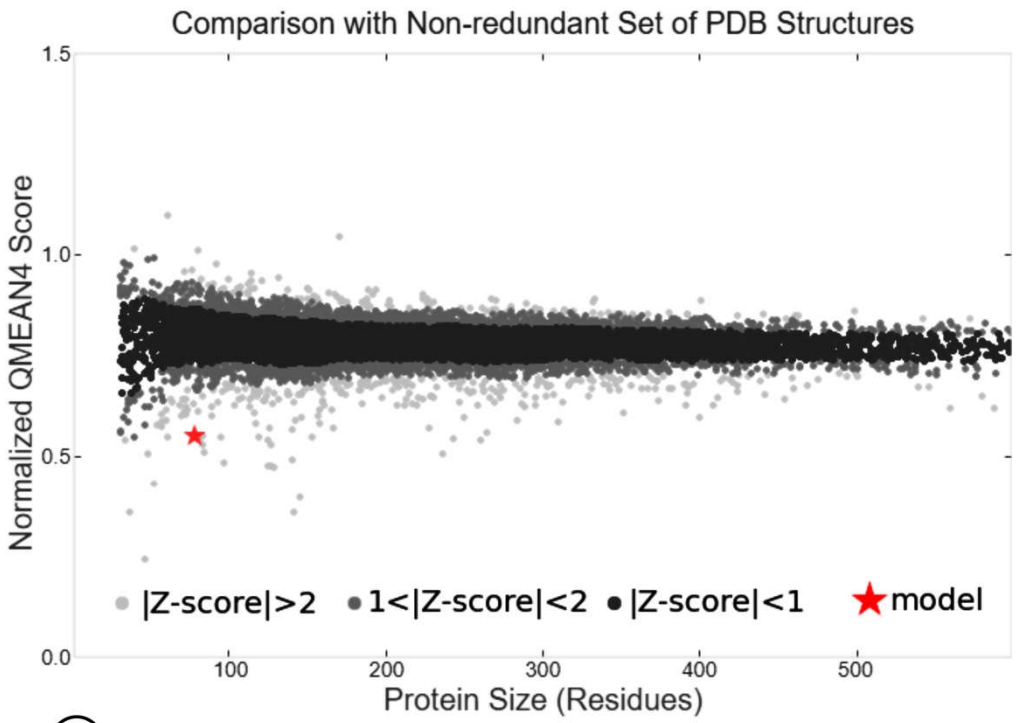

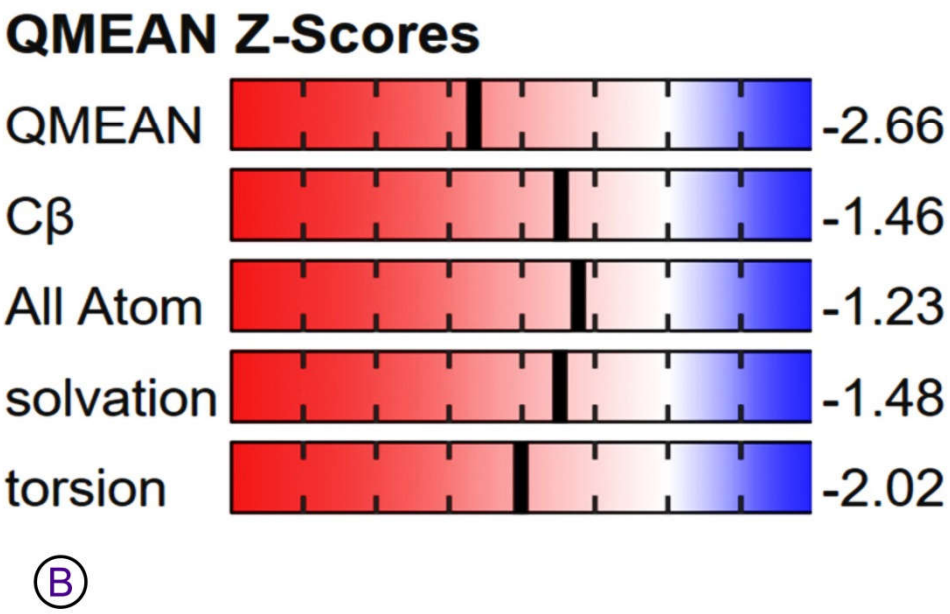

Figure 4.11: Structural validation of resilin protein model. (A) QMEAN score of structure of resilin protein model, (B) Graphical representation of the Z-Score

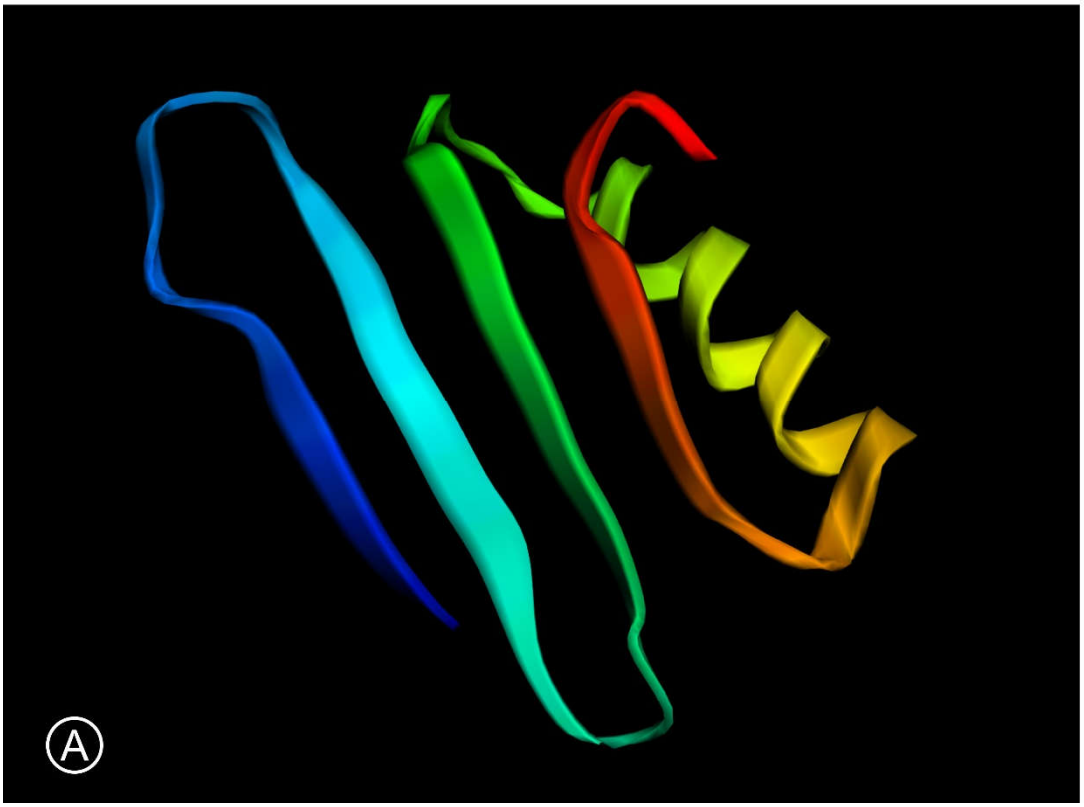

Figure 4.12: 3D structure of Resilin protein of *P. flavescens*

SUMMARY

The dragonflies exhibit unique flight characteristics; thus, the wing morphology and its influence on the flight have been studied extensively. The corrugated structure makes the wings stiffer and strengthens them. This makes the wing more lightweight and increases the aerodynamic performance of the dragonfly wings. In this study, we studied 26 dragonfly species' wing morphology, explicitly focusing on the diversity of wing venation patterns. The anal region of the hindwing and the venation patterns are the central wing characteristic features present in active and long-distance flight. The study documented three migratory species: *Pantala flavescens*, *Tholymis tillarga*, and *Tramea basilaris*. Among this species, *P. flavescens* is the longest migratory species. The wings of migratory dragonflies have more enormous and smoother wings with well-developed, large anal lobes. These differences between the migratory and non-migratory species might favour the gliding of migratory dragonflies. We noticed most of the changes in the hindwings.

The GMM analysis on the forewing and hindwings of selected dragonfly species proved that each species had its species boundary. From the analysis, we can conclude that the hind-wing venation analysis of dragonfly wings can be used as a prominent tool for species identification. In the morpho-phylogeny analysis, there is no phylogenetic signal in the forewing and hindwing (size and shape of the wings), which indicated that the morphological variability or diversity in the dragonfly was mainly modulated by the natural selection pressure nor by the evolutionary selection. Based on the environmental condition and associated requirements of the organism play a vital role in the wing morphological size and shape-related

variations. There is no proper close relationship between migratory and non-migratory species. For comparative purposes, we documented the phylogeny of wing morphology and COI-based phylogeny analysis. This irregular relationship between the migratory fly and the non-migratory indicates that this behaviour may have evolved due to natural selection pressure nor by evolutionary selection.

Migration-associated gene-based analysis is required for understanding the relationship between migratory and non-migratory dragonfly species. In the gut bacterial microbiome analysis, there is a significant difference between the gut bacterial microbiome of migratory (*P. flavescens*) and non-migratory species (*N. tullia*). Both species (migratory and non-migratory) were collected from the same region and at the same period. Even though they shared similar ecological and environmental factors, a significant difference in the gut-associated bacterial communities was observed. The food differences between these two species play an essential role in gut microbiome diversity. However, both species were collected from the same area in this study. Nevertheless, species-specific and sex-specific microbial community differences were documented in the *P. flavescens* and *N. tullia*.

The naiads and adult *P. flavescens* are one of the prominent predators that can be used for mosquito control. We studied the embryonic and post-embryonic development of *P. flavescens*. Culture standardisation is achieved through the supplementation of special nutrient composition. The unique nutrient solution can be used for successful laboratory-based mass culturing of *P. flavescens* and can be released into the agricultural field for control of pests. Dragonflies are potential biocontrol agents of major pests and vectors. This mass-rearing technique can be utilised in the Biological Control method of Integrated Pest Management.

Resilin protein plays an essential role in the elasticity of body parts in Arthropods. The high flapping, angle change, wing stretchability, and sudden modulation of wings in Odonates were mainly due to the presence of resilin protein in the wing joints. Resilin is primarily present in the vein junction, especially the flexible joints. It is also present in the anal region's veins of both the forewing and hindwing of *P. flavescens,* and this might be helping the *P. flavescens* during

migration. In the case of Odonate's, the resilin protein sequence is only available from *Ladona fulva* and *Aeshna sp*. Present study, that provides with the partial sequence of resilin from *P. flavescens*. This protein is highly stable, with a high level of ASA, and hydrophobic regions.

Future work related to dragonfly resilin protein may help explore its expression and functional characterisation for use in industry and biomedical applications.

FUTURE PERSPECTIVES

1. **Bioinspired Engineering:** Dragonfly wings are known for their intricate venation patterns and lightweight yet resilient structure. By understanding these patterns, engineers can design biomimetic materials for various applications such as lightweight structures, flexible electronics, and advanced aerospace materials.

2. **Medical Devices**: The study of wing resilin protein, which gives dragonflies their remarkable flexibility and durability, could inspire the development of biocompatible materials for medical devices such as implants, prosthetics, and surgical instruments. resilin protein could inspire advancements in biotechnology, such as the development of novel materials for tissue engineering, drug delivery systems, or biodegradable packaging.

3. **Biological Pest Control:** Understanding the relationship between dragonfly gut microbiome and their predatory behavior could inform strategies for biological pest control. Harnessing specific microbial communities that enhance predation could lead to more effective and environmentally friendly pest management techniques.

4. **Environmental Monitoring**: Dragonflies are sensitive to changes in water quality and habitat degradation. Monitoring the health of dragonfly populations through the analysis of wing venation patterns and gut microbiome could serve as a bioindicator for ecosystem health and assist in environmental conservation efforts.

Overall, the interdisciplinary study of dragonfly biology holds promise for a wide range of applications, from engineering and medicine to environmental monitoring and biotechnology.

PRESENTATIONS AND PUBLICATIONS

Presentations

Gayathri, M., & Y. Shibu Vardhanan (2023). Environmental stress monitoring through wing geometric morphometric analysis of wandering glider, *Pantala flavescens* (Odonata: Libellulidae). *International seminal on Ecotechnological Perspective for sustainable development.* MG University, Kerala. 21st & 22nd March, 2023.

Gayathri, M., & Y. Shibu Vardhanan (2023). Visualization of early developmental stages of the wandering glider, *Pantala flavescens* (Fabricius, 1798) embryos (Odonata: Libellulidae): A future biomarker. *2nd International conference on Advance Interdisciplinary Research (ICAIR-2023).* Digvijay Nath Post Graduate College, Gorakpur, UP. April 7 to 9, 2023.

Publications

Gayathri, M., Anand, P. P., & Y. Shibu Vardhanan. (2023). Visualization of early embryos of the wandering glider, *Pantala flavescens* (Fabricius, 1798) (Odonata: Libellulidae). *Aquatic Insects.* 44(4), 297-309. https://doi.org/10.1080/01650424.2023.2202182

Gayathri, M., Anand, P. P., & Y. Shibu Vardhanan. (2023). Wing size, shape, and asymmetry analysis of the wandering glider, *Pantala flavescens* (Odonata: Libellulidae) revealed that hindwings are more asymmetric than the forewings. *Biologia.*78, 2763. https://doi.org/10.1007/s11756-023-01404-8

Biologia
https://doi.org/10.1007/s11756-023-01396-5

ORIGINAL ARTICLE

Wing size, shape, and asymmetry analysis of the wandering glider, *Pantala flavescens* (Odonata: Libellulidae) revealed that hindwings are more asymmetric than the forewings

M. Gayathri[1] · P. P. Anand [1] · Y. Shibu Vardhanan[1]

Received: 9 September 2022 / Accepted: 15 March 2023

Abstract

The present study aimed to determine the wing asymmetry and sexual asymmetry of *Pantala flavescens* (Fabricius 1798) collected from a paddy field. *P. flavescens* is known as the longest migratory insect species and the morphological architecture of their hindwing aids in long-distance gliding. In our study, we collected F1 generation of male and female *P. flavescens* and used for geometric morphometric study to investigate wing asymmetry. We observed no difference in wing size between sexes from the study, but there are significant ($p < 0.05$) shape differences. The female population was more asymmetric than male population, with a high shape-related fluctuation asymmetry (FA). Discriminant function analysis was used to validate wing asymmetry (right-left) and sexual asymmetry of *P. flavescens*. Canonical variant analysis discriminated the forewings and hindwings of *P. flavescens* both sexes in a distinct morphospace. The PC's warp shape analysis proved that, when compared to forewings, the highest amount of shape variations was observed in hindwings, especially in anal lobe regions. Based on the results, pesticide and fertilizer used in the paddy fields are the primary reason for the high level of FA, and the morphological variations observed in the hindwings may influence the migratory behaviour of *P. flavescens.*

Keywords Wandering glider · Geometric morphometrics · Wing shape and size · Wing asymmetry · Fluctuation asymmetry

Introduction

Dragonflies and damselflies are well known for their remarkable flight abilities, which facilitating long-distance migration (Russell et al. 1998; Rajabi et al. 2016). Wing morphology and their unique architectural organization play an essential role in the high-flying maneuverability of dragonflies and damselflies (Rajabi et al. 2016). Approximately 6000 Odonata species are known to exist (Suhling et al. 2015), and it is estimated that only 25–50 of these species are migratory (Russell et al. 1998). *Pantala flavescens* (Fabricius 1798) (Globe skimmer or wandering glider) is the longest migratory species among dragonfly species and among all known insects (Hobson et al. 2012; May 2013; Chapman et al. 2015). And it is widely distributed throughout the tropics and many temperate areas (Hobson et al. 2012) and has been categorized as an obligate Intertropical Convergence Zone (ITCZ) migrant (Corbet 2004). In *P. flavescens,* multigenerational migration route from India to East Africa and back again, swarms of millions of *P. flavescens* can cover a total distance ranging from, or possibly exceeding, 14,000–18,000 km (Russell et al. 1998; Anderson 2009). In comparison to the forewing, the unique morphology of the hindwing aids in gliding of *P. flavescens,* and these features support long-distance migration (Garrison et al. 2006; May 2013; Suhling et al. 2015).

Compared to other dragonflies, migratory dragonflies were subjected to highly dynamic environmental modulations, which may have played a role in their morphological variations. Morphological variation is caused by developmental and environmental processes that result in differences between individuals and populations (Hoffmann

✉ P. P. Anand
anandpp633@gmail.com

✉ Y. Shibu Vardhanan
svardhanan@gmail.com

[1] Biochemistry and Toxicology Division, Department of Zoology, University of Calicut, Thenhipalam, Kerala 673 635, India

Published online: 30 March 2023

AQUATIC INSECTS
https://doi.org/10.1080/01650424.2023.2202182

Visualisation of early embryos of the wandering glider, *Pantala flavescens* (Fabricius, 1798) (Odonata: Libellulidae)

M. Gayathri, P. P. Anand and Y. Shibu Vardhanan

Biochemistry and Toxicology Division, Department of Zoology, University of Calicut, Thenhipalam, Kerala, India

ABSTRACT

The embryonic development of *Pantala flavescens* (Fabricius, 1798) is documented for the first time. In contrast to previously reported insect embryonic development, we describe the embryological development of *P. flavescens* in living conditions by focusing on its externally recognisable features, i.e., we conducted the study in a purely non-destructive manner. The entire embryonic development was completed within six to seven days. We pictured the eggs at successive embryonic developmental stages: embryogenesis starts, germband formation, segmentation, blastokinesis, appendage formation, and dorsal closure. These findings can be helpful in future studies regarding the impacts of pollutants and climate change on the early embryonic development of dragonflies.

ARTICLE HISTORY
Received 4 April 2022
Revised 17 November 2022
Accepted 7 December 2022

KEYWORDS
Dragonfly; embryology; light-microscopic imaging; wandering glider

Introduction

Embryogenesis, the mid-life cycle of insects, is recognised with different developmental stages such as zygote formation, morula formation, blastoderm formation, germ band formation, elongation, segmentation, appendage formation, and dorsal closure (Davis and Patel 2002). Hemimetabolous insects like Odonata show blastokinesis during their embryonic development and so embryogenesis can be divided into germ band formation, anatrepsis, intertrepsis, and katatrepsis (Masumoto and Machida 2006; Panfilio 2008; Donoughe and Extavour 2016). Tillyard (1917) conducted a detailed study on the biology of dragonflies, including their embryology. Ando (1962) studied the embryology of Odonata with special reference to *Epiophlebia surperstes* (Sélys, 1889) in Sélys-Longchamps and Palaeophlebia (1889) (Epiophlebiidae). Miyakawa (1987, 1990) carried out an elaborate work on the rotation of embryos in the eggs of some dragonflies (Odonata), studied the difference in the degree of rotation in seven dragonfly species, and compared the germ rudiment position in the egg. A preliminary study of egg chorion features in different dragonfly spp. (Anisoptera)

CONTACT P. P. Anand anandpp633@gmail.com Biochemistry and Toxicology Division, Department of Zoology, University of Calicut, Thenhipalam, Kerala673 635, India; Y. Shibu Vardhanan svardhanan@gmail.com Biochemistry and Toxicology Division, Department of Zoology, University of Calicut, Thenhipalam, Kerala673 635, India.

Published online 18 May 2023